# Bioinspired Molecular Engineering of Amino Acid and Arylenediimide Derivatives for Functional Applications

**A Thesis Submitted for the Degree of**

**Doctor of Philosophy**

**By**

**M. B. Avinash**

**Bioorganic Chemistry Laboratory, New Chemistry Unit**

**Jawaharlal Nehru Centre for Advanced Scientific Research**

**(A Deemed University)**

**Bengaluru-560064, India**

**January 2014**

# DEDICATED TO PROF. C. N. R. RAO

# CERTIFICATE

I hereby certify that the work described in this thesis entitled "**Bioinspired Molecular Engineering of Amino Acid and Arylenediimide Derivatives for Functional Applications**" has been carried out by **Mr. M. B. Avinash** under my supervision at the Bioorganic Chemistry Labortory, New Chemistry Unit, Jawaharlal Nehru Centre for Advanced Scientific Research, Bangalore, India and that it has not been submitted elsewhere for the award of any degree or diploma.

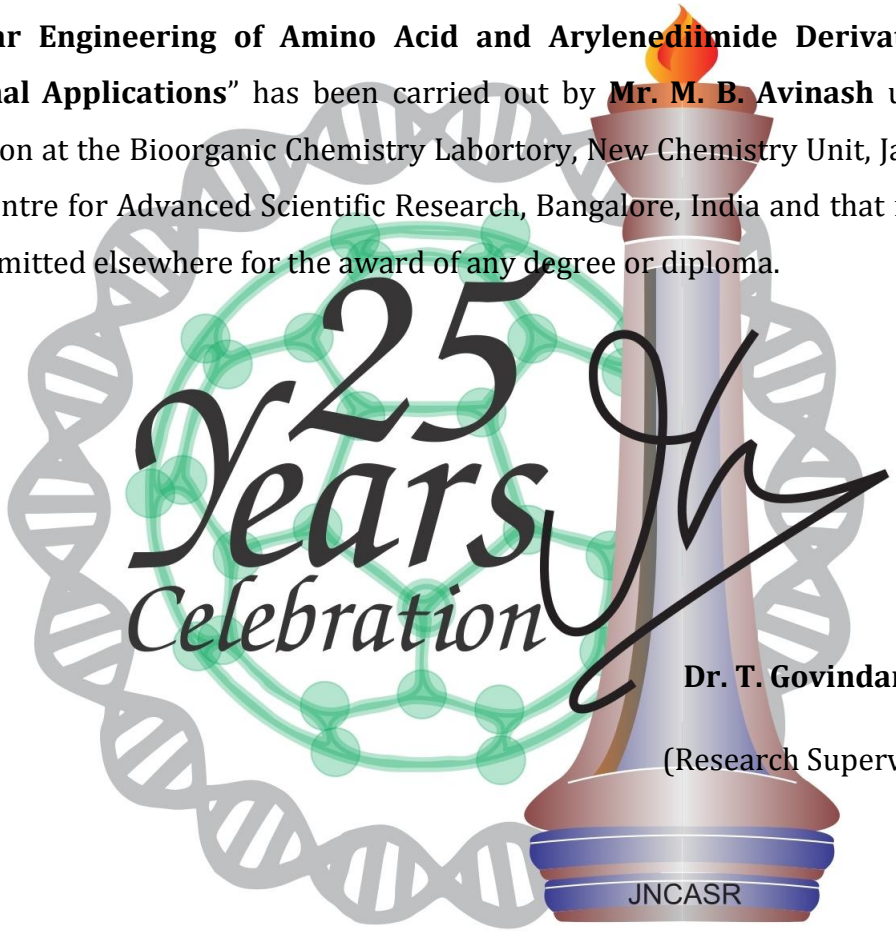


**Dr. T. Govindaraju**

(Research Supervisor)

# DECLARATION

I hereby declare that the matter embodied in the thesis entitled "**Bioinspired Molecular Engineering of Amino Acid and Arylenediimide Derivatives for Functional Applications**" is the resultant of the investigations carried out by me at the Bioorganic Chemistry Labortory, New Chemistry Unit, Jawaharlal Nehru Centre for Advanced Scientific Research, Bangalore, India under the supervision of **Dr. T. Govindaraju** and that it has not been submitted elsewhere for the award of any degree or diploma.

In keeping with the general practice in reporting the scientific observations, due acknowledgement has been made whenever the work described is based on the findings of other investigators. Any omission that might have occurred due to oversight or error in judgement is regretted.

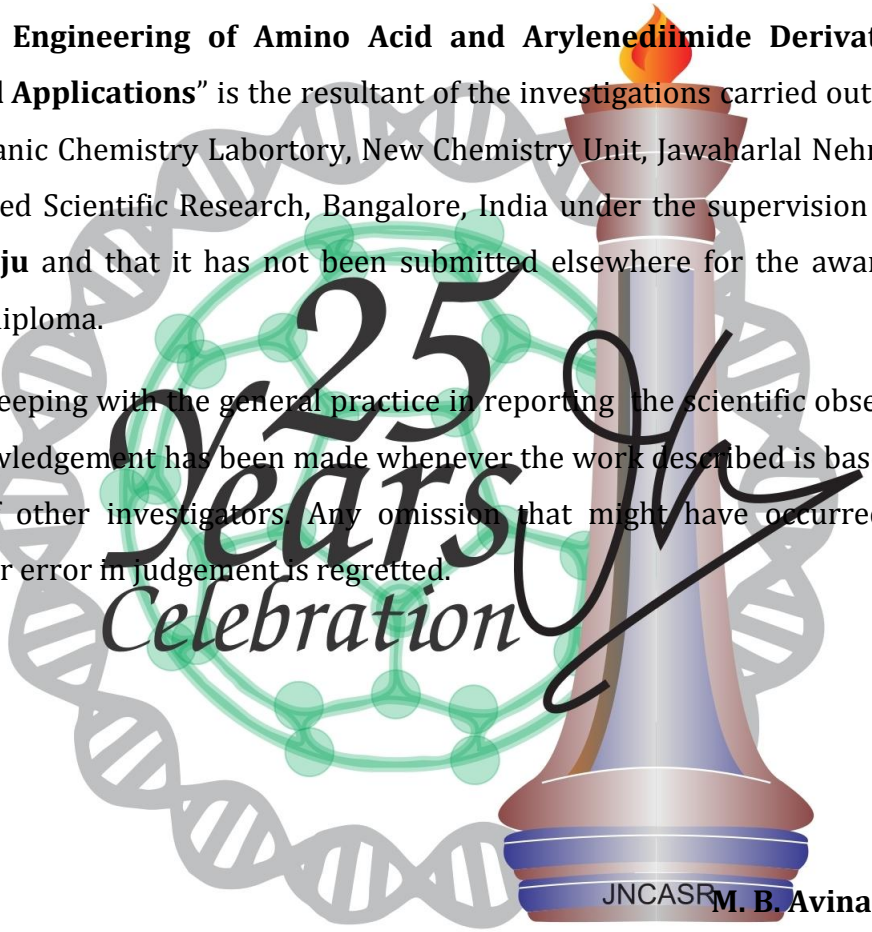


**M. B. Avinash**

(PhD Student)

# ACKNOWLEDGEMENTS

Firstly, I would like to thank my PhD research supervisor Dr. T. Govindaraju, with whom I had a roller coaster ride for the past five years. I thank him for his guidance, encouragement and the freedom that he offered to explore new things as well as a scenario to push me to my limits. Specially, I thank him for understanding me and for his patience, as many of my works were rather time consuming.

Nearly 15 years ago, I was inspired by Prof. C. N. R. Rao to indulge in research activities. Down the line, I was fortunate to work under him on several summer research projects. In many ways, he is the very reason why I am here today. His mere presence, ever-lasting enthusiasm and accomplishments have been an immense source of inspiration for excellence. I will be indebted to him for all the opportunities and support that he has bestowed on me for the last 10 years.

I would like to thank the faculty members of JNCASR namely Prof. S. M. Shivaprasad, Prof. Ranganathan, Prof. M. Eswaramoorthy, Prof. T. K. Maji, Dr. Subi J. George, Dr. T. Govindaraju, Prof. S. Balasubramanian, Prof. Shobhana Narasimhan and Prof. Amitabh Joshi for their fruitful courses.

I wouldn't have been better equipped for my PhD, if not for the guidance of Prof. A. Govindaraj, Dr. Kripa Sardar, Dr. Thirumurugan, Dr. Vivekchand, Dr. Kalyani and Dr. Gomathi, who were instrumental in teaching me the basics of research life during my summer project days.

Prof. S. N. Bhat and Prof. A. Govindaraj, who were the POCE coordinators have made huge difference to my research life and I am grateful to them for all their guidance, encouragement, affection and timely help.

I would like to thank Prof. Swapan K. Pati, Mr. Pralok K. Samanta, Prof. K. S. Narayan, Ms. Swati, Prof. U. Ramamurty, Mr. Devraj Raut, Prof. Carsten Schmuck and Ms. Elisabeth Verheggen for their valuable collaborations and thought-provoking discussions.

I thank Dr. K. S. Subrahmanyam, Dr. Y. Sundarayya, Mr. M. Shivaprasad, Mr. M. Pandeeswar, Mr. N. Nagarjun, Mr. K. V. Sandeepa and Mr. Ramakrishna for working with me on different research projects.

My PhD work wouldn't have be feasible without the friendly cooperation and technical aid of Mrs. Selvi (FESEM), Mrs. Usha (TEM), Mr. Basavaraj (AFM), Mr. Mahesh (NMR), Mr. Vasu (UV/PL/IR), Mr. Anil (PXRD), Mrs. Suma (Confocal), Mr. Peer/Mr. Munne Gowda/Mr. Dileep (Audio-Visual) and for which I am grateful.

I thank the then wardens Prof. A. Sundaresan, Dr. Kavita Jain, Prof. S. M. Shivaprasad, Dr. T. N. C. Vidya and sports coordinator Prof. Chandrabhas Narayana with whom I enjoyed additional responsibilities as a students and sports representative.

I am thankful to my lab-mates Dr. Maity, Mr. Pandu, Mr. Nagarjun, Mr. Shivaprasad, Mr. Rajasekhar, Ms. Suseela, Mr. Anand, Ms. Manju, Mr. Sandeepa, Mr. Manjunath, Mr. Sarkar, Mr. Manna, Mrs. Bhagya, Mrs. Mamata and Dr. Atul, with whom I have had some of the most memorable moments of my life.

I am thankful to our administrative officer Mr. A. N. Jayachandra for all his friendly affection, support and guidance.

This is my 10$^{th}$ year in JNC and in fact I have had the rare pleasure to stay for so long in my second home. I am grateful to JNC Faculties, Friends, Administrative Staff, Hostel Staff, Mess Workers, House Keeping Staff and Security Personnel for providing a congenial atmosphere and an opportunity to live my dream.

I thank all my well-wishers, friends, teachers and all those (either directly or indirectly) for influencing me in one way or the other.

Special thanks to my family members for their evergreen love, immaculate faith and relentless support in all phases of my life. Only they know how I have made this thesis possible and only I know how they have made this thesis possible.

# PREFACE

This PhD thesis has been categorized into four main chapters, namely, Introduction, Molecular Engineering, Molecular Biomimicry and Molecular Materials. The first chapter serves as an introduction to the thesis, outlining the fundamental aspects of molecular assembly and the essence of exploiting bioinspired designs for fundamental as well as technological implications. To put it in a nutshell, the Nature's archetypal molecular assemblies have been the result of rigorous natural selection and evolution over billions of years. Unsurprisingly, an eclectic approach to design and manufacture advanced materials necessarily include biomolecules due to their remarkable property of integrating structure, function and dynamics. It is thus believed that bioinspired design strategy will provide us with new opportunities to explore novel functional molecular materials and understand previously intractable complex biochemical phenomena.

With this premise in mind, thoughtful efforts were invoked to engineer the assemblies of arylenediimides *viz.* naphthalenediimides (NDIs) and perylenediimides (PDIs) upon derivatization with amino acids, which is especially interesting due to their wide spread applications in fields ranging from biomedicine to electronics. A wide variety of molecular designs were employed to exploit several non-covalent interactions like solvophobic, aromatic, hydrogen bonding, halogen bonding, van der Waals, metal coordination and charge transfer interactions, in an effort to find structure-property correlations. All these molecular design strategies are described in great detail as sub-chapters in the second chapter entitled Molecular Engineering.

In the third chapter, an ambitious effort was ventured to try and mimic biological processes occurring at the molecular-level or their assemblies, which forms the basis of a new discipline termed as Molecular Biomimicry. Herein, the first sub-chapter deals with the extremely slow dynamics of an abiotic helical assembly with an unusual relevance to the secondary structure of proteins, which finds importance with respect to prevalent protein folding mystery and the

associated conformational diseases. The second sub-chapter provides the first evidences for emergence and autoregulation in a dynamic molecular assembly. Emergence is a complex behavior occurring in the system due to a delicate interplay of multiple interactions, which are often unpredictable and unprecedented. On the other hand autoregulation is a mechanism by which a system actuates or modulates its responses depending on the external stimuli. We strongly believe that investigations of molecular systems having such behaviors could be instrumental in shedding novel insights about biochemical processes and also as an advanced means to treat biological ailments.

The fourth chapter entitled Molecular Materials is further divided into three sub-chapters. In the first sub-chapter, lotus effect inspired self-cleaning functional molecular material, developed by means of simple solution processable breath-figure technique (BFT) has been described. Using this approach, hydrophobic decorative molecular materials besides potential applications in electronics and miniaturized biochemical assays could be realized. On the other hand, simple modular peptides designed by a reductionistic approach are shown to mimic the mechanical properties of spider silk, which forms the basis for second sub-chapter. Such a design strategy holds promising applications as biological implants, biocompatible sutures, tissue engineering and other technologies. Finally, as our core functional molecule namely, NDIs are potential n-type organic semiconductors; the earlier embarked molecular structure-property correlation studies have led us to find very high electron mobilities even in their bulk state. The added advantage of solution processability engenders great promise in organic electronics.

In summary the thesis is structured in such a way that the first chapter provides the scope and objective of the work, while the second describes molecular engineering strategies by means of thoughtful exploration, the third renders interesting insights into complex biochemical processes and the fourth forms the basis for technological applications. The contents of this thesis are adapted from our publications listed in page 261, with permission of Wiley-VCH, RSC and ACS.

# TABLE OF CONTENTS

# CHAPTER 1 INTRODUCTION

## 1.1. Bioinspiration

The term bioinspiration relates to the design strategies that are inspired by mechanisms or laws or functions operating in biological systems.[1-14] Over the years, few other related terms are also being employed by several research groups, namely biomimetics (biomimicry), biotechnology, biokleptics and bionics. The term biomimetics is derived from the Greek word '*bios*' meaning '*life*' and '*mimesis*' meaning '*to imitate*'.[15-20] As early as 1969 Otto Schmitt coined the term biomimetics, which made its first appearance in Webster's Dictionary in 1974 with the definition, "the study of the formation, structure or function of biologically produced substances and materials (as enzymes or silk) and biological mechanisms and processes (as protein synthesis or photosynthesis) especially for the purpose of synthesizing similar products by artificial mechanisms which mimic natural ones". On the other hand, the term biotechnology refers to the technological application that uses biological systems, living organisms, or derivatives thereof, to make or modify products or processes for specific use.[21-24] Relatively an unknown term biokleptics deals with the usage of biological components to perform their natural function in a non-biological environment. The term bionics was coined by Jack Steele, which is defined as, "the application of biological methods and systems found in nature to the study and design of engineering systems for modern technology".[25-27]

It should be noted that the definitions of the above terms are also available in few other variations and a stringent distinction of these terminologies from one another is seldom simple. For a better understanding of the subtleties associated with these terminologies, interested readers are suggested to refer to a recent perspective article by Staniland *et. al.*.[28] Evidently the fields of biomimetics, biotechnology, biokleptics and

bionics derive its inspiration from the biological world in one way or the other, and hence by and large are the subsets of bioinspiration.

### 1.2. Why Bioinspiration?

Let us now address some of the most obvious questions as to why one has to undertake a bioinspired pathway? What are its benefits? How to make *de novo* designs? And so forth. We humans being the most intelligent species on this planet earth, have the capability to create and do things as per our whims and fancies. The irony is that, all of our methods can be mostly classified into the standard *heat*, *beat* and *treat* strategies. Unlike human's - way, Nature knows how to make even the most complex molecules, minerals as well as architectures, all in ambient temperatures and pressures. Interestingly, all of this is governed either directly or indirectly by a simple process known as self-assembly.[29-32] At the first outlook, this may not seem obvious. Just to elaborate on its importance, let us consider the formation of biominerals such as bones, teeth, sea-shells *etc*., which necessarily has to involve the organization of specific chemical entities into appropriate patterns and positions via a complicated interplay of molecular recognition and interactions to engender respective functions. Same is true for the intriguing architectures associated with cellular proteins, membranes, organelles, tissues and organisms. For instance, in order to biosynthesize a particular molecule, the respective enzymes (biomolecules) have to be assembled into a specific quaternary (native) structure and also the reagents has to be made available at the site of production via appropriate molecular recognition/interactions. All in all, the self-sustainability of the natural world involves the

auto-regulation of chemical interactions and their assembly. With this pretext, it is thus safe to say that the Nature's self-assembly approach has unparalleled superiority, efficiency and simplicity in tailoring organization with molecular-level precision. Nature's archetypal chemical engineering with specific structure-function relationship has thus inspired researchers to design novel biomimetics for advanced functional applications and to unravel the progressive evolution of self-organization towards complex matter.[33-35]

Although, the idea of mimicking is not new, we humans either knowingly or unknowingly have been inspired by the natural world since time immemorial. Not so obvious point to note is that the very process of learning our communicative language is by repeated imitation, and as a matter of fact we humans are the best imitators on this planet. Having a life span of several billions of years and with several millions of species, our natural world thrives on innumerable mysteries and engineering wonders. Therefore we strongly believe that the very process of imitation can aid us to decipher these secrets for a better understanding of our natural world. Moreover, it could also be a means to generate ingenious solutions to a wide range of our current engineering problems pertaining to energy, health and environment. Over the years, one such thought-process of mimicking bird's flight has led to multi-billion dollar aviation industry with a phenomenal impact on human's locomotion across the globe. Similarly, a wide variety of applications has been envisioned from the inspirations drawn from several biosystems, which in principle can bring about significant changes in our day-to-day activities.[1,4,7,8,18] In Table 1, we have provided a list of some of the interesting applications modeled on biological systems.

**Table 1.** Properties of some biological systems envisioned for various applications.

| Biological System | Property | Application |
|---|---|---|
| Plant Leaf | Photosynthesis | Energy Harvesting |
| Lotus Leaf | Superhydrophobicity | Self-Cleaning |
| Lizard | Sticking | Reversible Adhesives |
| Desert Beetle | Wettability | Fog Harvesting |
| Spider Silk | Strength<br>Toughness | Biological Implants<br>Automotives |
| Water Strider | Superhydrophobicity | Locomotion |
| Rice Leaf | Directional Wetting | Fluid Transport |
| Peacock Feather<br>Morpho Butterfly Wing<br>Beetle Shell | Structural Coloration | Beautification |
| Kingfisher Beak | Aerodynamics | Bullet Trains |
| Rodent Incisors | Chopping | Cutting Tool |
| Woodpecker Head | Shock Absorbers | Safety Equipments |
| Shark Skin | Wettability | Drag Reduction<br>Anti-biofouling |
| Termite Mound | Air Conditioning | Architectures |
| Mosquito Eye | Superhydrophobicity | Anti-fogging |
| Polar Bear Skin/Fur | Thermal Insulation | Artificial Fur/ Textiles |
| Bacteria Flagella | Propeller | Molecular Machines |
| Octopus | Maneuverability | Soft Robotics |
| Tortoise Beetle<br>Blue Damselfish | Stimuli Responsive<br>Structural Coloration | Camouflage |
| Deep-Sea Sponges | Glass | Optical Fibers |
| Bat | Echolocation | Navigation |

### 1.3. Self-assembly

Self-assembly is the process of formation of organized structure or pattern from a disordered system of pre-existing components as a consequence of specific, local

interactions among the components themselves, without an external guidance.[29,30] In general, self-assembly can be classified into two types as follows;

- Static self-assembly: The ordered state forms as the system approaches equilibrium, reducing its free energy and are primarily governed by thermodynamic properties of the system. Due to their tendency to equilibrate, this type of assembly facilitates self-healing properties.[29,30]
- Dynamic self-assembly: The ordered states are attained under non-equilibrium conditions and are essentially kinetically controlled systems. This type is especially interesting due to their pivotal role in living systems.[29,30]

### 1.4. Molecular self-assembly

If the constitutive components of a self-assembly process are molecules, then the process is termed as molecular self-assembly.[34,36-41] Molecular self-assembly can be further classified into two types namely,

- Intermolecular self-assembly: Herein the formation of organized structure or pattern involves the non-covalent interactions between neighboring molecules. The term molecular self-assembly generally refers to intermolecular self-assembly.
- Intramolecular self-assembly: Herein the formation of organized structure or pattern involves the non-covalent interactions within the different segments of a molecule. This type is commonly referred to a folding process.

## 1.5. Molecular interactions

In order to form an organized structure or pattern of a designer molecule, various non-covalent forces such as π-π stacking, hydrogen-bonding, van der Waals interactions, hydrophobic interactions, electrostatic interactions and/or metal co-ordinations are to be controlled effectively.[42-45] As these non-covalent forces are weak in nature, their effective control is most often tricky and a daunting task. In order to control molecular interactions, we employ supramolecular design principles.[46-54] Despite significant advances in supramolecular chemistry, direct control of molecular organization remains a challenging endeavor, and although we have improved our ability to tune the selectivity and specificity of weak, complicated molecular interactions, the field is still in its infancy. In this regard, designing and engineering the molecular organizations as per requirement needs to be the primary objective and future prospect of molecular self-assembly.

## 1.6. Molecular architectonics

After exploring the macroscopic world for several centuries and having visualized microscopic world for few decades, we are now venturing into the verge of controlling matter via pre-programmed assemblies. To construct such complex molecular systems, various weak non-covalent interactions have to be harnessed synchronously. This obligation of harvesting tricky intermolecular interactions cooperatively makes supramolecular engineering a challenging and intriguing endeavour.[55-62] To achieve this daunting task, several primitive yet elegant molecular designs involving hydrogen-bonding, metal coordination and/or aromatic interactions either in solution or at an

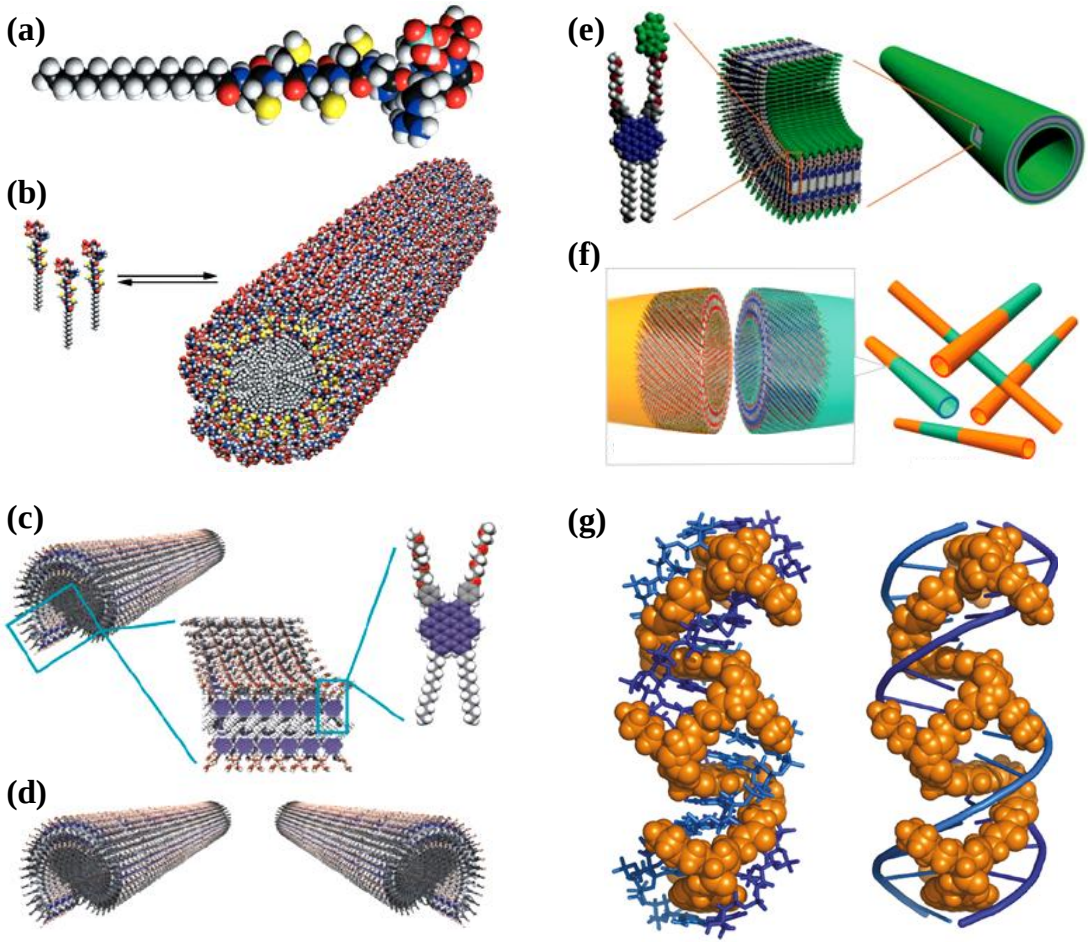


**Figure 1**. (a) Molecular model of an ingeniously designed peptide amphiphile, which directs the mineralization of hydroxyapatite to form a composite material. (b) Schematic representation of the self-assembly of peptide amphiphiles into cylindrical micelle. (c) Schematic representation of the structure of self-assembled grahitic nanotube obtained from hexabenzocoronene amphiphile. (d) Left and right-handed arrays of π-stacked hexabenzocoronene amphiphiles. (e) Schematic representation of the molecular organization of the photoconductive nanotube with a coaxial donor-acceptor configuration. The electron-accepting and donating functionalities are shown in green and blue respectively. (f) Schematic representation of the supramolecular linear heterojunction formed from fusing assemblies of distinct molecular components. (g) Molecular models of a sequence-specific threading tetra-intercalator having an extremely slow dissociation rate constant. (a) and (b) Adapted with permission of AAAS from reference 63. (c) and (d) Adapted with permission of National Academy of Sciences USA from reference 64. (e) Adapted with permission of AAAS from reference 65. (f) Adapted with permission of AAAS from reference 66. (g) Adapted with permission of NPG from reference 67.

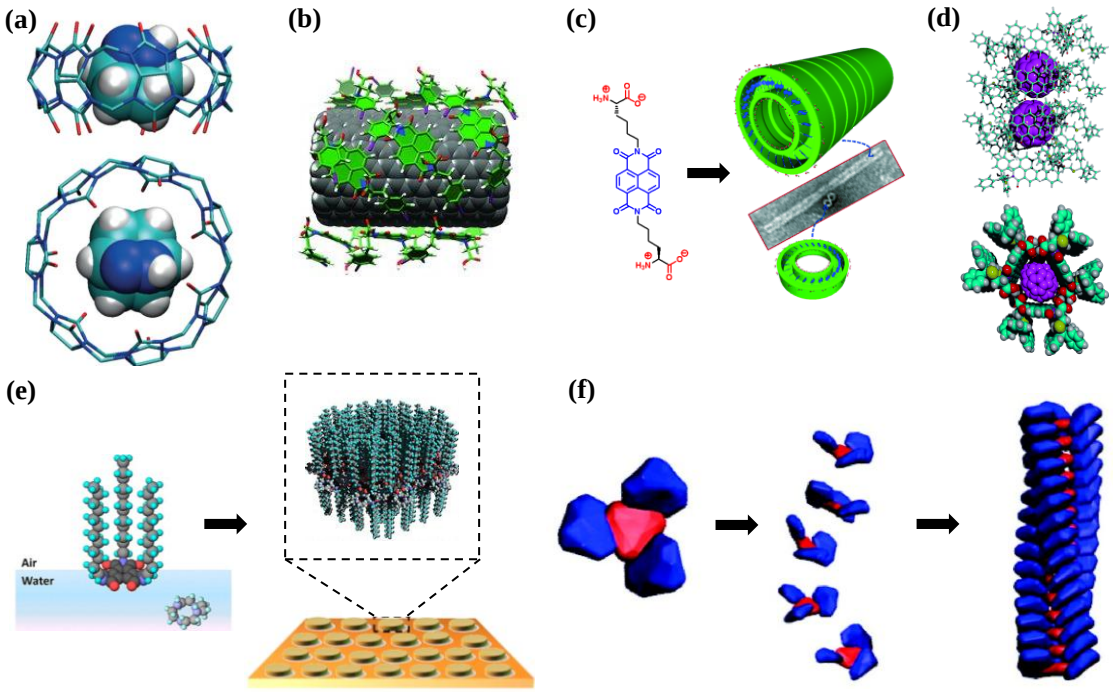


**Figure 2**. (a) Molecular models show the host-guest assembly (side- and top-view) formed by the complexation of cucurbit[*7*]uril with bicyclic azoalkane, which illustrates supramolecular reactivity occurring in molecular pockets. (b) Molecular mechanics minimized representation of naphthalenediimide (NDI) stacks self-assembled on the surface of a single-walled carbon nanotube (SWNT). This non-covalent surface encapsulation strategy facilitates internalization of SWNTs into cells. (c) Schematic representation of a supramolecular nanotube formed from an amphiphilic NDI derivative. The hierarchical nanotubes are formed via stacking of nanorings, which are formed from a monolayer of NDI derivatives. (d) Molecular models (side- and top-view) show the inclusion of $C_{60}$ in a NDI based helical nanotube. The poorly soluble $C_{60}$ molecules are solubilized by using these helical nanotubes. (e) Schematic representation of the formation of self-assembled molecular aggregates at the air-water interface. A convenient strategy to form regular-shaped self-assembled aggregates. (f) Schematic model of the self-assembly of twisted stacks of $C_3$ symmetric benzene-1,3,5-tricarbonamide derivatives. An interesting example of helical stacks of enantiomers having different stabilities. (a) Adapted with permission of NPG from reference 68. (b) Adapted with permission of Wiley-VCH from reference 69. (c) Adapted with permission of Wiley-VCH from reference 70. (d) Adapted with permission of Wiley-VCH from reference 71. (e) Adapted with permission of ACS from reference 72. (f) Adapted with permission of ACS from reference 73.

interface (liquid/liquid, solid/air etc.) have been attempted in the recent past.[74-78] During this journey, bio-inspired molecular designs as well as the entirely de novo designs have encountered both successes and failures. Although the successful ones were either because of serendipity or creativity, it is their combination with failures that has strengthened our supramolecular engineering skills (refer Figure 1, 2 for some interesting examples). Moreover, the supramolecular engineering of designed functional molecular modules to tailor-made architectures encompassing a detailed relationship between structural information and functional property has rarely been explored.[79-88] The process of custom-designing and/or molecularly engineering assemblies is conceptualized as molecular architectonics. Such an enabling technology with its characteristic chemical, physical and biological properties would undoubtedly make a tremendous impact in wide variety of fields pertaining to materials science and biomedicine.

### 1.7. Two-dimensional (2D) nanoarchitectonics

Herein, we describe the rationale for molecular designs and the nature of non-covalent interactions involved in 2D self-assembly. 2D nanoarchitectonics is the state of the art in supramolecular engineering.[62] It is the obligation to harvest intermolecular interactions cooperatively that makes 2D supramolecular engineering a challenging task and has remained elusive, until the last few years (Figure 3). Moreover, 2D architectonics is a much-needed significant milestone in the history of supramolecular engineering, as it fills up the missing link between zero-dimensional (0D; nanoparticles) and one-dimensional (1D) nanostructures (nanofibers/belts/helices) with the three-dimensional (3D) bulk

structures. Such an advancement has far-reaching consequences with a wide variety of applications, namely in the field of device fabrication, catalysis, sensing, separation, electronics, optoelectronics and biomaterials, amongst others.[89-93]

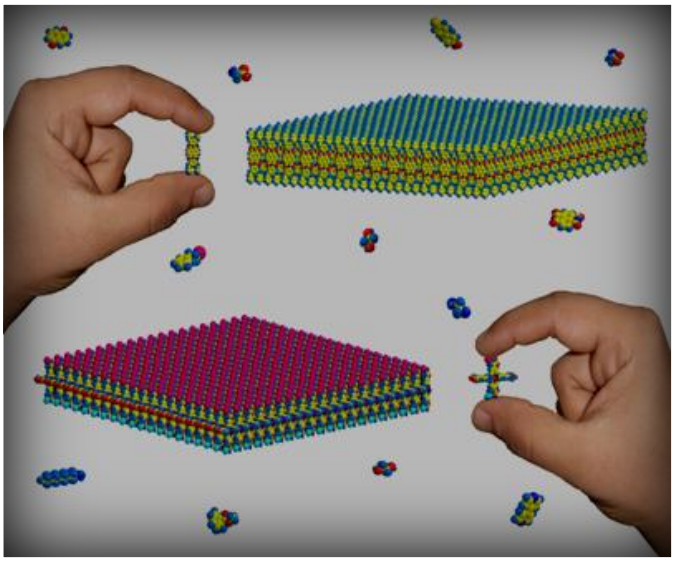

**Figure 3**. Schematic representation depicts the molecular designs to obtain two-dimensional assemblies from two orthogonal non-covalent interactions. Adapted with permission of RSC from reference 62.

Nanosheets are 2D architectures with a topographical thickness in the range of a typical monomer unit, up to 100 nm, while the lateral dimensions are of the order of few hundred nanometres to few microns or even larger. The process of custom-designing and engineering these nanosheets is conceptualized as 2D nanoarchitectonics.[92,93] This 2D nanoarchitectonics is an intriguing prospect (*vide infra*) for the simple reason that not much is known and hence it provides profuse opportunities for an inquisitive mind to explore and conquer. One such expedition has led to the discovery of graphene and its extraordinary properties.[94-97] In light of the technological applications foreseen in

graphene, it is imperative that one explores for alternatives as well.[62,89-91,93,98,99] In order to emphasize further and also to give an enticing flavour of this newly unfolding field of 2D nanoarchitectonics, we shall first describe what are known as S-layers.[100,101]

S-layers are one of the simplest yet highly sophisticated self-assembling systems commonly found as the crystalline surface layer proteins in bacteria and archaea. Remarkably, these periodic 2D structures are bestowed with precisely positioned functional groups, which render identical physicochemical properties on each molecular unit, down to the sub-nanometer level. More interestingly, even if isolated from their cell surface they are persistent in their ability to reassemble into 2D crystals. This inherently programmed assembly of S-layers has been explored in the recent past for applications in biotechnology, diagnostics, biomedicine, biomimetics, molecular nanotechnology and controlled biomineralization. Despite significant advances in this 2D biotemplating strategy, extremely low production yields, molecular size, stability, confined scope for functionalization and narrow operating conditions inhibit their optimal utilization. In this context, one has to look for novel 2D nanomaterials in an effort to find analogues, biomimics and to explore for even more exciting and fascinating materials with multifunctional technological implications.

For a regularly shaped 2D nanosheet like a square or rhombus, both the length and breadth in the lateral dimensions are equal. However, in other instances (*viz.* rectangle or parallelogram), a nominal value of length to breadth aspect ratio of ~10 or less are considered 2D, which also distinguishes them from 1D nanobelts and nanoribbons. Here the term 2D intends to emphasize that the extent of molecular interactions (driving force) across both the lateral directions (length and breadth) is

almost similar, unlike the dominant mono-directional (along the length) molecular interaction, as in the case of one-dimensional nanostructures.

In order to realize 2D molecular assembly one has to envision at least two molecular interactions (similar or different) acting approximately orthogonal to each other (Figure 4). These specific interactions can then extend along two lateral directions to result in 2D architectures. However, in designing such molecular systems, care must be taken in terms of chemical functionality and flexibility of the linker otherwise it might lead to 1D (or 0D) assembly. In addition, to compensate for the limitation associated with hydrogen-bonding-based assembly in polar solvents, hydrophobic and or electrostatic interactions could be incorporated into the molecular designs. Herein, relatively stronger electrostatic interactions could facilitate ionic assembly while the enhanced hydrophobic forces could facilitate aromatic stacking. However, finding that optimal molecular recipe and the appropriate solvent conditions to assemble in two lateral directions, could be a significant challenge. A similar strategy could also be extended to coordinate metal centers with suitably designed ligands. Alternatively, a better understanding of the nature of molecular interactions and the growth mechanisms are needed to achieve monodispersity in the shape, size and topographical thickness of 2D assembly.

Although graphene is the prime example of a 2D nanomaterial, supramolecularly engineered organic and hybrid analogues offer several advantages.[62,90,91] For example, large scale production of single-layer pristine graphene as well as uniform chemical functionalization has been one of the major concerns associated with graphene research. In contrast, supramolecular engineering of organic and hybrid 2D nanomaterials via solution processing facilitates large scale production by an efficient, inexpensive and

facile process, which are highly desirable for applications in optics and electronics. Moreover, with the inclusion of inorganic entities in the form of hybrid 2D nanomaterials, a wide variety of multifunctional properties like mechanical strength, magnetism, conductivity, photoluminescence, catalytic activity can also be harnessed.

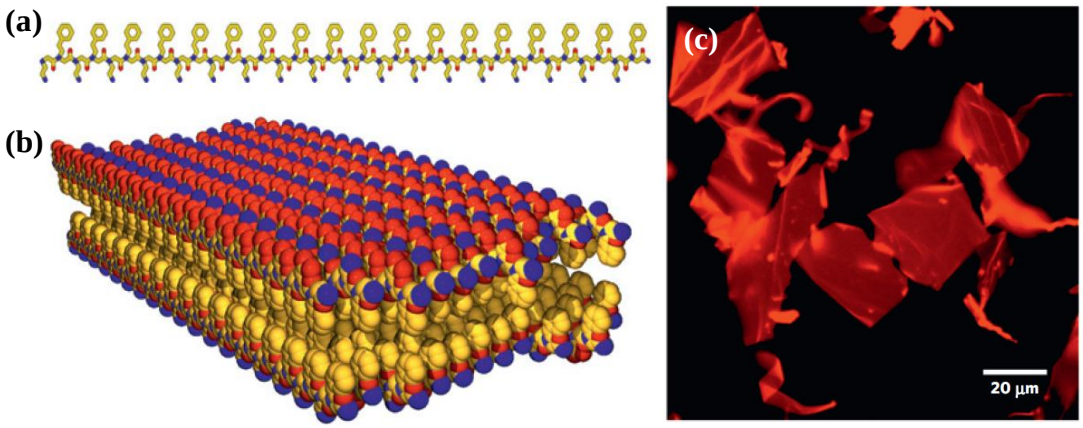


**Figure 4**. (a) Chemical structure of a positively charged peptoid amphiphile and the molecular model of the assembled sheets (b). (c) Fluorescent optical microscope image of the peptoid sheets stained with Nile Red. Adapted with permission of NPG from reference 102.

### 1.8. Our bioinspired approach

In recent years, the fabrication of designer molecules based advanced materials has gained unprecedented importance and interest due to their envisioned efficiency, specificity and complex operational capabilities.[33,34] However, construction of complex molecular systems represents a great challenge in chemistry and material science. Man's long standing quest for advanced molecular materials is inspired by Nature. Nature's archetypal molecular assemblies have been the result of rigorous natural selection and evolution over billions of years. Unsurprisingly, an eclectic approach to design and

manufacture advanced materials necessarily include biomolecules due to their remarkable property of integrating structure, function and dynamics.

It is thus believed that bio-inspired design strategies will provide us with new opportunities to explore novel functional molecular materials and understand previously intractable complex biochemical phenomena.[103-105] Among all biomolecules, amino acids are particularly appealing due to their remarkable molecular recognition, chirality and distinctive sequence specific self-assembling properties.[57,106] There are around 20

**Table 2.** List of amino acids with their distinct side chains

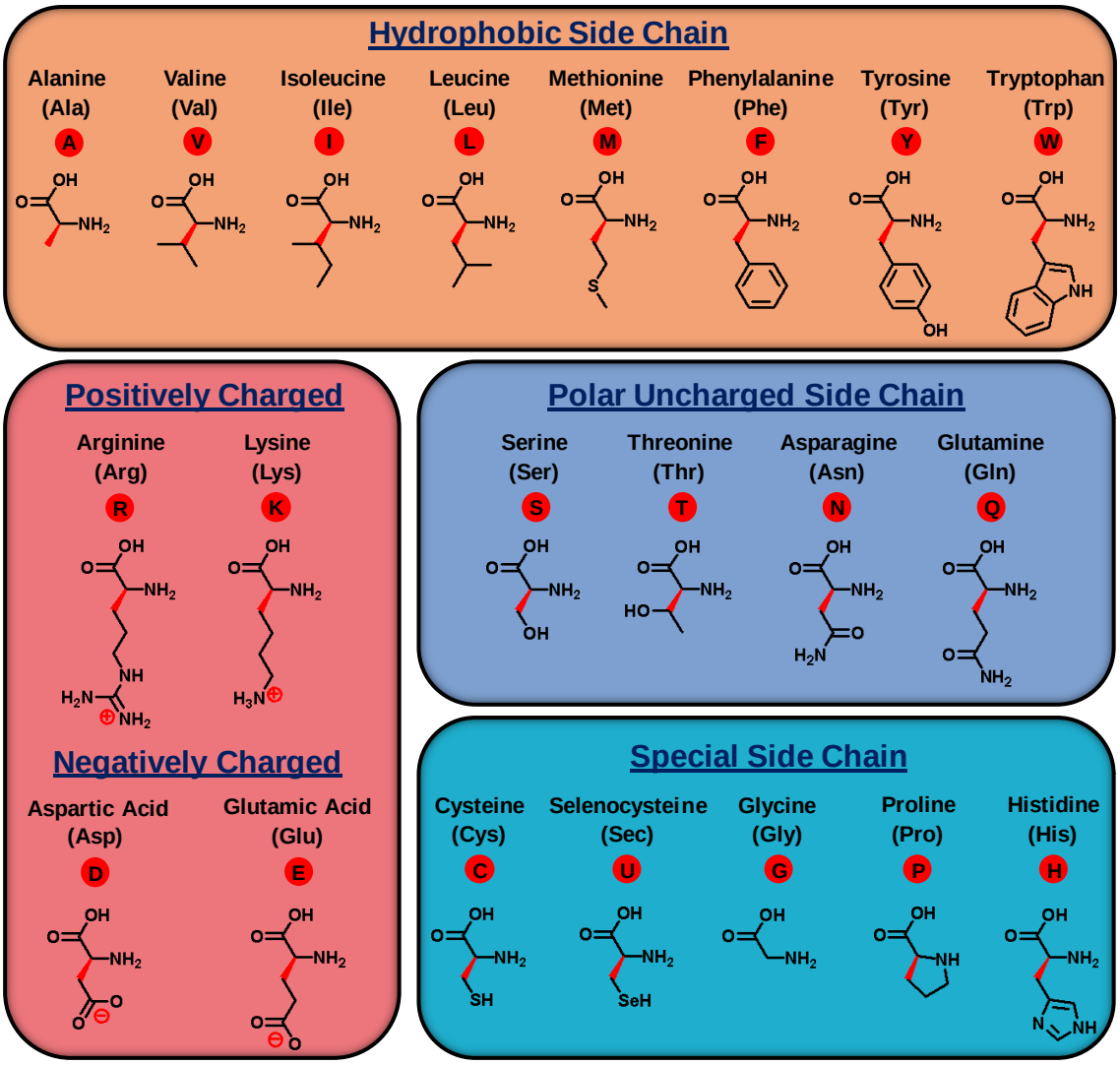

naturally occurring amino acids, each with its own unique size and functionality, which facilitates characteristic structural properties (Table 2). Unlike other auxiliaries, amino acids depending on their side chain functionality can furnish hydrophilic, hydrophobic and aromatic interactions in a single compact moiety. Moreover amino acids can facilitate metal binding, flexibility with respect to functionalization, pH sensitivity, stereospecificity and biocompatibility.

In our work, we have employed two basic design strategies, one wherein which various functional molecules were derivatized with amino acids in an effort to efficiently tailor their molecular assemblies and exploitation thereof for advanced properties (Figure 5). For this particular endeavour, we have specifically chosen two important members of arylenediimde family namely naphthalenediimide (NDI) and perylenediimide (PDI) as our functional molecules due to their wide variety of applications ranging from biomedicine to electronics.

The second design strategy was to identify a biological process or product and the mimic of which has to be developed by means of molecular self-assembly (Figure 5). Such design strategies could be instrumental in shedding interesting insights about the natural processes and could also provide opportunities to develop unprecedented functional molecular materials. We strongly believe that the scope to indulge in such bioinspired modular approach has far reaching consequences in the near future. With natural biological systems representing the benchmark standards, we anticipate that continued creative design strategies would lead to increasingly complex bio-inspired materials with multiple functions and advanced applications. As the natural world abounds with innumerable mysteries, the quest to develop advanced bioinspired

molecular materials will be a never ending process. With time, we can only hope to get better in terms of complexity, functionality and ultimately their practical applications in our day-to-day life.

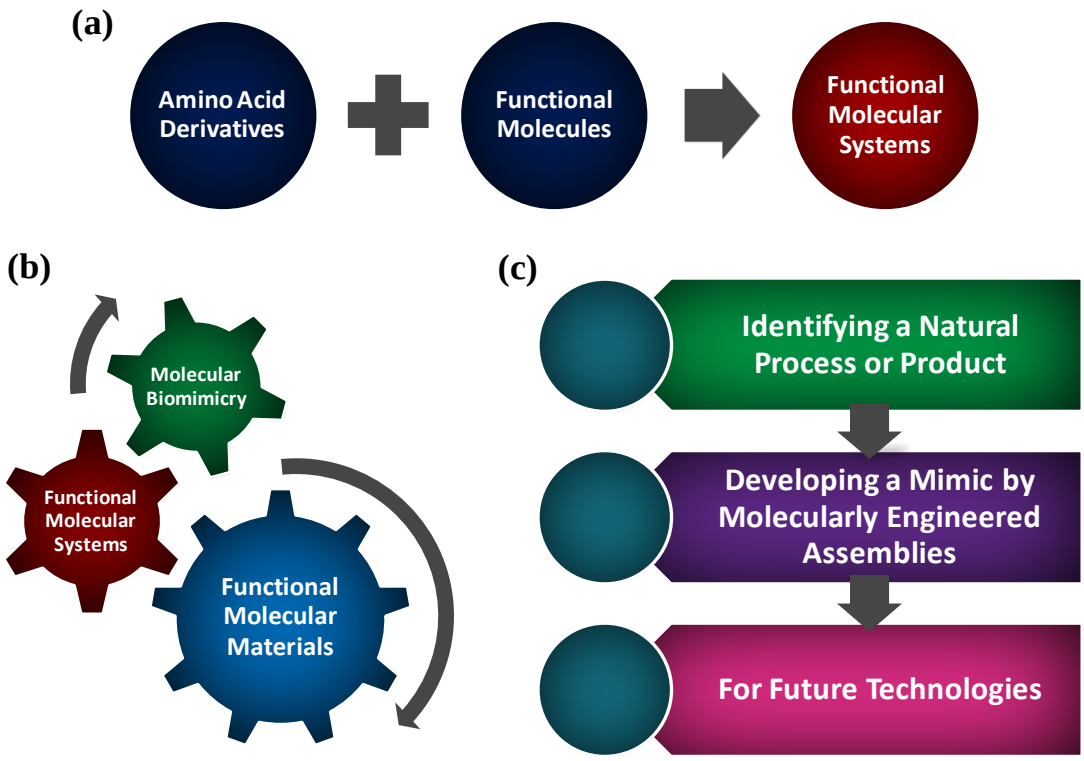


**Figure 5**. Schematic representation of the two design strategies employed in this thesis. (a) The first is to design functional molecular systems by conjugating functional molecules with amino acid derivatives. (b) Such functional molecular systems can lead to functional molecular materials and/or shed insights into certain biochemical processes, which is termed as molecular biomimicry. (c) The second strategy is to identify a natural process/product and to recreate it by molecular assemblies for technological applications.

## 1.9. Why arylenediimides?

Arylenediimides are the class of molecules that comprises of an aromatic core appended with two imide functionalities.[107] The main challenge in organizing aromatic moieties lies

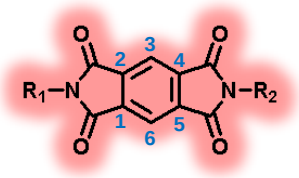


PyDI

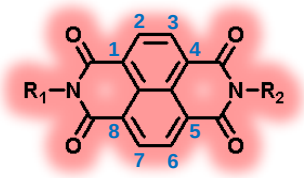


NDI

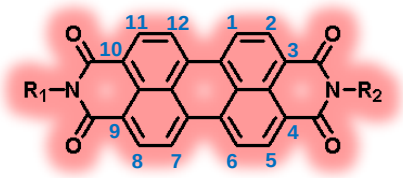


PDI

in controlling and optimizing the relatively strong π-π interactions by modulating their substituents. In our opinion, commonly employed strategy to functionalize arylenediimides (as a specific example or otherwise) with long-chain alkyl, alkoxy or phenyl substituent's seems to be not sufficient enough to modulate their properties efficiently.[108-111] The solubility is crucial for the solution processing of individual molecules, and this requires appropriate side-chain functionalities. Substitution with long or branched alkyl groups can aid solubility in organic non-polar solvents, while their solvo/hydrophobic effect in polar solvents can facilitate aromatic stacking. Generally, linear alkyl chains lead to 1D architectures while branched chains lead to 0D agglomerates. Increasing the size of the aromatic core can aid in molecular packing, but planarity, solubility as well as their effective π-π stacking can be affected.

Solvent–molecule interactions are yet another factor affecting the morphology of molecular self-assembly. Moreover, aggregation can vary from being spontaneous to being a rate-controlled process, depending on the alkyl chain length. In contrast to alkyl chains, alkoxy imide substituents (bolaamphiphiles), being hydrophilic, engenders solubility in polar solvents, although they can still be assembled in non-polar solvents. Amphiphiles with alkyl and alkoxy imide substituents on either side are also employed in molecular designs, while the incorporation of phenyl substituents offer rigidity and provide additional aromatic interactions. However, all these substituents are somewhat

restricted to simple, specific interactions such as hydrophobic, hydrophilic or aromatic interactions, and lack a combination of non-covalent forces that can act in a cooperative manner. This limitation led us to look for better alternatives, and we realized that a solution might lie with the naturally evolved amino acids (for the reasons described above). Thus an integration of the characteristic properties of arylenediimides (NDIs/PDIs) and that of amino acids could lead to unprecedented advanced molecular materials with electronics and biomedical applications amongst others.

In addition, it is interesting to note that the performance of an electronic device based on organic semiconductors primarily rely on the organization of π-conjugated materials.[112] To realize the extensive applications of organic electronic devices, both p- and n-type organic semiconductors are essential. The p-type organic semiconductors have been thoroughly investigated over recent decades, but the performance of n-type organic semiconductors has lagged behind that of p-type semiconductors.[113-116] NDIs/PDIs are among the most promising n-type organic semiconductors, and in spite of having a wide variety of applications (*vide supra*) in fields ranging from electronics to biomedicine, morphological modulation of NDIs/PDIs is largely unexplored.[57,67,117-127] For the potential applications of these organic semiconductors, there is a need to be able to tune the molecular interactions and thereby construct desired architectures.

### 1.10. Salient features of arylenediimides

NDIs and PDIs possess high electron affinity, good charge carrier mobility, excellent thermal and oxidative stability, making them promising candidates for organic electronics

applications namely organic field effect transistors (OFETs), photovoltaic devices and flexible displays.[107,117-119,123] The molecular planarity, rainbow fluorescence and the characteristic redox behaviour of NDI is especially intriguing.[117] DNA intercalation, antimicrobial and anticarcinogenic properties of NDIs render rather unique biomedical applications.[67,126,127] On the other hand, the near-unity fluorescence quantum yields of PDIs engender usage as industrial colorants in the form of dyes and pigments complementing their favorable photophysical and electrochemical properties. Utility of such excellent molecular characteristics of NDIs and PDIs have started emerging only in recent times and their full potentials are yet to be exploited.

### 1.11. NDIs and its molecular properties

The synthesis of NDI with symmetric imide substituents ($R_1 = R_2$) involves a simple one step procedure in which 1,4,5,8-naphthalenetetracarboxylic dianhydride is condensed with the appropriate amino acid in a high boiling solvent like isopropanol or *N*,*N*-dimethylformamide for 12-24 h at 70-110 $^{o}$C. Recently, Sanders and co-workers have reported a much simpler microwave-assisted synthetic procedure to obtain NDIs in very high yield within 5-10 min.[128] Moreover, the procedure provides control over stepwise condensation of α-amino acids with naphthalenetetracarboxylic dianhydride to result in unsymmetrical NDI derivatives ($R_1 \neq R_2$) in excellent yield. The energetics and the factors influencing the formation of *N*-desymmetrized NDIs by microwave-assisted synthesis are investigated very lately.[129]

The imide substituents in NDI have little effect on the molecular-level electronic and optical properties while significantly affects the solubility and molecular organization. However, with one or more substituents at positions 2, 3, 6 and 7, termed as core substituted NDIs (cNDIs) affect both electronic and optical properties.[117,124] cNDIs with electron donating substituents in the core generate a colorful push-pull system. The replacement of substituent's single atom is sufficient to tune the fluorescence in the entire visible spectrum, which is known as rainbow fluorescence. cNDIs with electron acceptors produce exceptionally π-acidic aromatic systems. The computed quadrupole moment $Q_{zz}$ for unsubstituted NDIs is -18.6 B (Buckinghams) whereas introduction of two cyano-acceptors in the core results in exceptional π-acidity with $Q_{zz}$ of -39.2 B. The elusive tetracyano cNDI possess the highest predicted $Q_{zz}$ of -55.5 B.

NDIs exhibit strong absorption bands, namely band I in the range of 300-400 nm and band II at ~235 nm, which are attributed to characteristic π-π* transitions of NDI chromophores polarized along the z and y axis respectively.[124] NDIs are weakly fluorescent with a 7 nm Stokes-shifted mirror-image emission bands. However, broad emission bands at ~ 475 nm are attributed to excimer-like emissions. NDIs can form stable radical anions in high yields either chemically or electrochemically at modest potentials (NDI: $E^1_{red}$ = -1.10 V vs. $Fc/Fc^+$ in $CH_2Cl_2$). The radical anions comprise of characteristic visible and near-infrared absorption bands at ~ 450 nm. The chiral supramolecular assemblies of NDIs exhibit strong exciton-coupled circular dichroism (CD).[130] The negative sign of the first cotton effect is ascribed to M-type of helicity while the positive sign of the first cotton effect to P-type of helicity. The amplitude of the CD signal depends on the molar extinction coefficient of the chromophore, twist angle,

intermolecular distance and the length of the supramolecular polymer. The planarity and high π-acidity of the NDI system is ideal for face-to-face π-stacking, while their enhanced solubility offers better processability than other aromatic imides. For additional information, interested readers are suggested to refer excellent reviews about 'Chemistry of naphthalenediimides' by Langford *et al.*[117] and 'Core-substituted naphthalenediimides' by Matile *et al.*[124]

### 1.12. PDIs and its molecular properties

The condensation of perylenetetracarboxylic dianhydride with an appropriate amino acid in imidazole or n-butanol at temperatures >110 °C for few hours, results in the formation of symmetrical PDI derivative ($R_1 = R_2$) in good yields.[131] However the unsymmetrical PDIs ($R_1 \neq R_2$) are obtained via multistep methods. One of the most commonly employed methods involve partial hydrolysis of symmetrical PDIs to perylene monoimide monoanhydride, which on subsequent imidization with the second amine or amino acid result in the unsymmetrical PDI in moderate yields. Substitutions at 1, 6, 7 and/or 12 positions of PDI are known as bay or core substituents. Substitutions at the bay positions are usually achieved via respective bromo or chloro bay substituted PDIs. PDIs typically exhibit strong vibronically structured absorptions with maxima at ~ 525 nm and molar absorptivities of the order of $10^5$ $M^{-1}cm^{-1}$. However, the emission spectrum is a small Stoke-shifted mirror image of absorption spectrum with near unity fluorescence quantum yields. The core substitutions significantly affect both absorption and emission properties of PDIs and moreover the steric effects imparted by core substituents can cause twisting

of PDI core, which strongly influences their aromatic stacking. A non-core substituted PDI possess two reversible reduction potentials (at ~ -1.0 and -1.2 V vs. $Fc/Fc^{+}$) and one reversible oxidation potential (at ~ +1.2 V). PDI radical anion exhibit characteristic absorption maxima at ~713 nm while the dianion at ~546 nm.

## 1.13. References

1. Chen, P.-Y.; McKittrick, J.; Meyers, M. A., Biological materials: Functional adaptations and bioinspired designs. *Prog. Mater. Sci.* **2012,** *57*, 1492-1704.

2. Sun, J.; Zuckermann, R. N., Peptoid Polymers: A Highly Designable Bioinspired Material. *ACS Nano* **2013,** *7*, 4715-4732.

3. Studart, A. R., Towards High-Performance Bioinspired Composites. *Adv. Mater.* **2012,** *24*, 5024-5044.

4. Zhao, Y.; Xie, Z.; Gu, H.; Zhu, C.; Gu, Z., Bio-inspired variable structural color materials. *Chem. Soc. Rev.* **2012,** *41*, 3297-3317.

5. Mohammed, J. S.; Murphy, W. L., Bioinspired Design of Dynamic Materials. *Adv. Mater.* **2009,** *21*, 2361-2374.

6. Kolle, M.; Lethbridge, A.; Kreysing, M.; Baumberg, J. J.; Aizenberg, J.; Vukusic, P., Bio-Inspired Band-Gap Tunable Elastic Optical Multilayer Fibers. *Adv. Mater.* **2013**, *25*, 2239-2245.

7. Bhushan, B., Biomimetics: lessons from nature–an overview. *Phil. Trans. R. Soc. A* **2009,** *367*, 1445-1486.

8. Wang, J.; Zhang, Y.; Wang, S.; Song, Y.; Jiang, L., Bioinspired colloidal photonic crystals with controllable wettability. *Acc. Chem. Res.* **2011,** *44*, 405-415.

9. Estroff, L. A.; Hamilton, A. D., At the interface of organic and inorganic chemistry: Bioinspired synthesis of composite materials. *Chem. Mater.* **2001,** *13*, 3227-3235.

10. Barron, A. E.; Zuckerman, R. N., Bioinspired polymeric materials: in-between proteins and plastics. *Curr. Opin. Chem. Biol.* **1999,** *3*, 681-687.

11. Xia, F.; Jiang, L., Bio-Inspired, Smart, Multiscale Interfacial Materials. *Adv. Mater.* **2008,** *20*, 2842-2858.

12. Fukuzumi, S., Bioinspired energy conversion systems for hydrogen production and storage. *Eur. J. Inorg. Chem.* **2008,** *2008*, 1351-1362.

13. Fukuzumi, S., Development of bioinspired artificial photosynthetic systems. *Phys. Chem. Chem. Phys.* **2008,** *10*, 2283-2297.

14. Sun, T.; Feng, L.; Gao, X.; Jiang, L., Bioinspired surfaces with special wettability. *Acc. Chem. Res.* **2005,** *38*, 644-652.

15. Kirshenbaum, K.; Zuckermann, R. N.; Dill, K. A., Designing polymers that mimic biomolecules. *Curr. Opin. Struct. Biol.* **1999,** *9*, 530-535.

16. Knowles, T. P.; Buehler, M. J., Nanomechanics of functional and pathological amyloid materials. *Nat. Nanotechnol.* **2011,** *6*, 469-479.

17. Kushner, A. M.; Guan, Z., Modular design in natural and biomimetic soft materials. *Angew. Chem. Int. Ed.* **2011,** *50*, 9026-9057.

18. Lepora, N. F.; Verschure, P.; Prescott, T. J., The state of the art in biomimetics. *Bioinspir. Biomim.* **2013,** *8*, 013001.

19. Tu, R. S.; Tirrell, M., Bottom-up design of biomimetic assemblies. *Adv. Drug Delivery Rev.* **2004,** *56*, 1537-1563.

20. Schutt, C. E.; Lindberg, U., The new architectonics: an invitation to structural biology. *Anat. Rec.* **2000,** *261*, 198-215.

21. Gartland, K.; Bruschi, F.; Dundar, M.; Gahan, P.; Viola Magni, M.; Akbarova, Y., Progress towards the 'Golden Age' of biotechnology. *Curr. Opin. Biotechnol.* **2013**, *24S*, S6-S13.

22. Chen, H.; Lin, Y., Promise and issues of genetically modified crops. *Curr. Opin. Plant biol.* **2013**,*16*, 255-260.

23. Hawkins, A. S.; McTernan, P. M.; Lian, H.; Kelly, R. M.; Adams, M. W., Biological conversion of carbon dioxide and hydrogen into liquid fuels and industrial chemicals. *Curr. Opin. Biotechnol.* **2013**, *24*, 376-384.

24. Bhullar, N. K.; Gruissem, W., Nutritional enhancement of rice for human health: the contribution of biotechnology. *Biotechnol. Adv.* **2013,** *31*, 50-57.

25. Wallace, G. G.; Higgins, M. J.; Moulton, S. E.; Wang, C., Nanobionics: the impact of nanotechnology on implantable medical bionic devices. *Nanoscale* **2012,** *4*, 4327-4347.

26. Ong, J. M.; da Cruz, L., The bionic eye: a review. *Clin. Experiment. Ophthalmol.* **2012,** *40*, 6-17.

27. Kim, S.; Laschi, C.; Trimmer, B., Soft robotics: a bioinspired evolution in robotics. *Trends Biotechnol.* **2013**, 31, 287-294.

28. Rawlings, A. E.; Bramble, J. P.; Staniland, S. S., Innovation through imitation: biomimetic, bioinspired and biokleptic research. *Soft Matter* **2012,** *8*, 6675-6679.

29. Whitesides, G. M.; Grzybowski, B., Self-assembly at all scales. *Science* **2002,** *295*, 2418-2421.

30. Whitesides, G. M.; Boncheva, M., Beyond molecules: Self-assembly of mesoscopic and macroscopic components. *Proc. Natl. Acad. Sci.USA* **2002,** *99*, 4769-4774.

31. Williams, R. J.; Smith, A. M.; Collins, R.; Hodson, N.; Das, A. K.; Ulijn, R. V., Enzyme-assisted self-assembly under thermodynamic control. *Nat. Nanotechnol.* **2008,** *4*, 19-24.

32. Winfree, E.; Liu, F.; Wenzler, L. A.; Seeman, N. C., Design and self-assembly of two-dimensional DNA crystals. *Nature* **1998,** *394*, 539-544.

33. Zhang, S.; Marini, D. M.; Hwang, W.; Santoso, S., Design of nanostructured biological materials through self-assembly of peptides and proteins. *Curr. Opin. Chem. Biol.* **2002,** *6*, 865-871.

34. Zhao, X.; Zhang, S., Molecular designer self-assembling peptides. *Chem. Soc. Rev.* **2006,** *35*, 1105-1110.

35. Lehn, J.-M., Toward complex matter: Supramolecular chemistry and self-organization. *Proc. Natl. Acad. Sci.USA* **2002,** *99*, 4763-4768.

36. Varghese, S.; Kumar, N. S. S.; Krishna, A.; Rao, D. S. S.; Prasad, S. K.; Das, S., Formation of Highly Luminescent Supramolecular Architectures Possessing Columnar Order from Octupolar Oxadiazole Derivatives: Hierarchical Self-Assembly from Nanospheres to Fibrous Gels. *Adv. Funct. Mater.* **2009,** *19*, 2064-2073.

37. Kumar, N.; Varghese, S.; Narayan, G.; Das, S., Hierarchical Self-Assembly of Donor–Acceptor-Substituted Butadiene Amphiphiles into Photoresponsive Vesicles and Gels. *Angew. Chem. Int. Ed.* **2006,** *45*, 6317-6321.

38. Ramaiah, D.; Neelakandan, P. P.; Nair, A. K.; Avirah, R. R., Functional cyclophanes: Promising hosts for optical biomolecular recognition. *Chem. Soc. Rev.* **2010,** *39*, 4158-4168.

39. Neelakandan, P. P.; Ramaiah, D., DNA-Assisted Long-Lived Excimer Formation in a Cyclophane. *Angew. Chem. Int. Ed.* **2008,** *47*, 8407-8411.

40. Moorthy, J. N.; Venkatakrishnan, P.; Natarajan, P.; Huang, D.-F.; Chow, T. J., De novo design for functional amorphous materials: synthesis and thermal and light-emitting properties of twisted anthracene-functionalized bimesitylenes. *J. Am. Chem. Soc.* **2008,** *130*, 17320-17333.

41. Moorthy, J. N.; Mandal, S.; Mukhopadhyay, A.; Samanta, S., Helicity as a Steric Force: Stabilization and Helicity-Dependent Reversion of Colored o-Quinonoid Intermediates of Helical Chromenes. *J. Am. Chem. Soc.* **2013,** *135*, 6872-6884.

42. Müller-Dethlefs, K.; Hobza, P., Noncovalent interactions: a challenge for experiment and theory. *Chem. Rev.* **2000,** *100*, 143-168.

43. Cook, J. L.; Hunter, C. A.; Low, C. M.; Perez-Velasco, A.; Vinter, J. G., Solvent effects on hydrogen bonding. *Angew. Chem. Int. Ed.* **2007,** *46*, 3706-3709.

44. Hunter, C. A.; Lawson, K. R.; Perkins, J.; Urch, C. J., Aromatic interactions. *J. Chem. Soc. Perkin Trans. 2* **2001,** 651-669.

45. Černý, J.; Hobza, P., Non-covalent interactions in biomacromolecules. *Phys. Chem. Chem. Phys.* **2007,** *9*, 5291-5303.

46. Lehn, J. M., Supramolecular chemistry—scope and perspectives molecules, supermolecules, and molecular devices (Nobel Lecture). *Angew. Chem., Int. Ed. Engl.* **1988,** *27*, 89-112.

47. Lehn, J. M., Perspectives in Supramolecular Chemistry—From Molecular Recognition towards Molecular Information Processing and Self-Organization. *Angew. Chem., Int. Ed. Engl.* **1990,** *29*, 1304-1319.

48. Zeng, F.; Zimmerman, S. C., Dendrimers in supramolecular chemistry: from molecular recognition to self-assembly. *Chem. Rev.* **1997,** *97*, 1681-1712.

49. Davis, A. P.; Wareham, R. S., Carbohydrate recognition through noncovalent interactions: a challenge for biomimetic and supramolecular chemistry. *Angew. Chem. Int. Ed.* **1999,** *38*, 2978-2996.

50. Schmuck, C.; Wienand, W., Highly stable self-assembly in water: ion pair driven dimerization of a guanidiniocarbonyl pyrrole carboxylate zwitterion. *J. Am. Chem. Soc.* **2003,** *125*, 452-459.

51. Chandler, D., Interfaces and the driving force of hydrophobic assembly. *Nature* **2005,** *437*, 640-647.

52. Schmuck, C.; Rehm, T.; Gröhn, F.; Klein, K.; Reinhold, F., Ion pair driven self-assembly of a flexible bis-zwitterion in polar solution: Formation of discrete nanometer-sized cyclic dimers. *J. Am. Chem. Soc.* **2006,** *128*, 1430-1431.

53. Lehn, J.-M., From supramolecular chemistry towards constitutional dynamic chemistry and adaptive chemistry. *Chem. Soc. Rev.* **2007,** *36*, 151-160.

54. Srinivas, G.; Pitera, J. W., Soft patchy nanoparticles from solution-phase self-assembly of binary diblock copolymers. *Nano Lett.* **2008,** *8*, 611-618.

55. Babu, S. S.; Prasanthkumar, S.; Ajayaghosh, A., Self-Assembled Gelators for Organic Electronics. *Angew. Chem. Int. Ed.* **2012,** *51*, 1766-1776.

56. Mayoral Munoz, M. J.; Fernandez, G., Metallosupramolecular amphiphilic π-systems. *Chem. Sci.* **2012,** *3*, 1395-1398.

57. Avinash, M. B.; Govindaraju, T., Amino Acid Derivatized Arylenediimides: A Versatile Modular Approach for Functional Molecular Materials. *Adv. Mater.* **2012,** *24*, 3905-3922.

58. Palma, C.-A.; Cecchini, M.; Samori, P., Predicting self-assembly: from empirism to determinism. *Chem. Soc. Rev.* **2012,** *41*, 3713-3730.

59. Giuseppone, N., Toward Self-Constructing Materials: A Systems Chemistry Approach. *Acc. Chem. Res.* **2012,** *45*, 2178-2188.

60. Aida, T.; Meijer, E. W.; Stupp, S. I., Functional Supramolecular Polymers. *Science* **2012,** *335*, 813-817.

61. Ciesielski, A.; Palma, C.-A.; Bonini, M.; Samorì, P., Towards Supramolecular Engineering of Functional Nanomaterials: Pre-Programming Multi-Component 2D Self-Assembly at Solid-Liquid Interfaces. *Adv. Mater.* **2010,** *22*, 3506-3520.

62. Govindaraju, T.; Avinash, M. B., Two-dimensional nanoarchitectonics: organic and hybrid materials. *Nanoscale* **2012,** *4*, 6102-6117.

63. Hartgerink, J. D.; Beniash, E.; Stupp, S. I., Self-assembly and mineralization of peptide-amphiphile nanofibers. *Science* **2001,** *294*, 1684-1688.

64. Jin, W.; Fukushima, T.; Niki, M.; Kosaka, A.; Ishii, N.; Aida, T., Self-assembled graphitic nanotubes with one-handed helical arrays of a chiral amphiphilic molecular graphene. *Proc. Natl. Acad. Sci. U. S. A.* **2005,** *102*, 10801-10806.

65. Yamamoto, Y.; Fukushima, T.; Suna, Y.; Ishii, N.; Saeki, A.; Seki, S.; Tagawa, S.; Taniguchi, M.; Kawai, T.; Aida, T., Photoconductive coaxial nanotubes of molecularly connected electron donor and acceptor layers. *Science* **2006,** *314*, 1761-1764.

66. Zhang, W.; Jin, W.; Fukushima, T.; Saeki, A.; Seki, S.; Aida, T., Supramolecular linear heterojunction composed of graphite-like semiconducting nanotubular segments. *Science* **2011,** *334*, 340-343.

67. Holman, G. G.; Zewail-Foote, M.; Smith, A. R.; Johnson, K. A.; Iverson, B. L., A sequence-specific threading tetra-intercalator with an extremely slow dissociation rate constant. *Nat. Chem.* **2011,** *3*, 875-881.

68. Lee, T.-C.; Kalenius, E.; Lazar, A. I.; Assaf, K. I.; Kuhnert, N.; Grün, C. H.; Jänis, J.; Scherman, O. A.; Nau, W. M., Chemistry inside molecular containers in the gas phase. *Nat. Chem.* **2013,** *5*, 376-382.

69. Hu, Z.; Pantoş, G. D.; Kuganathan, N.; Arrowsmith, R. L.; Jacobs, R. M. J.; Kociok-Köhn, G.; O'Byrne, J.; Jurkschat, K.; Burgos, P.; Tyrrell, R. M.; Botchway, S. W.; Sanders, J. K. M.; Pascu, S. I., Interactions Between Amino Acid-Tagged Naphthalenediimide and Single Walled

Carbon Nanotubes for the Design and Construction of New Bioimaging Probes. *Adv. Funct. Mater*. **2012,** *22*, 503-518.

70. Shao, H.; Seifert, J.; Romano, N. C.; Gao, M.; Helmus, J. J.; Jaroniec, C. P.; Modarelli, D. A.; Parquette, J. R., Amphiphilic Self-Assembly of an n-Type Nanotube. *Angew. Chem. Int. Ed.* **2010,** *49*, 7688-7691.

71. Pantoş, G. D.; Wietor, J. L.; Sanders, J. K., Filling helical nanotubes with C60. *Angew. Chem. Int. Ed.* **2007,** *46*, 2238-2240.

72. Mori, T.; Sakakibara, K.; Endo, H.; Akada, M.; Okamoto, K.; Shundo, A.; Lee, M. V.; Ji, Q.; Fujisawa, T.; Oka, K.; Matsumoto, M.; Sakai, H.; Abe, M.; Hill, J. P.; Ariga, K., Langmuir Nanoarchitectonics: One-Touch Fabrication of Regularly Sized Nanodisks at the Air–Water Interface. *Langmuir* **2012,** *29*, 7239-7248.

73. Danila, I.; Riobé, F.; Piron, F.; Puigmartí-Luis, J.; Wallis, J. D.; Linares, M.; Ågren, H.; Beljonne, D.; Amabilino, D. B.; Avarvari, N., Hierarchical Chiral Expression from the Nano- to Mesoscale in Synthetic Supramolecular Helical Fibers of a Nonamphiphilic C3-Symmetrical π-Functional Molecule. *J. Am. Chem. Soc.* **2011,** *133*, 8344-8353.

74. Fernández, G.; Pérez, E. M.; Sánchez, L.; Martín, N., Self-Organization of Electroactive Materials: A Head-to-Tail Donor–Acceptor Supramolecular Polymer. *Angew. Chem. Int. Ed.* **2008,** *47*, 1094-1097.

75. Llanes-Pallas, A.; Palma, C.-A.; Piot, L.; Belbakra, A.; Listorti, A.; Prato, M.; Samorì, P.; Armaroli, N.; Bonifazi, D., Engineering of Supramolecular H-Bonded Nanopolygons via Self-Assembly of Programmed Molecular Modules. *J. Am. Chem. Soc.* **2008,** *131*, 509-520.

76. Avinash, M. B.; Govindaraju, T., Extremely Slow Dynamics of an Abiotic Helical Assembly: Unusual Relevance to the Secondary Structure of Proteins. *J. Phys. Chem. Lett*. **2013,** *4*, 583-588.

77. Berl, V.; Huc, I.; Khoury, R. G.; Lehn, J.-M., Helical Molecular Programming: Supramolecular Double Helices by Dimerization of Helical Oligopyridine-dicarboxamide Strands. *Chem. Eur. J*. **2001,** *7*, 2810-2820.

78. Smulders, M. M. J.; Riddell, I. A.; Browne, C.; Nitschke, J. R., Building on architectural principles for three-dimensional metallosupramolecular construction. *Chem. Soc. Rev.* **2013,** *42*, 1728-1754.

79. Xue, Y.; Zimmt, M. B., Patterned Monolayer Self-Assembly Programmed by Side Chain Shape: Four-Component Gratings. *J. Am. Chem. Soc.* **2012,** *134*, 4513-4516.

80. Rosen, B. M.; Peterca, M.; Morimitsu, K.; Dulcey, A. E.; Leowanawat, P.; Resmerita, A.-M.; Imam, M. R.; Percec, V., Programming the Supramolecular Helical Polymerization of Dendritic

Dipeptides via the Stereochemical Information of the Dipeptide. *J. Am. Chem. Soc.* **2011,** *133*, 5135-5151.

81. Brodin, J. D.; Ambroggio, X. I.; Tang, C.; Parent, K. N.; Baker, T. S.; Tezcan, F. A., Metal-directed, chemically tunable assembly of one-, two- and three-dimensional crystalline protein arrays. *Nat. Chem.* **2012,** *4*, 375-382.

82. Fry, H. C.; Garcia, J. M.; Medina, M. J.; Ricoy, U. M.; Gosztola, D. J.; Nikiforov, M. P.; Palmer, L. C.; Stupp, S. I., Self-Assembly of Highly Ordered Peptide Amphiphile Metalloporphyrin Arrays. *J. Am. Chem. Soc.* **2012,** *134*, 14646-14649.

83. Charvet, R.; Yamamoto, Y.; Sasaki, T.; Kim, J.; Kato, K.; Takata, M.; Saeki, A.; Seki, S.; Aida, T., Segregated and Alternately Stacked Donor/Acceptor Nanodomains in Tubular Morphology Tailored with Zinc Porphyrin–C60 Amphiphilic Dyads: Clear Geometrical Effects on Photoconduction. *J. Am. Chem. Soc.* **2012,** *134*, 2524-2527.

84. Avinash, M. B.; Govindaraju, T., Engineering Molecular Organization of Naphthalenediimides: Large Nanosheets with Metallic Conductivity and Attoliter Containers. *Adv. Funct. Mater.* **2011,** *21*, 3875-3882.

85. Jiang, W.; Schalley, C. A., Integrative self-sorting is a programming language for high level self-assembly. *Proc. Natl. Acad. Sci.USA* **2009,** *106*, 10425-10429.

86. Oohora, K.; Burazerovic, S.; Onoda, A.; Wilson, Y. M.; Ward, T. R.; Hayashi, T., Chemically Programmed Supramolecular Assembly of Hemoprotein and Streptavidin with Alternating Alignment. *Angew. Chem. Int. Ed.* **2012,** *41*, 3818-3821.

87. Stulz, E., DNA Architectonics: towards the Next Generation of Bio-inspired Materials. *Chem. Eur. J.* **2012,** *18*, 4456-4469.

88. Moulin, E.; Cid, J.-J.; Giuseppone, N., Advances in Supramolecular Electronics – From Randomly Self-assembled Nanostructures to Addressable Self-Organized Interconnects. *Adv. Mater.* **2013,** *25*, 477-487.

89. Sakamoto, J.; van Heijst, J.; Lukin, O.; Schlüter, A. D., Two-Dimensional Polymers: Just a Dream of Synthetic Chemists? *Angew. Chem. Int. Ed.* **2009,** *48*, 1030-1069.

90. Osada, M.; Sasaki, T., Two-Dimensional Dielectric Nanosheets: Novel Nanoelectronics From Nanocrystal Building Blocks. *Adv. Mater.* **2012,** *24*, 210-228.

91. Mas-Balleste, R.; Gomez-Navarro, C.; Gomez-Herrero, J.; Zamora, F., 2D materials: to graphene and beyond. *Nanoscale* **2011,** *3*, 20-30.

92. Barth, J. V., Molecular Architectonic on Metal Surfaces. *Annu. Rev. Phys. Chem.* **2007,** *58*, 375-407.

93. Ariga, K.; Lee, M. V.; Mori, T.; Yu, X.-Y.; Hill, J. P., Two-dimensional nanoarchitectonics based on self-assembly. *Adv. Colloid Interface Sci.* **2010,** *154*, 20-29.

94. Novoselov, K. S.; Jiang, D.; Schedin, F.; Booth, T. J.; Khotkevich, V. V.; Morozov, S. V.; Geim, A. K., Two-dimensional atomic crystals. *Proc. Natl. Acad. Sci. U. S. A.* **2005,** *102*, 10451-10453.

95. Meyer, J. C.; Geim, A. K.; Katsnelson, M. I.; Novoselov, K. S.; Booth, T. J.; Roth, S., The structure of suspended graphene sheets. *Nature* **2007,** *446*, 60-63.

96. Rao, C. N. R.; Sood, A. K.; Subrahmanyam, K. S.; Govindaraj, A., Graphene: The New Two-Dimensional Nanomaterial. *Angew. Chem. Int. Ed.* **2009,** *48*, 7752-7777.

97. Avinash, M. B.; Subrahmanyam, K. S.; Sundarayya, Y.; Govindaraju, T., Covalent modification and exfoliation of graphene oxide using ferrocene. *Nanoscale* **2010,** *2*, 1762-1766.

98. Nag, A.; Raidongia, K.; Hembram, K. P. S. S.; Datta, R.; Waghmare, U. V.; Rao, C. N. R., Graphene Analogues of BN: Novel Synthesis and Properties. *ACS Nano* **2010,** *4*, 1539-1544.

99. Ramakrishna Matte, H. S. S.; Gomathi, A.; Manna, A. K.; Late, D. J.; Datta, R.; Pati, S. K.; Rao, C. N. R., MoS2 and WS2 Analogues of Graphene. *Angew. Chem. Int. Ed.* **2010,** *49*, 4059-4062.

100. Sleytr, U. B.; Messner, P.; Pum, D.; Sára, M., Crystalline Bacterial Cell Surface Layers (S Layers): From Supramolecular Cell Structure to Biomimetics and Nanotechnology. *Angew. Chem. Int. Ed.* **1999,** *38*, 1034-1054.

101. Schäffer, C.; Messner, P., Surface-layer glycoproteins: an example for the diversity of bacterial glycosylation with promising impacts on nanobiotechnology. *Glycobiology* **2004,** *14*, 31R-42R.

102. Nam, K. T.; Shelby, S. A.; Choi, P. H.; Marciel, A. B.; Chen, R.; Tan, L.; Chu, T. K.; Mesch, R. A.; Lee, B.-C.; Connolly, M. D.; Kisielowski, C.; Zuckermann, R. N., Free-floating ultrathin two-dimensional crystals from sequence-specific peptoid polymers. *Nat. Mater.* **2010,** *9*, 454-460.

103. Gazit, E., Self-assembled peptide nanostructures: the design of molecular building blocks and their technological utilization. *Chem. Soc. Rev.* **2007,** *36*, 1263-1269.

104. Cavalli, S.; Albericio, F.; Kros, A., Amphiphilic peptides and their cross-disciplinary role as building blocks for nanoscience. *Chem. Soc. Rev.* **2010,** *39*, 241-263.

105. Chen, C.-L.; Rosi, N. L., Peptide-Based Methods for the Preparation of Nanostructured Inorganic Materials. *Angew. Chem. Int. Ed.* **2010,** *49*, 1924-1942.

106. Johnson, J. C.; Korley, L. T., Enhanced mechanical pathways through nature's building blocks: amino acids. *Soft Matter* **2012,** *8*, 11431-11442.

107. Zhan, X.; Facchetti, A.; Barlow, S.; Marks, T. J.; Ratner, M. A.; Wasielewski, M. R.; Marder, S. R., Rylene and Related Diimides for Organic Electronics. *Adv. Mater.* **2011,** *23*, 268-284.

108. Tomasulo, M.; Naistat, D. M.; White, A. J. P.; Williams, D. J.; Raymo, F. M., Self-assembly of naphthalene diimides into cylindrical microstructures. *Tetrahedron Lett.* **2005,** *46*, 5695-5698.

109. Abraham, B.; McMasters, S.; Mullan, M. A.; Kelly, L. A., Reactivities of Carboxyalkyl-Substituted 1,4,5,8-Naphthalene Diimides in Aqueous Solution. *J. Am. Chem. Soc.* **2004,** *126*, 4293-4300.

110. Zang, L.; Che, Y.; Moore, J. S., One-Dimensional Self-Assembly of Planar π-Conjugated Molecules: Adaptable Building Blocks for Organic Nanodevices. *Acc. Chem. Res.* **2008,** *41*, 1596-1608.

111. Che, Y.; Datar, A.; Yang, X.; Naddo, T.; Zhao, J.; Zang, L., Enhancing One-Dimensional Charge Transport through Intermolecular π-Electron Delocalization: Conductivity Improvement for Organic Nanobelts. *J. Am. Chem. Soc.* **2007,** *129*, 6354-6355.

112. Hoeben, F. J. M.; Jonkheijm, P.; Meijer, E. W.; Schenning, A. P. H. J., About Supramolecular Assemblies of π-Conjugated Systems. *Chem. Rev.* **2005,** *105*, 1491-1546.

113. Wurthner, F., Perylene bisimide dyes as versatile building blocks for functional supramolecular architectures. *Chem. Commun.* **2004,** 1564-1579.

114. Mas-Torrent, M.; Rovira, C., Novel small molecules for organic field-effect transistors: towards processability and high performance. *Chem. Soc. Rev.* **2008,** *37*, 827-838.

115. Schenning, A. P. H. J.; Meijer, E. W., Supramolecular electronics; nanowires from self-assembled [small pi]-conjugated systems. *Chem. Commun.* **2005,** 3245-3258.

116. Würthner, F., Plastic Transistors Reach Maturity for Mass Applications in Microelectronics. *Angew. Chem. Int. Ed.* **2001,** *40*, 1037-1039.

117. Bhosale, S. V.; Jani, C. H.; Langford, S. J., Chemistry of naphthalene diimides. *Chem. Soc. Rev.* **2008,** *37*, 331-342.

118. Jones, B. A.; Facchetti, A.; Wasielewski, M. R.; Marks, T. J., Tuning Orbital Energetics in Arylene Diimide Semiconductors. Materials Design for Ambient Stability of n-Type Charge Transport. *J. Am. Chem. Soc.* **2007,** *129*, 15259-15278.

119. Katz, H. E.; Johnson, J.; Lovinger, A. J.; Li, W., Naphthalenetetracarboxylic Diimide-Based n-Channel Transistor Semiconductors: Structural Variation and Thiol-Enhanced Gold Contacts. *J. Am. Chem. Soc.* **2000,** *122*, 7787-7792.

120. Laquindanum, J. G.; Katz, H. E.; Dodabalapur, A.; Lovinger, A. J., n-Channel Organic Transistor Materials Based on Naphthalene Frameworks. *J. Am. Chem. Soc.* **1996,** *118*, 11331-11332.

121. Bhosale, R.; Misek, J.; Sakai, N.; Matile, S., Supramolecular n/p-heterojunction photosystems with oriented multicolored antiparallel redox gradients (OMARG-SHJs). *Chem. Soc. Rev.* **2010,** *39*, 138-149.

122. Oh, J. H.; Suraru, S. L.; Lee, W.-Y.; Könemann, M.; Höffken, H. W.; Röger, C.; Schmidt, R.; Chung, Y.; Chen, W.-C.; Würthner, F.; Bao, Z., High-Performance Air-Stable n-Type Organic Transistors Based on Core-Chlorinated Naphthalene Tetracarboxylic Diimides. *Adv. Funct. Mater.* **2010,** *20*, 2148-2156.

123. Wurthner, F.; Stolte, M., Naphthalene and perylene diimides for organic transistors. *Chem. Commun.* **2011,** *47*, 5109-5115.

124. Sakai, N.; Mareda, J.; Vauthey, E.; Matile, S., Core-substituted naphthalenediimides. *Chem. Commun.* **2010,** *46*, 4225-4237.

125. Bhosale, S. V.; Bhosale, S. V.; Kalyankar, M. B.; Langford, S. J., A Core-Substituted Naphthalene Diimide Fluoride Sensor. *Org. Lett.* **2009,** *11*, 5418-5421.

126. Tumiatti, V.; Milelli, A.; Minarini, A.; Micco, M.; Gasperi Campani, A.; Roncuzzi, L.; Baiocchi, D.; Marinello, J.; Capranico, G.; Zini, M.; Stefanelli, C.; Melchiorre, C., Design, Synthesis, and Biological Evaluation of Substituted Naphthalene Imides and Diimides as Anticancer Agent∞. *J. Med. Chem.* **2009,** *52*, 7873-7877.

127. Aveline, B. M.; Matsugo, S.; Redmond, R. W., Photochemical Mechanisms Responsible for the Versatile Application of Naphthalimides and Naphthaldiimides in Biological Systems. *J. Am. Chem. Soc.* **1997,** *119*, 11785-11795.

128. Pengo, P.; Pantoş, G. D.; Otto, S.; Sanders, J. K. M., Efficient and Mild Microwave-Assisted Stepwise Functionalization of Naphthalenediimide with α-Amino Acids. *J. Org. Chem.* **2006,** *71*, 7063-7066.

129. Tambara, K.; Ponnuswamy, N.; Hennrich, G.; Pantoş, G. D., Microwave-Assisted Synthesis of Naphthalenemonoimides and N-Desymmetrized Naphthalenediimides. *J. Org. Chem.* **2011,** *76*, 3338-3347.

130. Bulheller, B. M.; Pantos, G. D.; Sanders, J. K. M.; Hirst, J. D., Electronic structure and circular dichroism spectroscopy of naphthalenediimide nanotubes. *Phys. Chem. Chem. Phys.* **2009,** *11*, 6060-6065.

131. Huang, C.; Barlow, S.; Marder, S. R., Perylene-3,4,9,10-tetracarboxylic Acid Diimides: Synthesis, Physical Properties, and Use in Organic Electronics. *J. Org. Chem.* **2011,** *76*, 2386-2407.

# CHAPTER 2 MOLECULAR ENGINEERING

The chemistry of molecular assemblies involves weak yet complex non-covalent interactions such as π-π stacking, hydrogen-bonding, van der Waals interactions and solvo/hydrophobic interactions amongst others.[1-5] For potential applications as functional molecular materials, there is an inherent need to develop novel design strategies to effectively control the molecular interactions induced organizations and thereby pre-programmable molecular systems can be realized.[6-13] In this regard, we present a bio-inspired design strategy to tailor the self-assembly of NDIs (as a specific example) by incorporating minute structural mutations.[14] We envision the need for such a bio-inspired design strategy due to some of the limitations associated with the other strategies (as discussed in Chapter 1) that are being employed in the literature. These limitations led us to look for better alternatives, and we realized that a solution might lie with the naturally evolved amino acids, due to their extraordinary molecular recognition and sequence-specific self-assembling properties.

This chapter thus provides examples of amino acid functionalized NDI derivatives and the ways in which their molecular organizations can be engineered into distinct micro/nanoarchitectures, in an effort to try and understand their structure-property correlations.[15-17] By functionalizing naphthalenetetracarboxylic dianhydride with appropriate amino acid derivatives, the molecular assemblies of the resulting NDIs could be tailored into several 0D architectures namely nanospheres, nanocups, mesocups, microbowls, microspheres, microparticles, 1D architectures namely nanobelts, twisted nanoribbons, supercoiled helices, microfibers, and 2D architectures namely nanosheets, comb-edged nanoflakes, microsheets and fractals.

## 2.1. Tryptophan Derivatized Naphthalenediimides

Herein we report on an exclusive investigation of the molecular organization of NDI appended with two tryptophan moieties.[15] The choice of tryptophan as an imide substituent is unique due to its polar carboxylic acid group and an indole aromatic heterocycle offering both hydrophilic and hydrophobic properties in a single moiety. In addition, tryptophan provides interaction sites for metal binding, flexibility with regard to functionalization, and biocompatibility. This work demonstrates the possible ways in which various properties can be exploited. Tryptophan appended NDI (**NDI-Trp**) has excellent solubility in polar solvents. A small structural modification such as using the methyl ester of tryptophan (**NDI-TrpOMe**) improves solubility in non-polar solvents. All these features bring about drastic changes in the morphology of self-assembled NDIs by transforming them into well-defined architectures. These molecular assemblies have been thoroughly characterized by photophysical, spectroscopic and morphological studies. The molecular organization can be changed from nanospheres to particles, nanobelts, fibers and fractals. The latter possesses a broad range of applications due to their wide range of length scales.[18-19] Such drastic changes in the morphology of NDI architectures are striking evidences of the importance of these weak, complicated non-covalent forces.

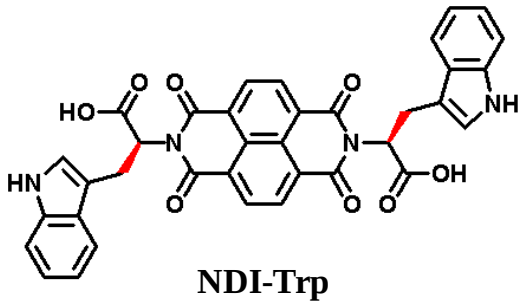


**NDI-Trp**

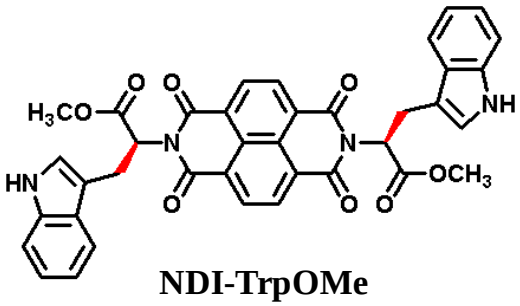


**NDI-TrpOMe**

### 2.1.1. Hydrophobic effect induced assembly

A typical UV-vis absorption spectra of **NDI-Trp** in acetonitrile (100 µM) shows absorption bands at 340 nm, 358 nm and 378 nm due to characteristic π-π* transitions (Figure 1a).[20,21] Increasing the solvent polarity by means of water (which has the highest hydrophobic effect) induces stacking interactions between the aromatic molecules. Water molecules solvating the aromatic surface have a higher energy than bulk water, and aromatic stacking reduces the total surface area exposed to water. The bathochromic shift of the absorption band with solvent polarity was observed for **NDI-Trp**. A bathochromic

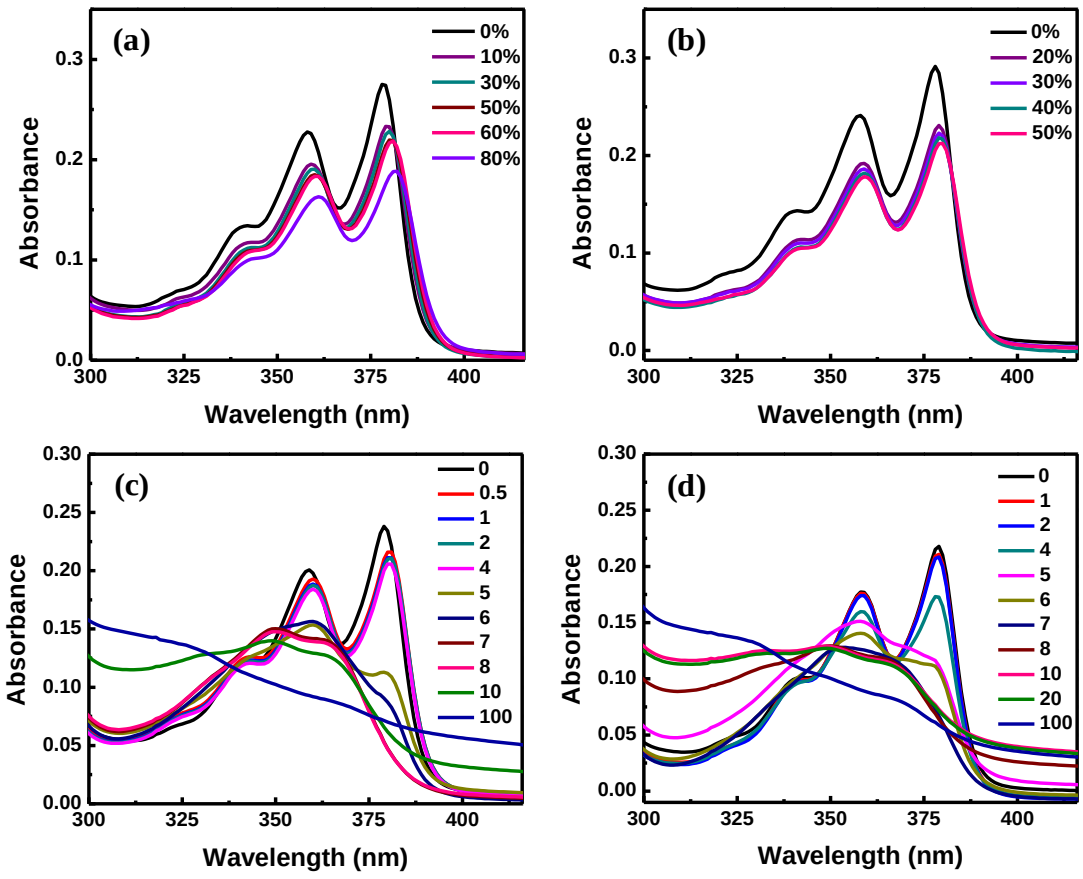


**Figure 1**. UV-vis spectra of **NDI-Trp** (a) and **NDI-TrpOMe** (b) in acetonitrile (100 µM) with increasing percentage of added water. UV-vis spectra of **NDI-Trp** (c) and **NDI-TrpOMe** (d) in 10% aqueous acetonitrile (100 µM) with the addition of NaOH (in equivalents).

shift of 2 nm, 4 nm and 6 nm for the 340 nm, 358 nm and 378 nm absorption bands was observed respectively. On the other hand, the absorption spectrum of **NDI-TrpOMe** in acetonitrile also possesses absorption bands at the same wavelength, as it is unaffected by methyl ester substitution (Figure 1b). The hydrophobic effect on **NDI-TrpOMe** in terms of bathochromicity was found to be minimal, as can be seen from the absorption spectra. A bathochromic shift of 1 nm and 2 nm for 358 nm and 378 nm bands respectively was observed, while 340 nm band was unaffected. Aromatic interactions are intriguing molecular recognition elements because they are expected to be strong in water due to their hydrophobic interactions.

### 2.1.2. Assembly in basic medium

Solvent-induced aggregation of **NDI-Trp** was found to be affected by protecting their free carboxylic acid groups with methyl esters, as in **NDI-TrpOMe**. In contrast, deprotonation of the carboxylic acid protons of **NDI-Trp** with an alkali such as sodium hydroxide (NaOH) shows interestingly different results. To a 10% aqueous acetonitrile solution of **NDI-Trp** (100 µM), NaOH was added portion-wise. The absorption bands for **NDI-Trp** were at 341 nm, 358 nm and 379 nm respectively in the absence of NaOH (Figure 1c). Successive addition resulted in a marginal bathochromic shift, up to a total of 4 equivalents of NaOH. With additional NaOH (5, 10, 20, 50 and 100 equivalents) the absorption bands show a strong hypsochromic shift. The absorption spectrum of **NDI-Trp** with 10 equivalents of NaOH contains bands at 331 nm, 349 nm and 364 nm. Further increase in the NaOH content resulted in a very broad band.

However, **NDI-TrpOMe** on NaOH treatment resulted in spectral features as shown in Figure 1d. It is not surprising that **NDI-TrpOMe** shows absorption spectra similar to that of **NDI-Trp** (except for the initial slight bathochromic shift). Hydrolysis of methyl ester in **NDI-TrpOMe** by added NaOH generates the respective sodium salt, as in the case of **NDI-Trp**. The differences between the spectral features of **NDI-Trp** and **NDI-TrpOMe** for the initial (although small shifts, but were consistent) equivalents of NaOH can be explained by means of the resulting side-products, water and methanol from **NDI-Trp** and **NDI-TrpOMe** respectively. The hydrophobic effect, which has been shown to cause the bathochromic shift (Figure 1a, 1b), is held responsible for the initial bathochromic shift observed in the case of **NDI-Trp**, as water is the byproduct. However, the weaker solvophobic interactions of methanol compared to water results in minimal bathochromic shifts, as observed in the case of **NDI-TrpOMe**. With more than 4 equivalents of NaOH, the imide rings of **NDI-Trp** and **NDI-TrpOMe** opens to form the naphthalene derivative.

### 2.1.3. Circular dichroism studies

To gain further insight into the mode of aggregation, we carried out CD studies on **NDI-Trp** and **NDI-TrpOMe**.[22-27] The CD spectrum of **NDI-Trp** in acetonitrile solution (100 μM) shows intense negative bands at 221 nm with a shoulder at 202 nm, and less intense bands at 276 nm, 335 nm, 352 nm and 372 nm (Figure 2a). The negative bands at 221 nm and 202 nm are attributed to n-π* and π-π* transitions of the imide chromophore respectively. The intense 221 nm band suggests possible additional contributions. The

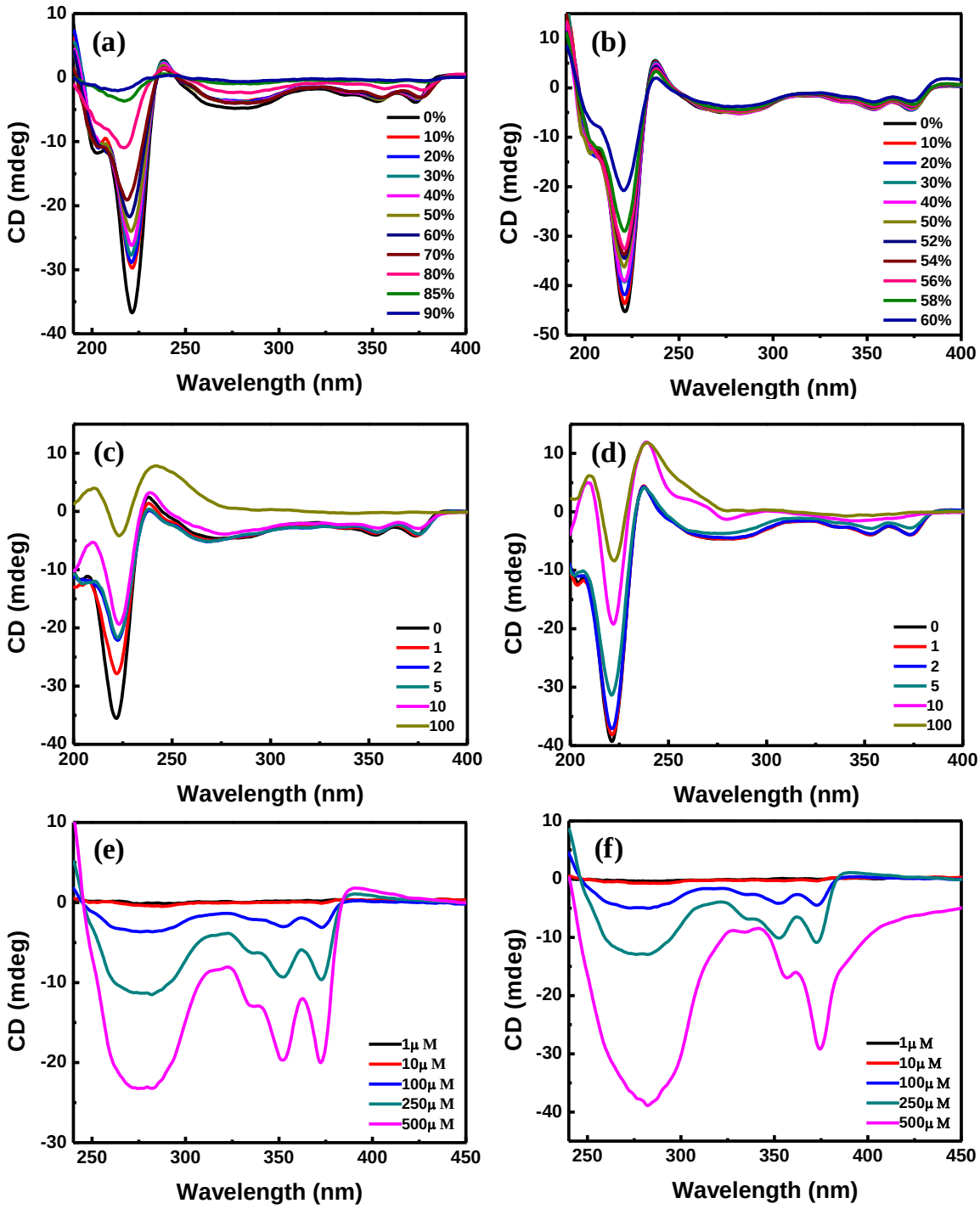


**Figure 2.** CD spectra of **NDI-Trp** (a) and **NDI-TrpOMe** (b) in acetonitrile (100 μM) with increasing percentage of added water. CD spectra of **NDI-Trp** (c) and **NDI-TrpOMe** (d) in 10% aqueous acetonitrile (100 μM) with added NaOH (in equivalents). Concentration dependent CD spectra of **NDI-Trp** (e) and **NDI-TrpOMe** (f) in acetonitrile.

close proximity of n-π* (221 nm) and π-π* (202 nm) transitions can facilitate mixing in a phenomenon known as the one-electron effect, which can enhance n-π* bands. However, the specific interactions with aromatic chromophores could also be responsible for the enhanced 221 nm band.[28,29] The band centered at 276 nm is due to the π-π* transitions of tryptophan, while those at 335 nm, 352 nm and 372 nm are due to that of NDI imposed by a chiral chemical environment.

Solvent-dependent CD studies on the aggregation mode of **NDI-Trp** are shown in Figure 2a. The negative band at 221 nm for **NDI-Trp** in acetonitrile was shifted to 213 nm ($\Delta\lambda$ = 8 nm) in 90% aqueous acetonitrile. The n-π* transition in amides is dependent on solvent, and increasing the solvent polarity by adding water shifts the n-π* transition to lower wavelengths. With increasing solvent polarity, the 221 nm (n-π* transition) band is quenched preferentially, rather than the 202 nm (π-π* transition) band. The spectral band features of **NDI-Trp** almost disappeared in 90% aqueous acetonitrile. The broad band centered at 276 nm was also found to quench with increasing solvent polarity, without any shift in band position. The π-π* transition bands of NDI at 335 nm, 352 nm and 372 nm were found to have a bathochromic shift to 337 nm, 357 nm and 378 nm respectively, similar to the bathochromic shift observed during absorption spectroscopic studies (Figure 1a). The CD study of hydrophobic effect on **NDI-TrpOMe** is shown in Figure 2b. **NDI-TrpOMe** exhibits a bathochromic shift with respect to NDI (π-π*) bands, but a hypsochromic shift with respect to the imide (221 nm) band, similar to **NDI-Trp**. In 60% aqueous acetonitrile, **NDI-TrpOMe** shows a 1 nm hypsochromic shift of the 221 nm band, and a 1 nm bathochromic shift for the 352 nm and 372 nm bands. The hypsochromic shift of the 221 nm band and the bathochromic shift of NDI bands

observed in CD measurements are due to the different mechanisms involved, as already discussed.

Surprisingly, **NDI-Trp** with NaOH was found to display a bathochromic shift of the 221 nm negative band (Figure 2c). A bathochromic shift of 2 nm was observed with 10 equivalents of NaOH. The bands above 240 nm showed minimal changes for various equivalents of NaOH. At 100 equivalents of NaOH, the bands above 240 nm completely disappeared. This is in agreement with the disappearance of the characteristic spectral features as observed in the absorption spectroscopic studies (Figure 1c). Interestingly, the 202 nm band due to the π-π* transition of imide was found to have a hypsochromic shift. The NaOH-mediated interaction of **NDI-Trp** is believed to shift the 202 nm band to below 200 nm. In addition, positive band-like features were observed at 210 nm and 240 nm. CD studies on **NDI-TrpOMe** with NaOH reveal spectral features similar to **NDI-Trp** (Figure 2d). A bathochromic shift of only 1 nm was observed for the 221 nm band in the case of **NDI-TrpOMe**.

Concentration-dependent CD studies of **NDI-Trp** and **NDI-TrpOMe** are shown in Figure 2e and Figure 2f respectively. The chiral-field-induced π-π* transitions of tryptophan result in a very broad negative band centered at 276 nm. However, the chiral-field-induced π-π* transitions of NDI result in negative bands at 335 nm, 352 nm and 372 nm. For low concentrations of **NDI-Trp** (1 μM and 10 μM) in acetonitrile these characteristic bands above 240 nm were not observed. Unlike **NDI-Trp**, the CD spectrum of 500 μM **NDI-TrpOMe** shows bands at 282 nm, 356 nm and 375 nm. The reduced solubility of **NDI-TrpOMe** is believed to aid in their molecular organization.

### 2.1.4. Vibrational spectroscopic studies

Vibrational spectroscopic studies of **NDI-Trp** and **NDI-TrpOMe** further revealed the changes in their vibrational modes (Figure 3). **NDI-TrpOMe** exhibits vibrational absorption frequencies at 1580 $cm^{-1}$, 1670 $cm^{-1}$ and 1706 $cm^{-1}$, among others. The vibrational frequency at 1706 $cm^{-1}$ is assigned to $\nu_{C=O}$ of carboxylic acid groups, 1580 $cm^{-1}$ to aromatic $\nu_{C=C}$ and the 1670 $cm^{-1}$ peak is attributed to the imide $\nu_{C=O}$ vibrational frequency, commonly known as the amide I band. The chemical environment constrained by conformation alters the amide I band, but the lack of conclusive structure–spectra correlations in the literature along with their several categories complicates the unambiguous assignment of amide I bands with the corresponding secondary structure. On the basis of the observed vibrational absorption frequency at 1670 $cm^{-1}$, we attribute **NDI-Trp** to a class of β-turn conformations.[30-33] **NDI-Trp** in 90% aqueous acetonitrile shows peaks at 1580 $cm^{-1}$, 1666 $cm^{-1}$ and 1704 $cm^{-1}$ corresponding to aromatic $\nu_{C=C}$, imide $\nu_{C=O}$ and $\nu_{C=O}$ of carboxylic acid functional groups respectively. These changes in the vibrational frequencies are attributed to hydrophobic-effect-induced structural variations.

In case of **NDI-TrpOMe** the peak at 1719 $cm^{-1}$ is attributed to ester $\nu_{C=O}$, and the 1580 $cm^{-1}$ peak to aromatic $\nu_{C=C}$, while the 1705 $cm^{-1}$ and 1678 $cm^{-1}$ peaks are assigned to the imide $\nu_{C=O}$ vibrational frequencies. **NDI-TrpOMe** showed slight changes in the vibrational modes in 60% aqueous acetonitrile. In another experiment NaOH was added portion-wise to an acetonitrile solution of **NDI-Trp**; the corresponding spectral changes are shown in Figure 4. With successive addition of NaOH, the carboxylic acid $\nu_{C=O}$ and imide carbonyl $\nu_{C=O}$ were found to shift towards lower frequencies. The carboxylic acid

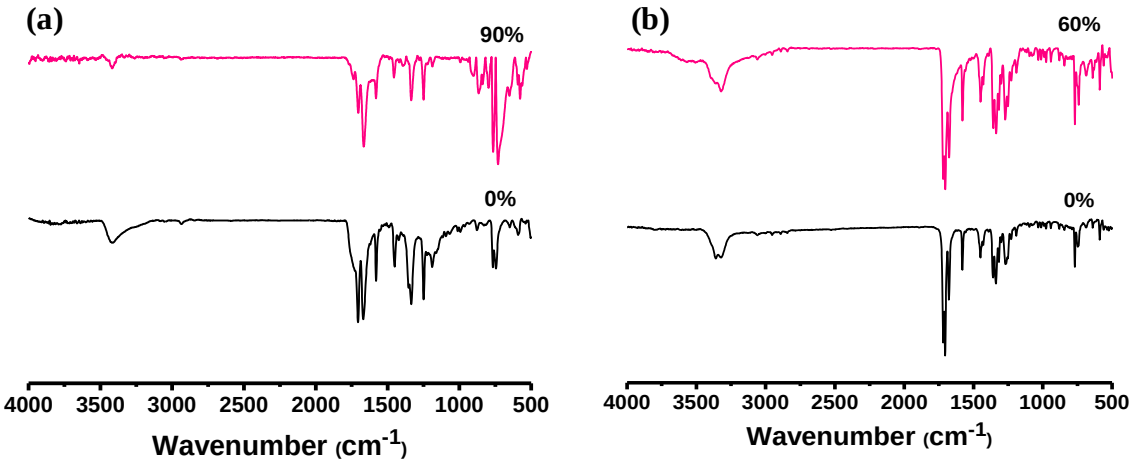


**Figure 3.** (a) and (b) IR spectra of **NDI-Trp** and **NDI-TrpOMe** in 0/60/90% aqueous acetonitrile respectively.

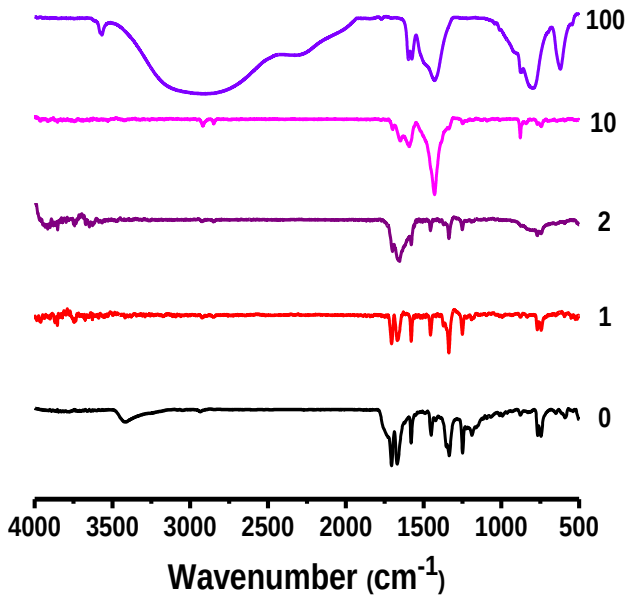


**Figure 4.** IR spectra of **NDI-Trp** (in acetonitrile) with the addition of NaOH (in equivalents).

$\nu_{C=O}$ was found to be at 1700 $cm^{-1}$, while the imide carbonyl $\nu_{C=O}$ at 1660 $cm^{-1}$ with 2 equivalents of NaOH (deprotonation of carboxylic acid protons). For 100 equivalents of NaOH, very broad vibrational modes at 620 $cm^{-1}$, 800 $cm^{-1}$, 1429 $cm^{-1}$, 1574 $cm^{-1}$, 1598 $cm^{-1}$ and ~3000 $cm^{-1}$ were observed.

### 2.1.5. Nuclear magnetic resonance (NMR) studies

NMR spectroscopic investigation further confirmed the structural changes occurring during the course of **NDI-Trp** aggregation. $^{1}$H NMR spectra for the solvent-dependent aggregation of **NDI-Trp** (aqueous $CD_3CN$ solution) is shown in Figure 5a. The hydrophobic-effect-induced stacking of **NDI-Trp** did not show significant changes in the naphthalene core proton resonances. The aromatic component (indole) of tryptophan shows interesting changes. The indole N–H proton resonating at $\delta$ = 8.91 ppm in $CD_3CN$ undergo a downfield shift to $\delta$ = 9.72 ppm in 65% aqueous $CD_3CN$. The labeled protons Hb, Hc, Hd and He experience an upfield shift, while Ha undergoes a downfield shift.

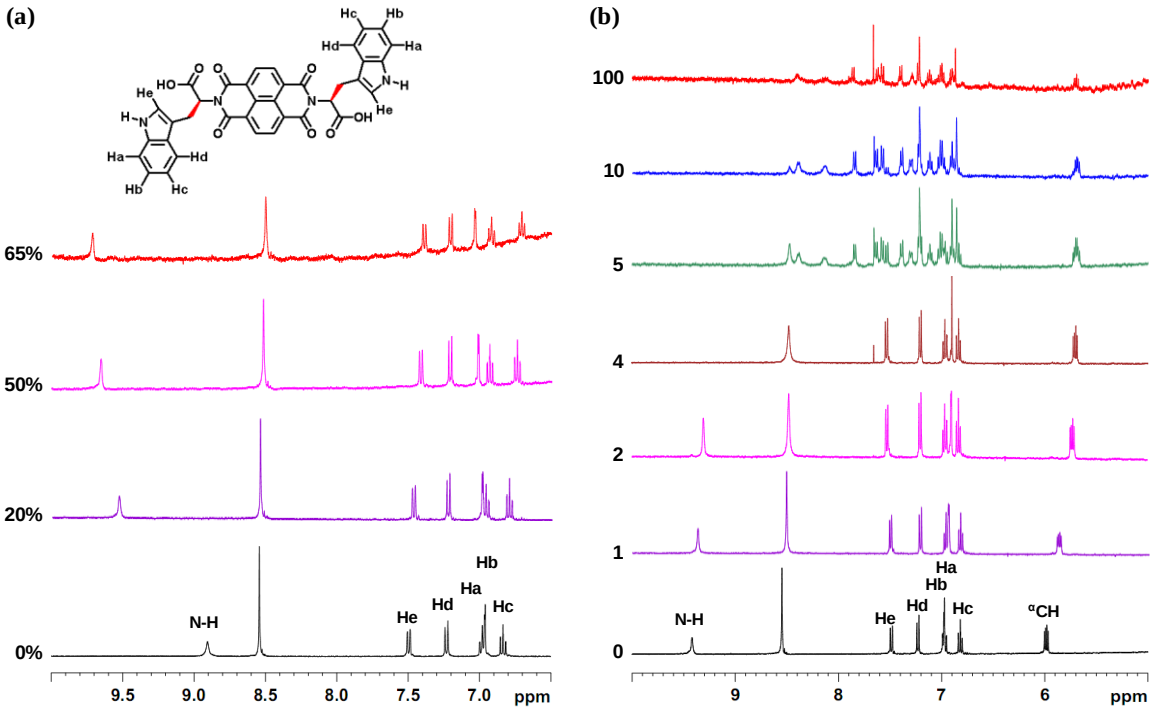


**Figure 5.** (a) Chemical structure of **NDI-Trp** with proton assignments (top) and $^{1}$H NMR spectra of **NDI-Trp** in $CD_3CN$ with varying percentage of added water (0-65%). (b) $^{1}$H NMR spectra of **NDI-Trp** in 10% aqueous $CD_3CN$ with increasing amount of added NaOH (0-100 equivalents). All the $^{1}$H NMR spectra were recorded with different equivalents of added NaOH maintaining the solvent composition of 10% aqueous $CD_3CN$.

However, the structural changes in **NDI-Trp** in the presence of NaOH are clearly evident from the $^{1}$H NMR studies (Figure 5b). On portion-wise addition of NaOH, the indole N–H proton shifts toward lower δ values. At 4 equivalents of NaOH the indole N–H disappears, indicating the abstraction of protons by NaOH. The naphthalene core protons undergo an upfield shift. The αCH also experiences an upfield shift from δ = 5.99 ppm to δ = 5.69 ppm, while protons Hb, Hc and Hd show minimal variations in the chemical shift. However, Ha and He protons have slight upfield and downfield shifts respectively. Addition of more than 4 equivalents of NaOH brings about significant changes in the $^{1}$H NMR of **NDI-Trp**. Chemical shifts observed in the aromatic region above 4 equivalents of NaOH are a clear indication of the structural changes occurring due to the presence of NaOH. $^{1}$H NMR studies shows the major variations in the proton resonances of tryptophan, and hence tryptophan and its indole moieties play a crucial role in determining the mode of aggregation.

### 2.1.6. Morphological studies

**NDI-Trp** forms spherical aggregates from acetonitrile solution as shown in the field-emission scanning electron microscopy (FESEM) image (Figure 6a). Transmission electron microscopy (TEM) image clearly showed the presence of solid nanospheres of **NDI-Trp** (Figure 6b). We obtained a maximum of 6 nm bathochromic shift (NDI electronic transitions) in absorption as well as CD studies, along with an 8 nm hypsochromic shift of the 221 nm band (CD) for **NDI-Trp** in 90% aqueous acetonitrile. Consequently, the FESEM micrograph showed the formation of particles of **NDI-Trp**

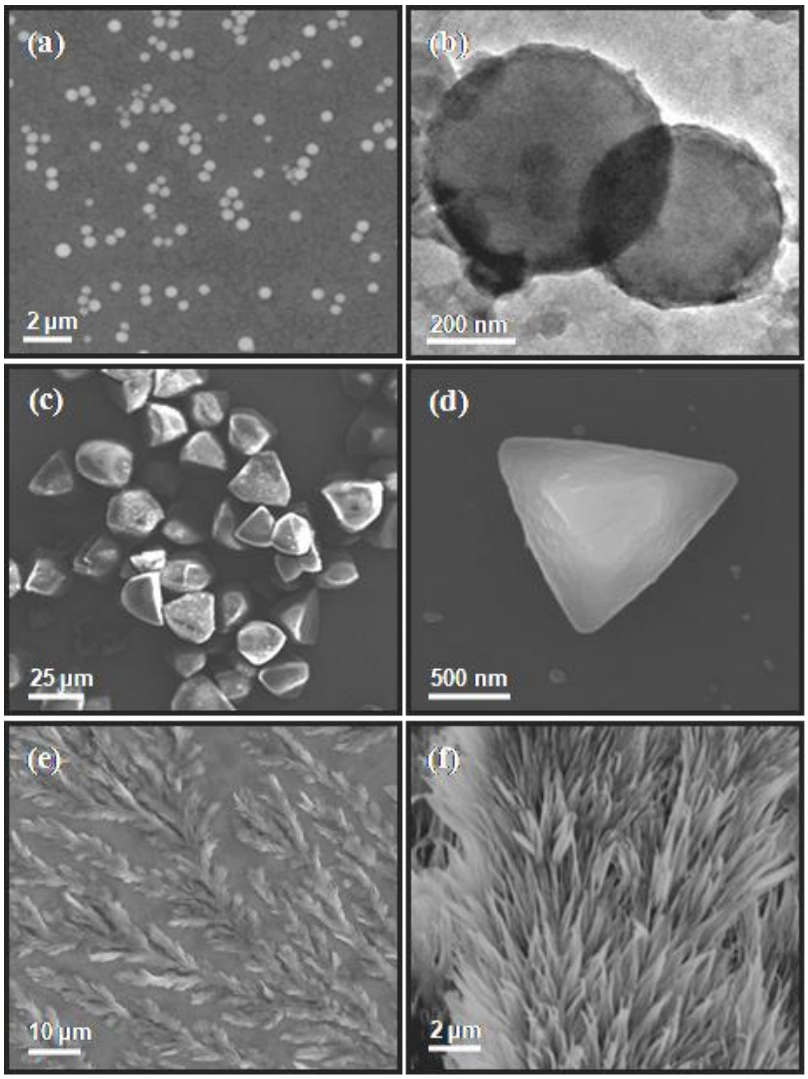


**Figure 6.** (a) FESEM micrograph of **NDI-Trp** nanospheres obtained from 100% acetonitrile solution. (b) The corresponding TEM micrograph of **NDI-Trp** nanospheres**.** (c) FESEM micrograph of **NDI-Trp** triangular particles obtained from 90% aqueous acetonitrile solution. (e) FESEM micrograph of **NDI-Trp** fractals formed by 10% aqueous acetonitrile solution containing 2 equivalents of NaOH. (d) and (f) are corresponding high magnification micrographs of (c) and (e) respectively.

from 90% aqueous acetonitrile (Figure 6c and 6d). The interplay between hydrogen bonding, solvophobic forces and aromatic stacking decides the molecular organization and hence their morphology. The intermolecular hydrogen bonding between carboxylic

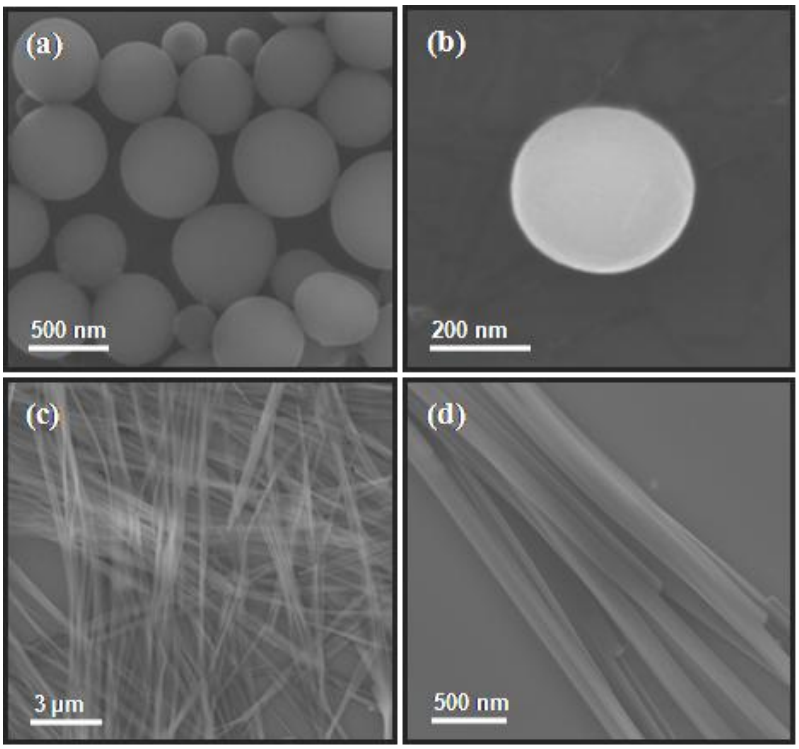


**Figure 7.** FESEM micrographs of **NDI-TrpOMe** nanospheres obtained from 100% acetonitrile solution (a) and fibers (bundle of nanobelts) obtained from 60% aqueous acetonitrile (c). (b) and (d) are the corresponding high magnification micrographs of (a) and (c) respectively.

acid groups of **NDI-Trp** in cooperation with the solvophobic and aromatic interaction leads to nanospheres in acetonitrile solution. The presence of water in aqueous acetonitrile solution of **NDI-Trp** disrupts the intermolecular hydrogen bonding. The particles are believed to be formed from disordered organization of **NDI-Trp**, as indicated by absorption and morphological studies.

**NDI-TrpOMe** also forms spherical aggregates from acetonitrile solution as shown in Figure 7a and 7b. The presence of the methyl ester of tryptophan in **NDI-TrpOMe** results in no significant changes in the aggregation mode with respect to **NDI-Trp** from acetonitrile solution. From the absorption spectroscopic study we had observed

a bathochromic shift of not more than 2 nm for the NDI π-π* transitions, a hypsochromic shift of 1 nm for the 221 nm (CD) band. Surprisingly, the molecular self-assembly of **NDI-TrpOMe** from 60% aqueous acetonitrile differs distinctly. **NDI-TrpOMe** forms fibers from 60% aqueous acetonitrile. The FESEM micrograph with a high aspect ratio fibers (bundle of nanobelts) is shown in Figure 7c and 7d. Atomic force microscopy (AFM) data revealed the transformation of **NDI-TrpOMe** nanospheres into nanobelts and then into microfibers (Figure 8a). The nanobelts bundle together to form long fibers that have a thickness of a few 100 nm to a few micrometers (Figure 8b). The formation of spherical aggregates from **NDI-TrpOMe** suggests that intermolecular hydrogen bonding (carboxylic groups) need not be necessary, as the aggregation is mainly facilitated by solvophobic and aromatic interactions. However, the presence of the methyl ester reduces the solubility in water, and moreover the dominance of hydrophobic forces in cooperation with aromatic interactions leads to 1D aggregation.

Analogous to the morphological changes induced by the bathochromic shift due to hydrophobic effect, NaOH too was found to affect the morphology. Deprotonation of the carboxylic acid protons in **NDI-Trp** was found to result in hardly any change in the absorption spectra. However, deprotonation results in drastic changes in the morphology of **NDI-Trp**. With 2 equivalents of NaOH, the formation of the sodium salt of **NDI-Trp** results in the formation of fractals (Figure 6e, 6f). For 10 equivalents of NaOH, distinct microstructures of **NDI-Trp** are formed. With further increase of NaOH (100 equivalents), agglomeration of **NDI-Trp** was observed. **NDI-TrpOMe** also results in similar fractals for 2 equivalents of NaOH and agglomerated masses for 100 equivalents of NaOH. We also studied the morphological changes as a function of concentration of

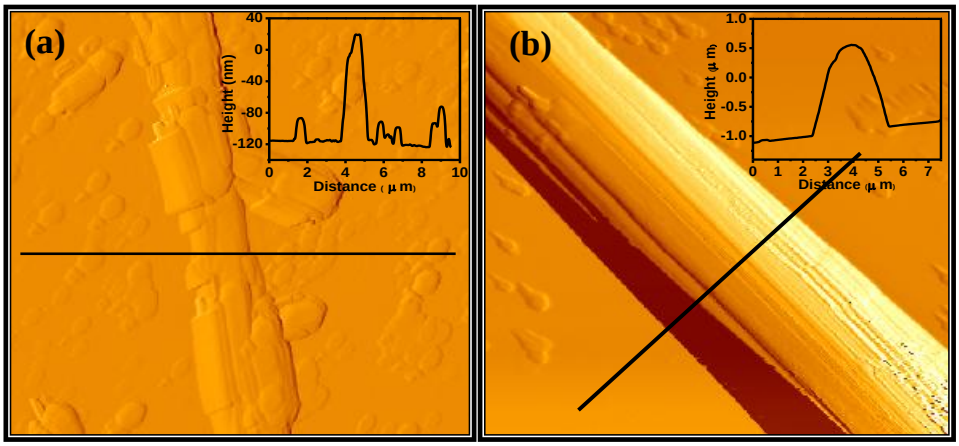


**Figure 8.** AFM image of **NDI-TrpOMe** showing (a) the structural transition from nanospheres to nanobelts and in turn into microfibers (60% aqueous acetonitrile), (b) microfiber (nanobelt bundles) formed from 60% aqueous acetonitrile. The insets in (a) and (b) are the corresponding height profiles.

NDIs. At higher concentration (1 mM) **NDI-Trp** agglomerates, while 1 mM **NDI-TrpOMe** transforms into 1D nanobelts. Relatively (**NDI-Trp**) reduced solubility rendered by the methyl ester functionality as well as the enhanced solvo/hydrophobic forces is believed to enforce 1D assembly of **NDI-TrpOMe**.

### 2.1.7. Conclusions

In an attempt to mimic Nature's versatility in terms of molecular recognition and the specific assembly properties embodied in amino acids, we have synthesized tryptophan-appended NDIs, **NDI-Trp** and **NDI-TrpOMe**. The tryptophan, as the imide substituent, possesses all the characteristics of a conventional substituent in a simple yet compact system. We were successful in tuning the morphology of NDIs to well-defined architectures including nanospheres, particles, nanobelts, fibers and fractals. Such drastic

change in the morphologies of **NDI-Trp** and **NDI-TrpOMe** is an illustration of the possibilities for extending morphology control mediated by molecular recognition. Our current work on tryptophan-appended NDI is an intriguing approach that, with further chemical modifications, has scope for electronic as well as biomedical applications. Tryptophan-appended NDIs are examples of compact model systems that should enable us to understand the relative contributions of non-covalent forces and to exploit them for useful applications

## 2.1.8. Experimental section

### *2.1.8.1. Materials and methods*

All the solvents and reagents were obtained from Sigma-Aldrich and used as received unless otherwise mentioned. $^{1}H$ and $^{13}C$ NMR were measured on a Bruker AV-400 spectrometer with chemical shifts reported as ppm (in $CDCl_3$/$CD_3CN$/DMSO-$d_6$, Tetramethylsilane as internal standard). Mass spectra were obtained from Shimadzu 2020 LC-MS. UV-vis spectra were recorded on a Perkin Elmer Model Lambda 900 spectrophotometer. Circular dichroism (CD) measurements were carried out on a Jasco J-810 spectropolarimeter. FESEM measurements were performed by using FEI Nova nanoSEM-600 equipped with field emission gun operating at 15 kV. AFM measurements were performed using Innova (Veeco) atomic force microscope. For FESEM and AFM measurements sample was taken on a fresh, ultra clean Si (111) substrate. TEM micrographs were obtained on a 200 mesh holey carbon supported copper grids. Elemental analysis was carried out on ThermoScientific FLASH 2000 Organic Element

Analyzer. IR spectra were recorded on a Bruker IFS 66/V spectrometer on a sodium chloride crystal.

### *2.1.8.2. Synthesis of tryptophan appended naphthalenetetracarboxylicdiimide* (NDI-Trp)

A modified procedure of Sanders and coworkers[34] has been employed to synthesize **NDI-Trp**. 1,4,5,8-Naphthalenetetracarboxylic dianhydride (200 mg, 0.74 mmol) and L-tryptophan (305 mg, 1.49 mmol) were suspended in DMF (20 mL) in a 250 mL Erlenmeyer flask. To this suspension was added 0.2 mL of triethylamine. The suspension was sonicated until the mixture became homogeneous. The reaction mixture was heated under microwave irradiation at full power for 3 min. in steps of 30 sec. and with 30 sec interval. The resulting dark brown oil was taken up into methanol (400 mL). The solution was added under stirring to 600 mL of 1N HCl. The resulting suspension was allowed to coagulate overnight and then filtered through a sintered glass funnel. The solid was then washed with 200 mL deionized water and dried in vacuo to obtain a brown solid of **NDI-Trp**. Yield 90%. $^1$H NMR: (400 MHz, DMSO-$d_6$) $\delta_{ppm}$ 3.46–3.52, (dd, 2H, $CH_2$, $J$ = 8 Hz, 8 Hz); 3.65-3.71 (dd, 2H, $CH_2$, $J$ = 8 Hz, 8 Hz); 5.84-5.87 (dd, 2H, αCH, $J$ = 8 Hz, 4 Hz); 6.78-6.82 (m, 2H, ArH); 6.92-6.96 (m, 2H, ArH); 7.04-7.05 (d, 2H, ArH, $J$ = 4 Hz); 7.19-7.21 (d, 2H, ArH, $J$ = 8 Hz); 7.46-7.48 (d, 2H, ArH, $J$ = 8 Hz); 8.61 (s, 4H, ArH); 10.64-

10.65 (d, 2H, NH, $J$ = 4 Hz); 12.99 (br, 2H, COOH). $^{13}$C NMR: (100 MHz, DMSO-$d_6$) $\delta_{ppm}$ 24.0, 54.2, 110.1, 111.2, 117.9, 118.2, 120.7, 123.6, 125.7, 125.9, 127.0, 131.1, 135.9, 162.0, 170.4. MS (EI): m/z = 641.16 $[M+H]^+$ for $C_{36}H_{25}N_4O_8$ (calc. 641.17). Elemental analysis: Found: C, 67.47; H, 3.83; N, 8.72; Calcd: C, 67.50; H, 3.78; N, 8.75 for $C_{36}H_{24}N_4O_8$.

### *2.1.8.3. Synthesis of tryptophan methylester appended naphthalenetetracarboxylicdiimide* (**NDI-TrpOMe**)

*Synthesis of L-Tryptophan methyl ester hydrochloride*: Anhydrous methanol (50 mL) was taken in a 100 mL 2-necked round bottom flask fitted with a reflux condenser and an additional dropping funnel and cooled to ice temperature. Acetyl chloride (3 mL) was added drop-wise through the dropping funnel. After 15 min, L-tryptophan (3 g) was added and the reaction mixture was refluxed at 70 °C for 6 h. The reaction mixture was vacuo dried to obtain L-tryptophan methyl ester hydrochloride in quantitative yield and used for further reaction without purification.

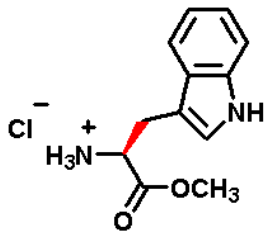


1,4,5,8-Naphthalenetetracarboxylic dianhydride (200 mg, 0.74 mmol) and L-tryptophan methyl ester hydrochloride (380 mg 1.49 mmol) were suspended in 20 mL of DMF in a 100 mL round bottom flask. To this suspension was added 0.5 mL of triethylamine under inert atmosphere. The reaction mixture was refluxed at 65 °C for 21 h. Solvent was evaporated under vacuo and the residue was purified by column chromatography (15 % methanol in chloroform). Yield 86%. $^1$H NMR: (400 MHz,

*CDCl*$_3$-$CF_3COOH$) $\delta_{ppm}$ 3.64–3.70, (dd, 2H, $CH_2$, *J* = 8 Hz, 8 Hz); 3.78-3.84, (dd, 2H, $CH_2$, *J* = 8 Hz, 8 Hz); 3.90 (s, 6H, $CH_3$); 6.12-6.16 (dd, 2H, αCH, *J* = 8 Hz, 4 Hz); 6.86-7.02 (m, 6H, ArH); 7.13-7.15 (d, 2H, ArH, *J* = 8 Hz); 7.46-7.48 (d, 2H, ArH, *J* = 8 Hz); 8.57 (s, 4H, ArH). $^{13}C$ NMR: (100 MHz, *CDCl*$_3$-$CF_3COOH$) $\delta_{ppm}$ 24.5, 53.9, 55.1, 110.2, 110.4, 118.6, 119.8, 122.4, 123.2, 126.1, 126.6, 127.2, 131.8, 136.1, 163.0, 172.5. MS (EI): m/z = 668.19 $[M]^+$ for $C_{38}H_{28}N_4O_8$ (calc. 668.19). Elemental analysis: Found: C, 68.23; H, 4.25; N, 8.35; Calcd: C, 68.26; H, 4.22; N, 8.38 for $C_{38}H_{28}N_4O_8$.

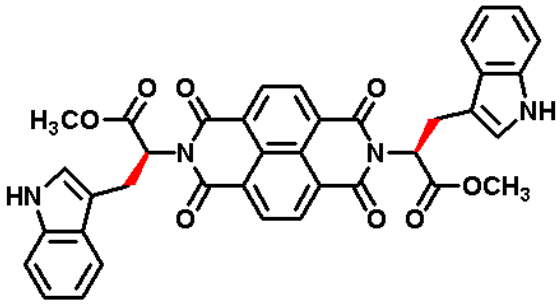

## 2.2. Phenylalanine Derivatized Naphthalenediimides

In this sub-chapter, we describe the novel molecularly engineered organization of NDIs into nanosheets, nanocups, mesocups, and bowl-like complex architectures.[16] Phenylalanine methylesters functionalized NDIs (**L-NDI** and **D-NDI**) were subjected to a simple solution processing technique to exploit the non-covalent interactions. Hydrophobic and π-π interactions enforce the self-assembly of L- and D-phenylalanine methylesters-appended NDIs into free-floating nanosheets with large lateral dimensions (Figure 9). To the best of our knowledge, we are, for the first time, disclosing the formation of large free-floating nanosheets by molecular self–assembly of an n-type organic semiconductor. Interestingly the nanosheets exhibit a remarkable conductivity of 1.6 $Scm^{-1}$. In organic-semiconductor films the mobility is mainly limited by molecular ordering and transport across the grain boundary.[35-39] This problem can be tackled by means of 1D molecular organization or growing films with large micrometer-sized grains. An alternative synergistic approach could be a 2D molecular organization. Consequently the self–assembled NDI nanosheets with large lateral dimension and high-level molecular ordering are certain to allow the fabrication of competent devices with ease.

On the other hand, solute-solvent interactions, involving chlorinated co-solvents, were used to obtain the attoliter ($10^{-18}$ L) containers. The composition and the type of chlorinated co-solvent employed resulted in the formation of nanocups, mesocups, and bowl-like architectures. Such ultra-small volume containers are particularly important in the emerging fields of miniaturized biochemical assays or single-molecule analysis.[40-42] These studies provide interesting insights of biological interactions at the molecular level, which are usually hidden in ensemble and time-averaging bulk experiments. Furthermore,

our NDI self-assembly based nanocups, mesocups, and bowls represent a novel class of ultra-low volume containers, which are unique from those obtained by etching (top-down) and emulsions, vesicles, or virus particles (bottom-up) approach.[43-46]

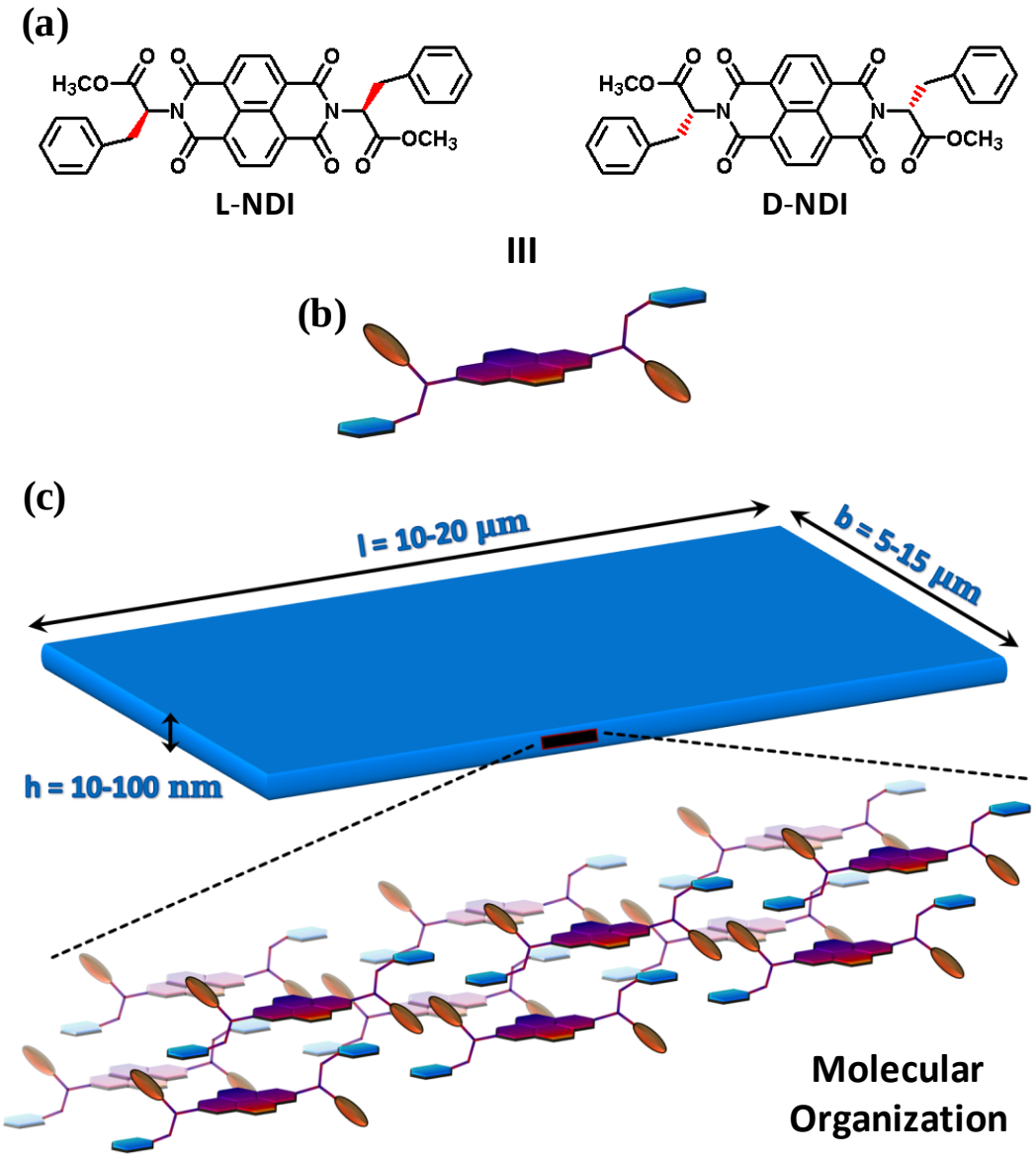


**Figure 9.** (a) Molecular Structures of phenylalanine methylester appended naphthalenediimides (**L-NDI** and **D-NDI**) with their pictorial representation (b). (c) Proposed molecular packing model for the self-assembled NDI nanosheets. *l* = length, *b* = width and *h* = height (thickness) of the nanosheet.

### 2.2.1. Highly crystalline large 2D nanosheets

#### *2.2.1.1. Photophysical studies*

The UV-vis absorption spectrum of **L-NDI** and **D-NDI** (100 μM) in acetonitrile exhibits strong absorption bands, namely band I in the range of 300-400 nm and band II at 235 nm (Figure 10a). Band I and II are attributed to characteristic π-π* transitions of NDI chromophores, polarized along the z and y axis, respectively. In 90% aqueous acetonitrile **L-NDI** and **D-NDI** undergo bathochromic shifts of 8 nm (band I) and 11 nm (band II) due to π-π stacking. A decrease in absorption intensity and a broadening of the band, accompanied by a red shift, indicate the presence of well-defined J-type aggregates. Interestingly **L-NDI** and **D-NDI** are weakly fluorescent in acetonitrile,[15,47,48] and showed a strong emission band in 90% aqueous acetonitrile centered at 475 nm with a shoulder at 530 nm (Figure 10b). The emission band is red shifted by 90 nm from its usual 7 nm Stokes-shifted weak mirror-image emission bands. This characteristic emission band is attributed to an excimer-like emission (excitation spectra not shown) due to the formation of ground-state aggregates.[47]

To gain further insights into the relative intermolecular orientation of the NDI chromophores, both **L-NDI** and **D-NDI** were subjected to circular dichroism (CD) studies. L- and D-phenylalanine methyl esters induce opposite chirality, as reflected in their mirror-image CD spectra in comparison to the NDI system, which is achiral under normal conditions (Figure 10c). The CD spectrum of **L-NDI** (100 μM) shows intense band at 215 nm and a less intense bands in the range of 225-400 nm. The 215 nm band is attributed to n-π* transitions of the imide chromophore. The less intense bands are due to

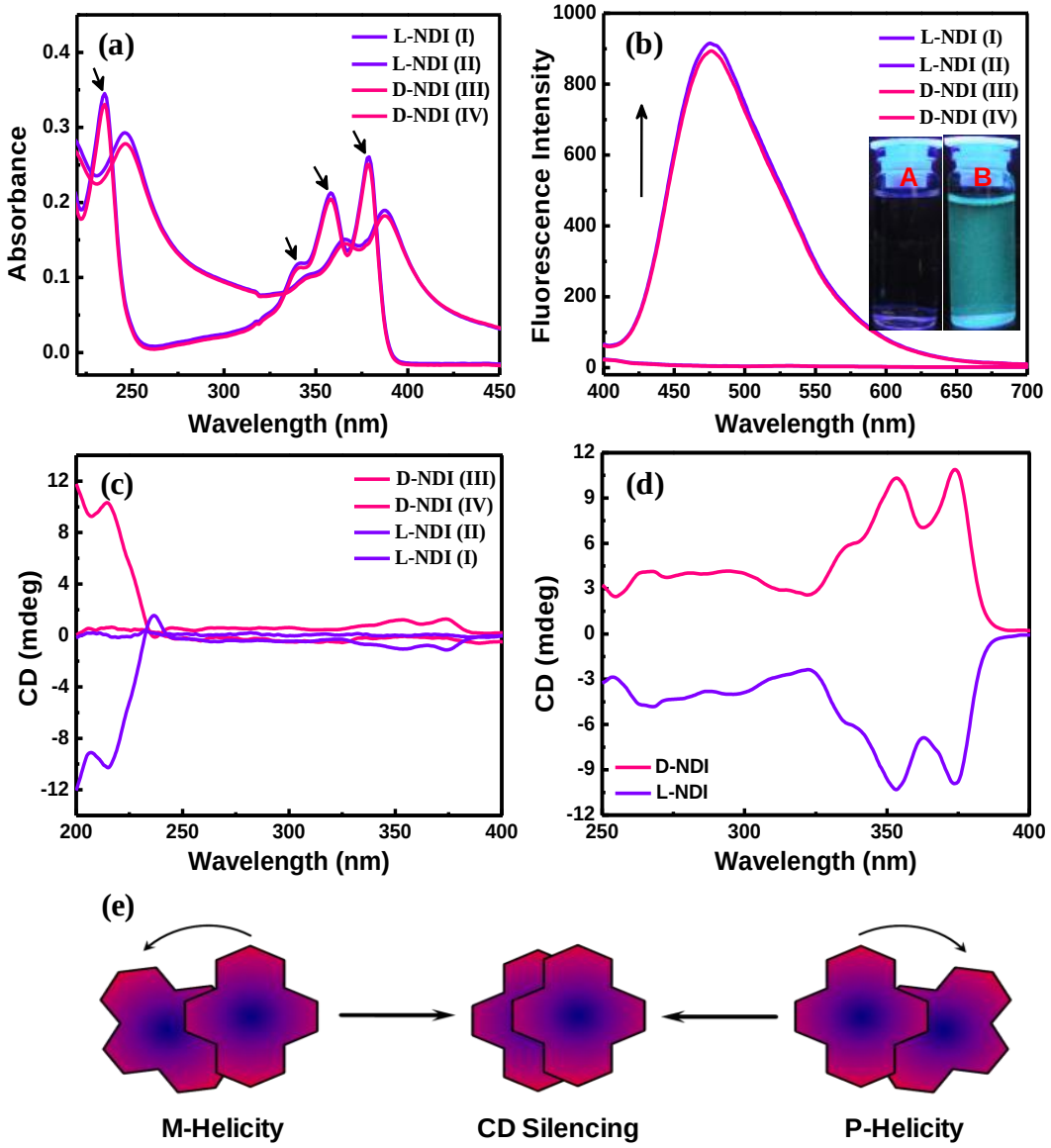


**Figure 10.** Photophysical studies of **L/D-NDI** (100 µM) in acetonitrile and 90% aqueous acetonitrile. (a) UV-vis absorption, (b) fluorescence emission and (c) circular dichroism (CD) spectra. (d) CD spectra of **L/D-NDI** (1 mM) in acetonitrile. Photographs of **L-NDI** in acetonitrile solution (A) and free-standing sheets with an excimer-like emission in 90% aqueous acetonitrile (B) under UV light. (e) Schematic representation of the transition of the angles between the *z*-polarized transition moments of stacked **L/D-NDI** chromophores. I): **L-NDI** in acetonitrile, II): **L-NDI** in 90% aqueous acetonitrile, III): **D-NDI** in acetonitrile and IV): **D-NDI** in 90% aqueous acetonitrile.

band I and band II electronic transitions of **L-NDI**. The CD spectrum for a relatively higher concentration of **L-NDI** (1 mM) clearly shows a strong Cotton effect (Figure 10d). The negative sign of the first Cotton effect (M-helicity) of **L-NDIs** in acetonitrile reflects the induction of supramolecular chirality to achiral NDI, on appending with the chiral L-phenylalanine methylester.[25,49]

Interestingly in 90% aqueous acetonitrile flat CD features were observed (Figure 10c). The increased hydrophobic forces impose a π-π stacking of the **L-NDI** chromophores. The observed CD silencing is thus attributed to the transition of the angles between the *z*-polarized transition moments of the stacked **L-NDI** chromophores towards zero (Figure 10e).[50] On the other hand, a complementary Cotton effect was observed for **D-NDI** (Figure 10c) with a positive sign of the first Cotton effect (P-helicity) in acetonitrile, and CD silencing in 90% aqueous acetonitrile, similar to that of **L-NDI**.

### *2.2.1.2. Characterization by microscopy and diffraction techniques*

FESEM revealed the formation of sheets with micrometer-size lateral dimension from 90% aqueous acetonitrile solution of **L-NDI** (Figure 11a). Similarly, **D-NDI** also self–assemble to form sheets in 90% aqueous acetonitrile. Furthermore free-floating sheets of **L-NDI** and **D-NDI** (100 μM, 90% aqueous acetonitrile) can be obtained within an hour of sample preparation. Such solution processing would lead to a convenient large-scale production of nanosheets for device applications without the need for sophisticated instrumentation. Thus, a formed free-floating sheet is an illustration of a successful molecular design and engineering with an optimal utilization of non-covalent

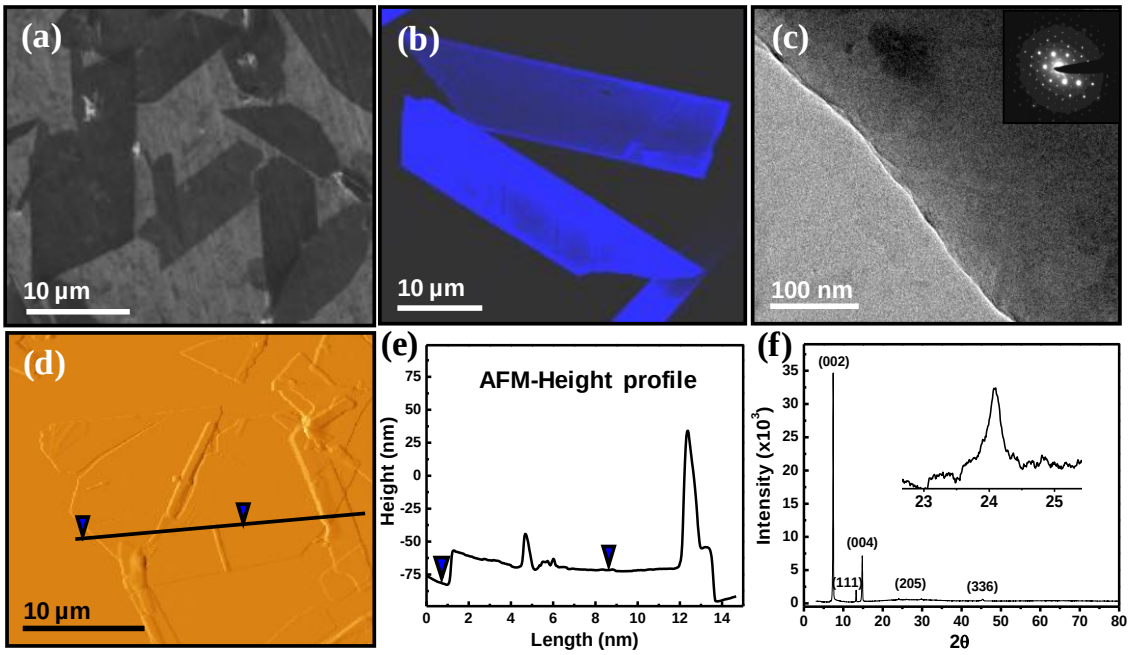


**Figure 11.** (a) FESEM, (b) fluorescence confocal (c) HRTEM and (d) AFM micrographs of **L-NDI** obtained from 90% aqueous acetonitrile. The inset in (c) is the SAED (selected area electron diffraction) pattern recorded on nanosheet revealing the single-crystalline ordering. (e) The corresponding height profile of AFM micrograph (d). The nanosheet possesses a typical height of ~10 nm. (f) Powder X-ray diffraction pattern of drop casted self-assembled **L-NDI** nanosheets. The inset corresponds to a *d* spacing of 3.68 Å.

interactions. In Figure 11b we show the confocal microscopy image of **L-NDI** sheets with a blue intrinsic fluorescence. The observed fluorescence is due to an excimer-like emission, as evident from fluorescence-spectroscopy studies. High-resolution transmission electron microscopy (HRTEM) image of **L-NDI** nanosheet is shown in Figure 11c. The selected-area electron diffraction (SAED) pattern recorded on these nanosheets exhibited well-resolved hexagonal spots, revealing the single-crystalline ordering (inset, Figure 11c) of the sample. An AFM image of the **L-NDI** sheets is shown in Figure 11d; the height profile reveals a 10 nm height for a typical sheet (Figure 11e). However, self-assembled nanosheets of NDI with topographical thicknesses (heights) of

10-100 nm can be obtained. Moreover, powder X-ray diffraction (PXRD) studies on **L-NDI** nanosheets showed a very high crystallinity along with a *d* spacing of 3.68 Å corresponding to π-π stacking (Figure 11f). The obtained diffraction peaks were indexed with the DICVOL program with lattice parameters of *a* = 9.81 Å and *c* = 23.88 Å in a tetragonal crystal system.

### *2.2.1.3. Solvophobic effect*

The UV-vis absorption spectra of **L-NDI** (100 µM) in dimethylformamide (DMF; Figure 12a) and dimethylsulphoxide (DMSO; Figure 12c) exhibit strong absorption bands

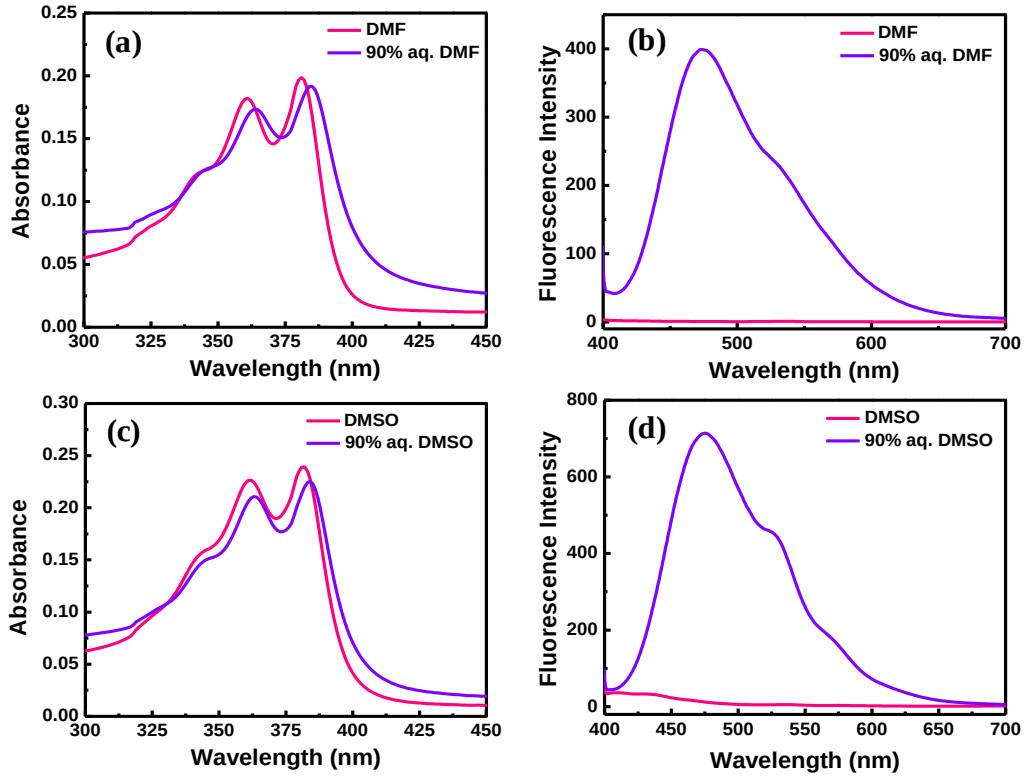


**Figure 12.** UV-vis spectra of 100 µM **L-NDI** in (a) DMF and 90% aqueous DMF, (c) DMSO and 90% aqueous DMSO. (b) and (d) the corresponding fluorescence spectra of (a) and (c) respectively.

corresponding to their characteristic π-π* transitions. In 90% aqueous DMF and 90% aqueous DMSO, both **L-NDI** and **D-NDI** undergo bathochromic shifts due to π-π stacking and exhibit excimer-like emission (Figure 12b and 12d). The high solvent polarity of DMF and DMSO in comparison with acetonitrile renders reduced influence by hydrophobic forces for their molecular organization. In 90% aqueous DMF, **L-NDI** organizes to form elongated belt-like sheets with ~100 µm length and 2-10 µm width (Figure 13a). On the contrary, in 90% aqueous DMSO, **L-NDI** organizes to form smaller (length 2-10 µm) but thicker sheets (thickness ~500 nm), as shown in Figure 13b. Thus, molecular organization of NDI into 2D sheets with varying dimensions can be obtained by using appropriate aqueous co-solvents.

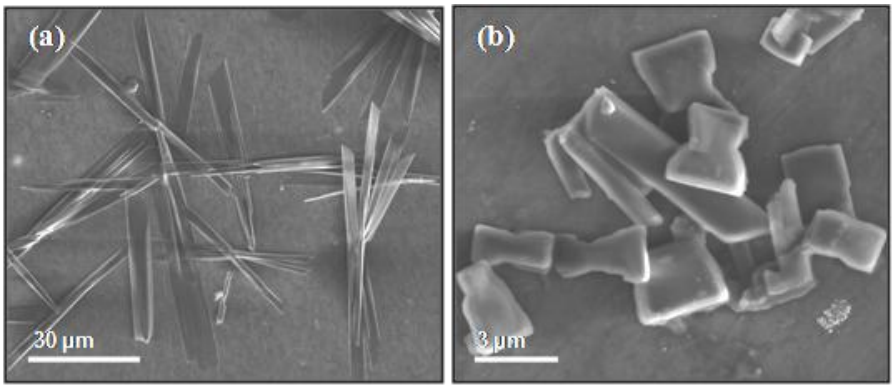


**Figure 13.** (a) and (b) FESEM micrograph of **L-NDI** in 90% aqueous DMF and 90% aqueous DMSO respectively.

### *2.2.1.4. Conductive atomic force microscopy*

A conductive AFM (C-AFM) technique was employed to study the conductivity of individual self-assembled nanosheets. Remarkably, the current–voltage (*I-V*)

characteristics of all measured **L-NDI** nanosheets displayed metallic conductivity. These *I-V* features were consistent throughout the length and width of the nanosheets, indicating persistent molecular ordering. A remarkable conductivity of 1.6 $Scm^{-1}$ was obtained for a nanosheet with the topographical thickness of 60 nm (Figure 14). Such metallic conductivities are reported only in heavily doped conducting polymers and small molecules.[51-55]

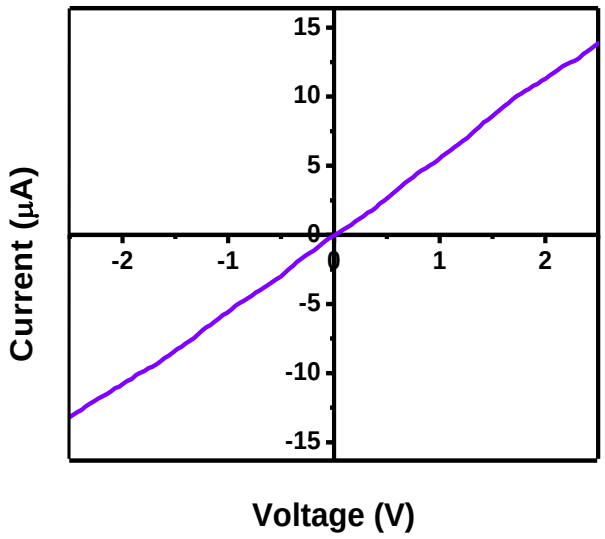


**Figure 14.** Current-voltage (I-V) characteristics obtained by C-AFM on a **L-NDI** nanosheet of 60 nm topographical thickness.

Furthermore, most of the organic semiconductors that exhibit high mobility (e.g., pentacene) adopt an edge-to-face herringbone structure with reduced intermolecular electronic couplings.[55] The observed metallic conductivity is attributed to the presence of high-level molecular ordering in **L-NDI** nanosheets. The molecular planarity of the NDI core and the ground-state molecular aggregation (excimer-like emission, CD silencing, and diffraction data) is envisioned to yield such high-level molecular ordering. The proposed model for the molecular packing of **L-NDI** and **D-NDI** is shown in Figure 9.

The methyl ester of phenylalanine in **L-NDI** and **D-NDI** systems initiate the molecular organization as a result of enhanced hydrophobic forces in 90% aqueous acetonitrile. The **L-NDI** chromophores undergo 1D π-π stacking in a direction perpendicular to the nanosheet surface. However the phenyl ring of phenylalanine facilitates a lateral organization to form 2D nanosheet architectures through interdigitation.[56]

### 2.2.2. Attoliter containers

#### *2.2.2.1. Halogen-bonding-mediated crystallization*

The single crystals of **L-NDI** were grown in chloroform. The crystal structure is composed of crystalline chloroform (Figure 15). The chlorine atoms were found to interact with the carbonyl oxygen of the methyl ester (3.02 Å; blue dotted line) and the carbonyl oxygen of naphthalenediimide (3.19 Å; green dotted line) in **L-NDI** by means of halogen bonding, as shown in Figure 15.[57-60] Halogen bonding is a highly directional non-covalent interaction (10-200 kJ $mol^{-1}$), which arises as a result of positive

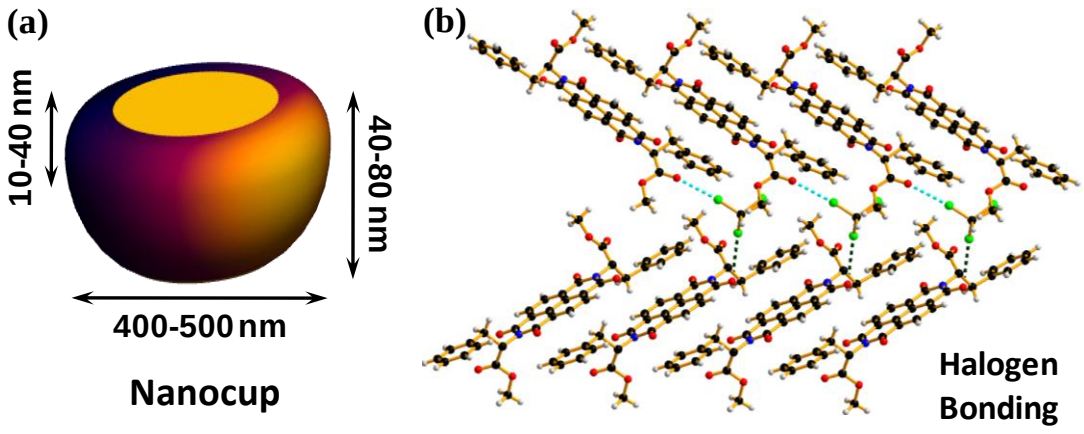


**Figure 15.** (a) Schematic of the **L-NDI** nanocup obtained from chlorinated co-solvent and (b) Molecular packing diagram for **L-NDI** single crystals grown in chloroform.

electrostatic potential developed along the carbon-halogen covalent bond. This σ-hole acts as an electrophillic species, which pulls the donor lone pair electrons closer towards the halogen atom and accounts for the orientation of the halogen bonds. Experimental studies have confirmed the theoretical prediction that electron density is anisotropically distributed around the halogen atom in organic halides.

### *2.2.2.2. Effect of chlorinated co-solvents - morphological studies*

The observed solute-solvent molecular interactions prompted us to investigate the probable role of chloroform in molecular organization. Consequently, the studies using chloroform as co-solvent resulted in interesting morphological changes (Figure 16). In chloroform alone, **L-NDI** forms random aggregates. However in 50% (v/v) chloroform/methanol, **L-NDI** organizes into cups of ~400 nm lateral widths, as shown in Figure 16a. Interestingly these cups were homogeneously distributed throughout the substrate. Furthermore in 10% (v/v) chloroform/methanol, **L-NDI** organizes into bigger cups with ~800 nm lateral width (Figure 16b). A careful inspection of the architectures obtained from 10% (v/v) chloroform/methanol reveals the presence of a few partially formed cup-like architectures. In addition, the occurrence of ridges within a fully formed bigger cup is in agreement with the dimensions of the smaller cup (lateral width: ~400 nm). Thus bigger cups are envisioned to be formed by the fusion of smaller cups. A typical bigger-cup formation involves the fusion of about four to six smaller cups. In methanol alone, the organization of **L-NDIs** into spherical structures was observed. Hence chloroform is believed to have a profound influence on the mode of aggregation.

For further verification, we used other chlorinated solvents, such as dichloromethane and carbon tetrachloride. **L-NDI** formed cups of ~700 nm in 10% (v/v) dichloromethane/ methanol. However 10% (v/v) carbontetrachloride/methanol results in bowl-like architectures of 1.5-2 μm (Figure 16c). Moreover in 10% (v/v) chloroform/acetonitrile **L-NDI** formed spherical aggregates. On the other hand, a dispersion of **L-NDI** in acetonitrile, when mixed with chloroform, resulted in cups of 300-700 nm lateral dimensions. These results clearly suggest that chlorinated co-solvents play a crucial role in the molecular organization of **L-NDI** into molecular containers. The nature of the halogen bonding driven by an appropriate chlorinated co-solvent determines the dimensions and morphology of the container. AFM studies on **L-NDI** cups obtained

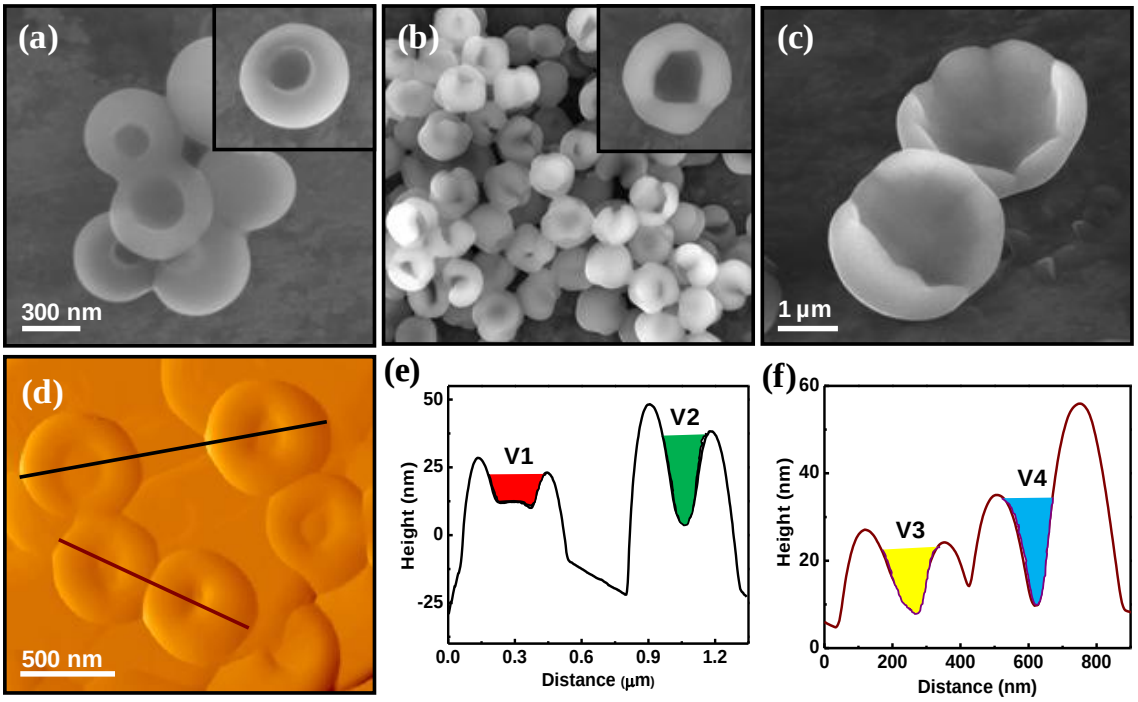


**Figure 16.** FESEM images of **L-NDI** (a) nanocups obtained from 50% (v/v) $CHCl_3$/MeOH, (b) mesocups obtained from 10% (v/v) $CHCl_3$/MeOH, (c) bowls from 10% (v/v) $CCl_4$/MeOH and (d) AFM micrograph of **L-NDI** nanocups obtained from 50% (v/v) $CHCl_3$/MeOH. The corresponding height profiles of (d) are shown in (e) and (f) respectively. Container volumes are indicated V1 (red), V2 (green), V3 (yellow) and V4 (cyan).

from 50% (v/v) chloroform/methanol revealed an overall diameter (thickness) of 400-500 nm and an exterior topographical height in the range of 40-80 nm (Figure 16d). The interior of the cup possess a typical height of 10-40 nm with an internal diameter [full width at half maximum (FWHM)] of 90-200 nm. An AFM image of these nanocups is shown in Figure 16d. The corresponding height profiles shown in Figure 16e and 16f accounts for a net volume of 0.58 (V1), 0.6 (V2), 0.19 (V3), and 0.2 (V4) attoliters.

The average volume capacity for the measured nanocups ranges from 0.1 to 1.5 attoliters. To demonstrate the utility, we made use of a femtojet technique to fill fluorescent dye into few **L-NDI** nanocontainers obtained on a glass/mica/aluminium substrate. Under appropriate experimental conditions, femtojet can inject liquid droplets of nanometer dimension. Dilute solutions of the analyte appended with fluorescent dyes

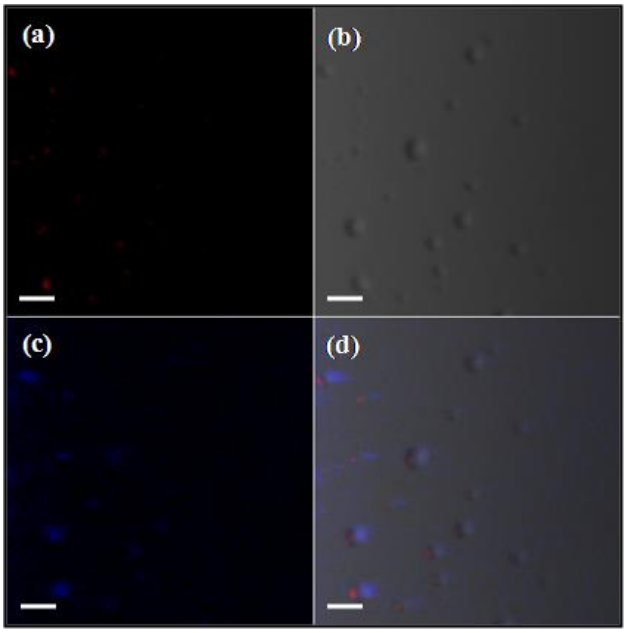


**Figure 17.** Fluorescence confocal micrographs of **L-NDI** mesocups on aluminium. (a) fluorescence micrograph obtained with an excitation at 543 nm (rhodamine) (b) bright field micrograph (c) two-photon fluorescence (**L-NDI**) micrograph and (d) overlay of (a), (b) and (c). Scale bar = 1 µm.

are commonly employed for biological assays. Herein, by using a femtojet technique, the fluorescent dye rhodamine was randomly sprinkled into an array of **L-NDI** containers and visualized with confocal microscopy (Figure 17). This illustrates the probable use of these ultrasmall containers for miniaturized applications. Furthermore, in order to passivate the surface, the self-assembled containers were gold coated by using a sputtering technique, which was confirmed by energy-dispersive X-ray analysis (EDAX) and FESEM studies.

### 2.2.3. Conclusions

We have shown a novel molecular design of NDI to engineer their organization into nanosheets, nanocups, mesocups, and bowl-like complex architectures. Phenylalanine methyl ester functionalized NDI was subjected to a simple solution processing technique to exploit non-covalent interactions. The successful molecular design comprises of methyl ester functionality to initiate molecular organization and the phenyl ring to facilitate lateral organization, as the NDI core experiences π-π stacking under enhanced hydrophobic (90% aqueous acetonitrile) forces. The subtle balance between hydrophobic and π-π interactions enforce the self-assembly of **L-NDI** and **D-NDI** into free-floating nanosheets with large lateral dimensions. The self-assembled nanosheets displayed excimer-like emissions. The molecular planarity of NDI core, well resolved electron diffraction, highly crystalline XRD patterns, CD silencing, and the spectroscopic data strongly emphasize the excellent crystallinity of nanosheets. The high degree of molecular ordering resulted in a metallic conductivity of 1.6 $Scm^{-1}$ of undoped **L-NDI**

nanosheets. On the contrary, **L-NDI** was organized into container-like complex architectures by employing chlorinated co-solvents. **L-NDI** was organized into nanocups of ~ 400 nm external lateral width. Furthermore, **L-NDI** was also organized into mesocup and bowl-like architectures. The dimensions and the morphology of the containers are mediated by halogen bonding with chlorinated co-solvents. Nanocups possess a net volume of 0.1-1.5 attoliters. These self–assembled attoliter containers are the first of its kind and may find use in miniaturized applications.

### 2.2.4. Experimental section

#### *2.2.4.1. Materials and methods*

1,4,5,8-Naphthalenetetracarboxylic dianhydride was obtained from Sigma–Aldrich. L-phenylalanine, D-phenylalanine, acetyl chloride, and triethylamine were obtained from Spectrochem Pvt. Ltd. Mumbai (India). All other reagents and solvents were of reagent grade and used without further purification.

*Absorption spectroscopy:* UV-vis spectra were recorded on a Perkin Elmer Model Lambda 900 spectrophotometer. A 100 μM solution of the sample was analyzed in quartz cuvette of 1 mm path length.

*Fluorescence spectroscopy:* Fluorescence spectra were recorded on a Perkin Elmer Model LS 55 spectrophotometer. A 100 μM solution of the sample were analyzed in a quartz cuvette of 1 mm path length with an excitation at 375 nm.

*NMR Spectroscopy, mass Spectrometry (MS), and elemental analysis:* $^{1}H$ and $^{13}C$ NMR were recorded on a Bruker AV-400 spectrometer with chemical shifts reported as ppm (in $CDCl_3$ with tetramethylsilane as internal standard). Mass spectra were obtained from Shimadzu 2020 LC-MS. Elemental analysis was carried out on ThermoScientific FLASH 2000 Organic Element Analyzer.

*Circular dichroism:* CD measurements were carried out on a Jasco J-810 spectropolarimeter under nitrogen atmosphere. 100 μM / 1 mM solutions of the sample were analyzed in quartz cuvette of 1 mm path length.

*Infrared (IR) spectroscopy:* IR spectra were recorded on a Bruker IFS 66/V spectrometer on a sodium chloride crystal. The liquid sample (free-floating sheets in case of 90% aqueous acetonitrile) was drop-casted and was allowed to dry naturally on the sodium chloride crystal.

*Field emission scanning electron microscopy:* FESEM images were acquired with a FEI Nova nanoSEM-600 equipped with a field-emission gun operating at 15 kV. The sample was prepared by drop-casting either onto a Al stub or on a Si(111) substrate.

*High-resolution transmission electron microscopy:* HRTEM measurements were performed on a JEOL, JEM 3010 instrument operated at 300 kV. The samples were prepared by drop-casting onto 200 mesh, holey, carbon-supported copper grids.

*Atomic force microscopy:* AFM images were acquired under ambient conditions using an Innova (Veeco) atomic force microscope in dynamic force (tapping) mode. The samples were prepared by drop-casting on freshly cleaved mica or Si(111). AFM section analysis was done offline.

*Current sensing (conductive) atomic force microscopy (C-AFM):* C-AFM was also performed using the above-mentioned Innova (Veeco) atomic force microscope. Pt/Ir coated Si tips with a tip radius (Max) of 25 nm (Bruker; Model: SCM-PIC) were employed. The samples were prepared by drop-casting on freshly cleaved highly oriented pyrolytic graphite (HOPG). *I-V* characteristics were obtained from several points on the self-assembled nanosheets of different topographical thickness (height). The value of the conductivity (σ) was calculated from the equation [$\sigma = d/(AR)$ $Scm^{-1}$], where $d$ is the sheet thickness/height (10–100 nm), $A$ is the area of the C-AFM probe in contact with the surface and computed as $\pi r^2$, assuming a contact radius of 25 nm between tip and sample. $R$ is the resistance of the sample, calculated from the inverse slope of the *I-V* curve.

*X-ray single-crystal measurement:* X-ray single-crystal structural data were collected on a Bruker Smart–CCD diffractometer equipped with a normal focus, 2.4 kW sealed tube X-ray source (Mo Kα radiation, 0.71073 Å), operating at 50 kV and 30 mA. An empirical absorption correction based on symmetry equivalent reflections was applied using the SADABS program.

*Powder X-ray diffraction (PXRD):* PXRD patterns were recorded with a Rigaku-99 (Miniflex) diffractometer using Cu Kα radiation (λ = 1.5406 Å). The free-floating self-assembled **L-NDI** nanosheets were drop-casted on a glass slide. The diffraction peaks were indexed with the DICVOL program.

*Gold sputtering:* Gold was sputtered with a Polaron SC502 Sputter Coater (FISONS Instruments) in Argon atmosphere.

*Femtojet technique:* The fluorescent dyes were injected by using Injectman NI2 coupled to a Femtojet (Eppendorf) setup. The dyes were injected by means of Femtotips with an injection pressure ($P_i$) of 15/25/50/200 hPa, an injection time ($t_i$) of 0.2 s and a compensation pressure ($P_c$) of 0 hPa. A 1 μM solution of rhodamine B base in 10:90 (v/v) $CHCl_3$: MeOH was employed.

*Fluorescence confocal microscopy:* Fluorescence confocal microscopy images were obtained from LSM 510 META-Carl Zeiss. A two-photon laser was employed to excite the self-assembled NDI nanosheets. An excitation wavelength of 543 nm was used to excite the rhodamine B base. The LSM image examiner was utilized for processing the images.

### *2.2.4.2. Synthesis of L-phenylalanine methylester appended naphthalenediimide* (L-NDI)

*Synthesis of L-phenylalanine methyl ester hydrochloride*: Anhydrous methanol (50 mL) was placed into a 100 mL two-necked round-bottom flask, fitted with a reflux condenser

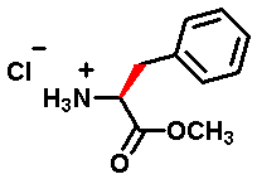


and an additional dropping funnel, and cooled to ice temperature (0 $^oC$). Acetyl chloride (3 mL) was added drop-wise through the dropping funnel. After 15 min, L-phenylalanine (3 g, 18.16 mmol) was added, and the reaction mixture was refluxed overnight at 70 $^oC$. The reaction mixture was dried in vacuo to obtain L-phenylalanine methyl ester hydrochloride in quantitative yield and used for further reaction without purification.

1,4,5,8-naphthalenetetracarboxylic dianhydride (200 mg, 0.74 mmol) and L-phenylalanine methyl ester hydrochloride (322 mg 1.49 mmol) were suspended in DMF

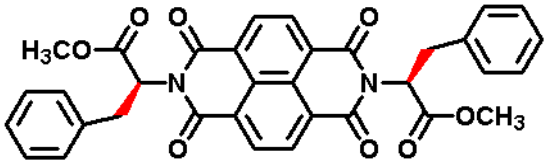


(20 mL) in a 100 mL round-bottom flask. To this suspension, triethylamine (0.6 mL) was added under inert atmosphere. The reaction mixture was refluxed at 75 $^{o}$C for 24 h. The solvent was evaporated in vacuo, and the residue was purified by column chromatography (1% methanol in chloroform). Yield 74%. $^{1}$H NMR (400 MHz, *CDCl$_3$*, δ): 8.63 (s, 4H), 7.1 (m, 10H), 6.02 (dd, 2H, *J* = 8Hz, 4Hz), 3.77 (s, 6H), 3.73 (dd, 2H, *J* = 8Hz, 4Hz), 3.50 (dd, 2H, *J* = 12 Hz, 4 Hz); $^{13}$C NMR (100 MHz, *CDCl$_3$*, δ) 169.6, 162.4, 136.9, 131.3, 129.2, 128.5, 126.9, 126.8, 126.3, 54.8, 52.8, 34.9; MS (EI): *m*/*z* = 590.16 $[M]^{+}$ for $C_{34}H_{26}N_2O_8$ (calc. 590.17); Elemental analysis: Calcd. for $C_{34}H_{26}N_2O_8$: C, 69.15; H, 4.44; N, 4.74. Found: C, 69.12; H, 4.48; N, 4.69.

### *2.2.4.3. Synthesis of D-phenylalanine methylester appended naphthalenediimide* (D-NDI)

*Synthesis of D-phenylalanine methyl ester hydrochloride*: Anhydrous methanol (50 mL)

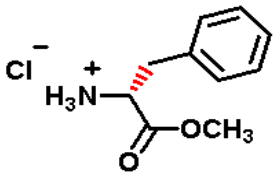


was placed into a 100 mL two-necked round bottom flask, fitted with a reflux condenser and an additional dropping funnel, and cooled to ice temperature (0 $^{o}$C). Acetyl chloride (3 mL) was added drop-wise through the dropping funnel. After 15 min, D-phenylalanine (3 g, 18.16 mmol) was added and the reaction mixture was refluxed overnight at 70 $^{o}$C. The reaction

mixture was dried in vacuo to obtain D-phenylalanine methyl ester hydrochloride in quantitative yield, which was used for further reaction without purification.

1,4,5,8-naphthalenetetracarboxylic dianhydride (200 mg, 0.74 mmol) and D-phenylalanine methyl ester hydrochloride (322 mg 1.49 mmol) were suspended in DMF

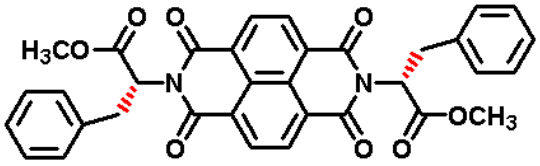


(20 mL) in a 100 mL round-bottom flask. To this suspension triethylamine (0.6 mL) was added under inert atmosphere. The reaction mixture was refluxed at 75 $^{o}$C for 24 h. The solvent was evaporated in vacuo and the residue was purified by column chromatography (1% methanol in chloroform). Yield 71%. $^{1}$H NMR (400 MHz, *CDCl*$_3$, δ): 8.63 (s, 4H), 7.1 (m, 10H), 6.02 (dd, 2H, *J* = 4Hz, 4Hz), 3.77 (s, 6H), 3.73 (dd, 2H, *J* = 8Hz, 4Hz), 3.50 (dd, 2H, *J* = 12 Hz, 4 Hz); $^{13}$C NMR (100 MHz, *CDCl*$_3$, δ) 169.6, 162.4, 136.9, 131.3, 129.2, 128.5, 126.9, 126.8, 126.4, 54.9, 52.8, 34.9; MS (EI): *m/z* = 590.18 $[M]^{+}$ for $C_{34}H_{26}N_2O_8$ (calc. 590.17); Elemental analysis: Calcd. for $C_{34}H_{26}N_2O_8$: C, 69.15; H, 4.44; N, 4.74. Found: C, 69.10; H, 4.49; N, 4.78.

## 2.3. Tailoring the π-π Stacking of Functional Modules

The elucidation of the complex factors that govern recognition events at the molecular level represents a daunting challenge in our quest to master the art of pre-programmed molecular assemblies.[61-67] In this context, we present the molecular architectonics of thoughtfully designed amino acid appended functional molecules **1**-**5** (Figure 18). NDI and pyrene were employed as functional modules due to their unusual topological shape similarity as well as complementary π-acidic and π-basic character, respectively.[17] In addition, we show that dyads of such unusual functional modules energetically favor alternate assembly in contrast to the predominant self-sorted assembly observed for single-component systems. Moreover, by incorporating minute structural mutations into the amino acid side-chains of **1**-**5**, we successfully tailored their assemblies into well-defined supramolecular architectures, namely supercoiled helices, twisted nanoribbons, nanobelts, comb-edged nanoflakes and nanosheets. A detailed analysis with the aid of experimental and theoretical studies has generated interesting insights into the factors that govern the recognition events at the molecular level.

As the performance of the electroactive molecular materials is essentially dependent on their molecular ordering, it is extremely important to develop novel modular approaches for tailoring their assemblies.[68-70] Interestingly, NDI is a highly π-acidic planar molecule with an estimated molecular quadrupole moment (*Qzz*) of +18.6 B (Buckinghams).[21] This π-acidic behaviour of NDI, which is in the range of explosive TNT, is an attractive property, because most aromatic compounds are π-basic, for example, benzene has a *Qzz* of -8.5 B, and pyrene has a *Qzz* of -13.8 B. Thus, NDI and pyrene exemplify a unique molecular (electron donor-acceptor) pair due to their

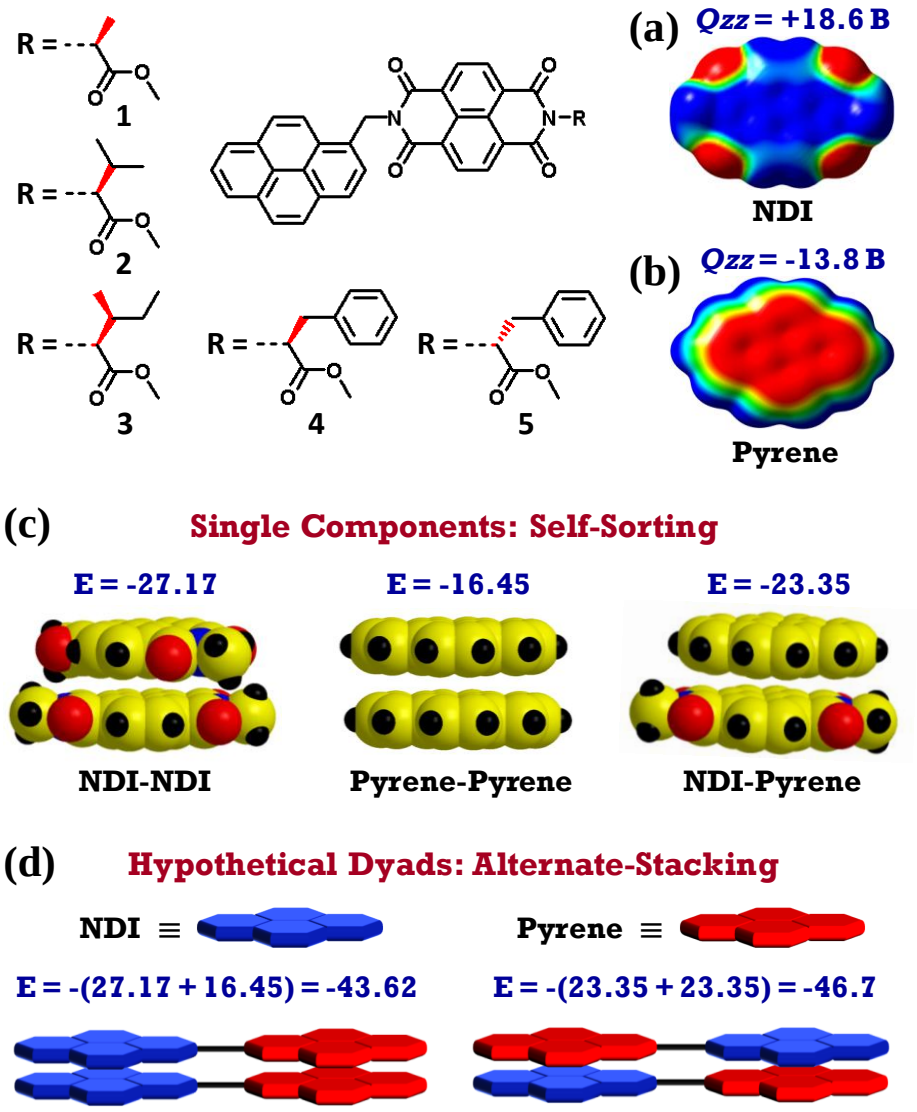


**Figure 18.** Molecular structures of designer functional molecules **1–5.** Blue colour signifies the topological shape similarity of naphthalenediimide (NDI) and pyrene. Electrostatic potential surfaces of (a) π-acidic NDI and (b) π-basic pyrene with their respective computed axial quadrupole moments *Qzz*. (c) Energy-minimized structures of NDI–NDI, pyrene–pyrene and NDI–pyrene stacking. (d) Schematic representation depicting the probable self-sorting or alternate stacking for hypothetical dyads of NDI and pyrene. The estimated interaction energies, *E* in kcal $mol^{-1}$, are shown in (c) and (d).

complementary π-character and also the unusual topological shape and the similarity of their molecular structures. However, the anticipated preferential alternate stacking of NDI and pyrene (when part of distinct molecular components), in contrast to their self-sorted

assemblies, are rarely realized due to their relatively weak non-covalent interaction energies.[71-81] On the other hand, exploitation of such donor/acceptor alternate stacking induced charge-transfer complexation (if extended to long-range order) is instrumental in obtaining excellent conduction through inherent doping as well as for the recently shown remarkable room-temperature ferroelectric property.[82,83] Thus, to extend the envisioned ordering from the molecular level to well-defined supramolecular architectures on a microscopic scale and also to explore systematic molecular structural mutation induced structure-property correlations, we have designed amino acid functionalized dyads of NDI and pyrene (**1**-**5**). The amino acid auxiliaries for tailoring the molecular assemblies were chosen on the basis of the phenomenal molecular/chiral recognition and distinctive sequence-specific self-assembling properties embodied in them as a result of over a billion years of stringent natural selection.[14] Specifically, by introducing minute molecular structural mutations in the side-chain of the amino acid auxiliary, striking variations in the supramolecular architectures, namely supercoiled helices, twisted nanoribbons, nanobelts, comb-edged nanoflakes and nanosheets, were realized.[17]

### 2.3.1. Photophysical studies

To understand the nature of the molecular assembly, we first subjected our functional molecules **1**-**5** to photophysical studies. The UV-vis absorption spectra of **1** in dimethylsulfoxide exhibits typical absorption bands in the region of 270–400 nm due to characteristic π-π* transitions polarized along the *z* and *y* axes of the NDI and pyrene chromophores (Figure 19a). Upon incremental addition of water to the DMSO solution of

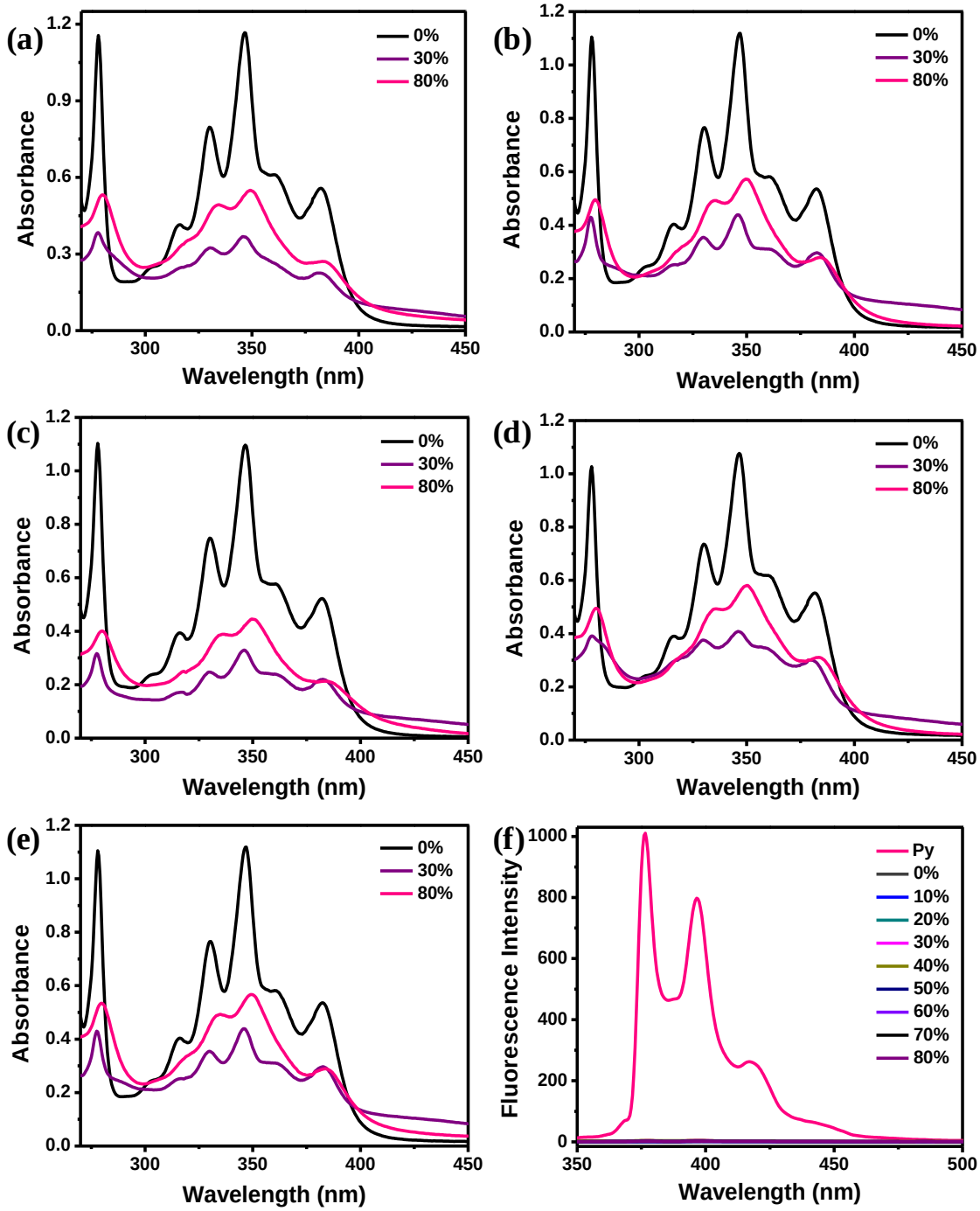


**Figure 19.** UV-vis absorption spectra of a 200 μM solution of (a) **1**, (b) **2**, (c) **3**, (d) **4** and (e) **5** in aqueous DMSO containing various percentages of water. (f) Fluorescence spectra of pyrenemethylamine hydrochloride (Py for comparsison) and 200 μM solution of **1** in aqueous DMSO. The values represent various percentages of water in aqueous DMSO.

**1**, a decrease in absorption intensity as well as broadening of the band was observed, which indicates molecular aggregation. Up to 30% aqueous DMSO, only a decrease in the absorption intensity was observed without any appreciable changes in the absorption maxima ($\lambda_{max}$). Interestingly, with a further increase in water content in the DMSO solution of **1**, a bathochromic shift of around 3 nm with respect to the band at 330 nm ($\lambda_{max}$), as well as an increase in the absorption intensity, was observed. Thus, these absorption characteristics of **1** suggest the formation of two different kinds of aggregates at 30% and 80% aqueous DMSO, which are termed as AGG1 and AGG2 (AGG = aggregate), respectively (see below). Similar spectral features were observed for **2-5** in aqueous DMSO, which suggests identical molecular aggregation behavior (Figure 19b-e). In addition, the fluorescence emission of both the pyrene and NDI units in **1-5** was found to be quenched in DMSO as well as in aqueous DMSO (Figure 19f). Interestingly, in aqueous DMSO, brick-red free-floating aggregates of **1-5** were found to form within a

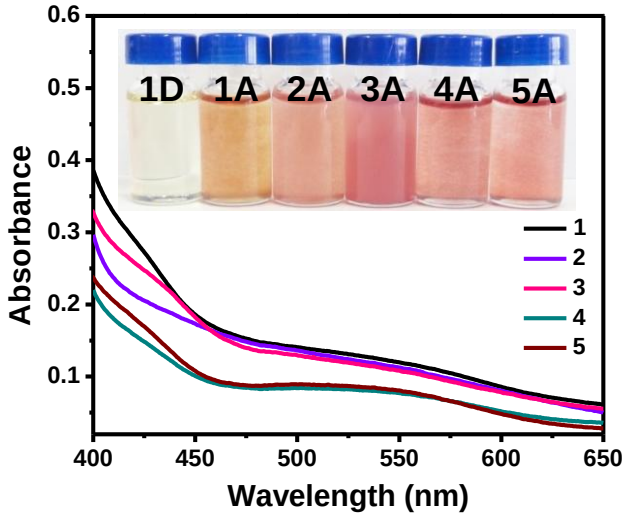


**Figure 20.** Absorption spectra of a 1 mM solution of **1–5** in 30% aqueous DMSO showing the charge-transfer band. The inset shows the characteristic brick-red free-floating aggregates formed in 1 mM solutions of **1–5** (1A–5A) in 30% aqueous DMSO within a few hours of sample preparation. 1D is a solution of **1** in DMSO alone.

couple of hours of sample preparation, which suggests a probable alternate stacking of NDI and pyrene (1A-5A; inset in Figure 20). Note that neither NDI nor pyrene are coloured in the visible region when dissolved individually (not shown) nor the dyad dissolved in only DMSO (1D; inset in Figure 20). Furthermore, the UV-vis spectra of **1-5** clearly show the characteristic broad absorption band in the region of 400-600 nm, which confirms the charge-transfer complexation of NDI and pyrene (Figure 20). The differences in the intensities of the charge-transfer bands for **1-5** can be ascribed to the steric and geometrical constraints in the complexes formed by NDI and pyrene.

### 2.3.2. Circular dichroism studies

To gain further insights into their mode of aggregation and also to detail the relationship between chirality and function, circular dichroism (CD) studies were performed. A DMSO solution of **3** did not show any CD features, which indicates the absence of excitonic coupling between the chromophores (Figure 21a). However, **3** in 30% aqueous DMSO exhibits a bisignated Cotton effect in the region of 270-400 nm, which corresponds to characteristic π-π* transitions of NDI and pyrene. The negative sign of the first Cotton effect indicates a left-handed (*M*-type) supramolecular helical organization of **3**. More interestingly, the transcription of molecular chirality from the L-isoleucine methyl ester is extended to the pyrene unit through the covalently interlinked NDI, which can be ascribed to the domino effect. The band at 278 nm, which is due to $S_0$-$S_3$ transitions in pyrene, shows a negative bisignated couplet centered at 280 nm, consistent with an *M*-type helical arrangement of adjacent pyrene transition dipoles within the

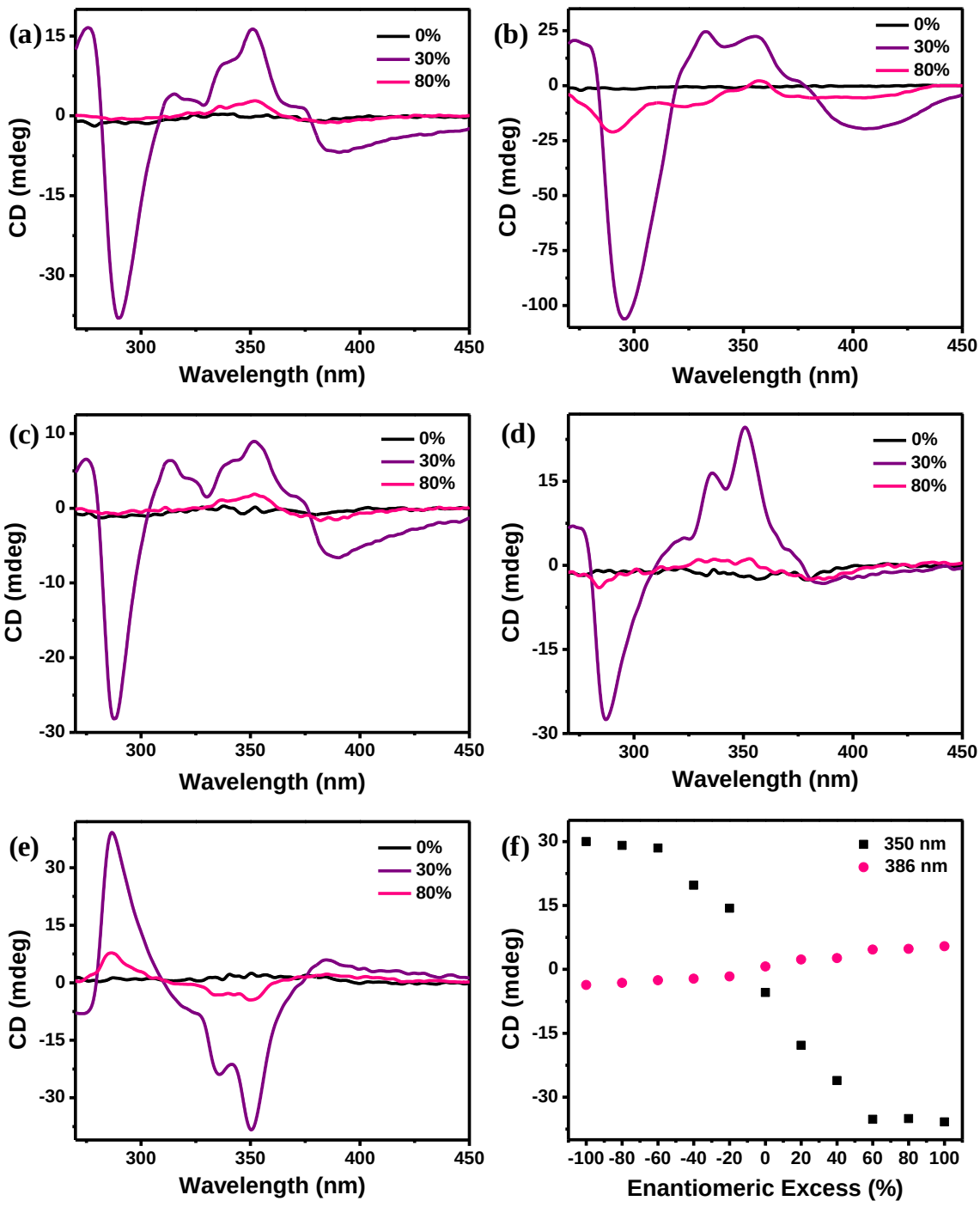


**Figure 21.** CD spectra of (a) **3**, (b) **1** (c) **2**, (d) **4** and (e) **5** in aqueous DMSO containing various percentages of water. (f) Results of majority-rule experiments for **4**/**5** monitored at 350 nm and 386 nm in 30% aqueous DMSO.

assembly. Furthermore, at 80% aqueous DMSO very weak CD signals are observed for **3**, which can be attributed to effective charge-transfer-induced CD silencing. Thus, the observed distinct CD spectral features of **3** in 30% and 80% aqueous DMSO is consistent with the two kinds of aggregates (AGG1 and AGG2; Figure 19a) found in absorption studies. Identical CD spectral characteristics were also observed for **1**, **2** and **4** (Figure 21b-d) in DMSO as well as in aqueous DMSO. However, **5** shows a complementary Cotton effect with a right-handed (*P*-type) supramolecular helicity as the transcription of chirality is from D-phenylalanine methyl ester (Figure 21e). Furthermore, we subjected the two enantiomers **4** and **5** to a majority-rules experiment to evaluate the amplification of chirality. The non-linear plot of CD amplitude versus enantiomeric excess indeed shows appreciable amplification in the majority-rules experiment (Figure 21f). PXRD patterns of **1**-**5** show reflections at around 3.36 Å, which corresponds to the inter-planar

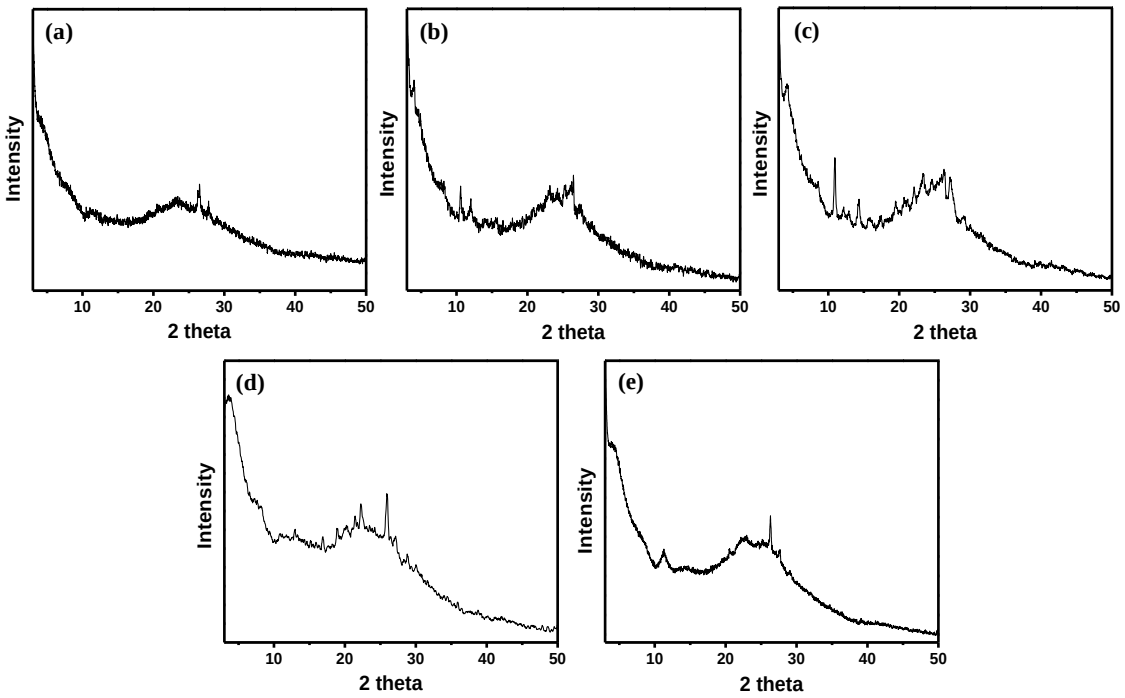


**Figure 22.** PXRD spectra of (a) **1**, (b) **2** (c) **3**, (d) **4** and (e) **5**.

distances between stacked NDI and pyrene (Figure 22). In addition, the reflection at around 21 Å in the small-angle region correlates well with the calculated end-to-end length of dimers of the functional molecules (~21 Å) and can thus be ascribed to the distance between their centers in two laterally assembled structures.

### 2.3.3. Morphological studies

The free-floating self-assembled aggregates of **1**-**5** formed in aqueous DMSO were subjected to morphological studies. The two kinds of aggregates, namely AGG1 and AGG2, formed from **1**-**5** in 30% and 80% aqueous DMSO, respectively, were investigated extensively under electron and scanning probe microscopes. The L-alanine methylester appended functional molecule **1** in 30% aqueous DMSO shows 2D sheet architectures (Figure 23a). Typically, these sheets have lengths of up to around 2 μm and widths in the range of 0.2-1.4 μm. The 2D sheet architecture emphasizes the fact that the tendency for molecular assembly (strength of inter molecular interactions) of **1** along its length and breadth is nearly equal. Although there is no clear demarcation between sheets and short belt-like architectures, we had earlier proposed that an aspect ratio (length to breadth) of ~10 corresponds to sheets, based on reports in the literature.[84] AFM revealed that the topographical thickness (height) of these sheets is in the range of 20-50 nm. However, **1** in 80% aqueous DMSO shows 1D belts with lengths in the order of several microns (Figure 23b). Interestingly, the widths of these belts are in between 100 nm and 500 nm, and their heights are 15-80 nm. Thus, it appears that in 80% aqueous DMSO, enhanced hydrophobic force induced aromatic stacking predominates along the length of

the belt in contrast to the van der Waals force driven lateral association of **1** along its breadth. Similarly, the L-valine methyl ester appended functional molecule **2** was found to assemble into 2D comb-edged flakes (Figure 23c) and 1D belts (Figure 23d) in 30% and 80% aqueous DMSO, respectively. The 2D comb-edged flakes are 1-2 μm in length with widths of 0.5-1 μm and heights in the range of 50-100 nm. The 1D belts of **2** are a few hundreds of microns long with their widths in the range of 50-300 nm.

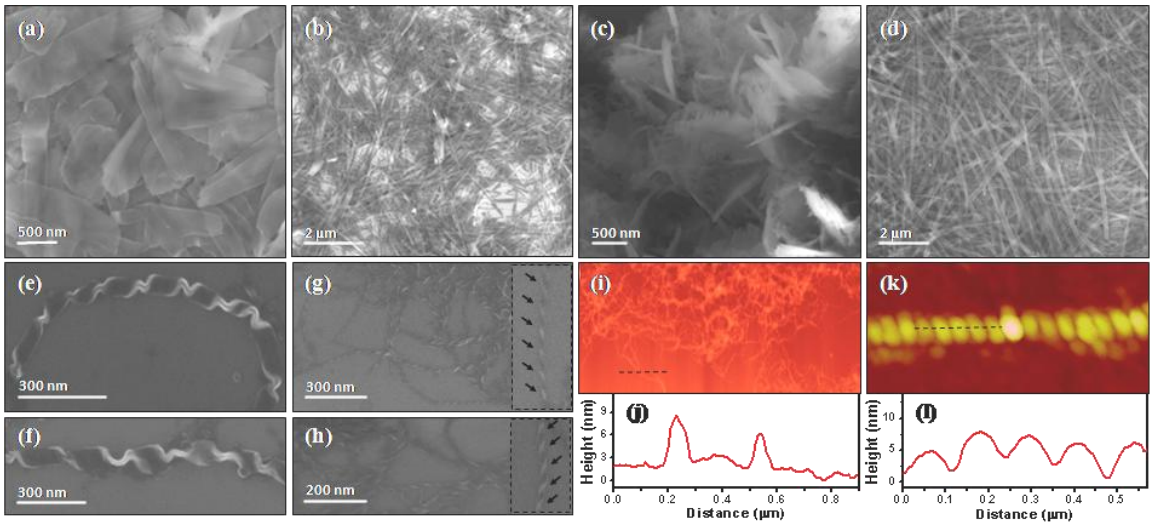


**Figure 23.** Field emission scanning electron microscopy (FESEM) images of (a) **1** in 30% aqueous DMSO, (b) **1** in 80% aqueous DMSO, (c) **2** in 30% aqueous DMSO, (d) **2** in 80% aqueous DMSO, (e) **3** in 30% aqueous DMSO, (f) **3** in 80% aqueous DMSO, (g) **4** in 30% aqueous DMSO and (h) **5** in 30% aqueous DMSO. The insets in (g) and (h) are high-resolution micrographs of the left- and right-handed supercoiled helices of **4** and **5**, respectively. (i) Atomic force microscopy (AFM) image of **4** in 30% aqueous DMSO and (j) the corresponding height profile along the dashed black line in (i). (k) AFM image of **5** in 30% aqueous DMSO and (l) the corresponding height profile along the dashed black line in (k).

On the other hand, 1D twisted ribbons are observed for L-isoleucine methyl ester appended functional molecule **3** in 30% aqueous DMSO (Figure 23e). Moreover, the

free-floating aggregates of **3** formed in 80% aqueous DMSO were also found to be 1D twisted ribbons (Figure 23f). These twisted ribbons have widths of 50-125 nm, topographical thicknesses of 35-60 nm and lengths of several microns. In addition, the pitch of the helix was found to be around 200 nm. Interestingly, L-phenylalanine methyl ester appended functional molecule **4** shows 1D supercoiled helix structures in both 30% and 80% aqueous DMSO (Figure 23g). Similarly, 1D supercoiled helix structures are observed for D-phenylalanine methyl ester appended functional molecule **5** (Figure 23h). The resultant supercoiled helix structures of **4** and **5** exhibit left- and right-handed helical signatures, which is consistent with the CD studies. The widths of these supercoiled helices were found to be around 100 nm, whereas the helical pitches are around 120 nm and the heights from 4 to 20 nm (Figure 23i–l). Although the photophysical studies of **3**-**5** showed the existence of two different kinds of aggregates (AGG1 and AGG2 in 30% and 80% aqueous DMSO, respectively), the absence of appreciable differences in their morphologies is believed to be a result of variations in structural organization that make minimal contributions to the overall supramolecular architecture. Subsequently, we carried out further studies to gain an understanding of the nature of the supramolecular architecture upon mixing **4** and **5** in a majority-rules experiment. This study showed the existence of both left- and right-handed supercoiled helices in the mixed sample, and in addition non-helical 1D belts were also observed (Figure 24). The formation of non-helical nanobelts is most likely due to the mixing of oppositely helical **4** and **5** into a single 1D architecture that nullifies the net helical contributions from **4** and **5**.

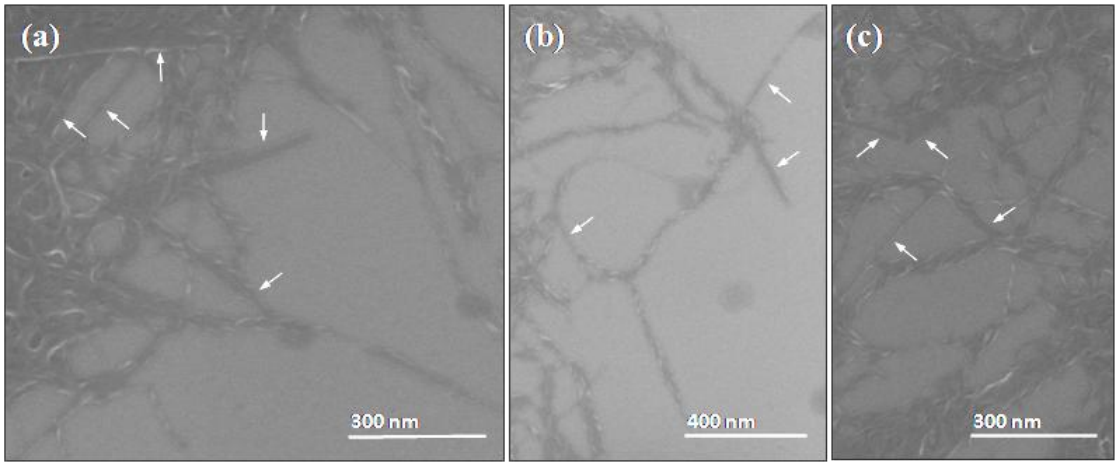


**Figure 24.** a), b) and c) FESEM images of **4** and **5** when subjected to Majority-rules experiment in 30% aqueous DMSO. The arrows show the non-helical belt like architectures.

### 2.3.4. Theoretical studies and discussion

The above-discussed 1D or 2D supramolecular architectures, namely nanobelts, twisted nanoribbons, supercoiled helices, comb-edged nanoflakes and nanosheets, formed by our functional molecules are a result of the information stored in their molecular structure, which ultimately governs the recognition events at the molecular level. The photophysical studies indeed confirmed that the NDI and pyrene units of the functional modules form stacks, supposedly due to the envisioned topological shape similarity and π-complementarity. However, to gain greater insights into the energetics as well as stereochemical and geometrical constraints of the functional molecules, ab initio DFT studies were performed by using the Gaussian 09 package.[85] For the DFT calculations, we employed the B3LYP exchange correlation functional with the 6-31+g(d,p) basis set for all atoms.[86] For the optimization of the dimer formed by homo- or hetero-stacking of two functional modules, we used the ωB97XD exchange correlation functional, which

includes empirical dispersion and long-range correlation with the 6-31g(d) basis set.[87,88] In general, when two different chromophores like NDI and pyrene are mixed, the result could be either a self-sorted (NDI–NDI and pyrene– pyrene) or alternate (NDI–pyrene) assembly. To predict the outcome of such a scenario, we estimated the interaction energies of hetero- and homo-stacked NDI and pyrene (Figure 18 and Table 1). The interaction energies for NDI-NDI, pyrene-pyrene and NDI-pyrene complexes are -27.17, -16.45 and -23.35 kcalmol$^{-1}$, respectively, which suggests that molecular self-sorting (driven mainly by the stacking of two π-acidic NDIs, which would experience reduced electrostatic repulsions) is most likely to predominate over alternate assembly unless aided by an additional molecular interaction.

Alternatively, interaction energies of -8.43 and -10.05 kcal mol$^{-1}$ were obtained for homo-stacked naphthalene (Nap) and 1,5-dihydroxynaphthalene (DHN), respectively (Figure 25), whereas hetero-stacked NDI-Nap and NDI-DHN have interaction energies of -17.39 and -19.85 kcal mol$^{-1}$, respectively (Figure 25). Consequently, an interaction energy difference of around 6 kcal mol$^{-1}$ between the hetero-stacks of NDI-pyrene (-23.35

**Table 1.** Computed interaction energies (*E*) of homo- and hetero-stacked functional modules.

| Functional Modules | *E* in kcal mol$^{-1}$ |
|---|---|
| NDI-NDI[a] | -27.17 |
| Pyrene-pyrene | -16.45 |
| Nap-Nap[b] | -8.43 |
| DHN-DHN[c] | -10.05 |
| NDI-pyrene | -23.35 |
| NDI-Nap | -17.39 |
| NDI-DHN | -19.85 |

[a] NDI = naphthalenediimide, [b] Nap = naphthalene, [c] DHN = 1,5-dihydroxynaphthalene.

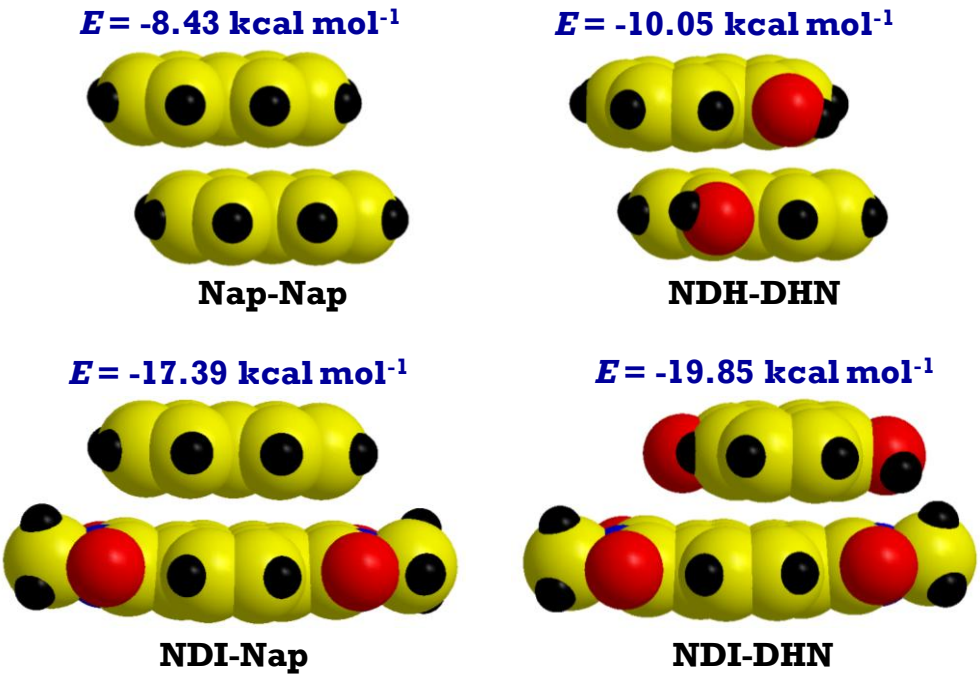


**Figure 25.** Energy-minimized structures of naphthalene–naphthalene (Nap–Nap), 1,5-dihydroxynaphthalene–1,5-dihydroxynaphthalene (DHN–DHN), naphthalenediimide–naphthalene (NDI-Nap) and naphthalenediimide–1,5-dihydroxynaphthalene (NDI–DHN) stacking with their respective estimated interaction energies (*E).*

kcal $mol^{-1}$) and NDI-Nap (-17.39 kcal $mol^{-1}$) can be ascribed to the topological shape similarity of NDI and pyrene. Unsurprisingly, in the literature, molecular NDI is most commonly found in a self-sorted assembly when mixed with donors like dialkoxynaphthalene (DAN) at room temperature.[89,90] On the other hand, mixing an oligomer/polymer of NDI with another oligomer/polymer of a donor like pyrene or DAN was found to facilitate charge-transfer complexation.[91,92] However, it should be noted that in the latter case, a 1:1 co-assembly of all NDI and pyrene/DAN units may not be feasible, and in addition a well-defined supramolecular architecture has not been realized to the best of our knowledge. Alternatively, a smarter design involving a dyad of NDI and pyrene should facilitate mixed stacking rather than a self-sorted assembly (Figure

18). Logically, the self-sorting of a hypothetical dyad of NDI-pyrene accounts for an interaction energy of -43.62 kcal $mol^{-1}$ [-(27.17 + 16.45) kcal $mol^{-1}$], whereas alternate stacking results in -46.7 kcal $mol^{-1}$ [–(23.35 + 23.35) kcal $mol^{-1}$]. To further validate our hypothesis, we first obtained energy-minimized structures of our functional molecules, which, as expected, revealed V-shaped structures due to the presence of the methylene linker between the NDI and pyrene units. The characteristic V-shaped geometric structure of the functional molecules allows four modes (I-IV) of dimerization (Figure 26a). Of these, mode IV has the most stable structure; the three remaining modes, I-III, are not so stable due to energetically unfavourable aromatic interactions and steric repulsions. The geometry optimizations of the dimers of **4** and **5** show alternate stacking of NDI and pyrene with interaction energies of -52.10 and -53.62 kcal $mol^{-1}$, respectively (Figure 26b,c). In addition, computational studies showed the charge-transfer interaction of NDI and pyrene units with $\lambda_{max}$ = 519 nm (Figure 27).

Having understood the origin and nature of the primary molecular interactions in our functional modules, that is, charge-transfer complexation, we performed additional analyses to account for the observed supramolecular architectonics. The resulting differences in the molecular assemblies of our functional molecules, namely, nanosheets and nanobelts from alanine derivative **1**, comb-edged nanoflakes and nanobelts from valine derivative **2**, twisted nanoribbons from isoleucine derivative **3** and supercoiled helices from phenylalanine derivatives **4** and **5**, can all be ascribed to molecular structural mutations in the side-chain of the amino acid (Figure 28 and Table 2). The side-chains of alanine, valine, isoleucine and phenylalanine possess an estimated hydrophobicity of 1.0, 2.2, 2.7 and 2.3 kcal $mol^{-1}$, respectively whereas their non-polar surface areas (excluding

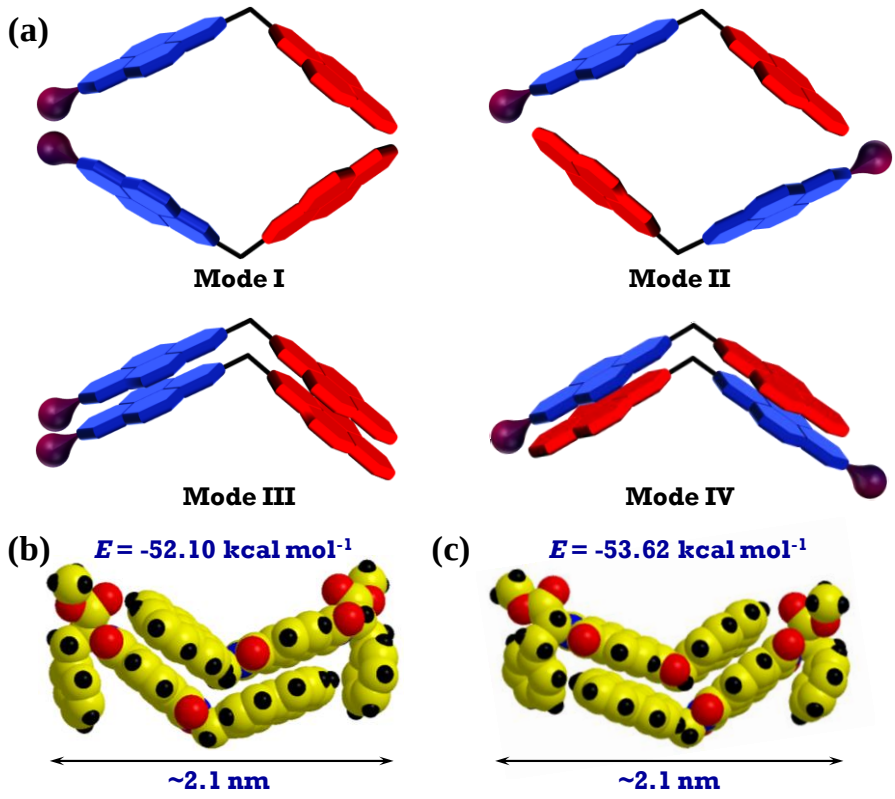


**Figure 26.** (a) Schematic representation of four plausible modes of dimerization for functional molecules **1**–**5**. (b,c) Energy-minimized structures of dimers of **4** and **5**,

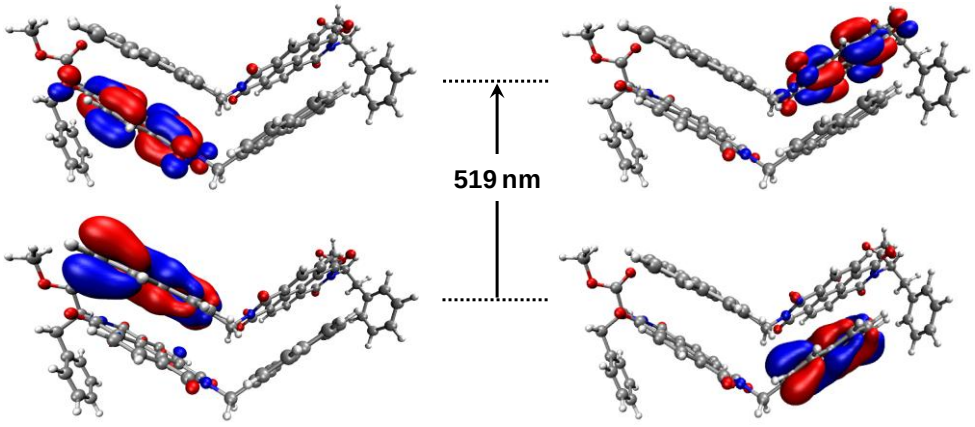


**Figure 27.** Molecular orbital diagrams depicting the charge-transfer interaction between NDI and pyrene in **4**. The value of 519 nm is the wavelength of the absorption maxima predicted by using time-dependent density functional theory (TD-DFT) as implemented in the Gaussian 09 package. The B3LYP exchange correlation was used for the TD-DFT calculations.

**Table 2.** Hydrophobicity and surface area of the amino acid functionalities.

| Functionality | Hydrophobicity[a] [kcal mol$^{-1}$] | Surface area[b] [Å$^2$] |
|---|---|---|
| alanine | 1.0 | 86 |
| valine | 2.2 | 135 |
| isoleucine | 2.7 | 155 |
| phenylalanine | 2.3 | 194 |

[a] Estimated hydrophobicity of the side-chain of the respective amino acid. [b] Non-polar surface area (excluding methyl ester functionality) of the respective amino acid.

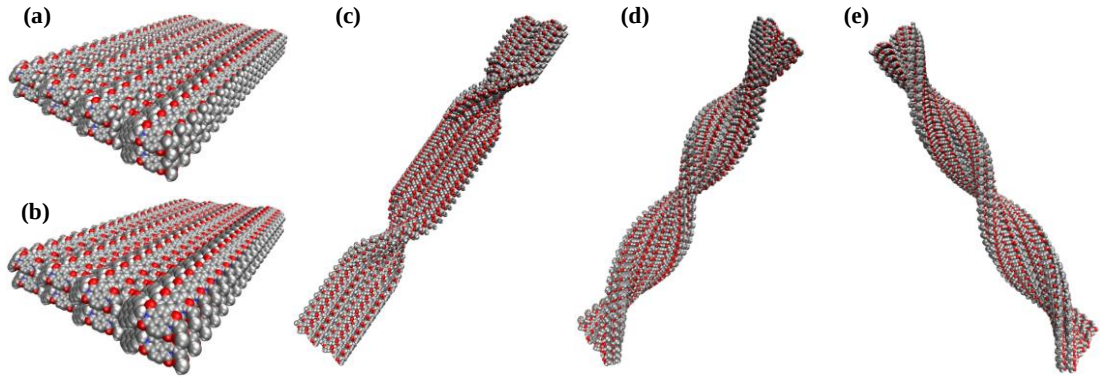


**Figure 28.** Schematic representation of the molecular organization of (a) **1**, (b) **2**, (c) **3**, (d) **4** and (e) **5** in aqueous DMSO. The energy-optimized structures obtained by using the B3LYP exchange correlation functional with the 6-31+g(d,p) basis set were employed to arrive at the proposed molecular packing models.

the methyl ester functionality) vary from 86 to 194 Å$^2$ (Table 2).[93] At the same time, the hydrophobic nature of the amino acid residues plays an equally important role by facilitating hydrophobic interactions in aqueous solutions. Moreover, based on our earlier experience we believe that the conversion of the carboxylic acid group of the amino acids into the methyl ester is necessary to eliminate any probable counter hydrophilic interactions in aqueous solution.[15] Although the steric bulkiness of the side-chain increases by a factor of 1.57 from alanine (86 Å$^2$) to valine (135 Å$^2$), it is believed that it

is still below the threshold for inducing helicity into the supramolecular architecture. However, the greater steric repulsion rendered by the side-chains of isoleucine (155 $Å^2$; 1.80 times that of alanine) and phenylalanine (194 $Å^2$; 2.25 times that of alanine) is thought to result in twisted belts and supercoiled helices, respectively. Moreover, the left- and right-handed supercoiled helical architectures of **4** and **5** arise from the transcription of chirality from the L- and D-phenylalanine methyl ester functionalities, respectively.

### 2.3.5. Conclusions

We have designed and developed amino acid appended functional molecules **1**-**5** comprising NDI and pyrene modules. These functional molecules are unique in terms of their design as they comprise topologically matching π-complementary modules. Such a design was envisioned to be the structural analogue of the lock-and-key model. Interestingly, the functional molecules **1**-**5** assembled into free-floating aggregates in aqueous DMSO due to enhanced hydrophobic forces in aqueous solutions. Moreover, we have shown that this design strategy was instrumental to exploit the intermolecular charge-transfer complexation of NDI and pyrene unlike the predominant self-sorted assembly observed for single-component systems. With the aid of DFT calculations we have shown that the alternate stacking of functional aromatic modules could be energetically controlled by smarter molecular designs. In addition, by incorporating systematic structural mutations into the side-chains of the amino acid auxiliaries, we have shown that the molecular assemblies can be tailored effectively to give well-defined 1D and 2D supramolecular nanoarchitectures. In particular, supercoiled helices, twisted

nanoribbons, nanobelts, comb-edged nanoflakes and nanosheets were realized through minute structural mutations in **1**-**5**. We further hope that this work will inspire the design and development of novel as well as improved molecular systems in an enduring effort to master the art of molecular programming and to decipher the role of molecular structure in complex biochemical processes through the intriguing systems-chemistry approach.

### 2.3.6. Experimental section

#### *2.3.6.1. Materials and methods*

1,4,5,8-Naphthalenetetracarboxylic dianhydride, 1-pyrenemethylamine hydrochloride and *N*, *N*-diisopropylethylamine were obtained from Sigma–Aldrich. L-Isoleucine, L-alanine, L-valine, L-phenylalanine, D-phenylalanine and acetyl chloride were obtained from Spectrochem Pvt. Ltd. Mumbai, India. All other reagents and solvents were of reagent- and spectroscopy grade and used without further purification. $^{1}H$ and $^{13}C$ NMR spectra were recorded at 298 K with a Bruker AV-400 spectrometer with chemical shifts reported in ppm (in [$D_6$] DMSO with tetramethylsilane as internal standard). Mass spectra were obtained with an HRMS 6200 series TOF/6500 series spectrometer (Agilent Technologies). Elemental analysis was carried out with a ThermoScientific FLASH 2000 Organic Element Analyzer.

*Absorption spectroscopy:* UV-vis spectra were recorded with a Perkin–Elmer Model Lambda 900 spectrophotometer. Samples (200 μM / 1 mM) were analysed in quartz cuvettes of 1 mm pathlength.

*Fluorescence spectroscopy:* Fluorescence spectra were recorded with a Perkin–Elmer Model LS-55 spectrophotometer. Samples (200 μM) were analysed in quartz cuvettes of 1 mm pathlength with excitation at 330 nm.

*Circular dichroism (CD) spectroscopy:* CD measurements were performed with a Jasco J-815 spectrometer under nitrogen. The sensitivity, time constant and scan rate were chosen appropriately. Samples (400 μM) were analysed in quartz cuvettes of 1 mm pathlength.

*Field-emission scanning electron microscopy (FESEM):* FESEM micrographs were acquired by using a FEI Nova nanoSEM-600 microscope equipped with a field-emission gun operating at 5 kV. Samples were prepared by drop-casting the free-floating aggregates on Si(111) substrate and allowing them to dry under ambient conditions.

*Atomic force microscopy (AFM):* AFM micrographs were acquired under ambient conditions with an Innova (Veeco) atomic force microscope in dynamic force (tapping) mode. The sample was prepared by drop-casting the free-floating aggregates on Si(111) substrate and allowing them to dry under ambient conditions. AFM section analysis was carried out offline.

*Powder X-ray diffraction (PXRD):* PXRD patterns were recorded with a Rigaku-99 (Miniflex) diffractometer by using Cu-$K_\alpha$ radiation ($\lambda$ = 1.5406 Å). The free-floating self-assembled aggregates of **1**-**5** were placed in a petridish and allowed to dry under ambient conditions. The solvent-free aggregates thus obtained were transferred to a glass slide to collect the diffraction data.

### *2.3.6.2. Synthesis of* 1

*Synthesis of L-alanine methyl ester hydrochloride:* Anhydrous methanol (50 mL) was placed in a 100 mL 2-necked round-bottom flask fitted with a reflux condenser and an additional dropping funnel, cooled to ice temperature. Acetyl chloride (3 mL) was added drop-wise through the dropping funnel. After 15 min, L-alanine (3 g) was added, and the reaction mixture was refluxed at 70 °C for 24 h ensuring complete conversion of the carboxylic acid to the methyl ester. The reaction mixture was vacuum-dried with successive co-evaporation with toluene to obtain the pure L-alanine methyl ester hydrochloride. $^{1}$H NMR (400 MHz, $D_2O$): δ = 4.26 (q, 1 H, α-carbon proton), 3.86 (s, 3 H, methyl ester protons), 1.59 (d, *J* = 8 Hz, 3 H, methyl protons) ppm.

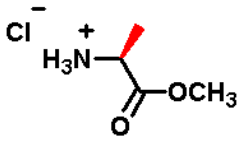


1,4,5,8-Naphthalenetetracarboxylic dianhydride (200 mg, 0.74 mmol), L-alanine methyl ester hydrochloride (104 mg 0.74 mmol) and 1-pyrenemethylamine hydrochloride (200 mg, 0.74 mmol) together with *N*,*N*-dimethylformamide (DMF) (20 mL) and *N*, *N*-diisopropylethylamine (1 mL) were heated at 110 °C for 36 h. Herein, mainly three products could be expected, *viz.* naphthalenediimide with L-alanine methyl ester as the imide substituents on both sides (denoted as Ala-NDI-Ala); naphthalenediimide with 1-pyrenemethylamine as the imide substituents on both sides (denoted as Py-NDI-Py); naphthalenediimide with L-alanine methyl ester and 1-pyrenemethylamine as the imide substituent on either sides (expected product **1**). The product pyrene-NDI-pyrene is insoluble in most of the solvents supposedly due to lack of any chemical functionality to

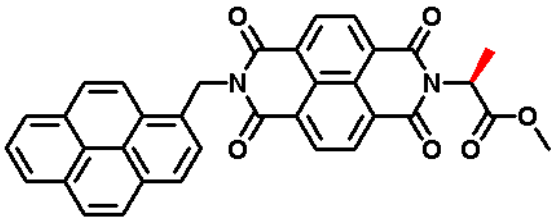

facilitate solubility. The product Ala-NDI-Ala is highly soluble in non-polar organic solvents like chloroform, while the expected product **1** (pyrene-NDI-Ala) possess limited solubility (ca. 1 mg/mL) in solvents like DMF and dimethylsulfoxide (DMSO). The resulting reaction mixture containing a precipitate was filtered, and the filtrate was dried under vacuum and then subjected to thorough washing with chloroform and methanol to obtain the expected product **1**. Yield 10 %. $^{1}$H NMR (400 MHz, [$D_6$] DMSO): δ = 8.75 (br., 4 H, NDI aromatic protons), 8.66 (br., 1 H, pyrene aromatic proton), 8.34 (br., 3 H, pyrene aromatic protons), 8.15 (br., 4 H, pyrene aromatic protons), 7.98 (br., 1H, pyrene aromatic proton), 6.06 (s, 2 H, methylene protons), 5.62 (br., 1 H, α-carbon proton), 3.65 (s, 3 H, methyl ester protons), 1.61 (d, *J* = 8 Hz, 3 H, methyl protons) ppm. HRMS (ESI): calcd. for $C_{35}H_{23}N_2O_6$ $[M + H]^+$ 567.1556; found 567.1522. $C_{35}H_{22}N_2O_6$ (566.15): calcd. C 74.20, H 3.91, N 4.94; found C 74.15, H 3.95, N 4.93.

### *2.3.6.3. Synthesis of* 2

*Synthesis of L-valine methyl ester hydrochloride:* Anhydrous methanol (50 mL) was placed in a 100 mL 2-necked round-bottom flask fitted with a reflux condenser and an additional dropping funnel, cooled to ice temperature. Acetyl chloride (3 mL) was added drop-wise through the dropping funnel. After 15 min, L-valine (3 g) was added, and the reaction mixture was refluxed at 70 °C for 24 h ensuring complete conversion of the carboxylic acid to the methyl ester. The reaction mixture was vacuum-dried with successive co-evaporation with toluene to obtain the pure L-valine methyl ester hydrochloride. $^{1}$H NMR (400 MHz,

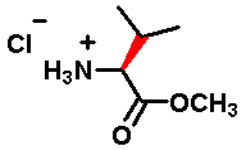

$D_2O$): δ = 4.05 (d, *J* = 4 Hz, 1 H, α-carbon proton), 3.87 (s, 3 H, methyl ester protons), 2.41-2.33 (m, 1H, β-carbon proton), 1.06 (dd, *J* = 4, 8 Hz, 6 H, methyl protons) ppm.

1,4,5,8-Naphthalenetetracarboxylic dianhydride (200 mg, 0.74 mmol), L-valine methyl ester hydrochloride (125 mg 0.74 mmol) and 1-pyrenemethylamine hydrochloride

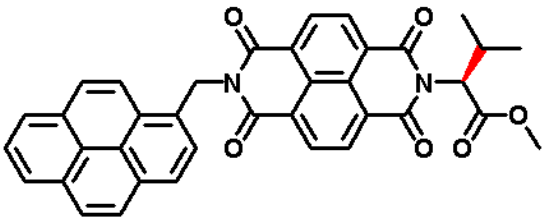

(200 mg, 0.74 mmol) together with DMF (20 mL) and *N*,*N*-diisopropylethylamine (1 mL) were heated at 110 °C for 36 h. Here also three main products could be expected as described above. The resulting reaction mixture containing a precipitate was filtered, and the filtrate was dried under vacuum and then subjected to thorough washing with chloroform and methanol to obtain the expected product **2**. Yield 12%. $^1$H NMR (400 MHz, [$D_6$] DMSO): δ = 8.68 (br., 4 H, NDI aromatic protons), 8.60 (d, *J* = 8 Hz, 1 H, pyrene aromatic proton), 8.31-8.25 (m, 3 H, pyrene aromatic protons), 8.14-8.04 (m, 4 H, pyrene aromatic protons), 7.95-7.90 (m, 1 H, pyrene aromatic proton), 6.00 (s, 2 H methylene protons), 5.16 (d, *J* = 8 Hz, 1 H, α-carbon proton), 3.63 (s, 3 H, methyl ester protons), 2.73–2.67 (m, 1 H, β-carbon proton), 1.25 (d, *J* = 4 Hz, 3 H, methyl protons), 0.76 (d, *J* = 8 Hz, 3 H , methyl protons) ppm. HRMS (ESI): calcd. for $C_{37}H_{27}N_2O_6$ $[M + H]^+$ 595.1869; found 595.1838. $C_{37}H_{26}N_2O_6$ (594.18): calcd. C 74.74, H 4.41, N 4.71; found C 74.76, H 4.44, N 4.69.

### *2.3.6.4. Synthesis of* 3

*Synthesis of L-isoleucine methyl ester hydrochloride:* Anhydrous methanol (50 mL) was placed in a 100 mL 2-necked round-bottom flask fitted with a reflux condenser and an additional dropping funnel, cooled to ice temperature. Acetyl chloride (3 mL) was added drop-wise through the dropping funnel. After 15 min, L-isoleucine (3 g) was added, and the reaction mixture was refluxed at 70 °C for 24 h ensuring complete conversion of the carboxylic acid to the methyl ester. The reaction mixture was vacuum-dried with successive co-evaporation with toluene to obtain the pure L-isoleucine methyl ester hydrochloride. $^{1}$H NMR (400 MHz, $D_2O$): d = 4.17 (d, *J* = 4 Hz,1 H, α-carbon proton), 3.89 (s, 3 H, methyl ester protons), 2.17-2.07 (m, 1 H, β-carbon proton), 1.57-1.47 (m, 1 H, γ-carbon proton), 1.43-1.32 (m, 1 H, γ-carbon proton), 1.06 (d, *J* = 8 Hz, 3 H, methyl protons), 0.98 (t, 3 H, methyl protons) ppm.

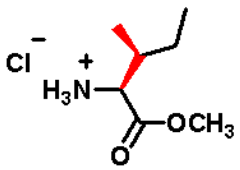


1,4,5,8-Naphthalenetetracarboxylic dianhydride (200 mg, 0.74 mmol), L-isoleucine methyl ester hydrochloride (135 mg 0.74 mmol) and 1-pyrenemethylamine hydrochloride (200 mg, 0.74 mmol) together with DMF (20 mL) and *N*, *N*-diisopropylethylamine (1 mL) were heated at 110 °C for 36 h. Here also three main products could be expected as described above. The resulting reaction mixture containing a precipitate was filtered, and the filtrate was dried under vacuo and then subjected to thorough washing with chloroform and methanol to obtain the expected product **3**. Yield 13 %. $^{1}$H NMR (400 MHz, [$D_6$] DMSO): δ = 8.76-8.71 (m, 4 H, NDI aromatic protons),

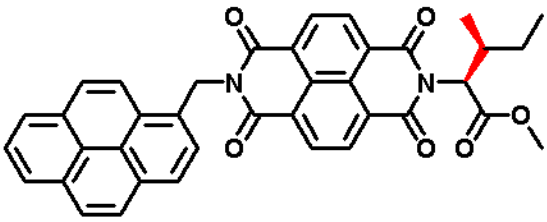

8.63 (d, *J* = 8 Hz, 1 H, pyrene aromatic proton), 8.34-8.28 m, 3 H, (pyrene aromatic protons), 8.16-8.07 (m, 4 H, pyrene aromatic protons), 7.95 (d, 1 H, *J* = 8 Hz, pyrene aromatic proton), 6.05 (s, 2 H, methylene protons), 5.25 (d, *J* = 8 Hz, 1 H, α-carbon proton), 3.61 (s, 3 H, methyl ester protons), 2.73-2.71 (m, 1 H, β-carbon proton), 1.33-1.27 (m, 1 H, γ-carbon proton), 1.22 (d, *J* = 8 Hz, 3 H, methyl protons), 0.98-0.92 (m, 1 H, γ-carbon proton), 0.76 (t, 3 H, methyl protons) ppm. HRMS (ESI): calcd. for $C_{38}H_{29}N_2O_6$ $[M+H]^+$ 609.2026; found 609.1996. $C_{38}H_{28}N_2O_6$ (608.19): calcd. C 74.99, H 4.64, N 4.60; found C 74.95, H 4.68, N 4.57.

### *2.3.6.5. Synthesis of* 4

*Synthesis of L-phenylalanine methyl ester hydrochloride:* Anhydrous methanol (50 mL) was placed in a 100 mL 2-necked roundbottom flask fitted with a reflux condenser and an additional dropping funnel, cooled to ice temperature. Acetyl chloride (3 mL) was added drop-wise through the dropping funnel. After 15 min, L-phenylalanine (3 g) was added, and the reaction mixture was refluxed at 70 °C for 24 h ensuring complete conversion of the carboxylic acid to the methyl ester. The reaction mixture was vacuum-dried with successive co-evaporation with toluene to obtain the pure L-phenylalanine methyl ester hydrochloride. $^1$H NMR (400 MHz, $D_2O$): δ = 7.50-7.33 (m, 5 H, phenyl aromatic protons), 4.49 (t, 1 H, α-carbon proton), 3.89 s, 3 H, (methyl ester protons), 3.41 (dd, *J* = 4, 8 Hz, 1 H, methylene proton), 3.30 (dd, *J* = 4, 8 Hz, 1 H, methylene proton) ppm.

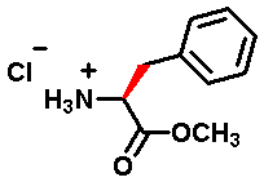

1,4,5,8-Naphthalenetetracarboxylic dianhydride (200 mg, 0.74 mmol), L-phenylalanine methyl ester hydrochloride (160 mg 0.74 mmol) and 1-pyrenemethylamine hydrochloride (200 mg, 0.74 mmol) together with DMF (20 mL) and *N*, *N*-diisopropylethylamine (1 mL) were heated at 110 °C for 36 h. Here also three main products could be expected as described above. The resulting reaction mixture containing a precipitate was filtered, and the filtrate was dried under vacuum and then subjected to thorough washing with chloroform and methanol to obtain the expected product **4**. Yield 13 %. $^1$H NMR (400 MHz, [$D_6$] DMSO): δ = 8.72-8.61 (m, 5 H, NDI and pyrene aromatic protons), 8.36-8.30 (m, 3 H, pyrene aromatic protons), 8.16-8.08 (m, 4 H, pyrene aromatic protons), 7.98 (d, 1 H, *J* = 8 Hz, pyrene aromatic proton), 7.19-7.05 (m, 5 H, phenyl aromatic protons), 6.04 (br., 3 H, α-carbon and methylene protons), 3.69 (s, 3 H, methyl ester protons), 3.66-3.59 (m, 1 H, methylene proton), 3.44-3.37 (m, 1 H, methylene proton) ppm. HRMS (ESI): calcd. for $C_{41}H_{27}N_2O_6$ $[M+H]^+$ 643.1869; found 643.1836. $C_{41}H_{26}N_2O_6$ (642.18): calcd. C 76.63, H 4.08, N 4.36; found C 76.61, H 4.12, N 4.33.

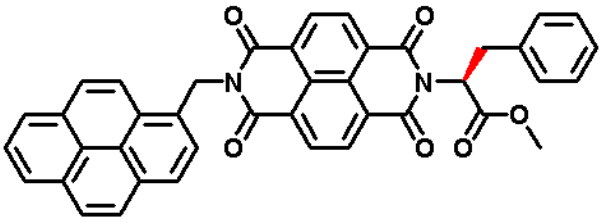

### *2.3.6.6. Synthesis of* **5**

*Synthesis of D-phenylalanine methyl ester hydrochloride:* Anhydrous methanol (50 mL) was placed in a 100 mL 2-necked round-bottom flask fitted with a reflux condenser and an additional dropping funnel, cooled to ice temperature. Acetyl chloride (3 mL) was

added drop-wise through the dropping funnel. After 15 min, D-phenylalanine (3 g) was added, and the reaction mixture was refluxed at 70 °C for 24 h ensuring complete

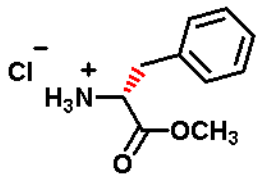


conversion of the carboxylic acid to the methyl ester. The reaction mixture was vacuum dried with successive co-evaporation with toluene to obtain the pure D-phenylalanine methyl ester hydrochloride. $^1$H NMR (400 MHz, $D_2O$): δ = 7.51-7.33 (m, 5 H, phenyl aromatic protons), 4.48 (t, 1 H, α-carbon proton), 3.88 (s, 3 H, methyl ester protons), 3.41 (dd, *J* = 4, 8 Hz, 1 H, methylene proton), 3.31 (dd, *J* = 4, 8 Hz, 1 H, methylene proton) ppm.

1,4,5,8-Naphthalenetetracarboxylic dianhydride (200 mg, 0.74 mmol), D-phenylalanine methyl ester hydrochloride (160 mg 0.74 mmol) and 1-pyrenemethylamine

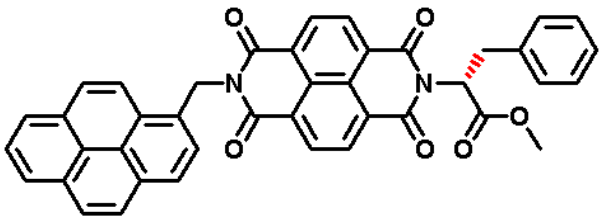


hydrochloride (200 mg, 0.74 mmol) together with DMF (20 mL) and *N*, *N*-diisopropylethylamine (1 mL) were heated at 110 °C for 36 h. Here also three main products could be expected as described above. The resulting reaction mixture containing a precipitate was filtered, and the filtrate was dried under vacuum and then subjected to thorough washing with chloroform and methanol to obtain the expected product **5**. Yield 12 %. $^1$H NMR (400 MHz, [$D_6$] DMSO): δ = 8.74-8.60 (m, 5 H, NDI and pyrene aromatic protons), 8.36-8.30 (m, 3 H, pyrene aromatic protons), 8.17-8.07 (m, 4 H, pyrene aromatic protons), 7.98 (d, *J* = 8 Hz, 1 H, pyrene aromatic proton), 7.19-7.06 (m, 5 H, phenyl aromatic protons), 6.03 (br., 3 H, α-carbon and methylene protons), 3.69 (s, 3 H, methyl ester protons), 3.66-3.58 (m, 1 H, methylene proton), 3.44-3.37 (m, 1 H, methylene proton) ppm. HRMS (ESI): calcd. for $C_{41}H_{27}N_2O_6$ $[M+H]^+$ 643.1869; found

643.1832. $C_{41}H_{26}N_2O_6$ (642.18): calcd. C 76.63; H 4.08, N 4.36; found C 76.64, H 4.10, N 4.38.

### 2.3.7. Appendix

- $^{1}H$ and $^{13}C$ NMR of **NDI-Trp**
- $^{1}H$ and $^{13}C$ NMR of **NDI-TrpOMe**
- $^{1}H$ and $^{13}C$ NMR of **L-NDI**
- $^{1}H$ and $^{13}C$ NMR of **D-NDI**
- $^{1}H$ NMR and HRMS of **1**
- $^{1}H$ NMR and HRMS of **2**
- $^{1}H$ NMR and HRMS of **3**
- $^{1}H$ NMR and HRMS of **4**
- $^{1}H$ NMR and HRMS of **5**
- Crystal data for **L-NDI**

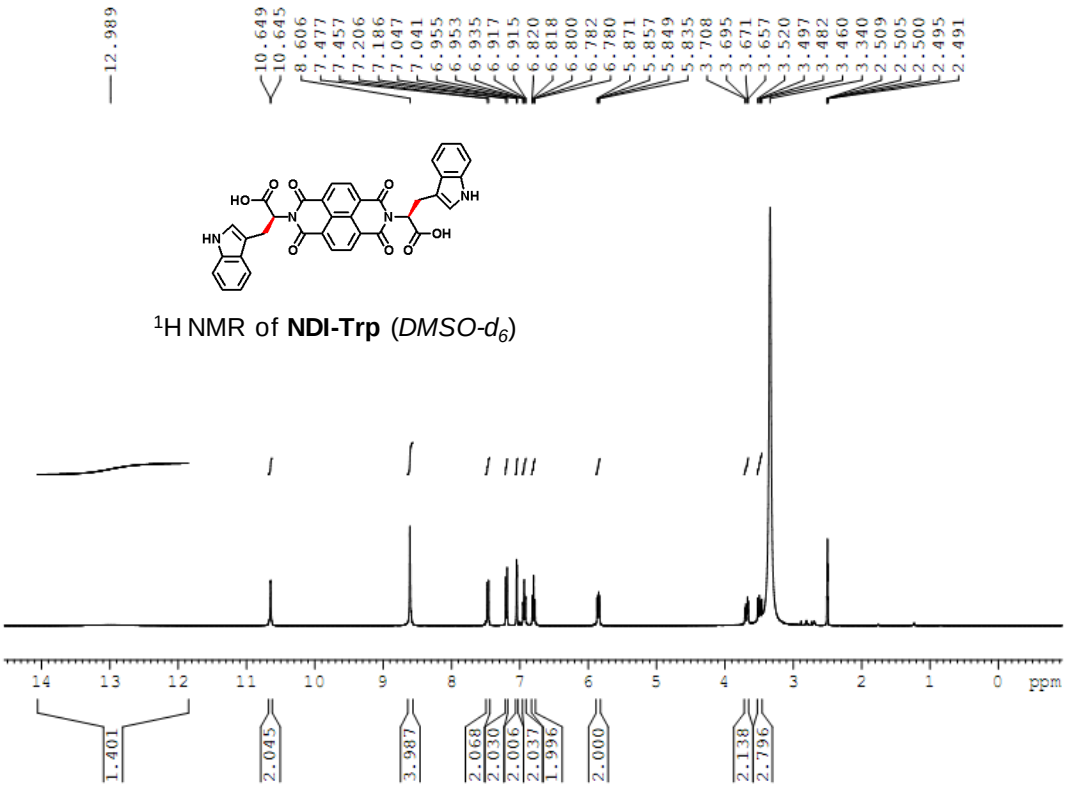


$^{1}$H NMR of **NDI-Trp** (*DMSO-$d_6$*)

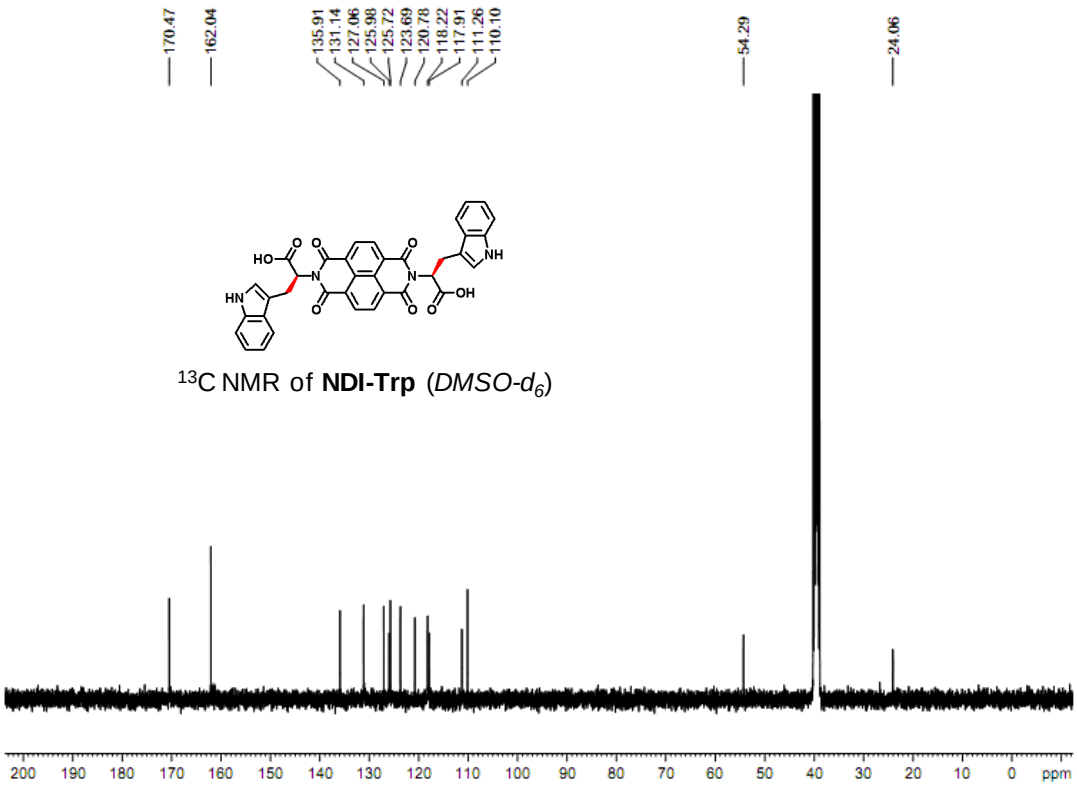


$^{13}$C NMR of **NDI-Trp** (*DMSO-$d_6$*)

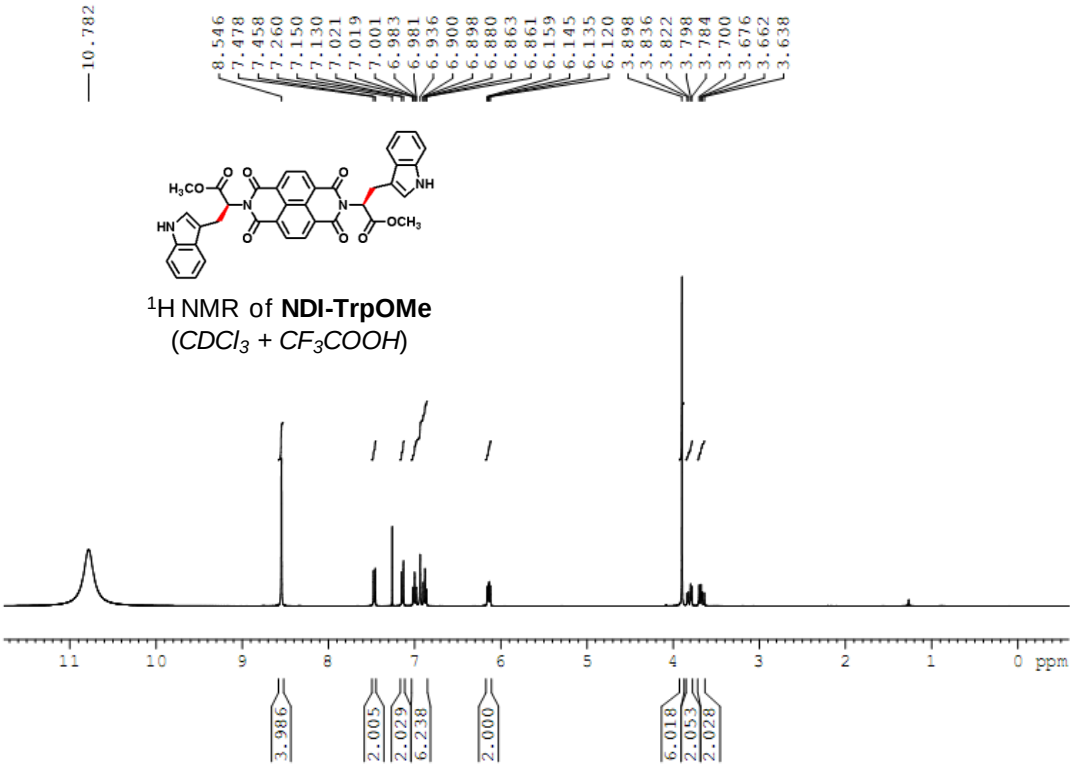


$^{1}$H NMR of **NDI-TrpOMe**
(*$CDCl_3$ + $CF_3COOH$*)

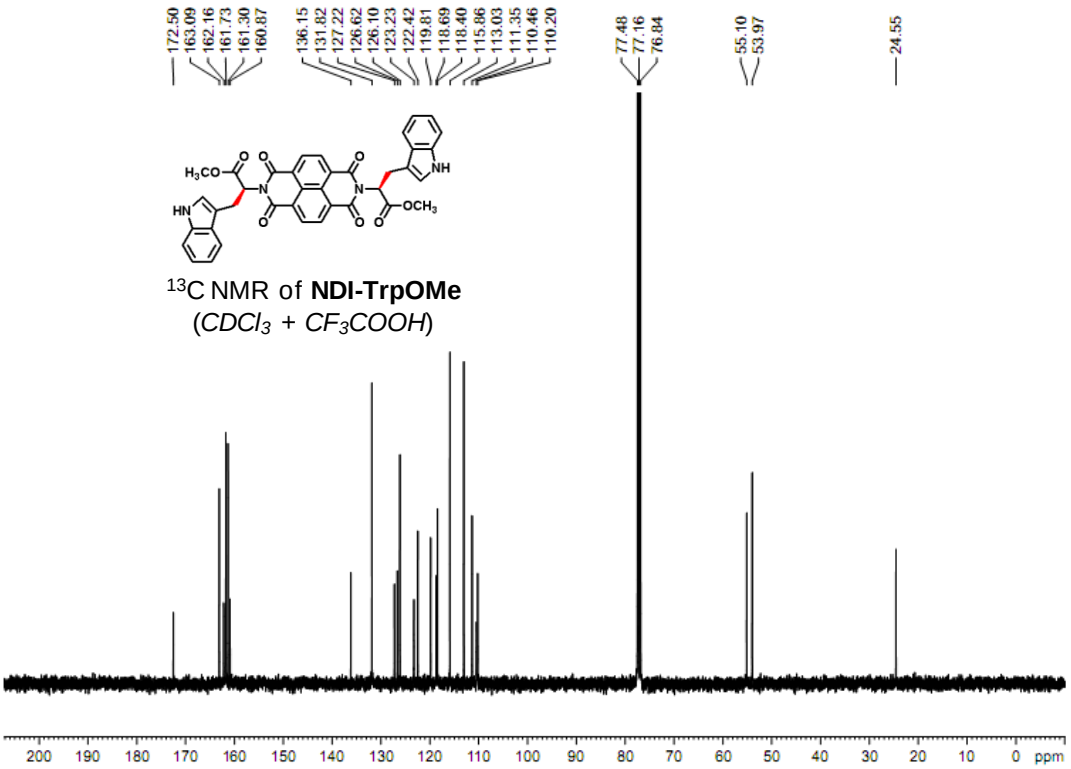


$^{13}$C NMR of **NDI-TrpOMe**
(*$CDCl_3$ + $CF_3COOH$*)

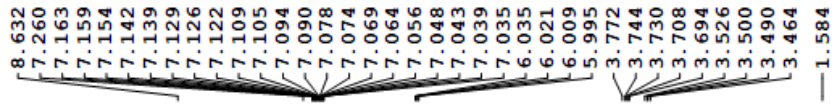


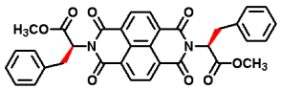


$^{1}$H NMR of **L-NDI** (*CDCl$_3$*)

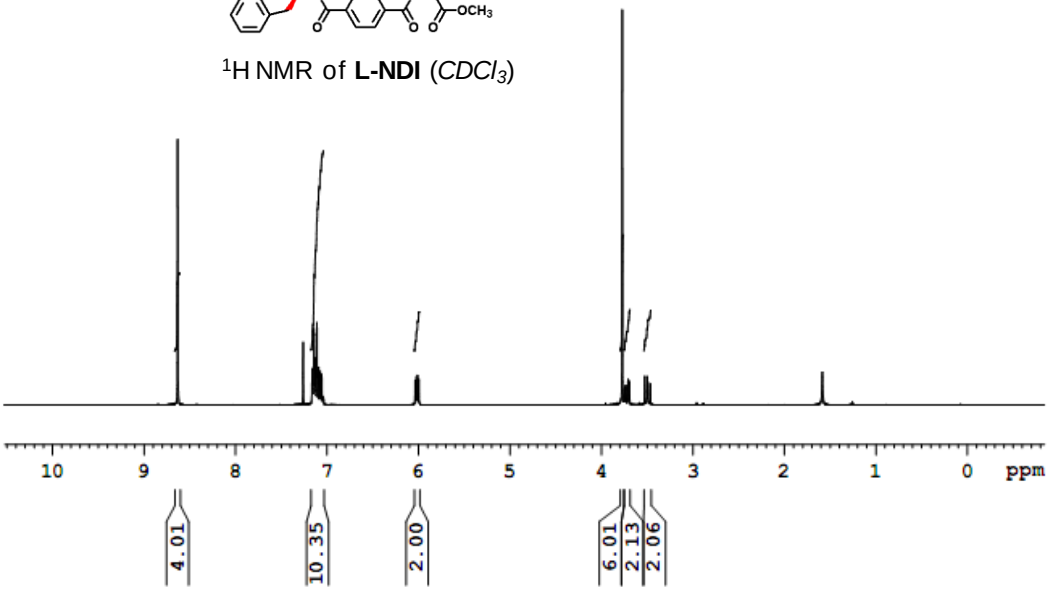



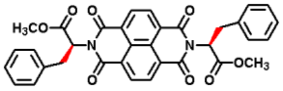


$^{13}$C NMR of **L-NDI** (*CDCl$_3$*)

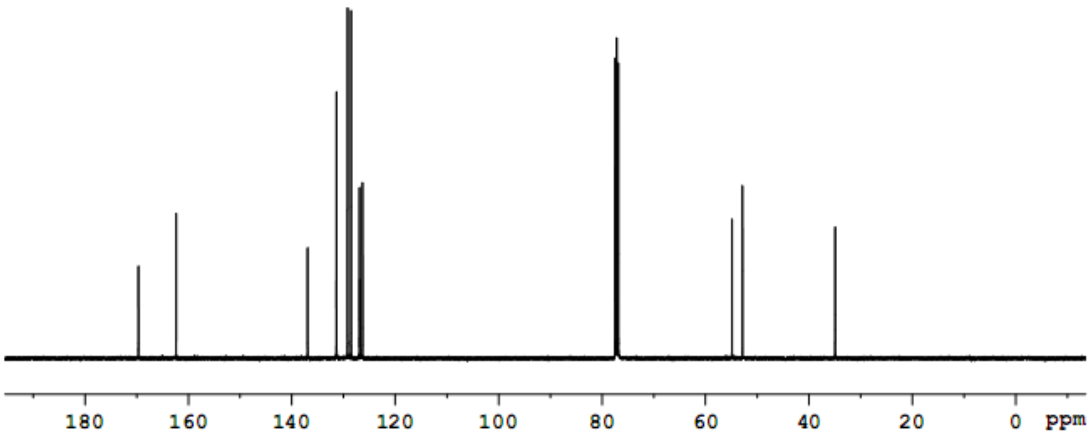

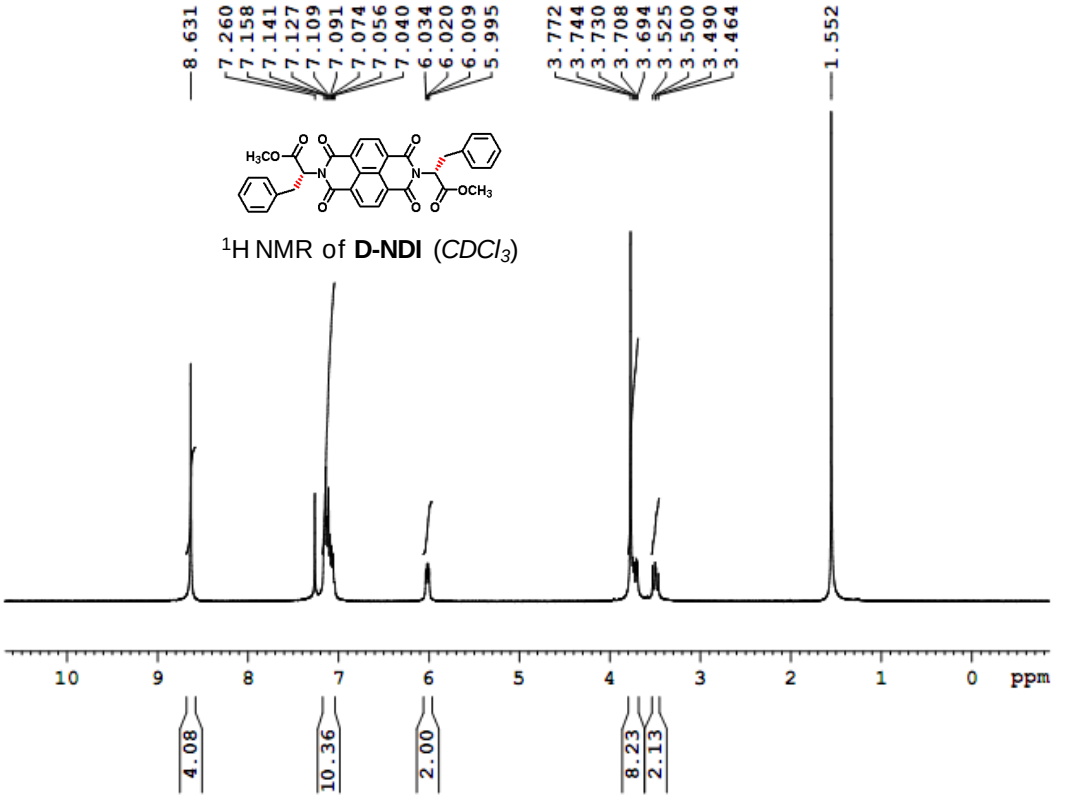


$^{1}$H NMR of **D-NDI** ($CDCl_3$)

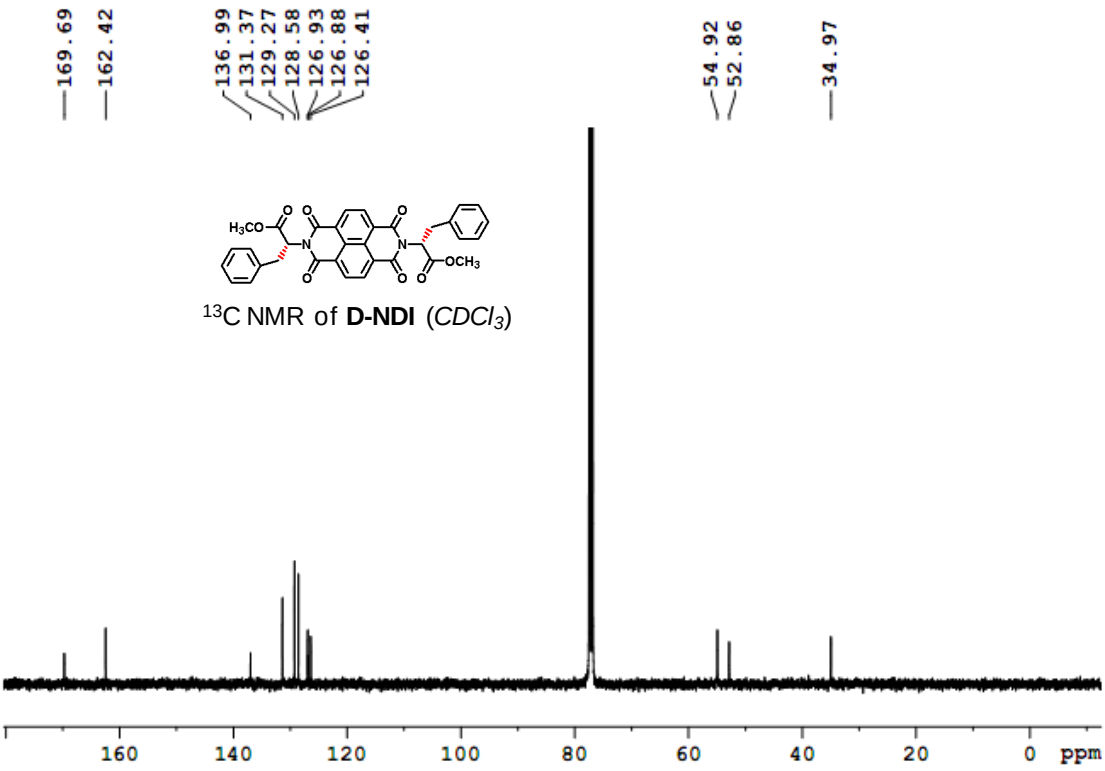


$^{13}$C NMR of **D-NDI** ($CDCl_3$)

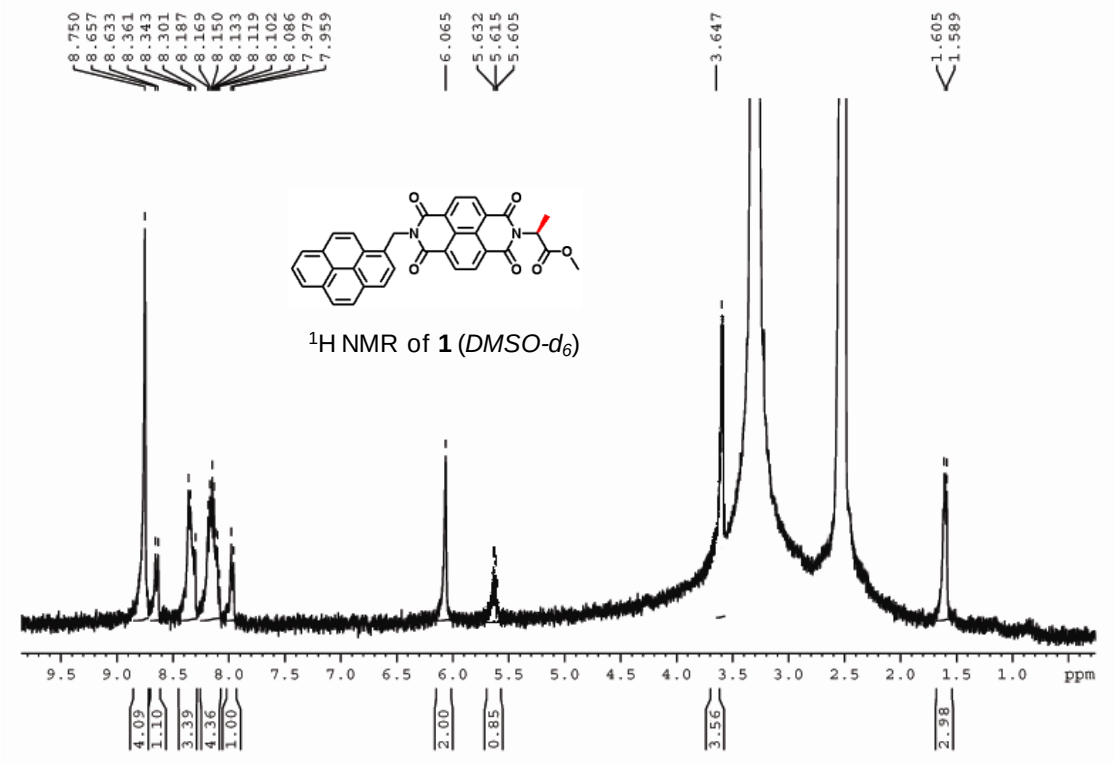


$^1$H NMR of **1** (*DMSO-$d_6$*)

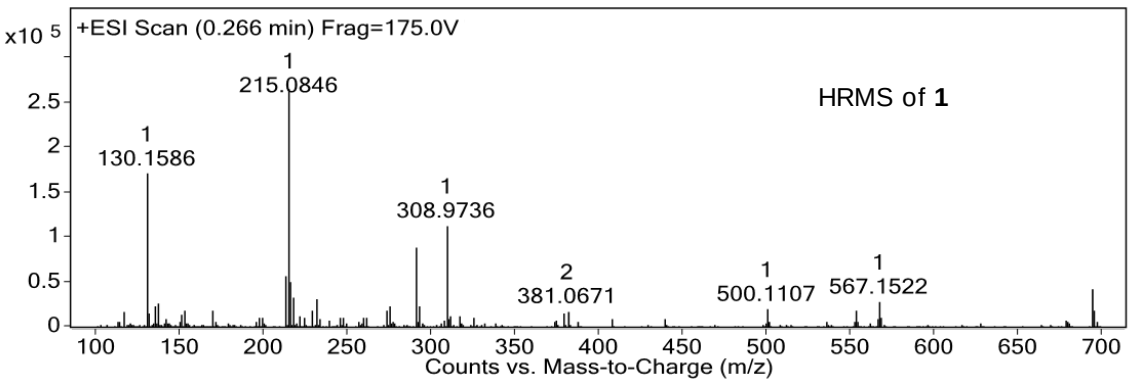

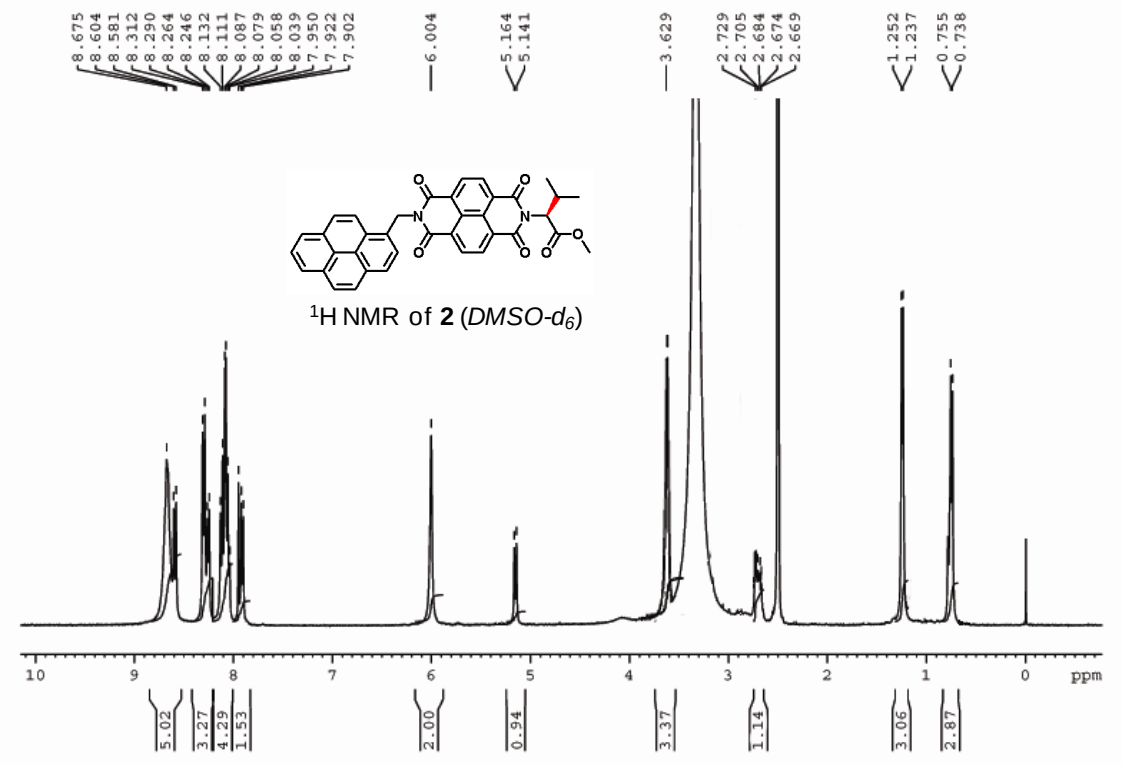


$^1$H NMR of **2** (*DMSO-d$_6$*)

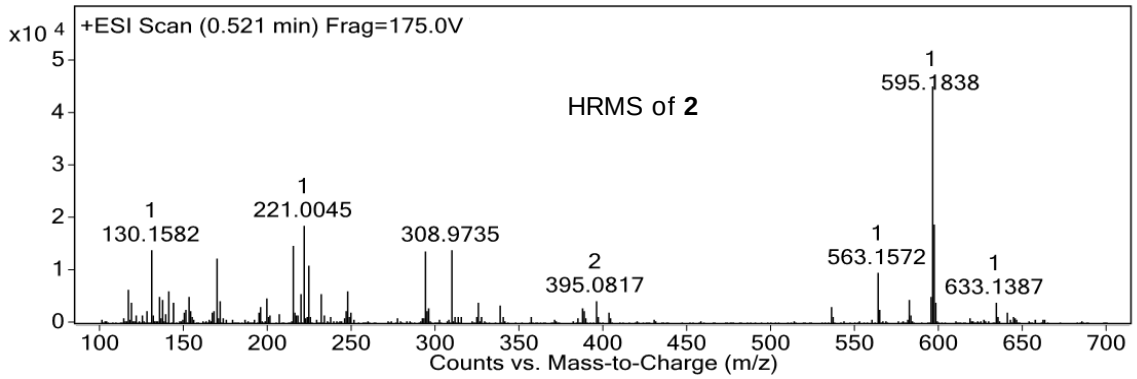


HRMS of **2**

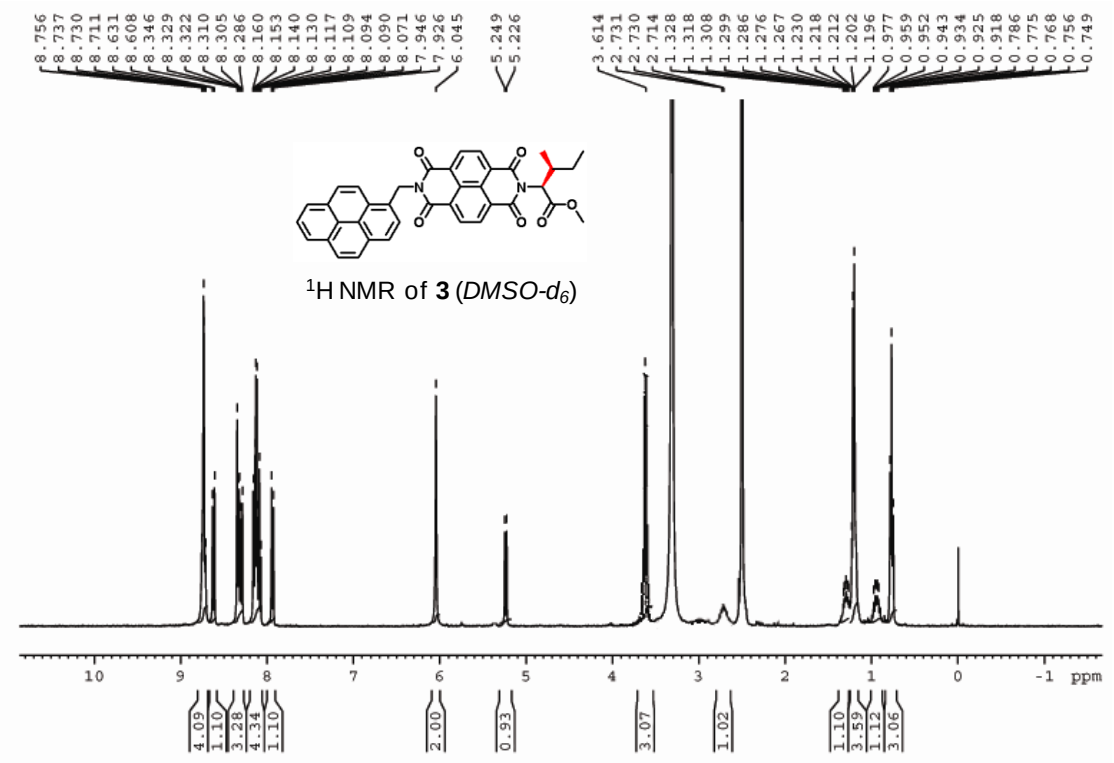


$^1$H NMR of **3** (*DMSO-d$_6$*)

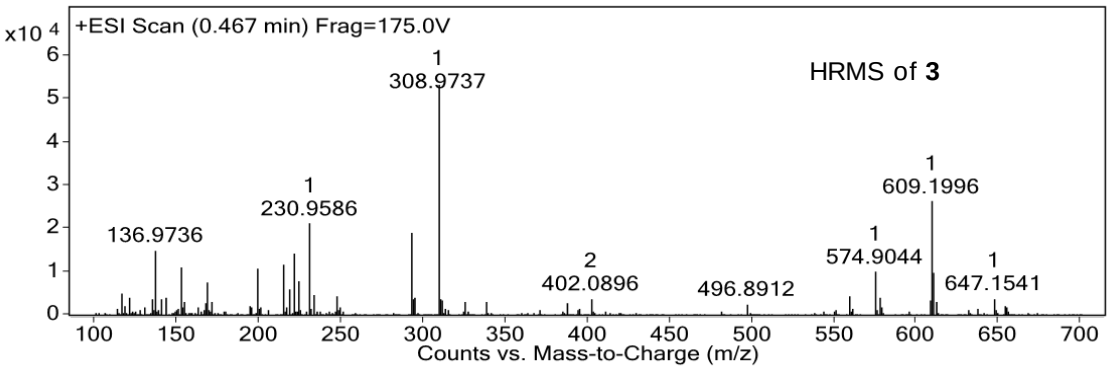

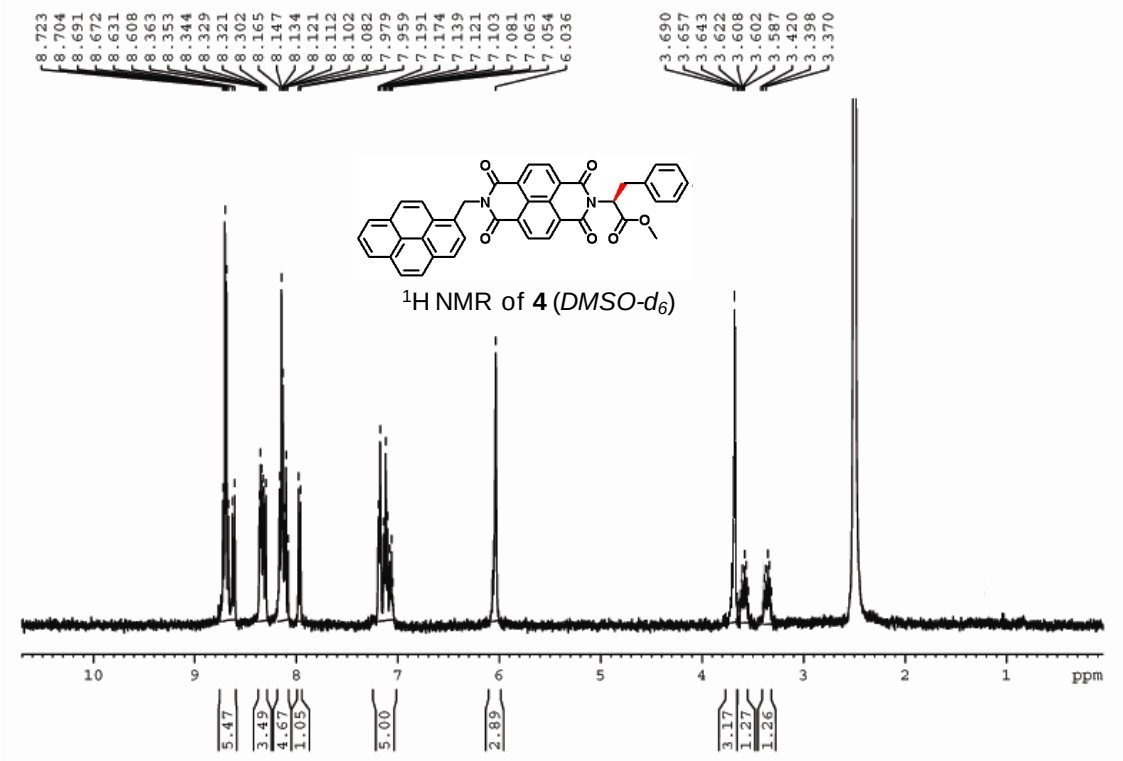


$^1$H NMR of **4** (*DMSO-d$_6$*)

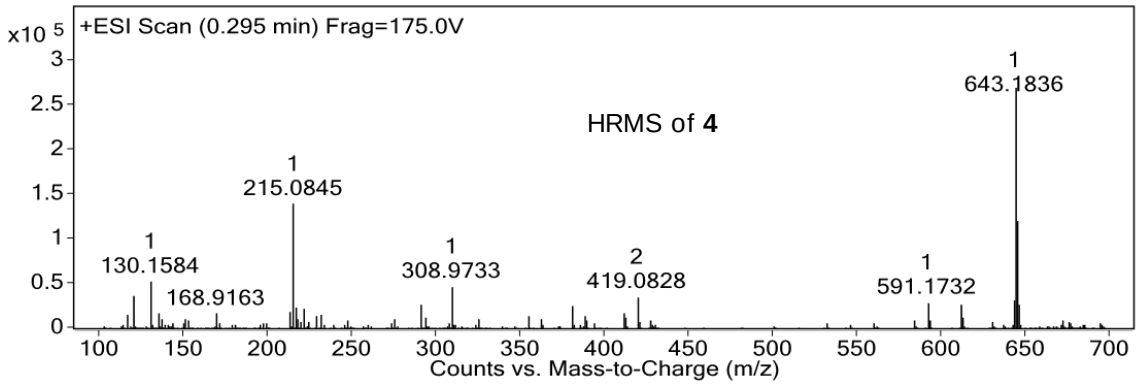

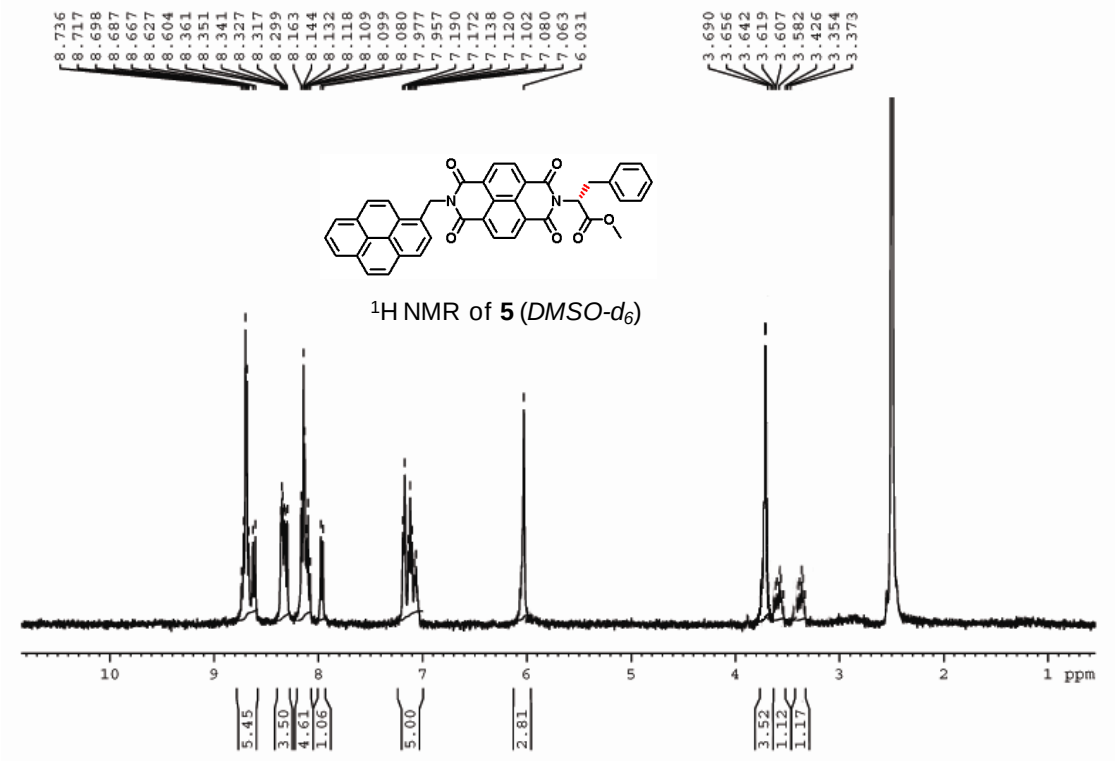


$^1$H NMR of **5** (*DMSO-$d_6$*)

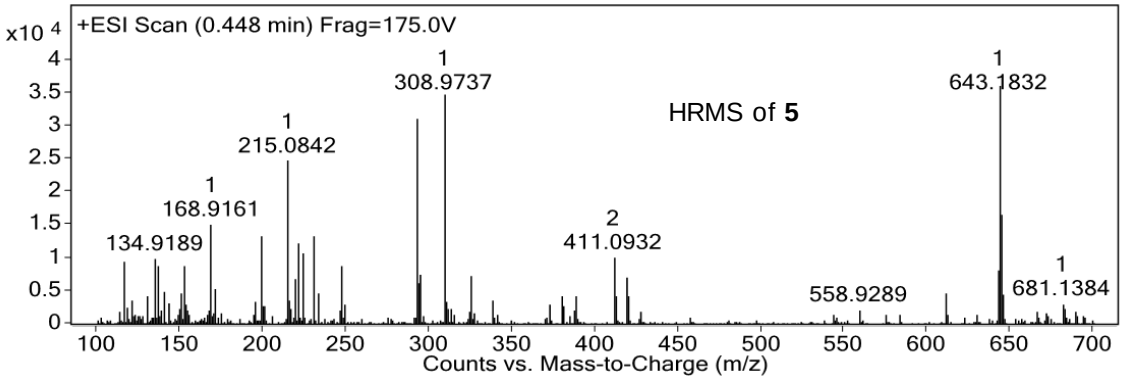

Crystal data for **L-NDI**: Formula $C_{35}H_{25}N_2O_8Cl_3$, Mr = 700.72, Monoclinic, Space group $P_{21}$ (no. 4), a = 8.0720(9) Å, b = 25.548(3) Å, c = 8.2074(9) Å, β = 112.362(2)°, V = 1565.3(3) $Å^3$, Z = 2, $\rho_{calc}$ =1.502 g $cm^{-3}$, μ (MoKα) = 0.352 $mm^{-1}$, T = 293 K, λ ( MoKα) = 0.71073 Å, θmax = 28.0°, Total data = 17985, Unique data = 7297, (Rint = 0.046), Observed data [I > 2σ(I)] = 6375, R = 0.0576, Rw = 0.1278, GOF = 1.10. CCDC 813796 contains the supplementary crystallographic data for this paper. These data can be obtained free of charge from The Cambridge Crystallographic Data Centre via www.ccdc.cam. ac.uk/data_request/cif.

### 2.3.8. References

1. Ariga, K.; Hill, J. P.; Lee, M. V.; Vinu, A.; Charvet, R.; Acharya, S., Challenges and breakthroughs in recent research on self-assembly. *Sci. Tech. Adv. Mater.* **2008,** *9*, 014109.

2. Corbett, P. T.; Leclaire, J.; Vial, L.; West, K. R.; Wietor, J.-L.; Sanders, J. K.; Otto, S., Dynamic combinatorial chemistry. *Chem. Rev.* **2006,** *106*, 3652-3711.

3. Ariga, K.; Lee, M. V.; Mori, T.; Yu, X.-Y.; Hill, J. P., Two-dimensional nanoarchitectonics based on self-assembly. *Adv. Colloid Interface Sci.* **2010,** *154*, 20-29.

4. Babu, S. S.; Prasanthkumar, S.; Ajayaghosh, A., Self-Assembled Gelators for Organic Electronics. *Angew. Chem. Int. Ed.* **2012,** *51*, 1766-1776.

5. Pérez-García, L.; Amabilino, D. B., Spontaneous resolution under supramolecular control. *Chem. Soc. Rev.* **2002,** *31*, 342-356.

6. Moulin, E.; Cid, J.-J.; Giuseppone, N., Advances in Supramolecular Electronics – From Randomly Self-assembled Nanostructures to Addressable Self-Organized Interconnects. *Adv. Mater.* **2013,** *25*, 477-487.

7. Dsouza, R. N.; Pischel, U.; Nau, W. M., Fluorescent dyes and their supramolecular host/guest complexes with macrocycles in aqueous solution. *Chem. Rev.* **2011,** *111*, 7941-7980.

8. Pérez-García, L.; Amabilino, D. B., Spontaneous resolution, whence and whither: from enantiomorphic solids to chiral liquid crystals, monolayers and macro-and supra-molecular polymers and assemblies. *Chem. Soc. Rev.* **2007,** *36*, 941-967.

9. Ariga, K.; Hill, J. P.; Ji, Q., Layer-by-layer assembly as a versatile bottom-up nanofabrication technique for exploratory research and realistic application. *Phys. Chem. Chem. Phys.* **2007,** *9*, 2319-2340.

10. Pantoş, G. D.; Wietor, J. L.; Sanders, J. K., Filling helical nanotubes with C60. *Angew. Chem. Int. Ed.* **2007,** *46*, 2238-2240.

11. Tanaka, H.; Litvinchuk, S.; Tran, D.-H.; Bollot, G.; Mareda, J.; Sakai, N.; Matile, S., Adhesive π-clamping within synthetic multifunctional pores. *J. Am. Chem. Soc.* **2006,** *128*, 16000-16001.

12. Mohanty, J.; Nau, W. M., Ultrastable rhodamine with cucurbituril. *Angew. Chem. Int. Ed.* **2005,** *44*, 3750-3754.

13. Su, B.; Wu, Y.; Jiang, L., The art of aligning one-dimensional (1D) nanostructures. *Chem. Soc. Rev.* **2012,** *41*, 7832-7856.

14. Avinash, M. B.; Govindaraju, T., Amino Acid Derivatized Arylenediimides: A Versatile Modular Approach for Functional Molecular Materials. *Adv. Mater.* **2012,** *24*, 3905-3922.

15. Avinash, M.; Govindaraju, T., A bio-inspired design strategy: Organization of tryptophan-appended naphthalenediimide into well-defined architectures induced by molecular interactions. *Nanoscale* **2011,** *3*, 2536-2543.

16. Avinash, M. B.; Govindaraju, T., Engineering Molecular Organization of Naphthalenediimides: Large Nanosheets with Metallic Conductivity and Attoliter Containers. *Adv. Funct. Mater.* **2011,** *21*, 3875-3882.

17. Avinash, M. B.; Samanta, P. K.; Sandeepa, K. V.; Pati, S. K.; Govindaraju, T., Molecular Architectonics of Stereochemically Constrained π-Complementary Functional Modules. *Eur. J. Org. Chem.* **2013,** *2013*, 5838-5847.

18. Lomander, A.; Hwang, W.; Zhang, S., Hierarchical Self-Assembly of a Coiled-Coil Peptide into Fractal Structure. *Nano Lett.* **2005,** *5*, 1255-1260.

19. Wang, W.; Chau, Y., Self-assembled peptide nanorods as building blocks of fractal patterns. *Soft Matter* **2009,** *5*, 4893-4898.

20. Bhosale, S. V.; Jani, C. H.; Langford, S. J., Chemistry of naphthalene diimides. *Chem. Soc. Rev.* **2008,** *37*, 331-342.

21. Sakai, N.; Mareda, J.; Vauthey, E.; Matile, S., Core-substituted naphthalenediimides. *Chem. Commun.* **2010,** *46*, 4225-4237.

22. Berova, N.; Nakanishi, K.; Woody, R. W., *Circular dichroism: principles and applications*. Wiley-VCH New York: 2000; Vol. 912.

23. Kelly, S. M.; Jess, T. J.; Price, N. C., How to study proteins by circular dichroism. *BBA-Proteins Proteom.* **2005,** *1751*, 119-139.

24. Polavarapu, P. L., Why is it important to simultaneously use more than one chiroptical spectroscopic method for determining the structures of chiral molecules? *Chirality* **2008,** *20*, 664-672.

25. Simonyi, M.; Bikadi, Z.; Zsila, F.; Deli, J., Supramolecular exciton chirality of carotenoid aggregates. *Chirality* **2003,** *15*, 680-698.

26. Harada, N.; Nakanishi, K., Exciton chirality method and its application to configurational and conformational studies of natural products. *Acc. Chem. Res.* **1972,** *5*, 257-263.

27. Palmans, A. R.; Meijer, E. e. W., Amplification of chirality in dynamic supramolecular aggregates. *Angew. Chem. Int. Ed.* **2007,** *46*, 8948-8968.

28. Arnold, G. E.; Day, L. A.; Dunker, A. K., Tryptophan contributions to the unusual circular dichroism of fd bacteriophage. *Biochemistry* **1992,** *31*, 7948-7956.

29. Ma, M.; Kuang, Y.; Gao, Y.; Zhang, Y.; Gao, P.; Xu, B., Aromatic−Aromatic Interactions Induce the Self-Assembly of Pentapeptidic Derivatives in Water To Form Nanofibers and Supramolecular Hydrogels. *J. Am. Chem. Soc.* **2010,** *132*, 2719-2728.

30. Demirdöven, N.; Cheatum, C. M.; Chung, H. S.; Khalil, M.; Knoester, J.; Tokmakoff, A., Two-Dimensional Infrared Spectroscopy of Antiparallel β-Sheet Secondary Structure. *J. Am. Chem. Soc.* **2004,** *126*, 7981-7990.

31. Surewicz, W. K.; Mantsch, H. H.; Chapman, D., Determination of protein secondary structure by Fourier transform infrared spectroscopy: A critical assessment. *Biochemistry* **1993,** *32*, 389-394.

32. Khurana, R.; Fink, A. L., Do Parallel β-Helix Proteins Have a Unique Fourier Transform Infrared Spectrum? *Biophys. J.* **2000,** *78*, 994-1000.

33. Dettin, M.; Falcigno, L.; Campanile, T.; Scarinci, C.; D'Auria, G.; Cusin, M.; Paolillo, L.; Di Bello, C., A type-II β-turn, proline-containing, cyclic pentapeptide as a building block for the construction of models of the cleavage site of pro-oxytocin. *J. Pept. Sci.* **2001,** *7*, 358-373.

34. Pengo, P.; Pantoş, G. D.; Otto, S.; Sanders, J. K. M., Efficient and Mild Microwave-Assisted Stepwise Functionalization of Naphthalenediimide with α-Amino Acids. *J. Org. Chem.* **2006,** *71*, 7063-7066.

35. Anthony, J. E.; Facchetti, A.; Heeney, M.; Marder, S. R.; Zhan, X., n-Type Organic Semiconductors in Organic Electronics. *Adv. Mater.* **2010,** *22*, 3876-3892.

36. Zang, L.; Che, Y.; Moore, J. S., One-Dimensional Self-Assembly of Planar π-Conjugated Molecules: Adaptable Building Blocks for Organic Nanodevices. *Acc. Chem. Res.* **2008,** *41*, 1596-1608.

37. Bhosale, R.; Misek, J.; Sakai, N.; Matile, S., Supramolecular n/p-heterojunction photosystems with oriented multicolored antiparallel redox gradients (OMARG-SHJs). *Chem. Soc. Rev.* **2010,** *39*, 138-149.

38. Schenning, A. P. H. J.; Meijer, E. W., Supramolecular electronics; nanowires from self-assembled π-conjugated systems. *Chem. Commun.* **2005,** 3245-3258.

39. Carroll, R. L.; Gorman, C. B., The Genesis of Molecular Electronics. *Angew. Chem. Int. Ed.* **2002,** *41*, 4378-4400.

40. Chiu, D. T.; Lorenz, R. M., Chemistry and Biology in Femtoliter and Picoliter Volume Droplets. *Acc. Chem. Res.* **2009,** *42*, 649-658.

41. Xu, W.; Sims, C. E.; Allbritton, N. L., Microcup Arrays for the Efficient Isolation and Cloning of Cells. *Anal. Chem.* **2010,** *82*, 3161-3167.

42. Gorris, H. H.; Walt, D. R., Analytical chemistry on the femtoliter scale. *Angew. Chem. Int. Ed.* **2010,** *49*, 3880-3895.

43. Rondelez, Y.; Tresset, G.; Tabata, K. V.; Arata, H.; Fujita, H.; Takeuchi, S.; Noji, H., Microfabricated arrays of femtoliter chambers allow single molecule enzymology. *Nat Biotech* **2005,** *23*, 361-365.

44. Jagadeesan, D.; Mansoori, U.; Mandal, P.; Sundaresan, A.; Eswaramoorthy, M., Hollow Spheres to Nanocups: Tuning the Morphology and Magnetic Properties of Single-Crystalline α-Fe2O3 Nanostructures. *Angew. Chem. Int. Ed.* **2008,** *47*, 7685-7688.

45. Krishna, K. S.; Mansoori, U.; Selvi, N. R.; Eswaramoorthy, M., Form Emerges from Formless Entities: Temperature-Induced Self-Assembly and Growth of ZnO Nanoparticles into Zeptoliter Bowls and Troughs. *Angew. Chem. Int. Ed.* **2007,** *46*, 5962-5965.

46. John, N. S.; Selvi, N. R.; Mathur, M.; Govindarajan, R.; Kulkarni, G. U., A Facile Method of Producing Femtoliter Metal Cups by Pulsed Laser Ablation. *J. Phys. Chem. B* **2006,** *110*, 22975-22978.

47. Andric, G.; Boas, J. F.; Bond, A. M.; Fallon, G. D.; Ghiggino, K. P.; Hogan, C. F.; Hutchison, J. A.; Lee, M. A.; Langford, S. J.; Pilbrow, J. R.; Troup, G. J.; Woodward, C. P., Spectroscopy of Naphthalene Diimides and Their Anion Radicals*. *Aust. J. Chem.* **2004,** *57*, 1011-1019.

48. Ozser, M. E.; Uzun, D.; Elci, I.; Icil, H.; Demuth, M., Novel naphthalene diimides and a cyclophane thereof: synthesis, characterization, photophysical and electrochemical properties. *Photochem. Photobiol. Sci.* **2003,** *2*, 218-223.

49. Gawroński, J.; Brzostowska, M.; Kacprzak, K.; Kołbon, H.; Skowronek, P., Chirality of aromatic bis-imides from their circular dichroism spectra. *Chirality* **2000,** *12*, 263-268.

50. Sakai, N.; Talukdar, P.; Matile, S., Use of the exciton chirality method in the investigation of ligand-gated synthetic ion channels. *Chirality* **2006,** *18*, 91-94.

51. Li, R.; Hu, W.; Liu, Y.; Zhu, D., Micro- and Nanocrystals of Organic Semiconductors. *Acc. Chem. Res.* **2010,** *43*, 529-540.

52. Chang, S.-S.; Wu, C.-G., Effects of Polymerization Media on the Nanoscale Conductivity and Current−Voltage Characteristics of Chemically Synthesized Polyaniline Films. *J. Phys. Chem. B* **2005,** *109*, 18275-18282.

53. Prasanthkumar, S.; Gopal, A.; Ajayaghosh, A., Self-Assembly of Thienylenevinylene Molecular Wires to Semiconducting Gels with Doped Metallic Conductivity. *J. Am. Chem. Soc.* **2010,** *132*, 13206-13207.

54. Refat, M. S.; Killa, H.; Grabchev, I.; Mansour, A. F.; El-Sayed, M. Y., Interaction of N, N'-bis [2-N, N-dimethylaminoethyl)]-1, 4, 6, 8-naphthalene-diimide with para substituted phenols: preparation and spectroscopic characterization of charge-transfer complexes and their conductivity measurements with polystyrene composites. *Can. J. Anal. Sci. Spectrosc.* **2007,** *52*, 75-90.

55. Roberson, L. B.; Kowalik, J.; Tolbert, L. M.; Kloc, C.; Zeis, R.; Chi, X.; Fleming, R.; Wilkins, C., Pentacene Disproportionation during Sublimation for Field-Effect Transistors. *J. Am. Chem. Soc.* **2005,** *127*, 3069-3075.

56. Govindaraju, T.; Pandeeswar, M.; Jayaramulu, K.; Jaipuria, G.; Atreya, H. S., Spontaneous self-assembly of designed cyclic dipeptide (Phg-Phg) into two-dimensional nano- and mesosheets. *Supramol. Chem.* **2011,** *23*, 487-492.

57. Metrangolo, P.; Meyer, F.; Pilati, T.; Resnati, G.; Terraneo, G., Halogen Bonding in Supramolecular Chemistry. *Angew. Chem. Int. Ed.* **2008,** *47*, 6114-6127.

58. Politzer, P.; Lane, P.; Concha, M.; Ma, Y.; Murray, J., An overview of halogen bonding. *J. Mol. Model.* **2007,** *13*, 305-311.

59. Metrangolo, P.; Neukirch, H.; Pilati, T.; Resnati, G., Halogen Bonding Based Recognition Processes: A World Parallel to Hydrogen Bonding†. *Acc. Chem. Res.* **2005,** *38*, 386-395.

60. Adler, M.; Kochanny, M. J.; Ye, B.; Rumennik, G.; Light, D. R.; Biancalana, S.; Whitlow, M., Crystal Structures of Two Potent Nonamidine Inhibitors Bound to Factor Xa. *Biochemistry* **2002,** *41*, 15514-15523.

61. Saleh, N. i.; Koner, A. L.; Nau, W. M., Activation and Stabilization of Drugs by Supramolecular pKa Shifts: Drug-Delivery Applications Tailored for Cucurbiturils. *Angew. Chem. Int. Ed.* **2008,** *47*, 5398-5401.

62. Burnworth, M.; Tang, L.; Kumpfer, J. R.; Duncan, A. J.; Beyer, F. L.; Fiore, G. L.; Rowan, S. J.; Weder, C., Optically healable supramolecular polymers. *Nature* **2011,** *472*, 334-337.

63. Oohora, K.; Burazerovic, S.; Onoda, A.; Wilson, Y. M.; Ward, T. R.; Hayashi, T., Chemically Programmed Supramolecular Assembly of Hemoprotein and Streptavidin with Alternating Alignment. *Angew. Chem. Int. Ed.* **2012,** *51*, 3818-3821.

64. Boekhoven, J.; Brizard, A. M.; van Rijn, P.; Stuart, M. C.; Eelkema, R.; van Esch, J. H., Programmed Morphological Transitions of Multisegment Assemblies by Molecular Chaperone Analogues. *Angew. Chem.Int. Ed.* **2011,** *50*, 12285-12289.

65. Jiang, W.; Schalley, C. A., Integrative self-sorting is a programming language for high level self-assembly. *Proc. Natl. Acad. Sci.USA* **2009,** *106*, 10425-10429.

66. Muscat, R. A.; Bath, J.; Turberfield, A. J., A programmable molecular robot. *Nano Lett.* **2011,** *11*, 982-987.

67. Winfree, E.; Liu, F.; Wenzler, L. A.; Seeman, N. C., Design and self-assembly of two-dimensional DNA crystals. *Nature* **1998,** *394*, 539-544.

68. Ratner, M. A., Introducing molecular electronics. *Mater.Today* **2002,** *5*, 20-27.

69. Li, J.; Zhao, Y.; Tan, H. S.; Guo, Y.; Di, C.-A.; Yu, G.; Liu, Y.; Lin, M.; Lim, S. H.; Zhou, Y., A stable solution-processed polymer semiconductor with record high-mobility for printed transistors. *Sci. Rep.* **2012,** *2*, 754.

70. Coropceanu, V.; Cornil, J.; da Silva Filho, D. A.; Olivier, Y.; Silbey, R.; Brédas, J.-L., Charge transport in organic semiconductors. *Chem. Rev.* **2007,** *107*, 926-952.

71. Kumar, N. S. S.; Gujrati, M. D.; Wilson, J. N., Evidence of preferential π-stacking: a study of intermolecular and intramolecular charge transfer complexes. *Chem. Commun.* **2010,** *46*, 5464-5466.

72. Sakai, N.; Bhosale, R.; Emery, D.; Mareda, J.; Matile, S., Supramolecular n/p-Heterojunction Photosystems with Antiparallel Redox Gradients in Electron- and Hole-Transporting Pathways. *J. Am. Chem. Soc.* **2010,** *132*, 6923-6925.

73. Cougnon, F. B. L.; Au-Yeung, H. Y.; Pantoş, G. D.; Sanders, J. K. M., Exploring the Formation Pathways of Donor−Acceptor Catenanes in Aqueous Dynamic Combinatorial Libraries. *J. Am. Chem. Soc.* **2011,** *133*, 3198-3207.

74. Burattini, S.; Greenland, B. W.; Merino, D. H.; Weng, W.; Seppala, J.; Colquhoun, H. M.; Hayes, W.; Mackay, M. E.; Hamley, I. W.; Rowan, S. J., A Healable Supramolecular Polymer

Blend Based on Aromatic π-π Stacking and Hydrogen-Bonding Interactions. *J. Am. Chem. Soc.* **2010,** *132*, 12051-12058.

75. Murase, T.; Otsuka, K.; Fujita, M., Pairwise Selective Formation of Aromatic Stacks in a Coordination Cage. *J. Am. Chem. Soc.* **2010,** *132*, 7864-7865.

76. Liu, K.; Wang, C.; Li, Z.; Zhang, X., Superamphiphiles Based on Directional Charge-Transfer Interactions: From Supramolecular Engineering to Well-Defined Nanostructures. *Angew. Chem. Int. Ed.* **2011,** *50*, 4952-4956.

77. Alvey, P. M.; Reczek, J. J.; Lynch, V.; Iverson, B. L., A Systematic Study of Thermochromic Aromatic Donor−Acceptor Materials. *J. Org. Chem.* **2010,** *75*, 7682-7690.

78. Gunderson, V. L.; Krieg, E.; Vagnini, M. T.; Iron, M. A.; Rybtchinski, B.; Wasielewski, M. R., Photoinduced Singlet Charge Transfer in a Ruthenium(II) Perylene-3,4:9,10-bis(dicarboximide) Complex. *J. Phys. Chem. B* **2011,** *115*, 7533-7540.

79. Koshkakaryan, G.; Klivansky, L. M.; Cao, D.; Snauko, M.; Teat, S. J.; Struppe, J. O.; Liu, Y., Alternative Donor−Acceptor Stacks from Crown Ethers and Naphthalene Diimide Derivatives: Rapid, Selective Formation from Solution and Solid State Grinding. *J. Am. Chem. Soc.* **2009,** *131*, 2078-2079.

80. Klivansky, L. M.; Hanifi, D.; Koshkakaryan, G.; Holycross, D. R.; Gorski, E. K.; Wu, Q.; Chai, M.; Liu, Y., A complementary disk-shaped π electron donor-acceptor pair with high binding affinity. *Chem. Sci.* **2012,** *3*, 2009-2014.

81. Tu, S.; Kim, S. H.; Joseph, J.; Modarelli, D. A.; Parquette, J. R., Self-Assembly of a Donor–Acceptor Nanotube. A Strategy To Create Bicontinuous Arrays. *J. Am. Chem. Soc.* **2011,** *133*, 19125-19130.

82. Yu, W.; Wang, X.-Y.; Li, J.; Li, Z.-T.; Yan, Y.-K.; Wang, W.; Pei, J., A photoconductive charge-transfer crystal with mixed-stacking donor-acceptor heterojunctions within the lattice. *Chem. Commun.* **2013,** *49*, 54-56.

83. Tayi, A. S.; Shveyd, A. K.; Sue, A. C. H.; Szarko, J. M.; Rolczynski, B. S.; Cao, D.; Kennedy, T. J.; Sarjeant, A. A.; Stern, C. L.; Paxton, W. F.; Wu, W.; Dey, S. K.; Fahrenbach, A. C.; Guest, J. R.; Mohseni, H.; Chen, L. X.; Wang, K. L.; Stoddart, J. F.; Stupp, S. I., Room-temperature ferroelectricity in supramolecular networks of charge-transfer complexes. *Nature* **2012,** *488*, 485-489.

84. Govindaraju, T.; Avinash, M. B., Two-dimensional nanoarchitectonics: organic and hybrid materials. *Nanoscale* **2012,** *4*, 6102-6117.

85. Frisch, M.; Trucks, G.; Schlegel, H.; Scuseria, G.; Robb, M.; Cheeseman, J.; Scalmani, G.; Barone, V.; Mennucci, B.; Petersson, G., Gaussian 09, Revision A. 1; Gaussian, Inc: Wallingford, CT, 2009.

86. Miehlich, B.; Savin, A.; Stoll, H.; Preuss, H., Results obtained with the correlation energy density functionals of becke and Lee, Yang and Parr. *Chem. Phys. Lett.* **1989,** *157*, 200-206.

87. Chai, J.-D.; Head-Gordon, M., Long-range corrected hybrid density functionals with damped atom-atom dispersion corrections. *Phys. Chem. Chem. Phys.* **2008,** *10*, 6615-6620.

88. Chai, J.-D.; Head-Gordon, M., Systematic optimization of long-range corrected hybrid density functionals. *J. Chem. Phys.* **2008,** *128* , 084106.

89. Das, A.; Molla, M. R.; Maity, B.; Koley, D.; Ghosh, S., Hydrogen-Bonding Induced Alternate Stacking of Donor (D) and Acceptor (A) Chromophores and their Supramolecular Switching to Segregated States. *Chem. Eur. J.* **2012,** *18*, 9849-9859.

90. Molla, M. R.; Das, A.; Ghosh, S., Chiral induction by helical neighbour: spectroscopic visualization of macroscopic-interaction among self-sorted donor and acceptor π-stacks. *Chem. Commun.* **2011,** *47*, 8934-8936.

91. Fox, J.; Wie, J. J.; Greenland, B. W.; Burattini, S.; Hayes, W.; Colquhoun, H. M.; Mackay, M. E.; Rowan, S. J., High-Strength, Healable, Supramolecular Polymer Nanocomposites. *J. Am. Chem. Soc.* **2012,** *134*, 5362-5368.

92. Bradford, V. J.; Iverson, B. L., Amyloid-like Behavior in Abiotic, Amphiphilic Foldamers. *J. Am. Chem. Soc.* **2008,** *130*, 1517-1524.

93. Andrew Karplus, P., Hydrophobicity regained. *Protein Sci.* **1997,** *6*, 1302-1307.

# CHAPTER 3 MOLECULAR BIOMIMICRY

The extraordinary molecular recognition, self-replication, autocatalysis, self-healing, photosynthesis, autoregulation, synthesis of proteins/biominerals/bioarchitectures, and so forth are some of the hallmark processes occurring under ambient conditions in biological systems.[1-6] Undoubtedly, these archetypal bioprocesses are crucial for the existence as well as functioning of life.[7-10] An effort to understand these processes occurring at the molecular and/or at its assembly-level via an act of imitation forms the basis of a newly emerging discipline termed as molecular biomimicry.[11-16] Such an endeavor not only sheds novel insights into the biochemical processes but also provides ambitious opportunities for the intriguing prospects of systems chemistry, synthetic biology, as well as an advanced means to aid biological ailments.[17-26]

Although, the current advancement in science and technology can empower us to see atoms and molecules, there is an inherent dearth of design strategies to efficiently manipulate their assemblies and to furnish biological functionalities.[27-29] In this regard, we propose a bioinspired design strategy as an eclectic approach to mimic bioprocesses, which in turn may give rise to biological functionalities.[30] In this chapter, we provide two sets of functional molecular systems, which exhibit unprecedented molecular behaviors having relevance to biological systems. In the first sub-chapter, we show the extremely slow dynamic assembly of our functional molecule with an unusual relevance to the secondary structure of proteins. In the second sub-chapter, we describe probably the most complicated synthetic molecular assembly that has ever been reported, to the best of our knowledge. In the latter case we present the examples of autoregulatory and emergent behaviors in a man-made dynamic molecular assembly.

## 3.1. Extremely Slow Dynamics of an Abiotic Helical Assembly - Unusual Relevance to the Secondary Structure of Proteins

In this work, we describe the self-assembly of three PDIs namely **1**, **2**, and **3** obtained by functionalizing with isoleucine, phenylalanine, and alanine methylesters, respectively.[31] In particular, **1** exhibited an unusual molecular assembly behavior with an extremely slow rate of helical organization over a day's time. Further, temperature-dependent studies showed that this slow dynamics of organization was under kinetic control, unlike the ubiquitous thermodynamically controlled synthetic assemblies.[32,33] Surprisingly, the molecular assembly was not reversible upon thermal treatment, which was supposedly due to heat-induced conformational modifications in the isoleucine side chain of **1**. However, the so-formed random aggregates of thermally treated **1** could be made reversible only upon addition of thermally untreated aggregates of **1**, which act as seeds. This intriguing molecular assembly behavior and the slow dynamics provided us a rare opportunity to find an unusual correlation with the secondary structure of proteins.

It is interesting to note that the majority of the freshly biosynthesized proteins must transform to their native three-dimensional conformation in order to be functional or biologically active, by a process known as protein folding.[34,35] It was estimated that even

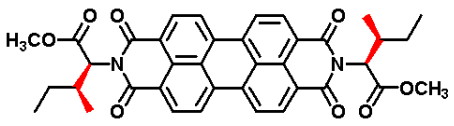


**1**

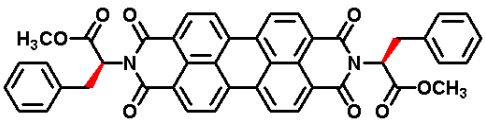


**2**

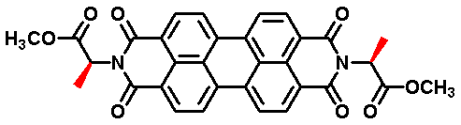


**3**

a small protein of 100 amino acids would take an astronomical length of time to reach its native conformation if the folding were to be a random process.[36] In contrast, protein folding typically occurs in the time scale of microseconds to few milliseconds (most often aided by chaperones, heat shock proteins, and/or folding catalysts), which is indeed a testimony to Nature's ingenious solutions to complex problems.[37] Although Anfinsen's hypothesis suggested that all of the information for transition of a random coil to the native structure is stored in the protein sequence, it is still not yet clear exactly how the sequence encodes such complex characteristics.[38,39] Solving this mystery demands novel approaches or advanced experimental/computational methodologies or a combination thereof.[40] It is in this context that we believe that simple bio-mimicking molecular systems like **1** could bring about novel perspectives to understand the complex protein folding problem via their intricate molecular mechanistic details. In addition, such studies could be instrumental in understanding the protein conformational diseases, namely, Alzheimer's, Parkinson's, Huntington's, cancer, cataracts, and cystic fibrosis among others caused due to protein misfolding.[41]

### 3.1.1. Spontaneous helical assembly

The molecular self-assemblies of **1**, **2**, and **3** were studied in 2,2,2-trifluoroethanol (TFE), dimethylsulfoxide (DMSO), as well as their aqueous solutions (Figure 1,2). Absorption studies of **1** in TFE showed typical vibronically structured spectra with maxima at 460, 490, and 526 nm (Figure 1a). The incremental addition of water resulted in hypochromic effect due to enhanced hydrophobic-force-induced aggregation of **1** (Figure 1a).

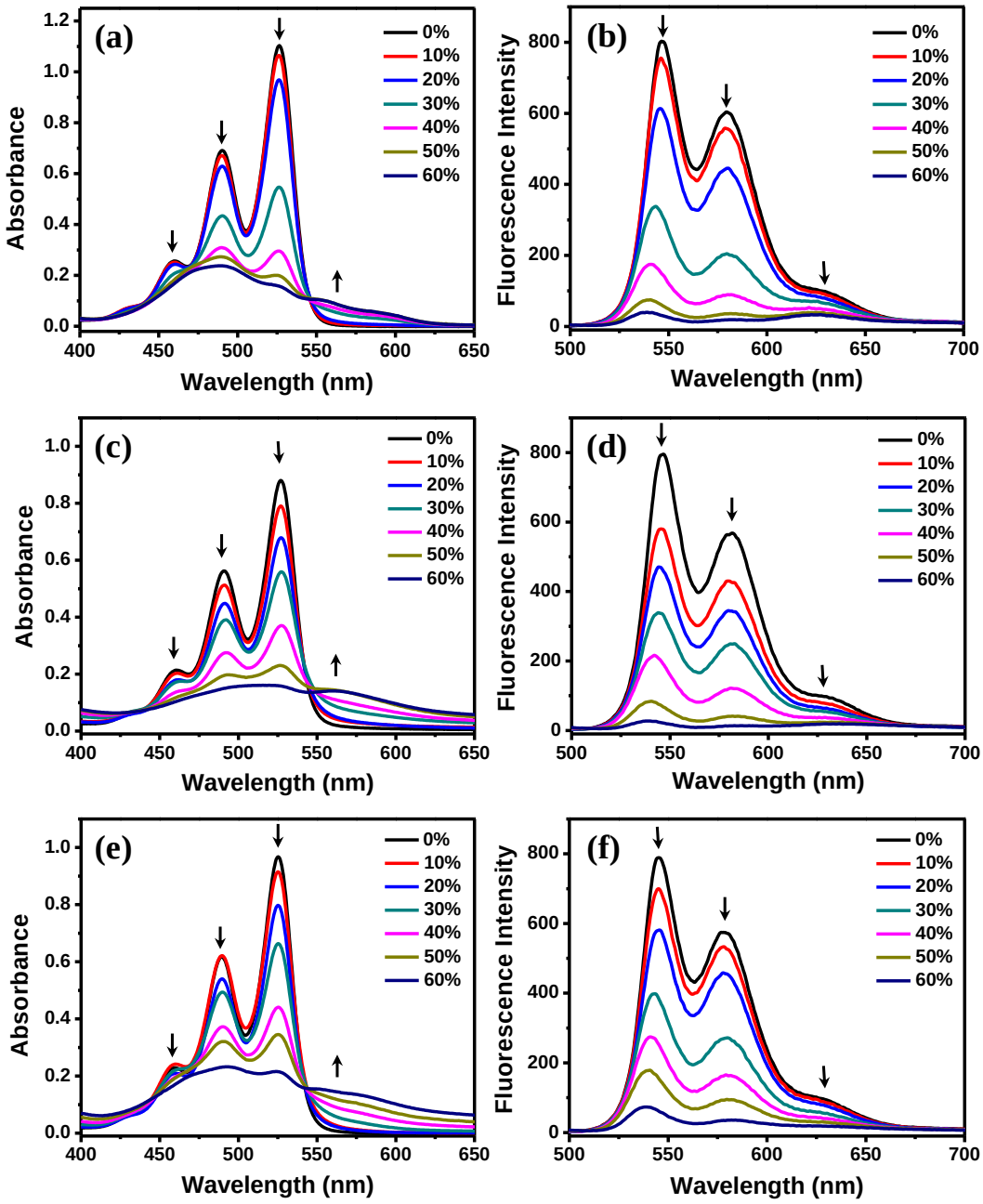


**Figure 1**. (a), (c) and (e) Absorption, (b), (d) and (f) fluorescence (excitation at 480 nm) spectra of 200 μM solution of **1**, **2** and **3** respectively at 298 K. The values represent the percentages of water in aqueous solution of TFE.

Fluorescence studies showed 20 nm Stokes-shifted mirror image emission bands, while the aggregation in the aqueous solutions resulted in quenching of fluorescence (Figure 1b). Similar spectral features were also observed for **2** and **3** in aqueous solutions of TFE

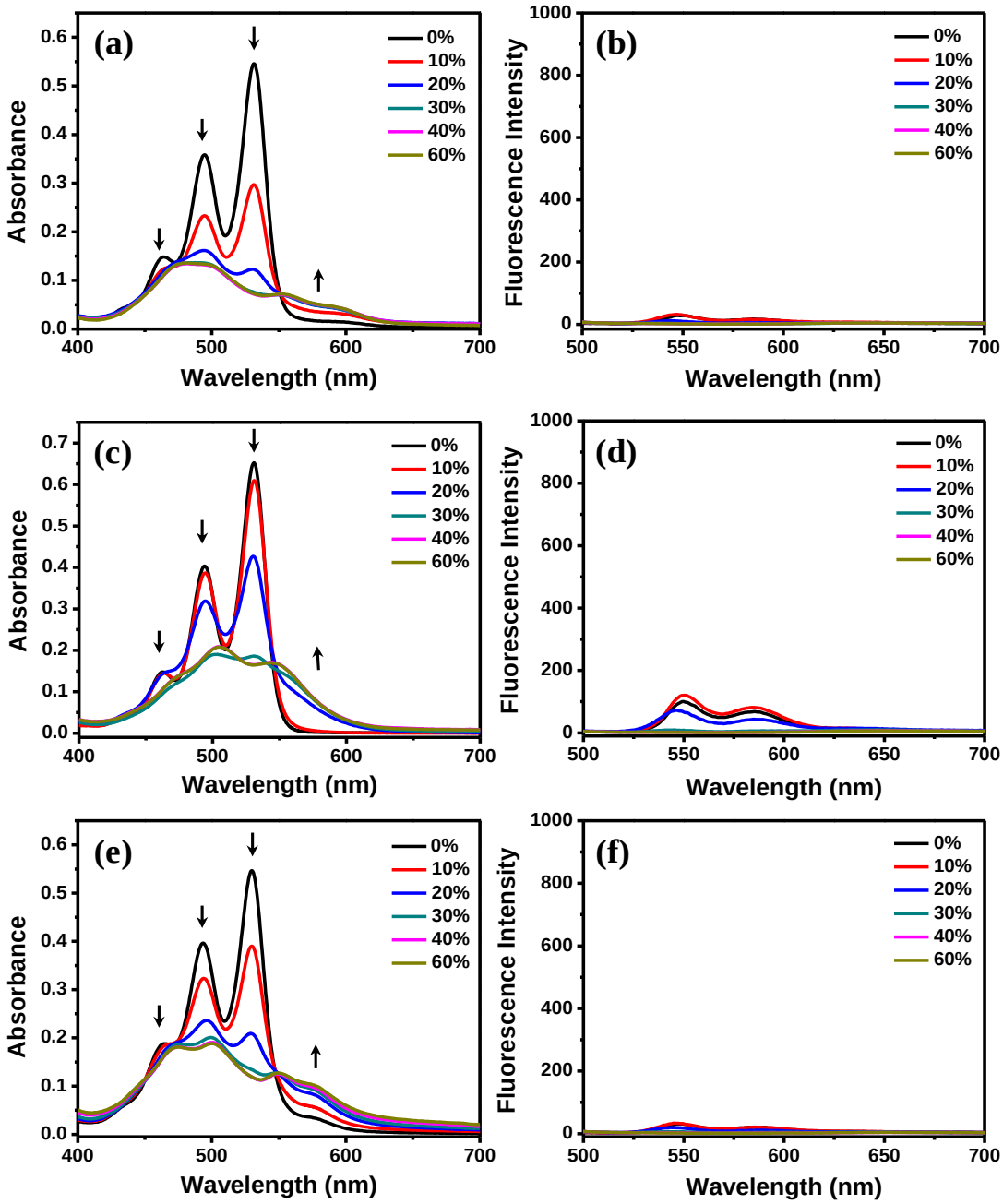


**Figure 2**. (a), (c) and (e) Absorption, (b), (d) and (f) fluorescence (excitation at 480 nm) spectra of 200 μM solution of **1**, **2** and **3** respectively at 298 K. The values represent the percentages of water in aqueous solution of DMSO.

(Figure 1c-f). On the contrary, **1**, **2**, and **3** in aqueous DMSO exhibited a hypochromic effect for ≤30% v/v of water in DMSO (Figure 2). With further increase in water content,

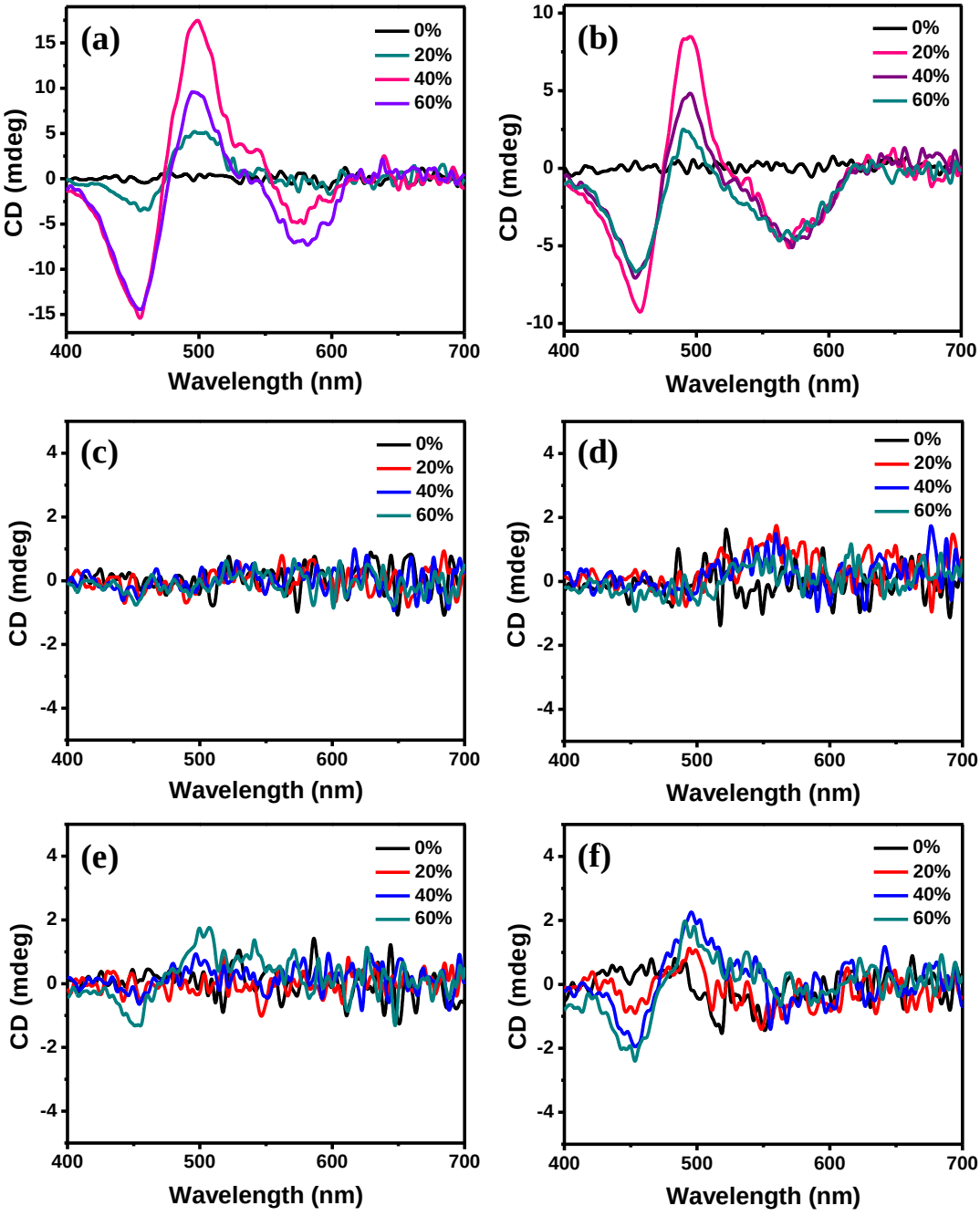


**Figure 3**. CD spectra of 200 μM solution of (a, b) **1**, (c, d) **2** and (e, f) **3** at 298 K. (a), (c) and (e) are in aqueous TFE while (b), (d) and (f) in aqueous DMSO. (a-f) Spectra of as-prepared (prepared by successive dissolution and solvent mixing) samples. The values represent the percentages of water in aqueous solution of TFE or DMSO.

a bathochromic shift was observed, and ultimately a shift of 23, 14, and 18 nm (with respect to $\lambda_{max}$ = 530 nm) was found for **1**, **2**, and **3** in 60% v/v of water in DMSO.

To gain further insights into the nature of intermolecular interactions, CD spectroscopy studies were performed. CD spectra of **1** in TFE showed no characteristic exciton coupled cotton effect, which could be ascribed for a molecularly dissolved state (Figure 3a, black trace). However, in aqueous TFE bisignated CD features were observed and a negative sign of the first cotton effect was ascribed to M-type helicity. In contrast, **2** did not show any cotton effect both in TFE and in aqueous TFE (Figure 3c). On the other hand, absorption and fluorescence studies had revealed that **2** was aggregated in aqueous TFE. Thus, the absence of CD features for a chiral molecule like **2**, even in the aggregated state could be ascribed either due to probable CD silencing or to phenyl-substituent induced hindrance for excitonic coupling.[42] Further, **3** also did not show any cotton effect in aqueous TFE, which is most likely due to CD silencing as the methyl substituent would be sterically less bulky (Figure 3e). Molecular aggregation behavior of **1** (Figure 3b), **2** (Figure 3d), and **3** (Figure 3f) in aqueous DMSO was also along similar lines to that in aqueous TFE.

### 3.1.2. Extremely slow dynamics of an abiotic helical assembly

Serendipitously, we found that the aged sample of **1** showed a bisignated cotton effect in DMSO alone (Figure 4a), in contrast to the CD-inactive characteristics observed earlier (Figure 3b, black trace). Further investigations to understand the origin of such molecular

assembly behavior led us to some remarkable conclusions. Time-dependent CD studies of **1** in DMSO alone revealed the gradual transition from a molecularly dissolved state of an as-prepared sample to a supramolecular chiral assembly over a day's time (Figure 4a). Typically, chiral molecules undergo helical assembly either in a specific solvent or in a mixture of solvents almost instantaneously, which is in total contrast to the extremely slow dynamics of **1** observed in DMSO.[43] A plot of CD intensity as a function of time shows a sigmoidal-like correlation indicative of isodesmic growth (Figure 4b). Further, concentration-dependent studies of **1** in DMSO were performed to find the critical

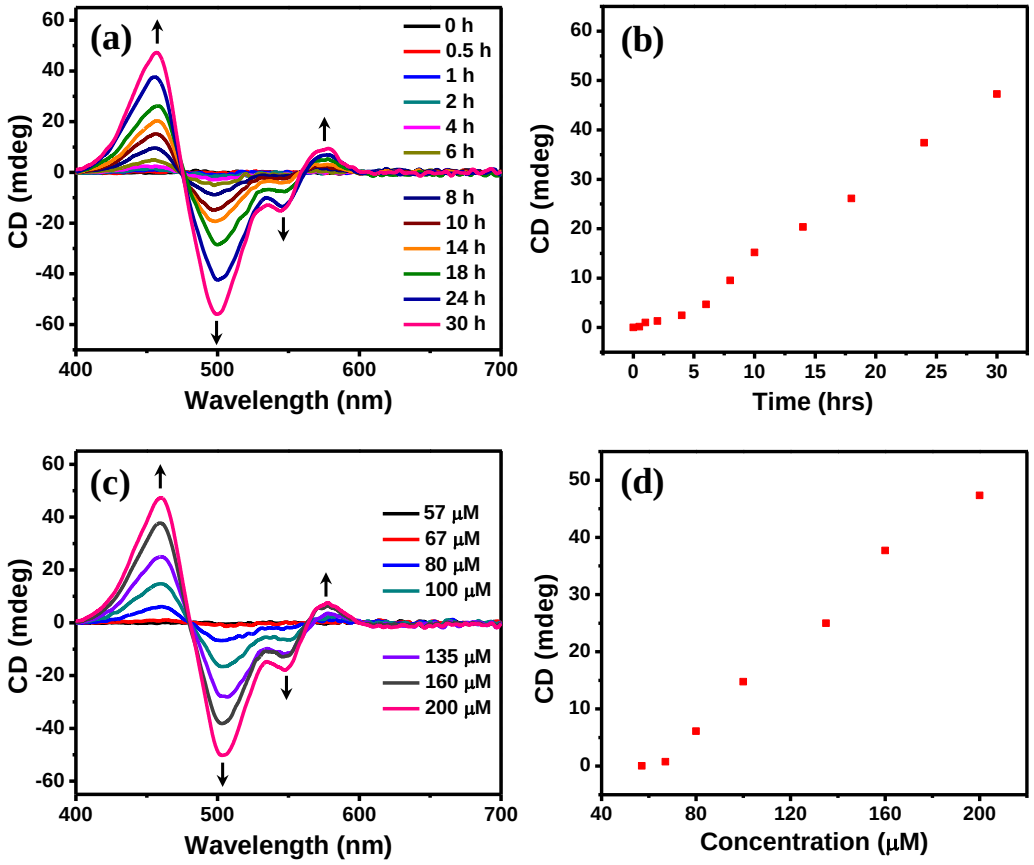


**Figure 4**. (a) Time dependent CD spectra of 200 μM solutions of **1** in DMSO. (b) Time dependent CD spectra of 200 μM solutions of **1** in DMSO monitored at 457 nm. (c) Concentration dependent CD spectra of **1** in DMSO for aged (30 h) sample. (d) Concentration dependent CD spectra of 200 μM solutions of **1** in DMSO monitored at 457 nm.

concentration of the helical assembly (Figure 4c). However, a sigmoidal-like correlation was not obvious for the plot of CD intensity as a function of the molar concentration of **1** in DMSO (Figure 4d).

Thus, variable temperature CD studies were carried out for accurate determination of the supramolecular growth mechanism and to obtain the thermodynamic parameters. For this experiment, the CD intensity at 500 nm was recorded at 0.1 K intervals with a ramp rate of 1 K $min^{-1}$ during heating or cooling cycles between 298 and 363 K. Upon heating, as expected, **1** in DMSO was found to undergo supramolecular depolymerization from its aggregated state to its molecularly dissolved state (Figure 5a,b). However, upon cooling under the same conditions, **1** was totally CD-inactive from 363 to 298 K (Figure 5b). This difference in the trajectories of heating and cooling cycles known as hysteresis, indicates that the self-assembly is not under thermodynamic control.[44] We have termed this transition of **1** from the aggregated state to the molecularly dissolved state as chiral denaturation. Moreover, it was interesting to note that the trajectory obtained during the heating cycle for these kinetically controlled aggregates was also sigmoidal in nature. These temperature-dependent CD data were normalized to obtain the degree of aggregation $\alpha$ which was then fitted to the isodesmic model, as prevalent in the literature (Figure 5c).[43-46] For a 200 μM concentration of **1**, the melting temperature $T_M$ (defined as the temperature for which $\alpha = 0.5$) was found to be 316.6 K. The calculated values of the molar enthalpy ($\Delta H$), the number-averaged degree of polymerization ($DP_N$), and the association constant (K) at 303 K were -195 kJ $mol^{-1}$, 4.36, and $7.32 \times 10^4$ $M^{-1}$, respectively, and evidently are not the true thermodynamic values because the molecular system is not under thermodynamic equilibrium.

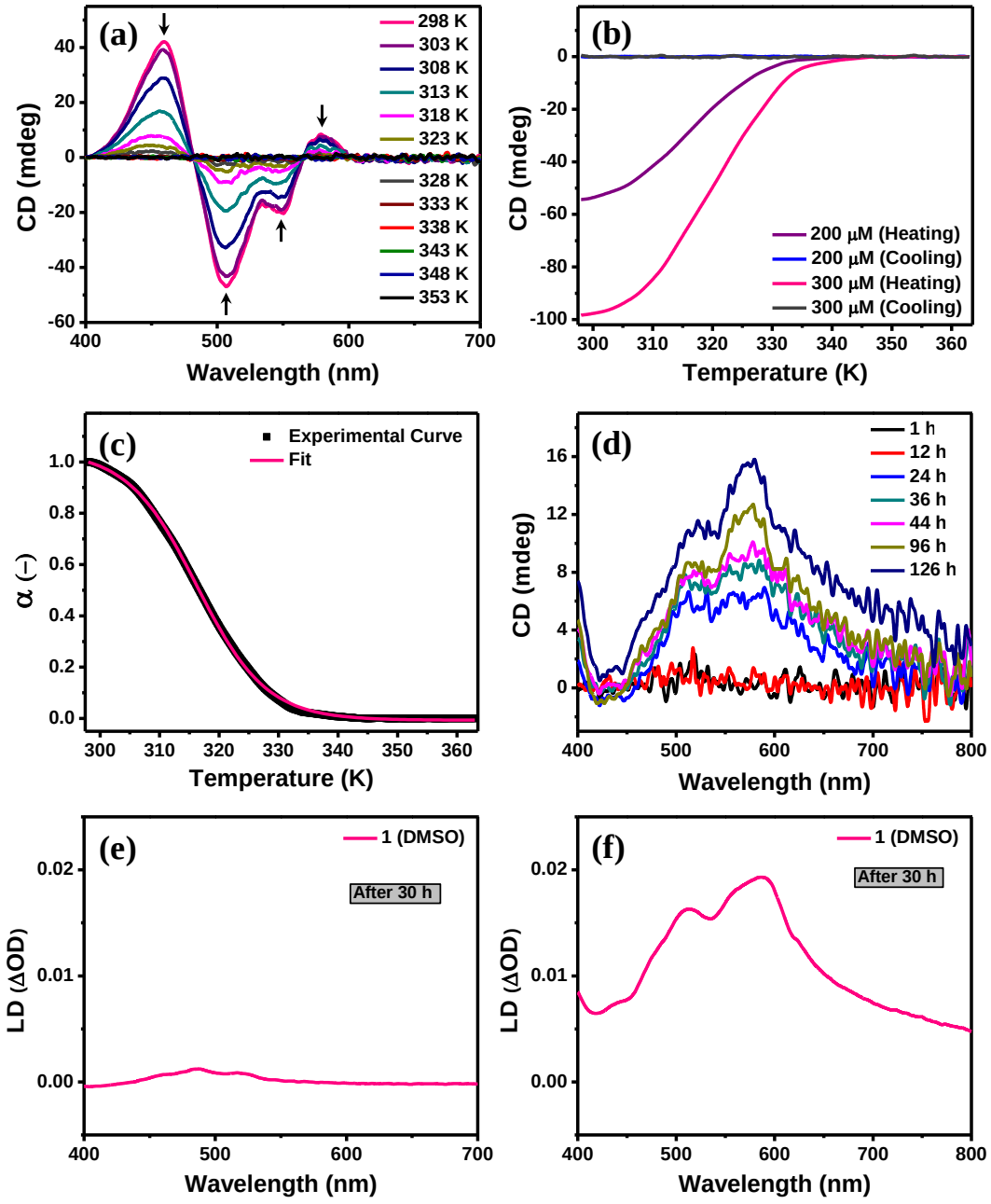


**Figure 5**. (a) CD spectra of 200 μM solution of **1** in DMSO at respective temperature. (b) Temperature dependent CD spectra of **1** in DMSO monitored at 500 nm. (a) and (b) For aged (30 h) sample. (c) Temperature dependent degree of aggregation, α calculated from CD intensity at 500 nm and the corresponding isodesmic fit. (d) Time dependent CD spectra of **1** (200 μM) in DMSO after chiral denaturation. The spectral features are LD induced artifacts. LD spectra of 200 μM solution of **1** in DMSO (e) non denatured and (f) chiral denatured.

Although CD was inactive for **1** during the cooling cycle, we were hoping that the supramolecular helical assembly could be regained over a period of time due to its slow dynamics. This chiral denatured sample when monitored at regular time intervals over a day's time revealed only a broad spectra stretching from 400 to 800 nm (Figure 5d), which was totally different from the non-denatured (having bisignated CD as in Figure 4a) sample of **1**. Similar broad non-bisignated CD features were found even after 5 day's time. This chiral denatured sample when subjected to linear dichroism (LD) studies showed considerable enhancement in the absorption in comparison to the non-denatured sample, suggesting a probable LD-induced artifact (Figure 5e,f). This suggests that **1** loses its specific supramolecular chiral handedness upon heating and ultimately ends up with random aggregation. Such heat-induced irreversible denaturation behavior for a simple and small supramolecular helical system like **1** was especially intriguing.

Having understood the thermally irreversible helical assembly behavior of **1**, we explored further to know if it can be made reversible. If this chiral denatured sample was assumed to be a molecular entity having no bias for specific handedness (which is why it leads to random aggregation), then a fresh non-denatured sample should be able to induce specific handedness by means of the seeding effect. When a fixed concentration of non-denatured sample (Figure 6a, navy blue trace) was mixed with the chiral denatured sample, it indeed induced specific handedness to the denatured sample, as can be inferred from the CD spectra (Figure 6a). Herein, the assignment of the chirality amplification process to the seeding effect, instead of the sergeants-and-soldiers or majority rules type is mainly due to their definitions as such.[43] Although one can ascribe our system to a sergeants-and-soldiers amplification pathway over the majority-rules type due to the

observed chiral denaturation (CD silencing upon heating), it is the absence of strong acidic/basic conditions and/or the heat-induced racemization pathway (to the best of our knowledge) that prompted us to ascribe it to the seeding effect.

Interestingly, incremental addition of water to a day's old sample of **1** in DMSO was found to exhibit CD features (Figure 6b) similar to that of a kinetically controlled

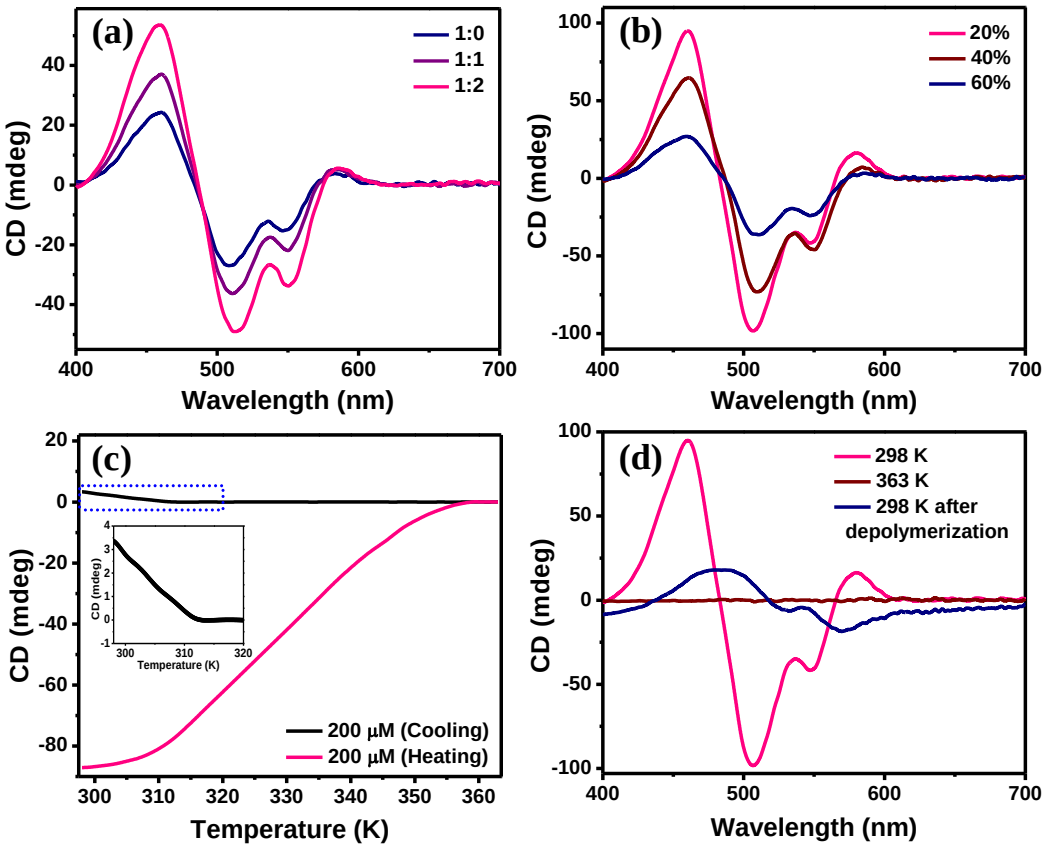


**Figure 6**. (a) CD spectra of fixed concentration (1 mole) of non-denatured aggregates of **1** (navy blue trace) added with chiral denatured sample (navy blue: 0, purple: 1 and pink: 2 mole respectively). (b) CD spectra of 200 μM solutions of **1** in aqueous DMSO. The values represent the percentages of water in aqueous DMSO. (c) Temperature dependent CD spectra of **1** in 20 % aqueous DMSO monitored at 505 nm. The inset is the enlarged spectra for the region shown in dotted blue box. (d) CD spectra of **1** in 20 % aqueous DMSO recorded at specific temperatures. For (b), (c) and (d) the samples were prepared by employing a day's old solution of **1** in DMSO.

assembly as in Figure 4a, which is different from CD spectra recorded for an as-prepared sample with incremental addition of water (Figure 3b). Further, in order to check the effect of heat on the assembly of an aged sample of **1** in DMSO upon addition of water, a variable-temperature-dependent study of **1** in 20% aqueous DMSO was performed. Here as well, upon heating the supramolecular aggregates of **1** depolymerized to reach a molecularly dissolved state (Figure 6c). However, upon cooling, the CD signal started to emerge below 312 K (Figure 6c). The CD spectra acquired for **1** in 20% aqueous DMSO at 298, 363, and back again at 298 K after supramolecular depolymerization showed distinct cotton effects (Figure 6d).

Interestingly, the latter spectra obtained at 298 K after depolymerization had similar spectral features to that obtained for an as-prepared sample of **1** in 20% aqueous DMSO (compare with Figure 3b, pink trace). The probable reason for such aggregation behavior could be that once the kinetically controlled aggregates are formed over a day's time, the hydrophobic forces (rendered by water) have minimal effect and thus, the CD features prevail even in the presence of water. Only when these kinetically controlled aggregates depolymerize at high temperature do the hydrophobic effect predominate and thereby CD features as seen in Figure 3b are regained below 312 K. Moreover, the occurrence of CD spectral features for **1** in a 20% aqueous DMSO upon a heating-cooling cycle further reiterates that the compound is not a racemic mixture (equivalent to an achiral entity in terms of CD inactivity) and hence cannot be ascribed to the sergeants-and-soldiers amplification pathway. Further, it should be noted that **2** in DMSO as well as **1** in TFE were CD-inactive even after 2 months of sample preparation, while **3** in DMSO

exhibited weak CD signals in about 2 month's time (Figure 7). Therefore, the observed slow dynamics of **1** in DMSO could be attributed to their reduced solubility as well as to the solvatophobic-force-induced helical assembly rendered by a relatively bulkier side chain of isoleucine.

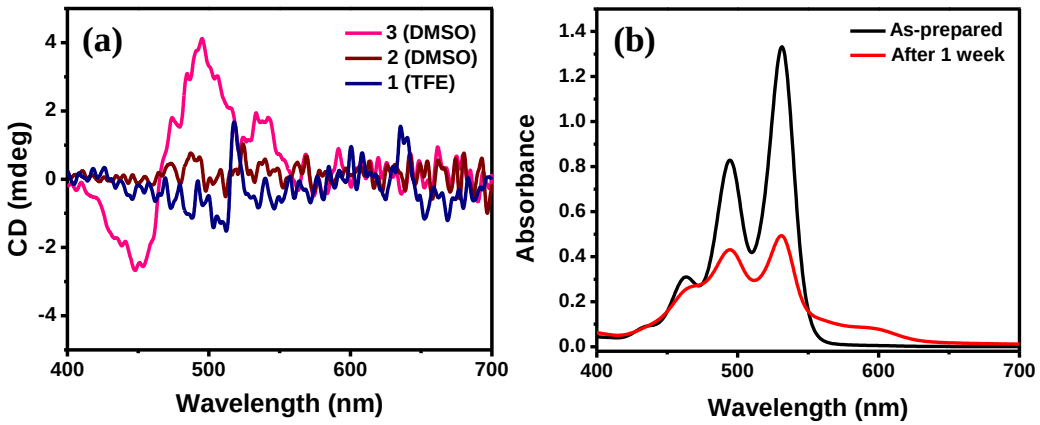


**Figure 7**. (a) CD spectra of **1**, **2** and **3** recorded after 2 months of their sample preparation. (b) Time dependent absorption spectra of as-prepared 200 μM solution of **1** in DMSO and after one week.

### 3.1.3. NMR and DLS studies

In order to address the conformational changes occurring in **1**, we first carried out temperature-dependent $^{1}$H NMR studies. The compound **1** was found to be thermally stable at temperatures as high as 363 K, which is in agreement with the literature (Figure 8).[47] At this high temperature, very minute variations in the chemical shift values were observed due to the deshielding effect, which retraces back upon cooling to room temperature. This study only helped us to prove that **1** is thermally stable, while the chemical shift values were minimal to account for conformational changes. The nature of conformational changes remains to be addressed and may need high-level theoretical

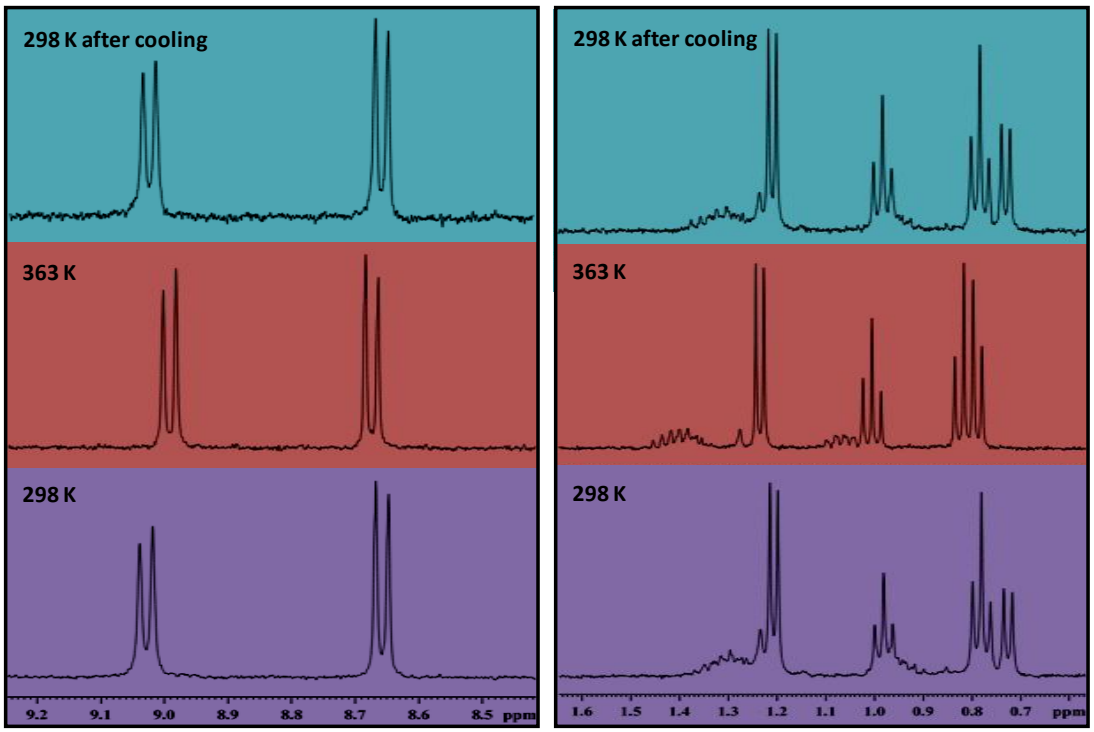


**Figure 8**. Temperature dependent $^{1}$H NMR of 200 μM DMSO-$d_6$ solution of **1** showing the enlarged portion corresponding to perylenediimide core and side chain of isoleucine.

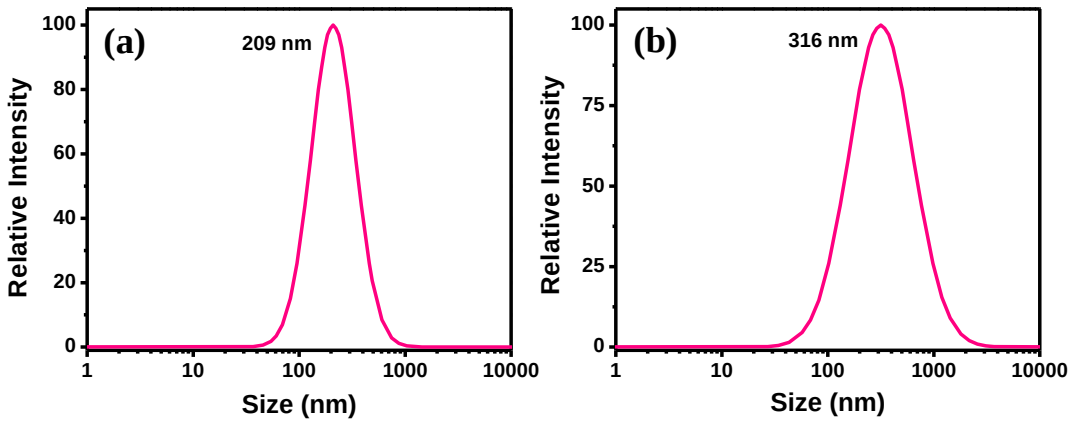


**Figure 9**. Dynamic light scattering (DLS) spectra of 200 μM DMSO solution of **1** (a) 30 h aged and (b) after one week following a heating-cooling cycle (chiral denatured).

studies and computational simulations. Further, we performed dynamic light scattering (DLS) studies, which show that there are no aggregates in the as-prepared 200 μM

DMSO solution of **1** (data not shown). However, aging as well as following the heating cooling cycle showed the presence of aggregates (Figure 9). This can thus believed to rule out the transition from one aggregate to another and thereby supports our correlation with the secondary structure of proteins via an extremely slow kinetic pathway.

### 3.1.4. Discussion and conclusions

A schematic representation depicting the unusual correlation between the abiotic helical assembly/reassembly of **1** and the secondary structure of the protein is shown in Figure 10. The supramolecular helical assembly of **1** is on an average 10 orders of magnitude slower than the protein's microsecond kinetics. Such slow dynamics are advantageous from an experimental perspective to probe the folding pathway but may not be for routine

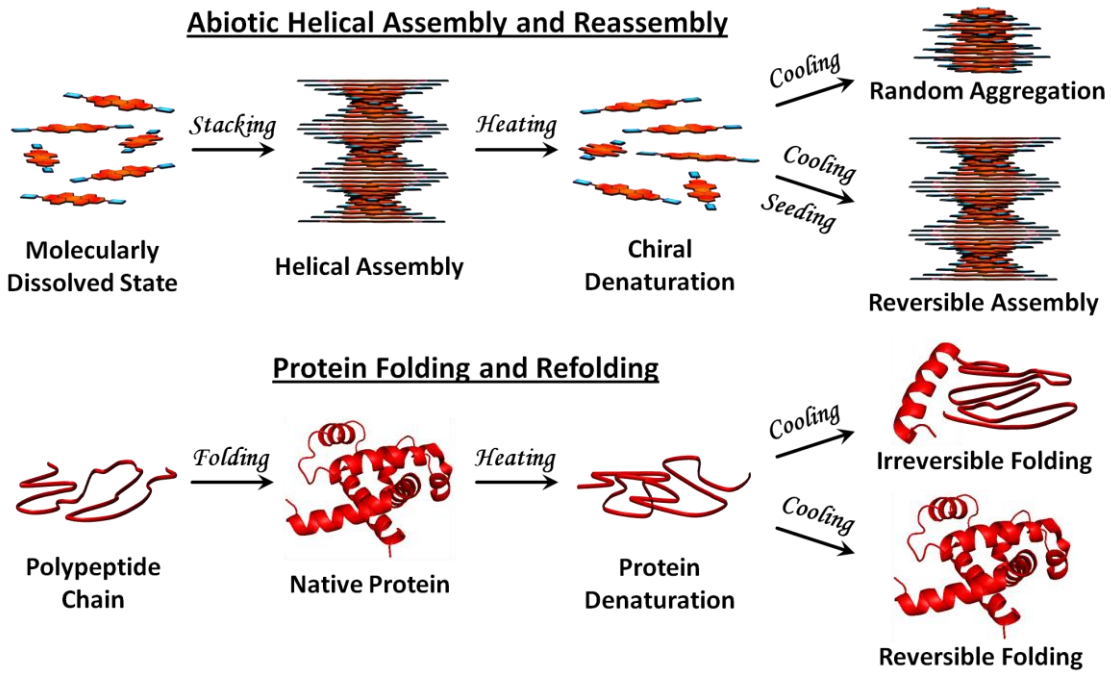


**Figure 10**. A schematic representation to depict the relevance of the abiotic helical assembly and reassembly of **1** with the (secondary structure) protein folding and refolding. Not to scale.

computational simulations. Unlike proteins, the aggregation of **1** was mainly driven by solvatophobic forces and stabilized by aromatic interactions of the perylenediimide core without any contributions from hydrogen bonding. The heat-induced irreversible chiral denaturation and the formation of random aggregates of **1** in DMSO are especially intriguing, which can be attributed to conformational changes in the side chain of the isoleucine methylester functionality. The unusual molecular assembly/reassembly behavior of **1** could thus be visualized as an extremely simplified model representing the complex protein folding problem, which has both merits and demerits of its own. Moreover, it should be noted that molecular-level experimental understanding of protein folding is not known except for the mutation-based studies in protein engineering. We hope that this work will stimulate researchers to develop improved designer molecules for obtaining clearer and finer details of protein folding as well as a means for *de novo* functional peptides and proteins having hitherto unknown properties and functions.

### 3.1.5. Experimental section

#### *3.1.5.1. Materials and methods*

Perylene-3,4,9,10-tetracarboxylic dianhydride was obtained from Sigma-Aldrich. L-isoleucine, L-phenylalanine, L-alanine, acetyl chloride, imidazole and triethylamine were obtained from Spectrochem Pvt. Ltd. Mumbai (India). All other reagents and solvents were of reagent grade and used without further purification. $^{1}H$ and $^{13}C$ NMR were recorded on a Bruker AV-400 spectrometer with chemical shifts reported as ppm (in $CDCl_3$ with tetramethylsilane as internal standard). Mass spectra were obtained from

Shimadzu 2020 LC-MS. Elemental analysis was carried out on ThermoScientific FLASH 2000 Organic Element Analyzer.

*Absorption spectroscopy*: UV-vis spectra were recorded on a Perkin Elmer Model Lambda 900 spectrophotometer. 200 μM of the sample prepared from 1 mM stock solution was analyzed in quartz cuvette of 1 mm path length.

*Fluorescence spectroscopy*: Fluorescence spectra were recorded on a Perkin Elmer Model LS 55 spectrophotometer. 200 μM of the sample prepared from 1 mM stock solution was analyzed in quartz cuvette of 1 mm path length with an excitation at 480 nm.

*Circular dichroism (CD) spectroscopy*: CD measurements were carried out on a Jasco J-815 spectrometer under nitrogen atmosphere. The sensitivity, time constant and scan rate were chosen appropriately. Temperature dependent measurements were performed employing Peltier-type temperature controller (CDF-4265/15) in the range of 298 K to 363 K with a ramp rate of 1 K $min^{-1}$. Required concentration of the sample was prepared from 1 mM stock solution and analyzed in quartz cuvette of 1 mm path length. The time dependent studies were performed with respect to the time of preparation of 1 mM stock solution of **1**.

*Dynamic light scattering analysis*: The self-assembled aggregate size measurements were carried out using ZetaPALS, Zeta Potential Analyzer (Brookhaven Instruments Corporation, USA) by employing 200 μM DMSO solution of **1**.

*Polarimeter*: The specific optical rotation of chiral perylenediimides was obtained by using Digital Polarimeter P-2000 (Jasco Corporation, Japan).

### *3.1.5.2. Synthesis of L-isoleucine methylester appended perylenediimide* (1)

*Synthesis of L-isoleucine methylester hydrochloride*: Anhydrous methanol (50 mL) was

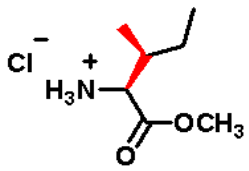

taken in a 100 mL 2-necked round bottom flask fitted with a reflux condenser and an additional dropping funnel and cooled to ice temperature. Acetyl chloride (3 mL) was added drop-wise through the dropping funnel. After 15 min, L-isoleucine (3 g) was added and the reaction mixture was refluxed at 70 °C for overnight. The reaction mixture was vacuo dried to obtain L-isoleucine methylester hydrochloride in quantitative yield and used for further reaction without purification.

Perylene-3,4,9,10-tetracarboxylic dianhydride (500 mg, 1.28 mmol), L-isoleucine methylester hydrochloride (463 mg 2.55 mmol) and imidazole (10 g) taken in a 100 mL

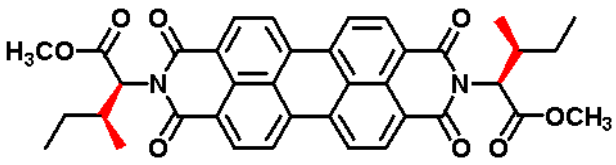

round bottom flask was heated at 110 °C for 2 h. To the reaction mixture ~ 200 mL ethanol and ~ 300 mL of 1 N HCl was added. The reaction contents were shaken vigorously and were allowed to precipitate overnight. The precipitate was washed with distilled water till a neutral pH was obtained for the aqueous filtrate. The product was further purified by column chromatography (0.5 % methanol in chloroform). Yield 65%. $^{1}$H NMR (400 MHz, *CDCl$_3$*): δ 8.71 (dd, 8H, J = 8Hz, 4Hz), 5.47 (d, 2H, J = 8Hz), 3.72 (s, 6H), 2.68 (m, 2H), 1.30 (m, 6H), 1.04 (m, 4H), 0.82 (m, 6H). $^{13}$C NMR (100 MHz, *CDCl$_3$*): δ 170.3, 163.4, 135.1, 132.2, 129.8, 126.7, 123.5, 123.1, 58.4, 52.4, 33.9, 33.8, 28.4, 25.4, 18.1, 15.1, 11.5, 11.2. MS (EI): Found m/z = 646.31 $[M]^+$ for $C_{38}H_{34}N_2O_8$ (calcd.

646.23). Elemental analysis: Found C, 70.55; H, 5.34; N, 4.36; calcd: C, 70.58; H, 5.30; N, 4.33 for $C_{38}H_{34}N_2O_8$.

### *3.1.5.3. Synthesis of L-phenylalanine methylester appended perylenediimide* (2)

*Synthesis of L-phenylalanine methylester hydrochloride*: Anhydrous methanol (50 mL) was taken in a 100 mL 2-necked round bottom flask fitted with a reflux condenser and an

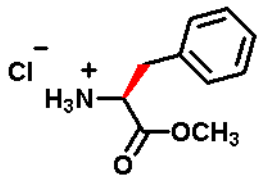


additional dropping funnel and cooled to ice temperature. Acetyl chloride (3 mL) was added drop-wise through the dropping funnel. After 15 min., L-phenylalanine (3 g) was added and the reaction mixture was refluxed at 70 °C for overnight. The reaction mixture was vacuo dried to obtain L-phenylalanine methylester hydrochloride in quantitative yield and used for further reaction without purification.

Perylene-3,4,9,10-tetracarboxylic dianhydride (200 mg, 0.51 mmol), L-phenylalanine methylester hydrochloride (220 mg 1.02 mmol) and imidazole (5 g) taken

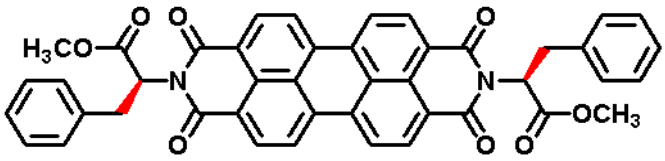


in a 100 mL round bottom flask was heated at 110 °C for 2 h. To the reaction mixture ~ 200 mL ethanol and ~ 300 mL of 1 N HCl was added. The reaction contents were shaken vigorously and allowed to precipitate overnight. The precipitate was washed with distilled water till a neutral pH was obtained for the aqueous filtrate. The product was further purified by column chromatography (0.5 % methanol in chloroform). Yield 69%. $^1$H NMR (400 MHz, *$CDCl_3$*): δ 8.56 (d, 4H, J = 8Hz), 8.48 (d, 4H, J = 8Hz), 7.23 (d, 4H,

J = 8Hz), 7.15 (t, 4H), 7.07 (t, 2H), 6.07 (t, 2H), 3.80 (s, 6H), 3.76 (dd, 2H, J = 8Hz, 4Hz), 3.55 (dd, 2H, J = 8Hz, 12Hz). $^{13}$C NMR (100 MHz, *CDCl$_3$*): δ 170.2, 162.9, 137.5, 134.7, 131.8, 129.4, 128.5, 126.8, 126.4, 123.2, 122.9, 54.6, 52.8, 35.1. MS (EI): Found m/z = 714.31 $[M]^+$ for $C_{44}H_{30}N_2O_8$ (calcd 714.20). Elemental analysis: Found C, 73.90; H, 4.28; N, 3.88; Calcd: C, 73.94; H, 4.23; N, 3.92 for $C_{44}H_{30}N_2O_8$.

### *3.1.5.4. Synthesis of L-alanine methylester appended perylenediimide* (3)

*Synthesis of L-alanine methylester hydrochloride*: Anhydrous methanol (50 mL) was taken in a 100 mL 2-necked round bottom flask fitted with a reflux condenser and an additional dropping funnel and cooled to ice temperature. Acetyl chloride (3 mL) was added drop wise through the dropping funnel. After 15 min., L-alanine (3 g) was added and the reaction mixture was refluxed at 70 °C for overnight. The reaction mixture was vacuo dried to obtain L-alanine methylester hydrochloride in quantitative yield and used for further reaction without purification.

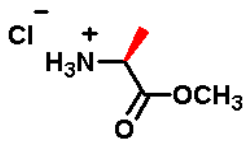


Perylene-3,4,9,10-tetracarboxylic dianhydride (500 mg, 1.27 mmol), L-alanine methylester hydrochloride (354 mg 2.55 mmol) and imidazole (10 g) taken in a 100 mL round bottom flask was heated at 110 °C for 2 h. To the reaction mixture ~ 200 mL ethanol and ~ 300 mL of 1 N HCl was added. The reaction contents were shaken vigorously and allowed to precipitate overnight. The precipitate was washed with distilled water till a neutral pH

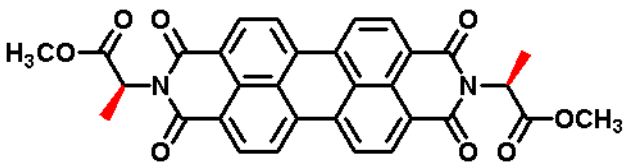

was obtained for the aqueous filtrate. The product was further purified by column chromatography (0.5 % methanol in chloroform). Yield 52%. $^{1}$H NMR (400 MHz, *CDCl$_3$*): δ 8.68 (dd, 8H, J = 4Hz, 8Hz), 5.79 (q, 2H), 3.77 (s, 6H), 1.75 (d, 6H, J = 8Hz). $^{13}$C NMR (100 MHz, *CDCl$_3$*): δ 170.9, 162.9, 135.1, 132.0, 129.9, 126.8, 123.5, 123.4, 52.7, 49.5, 29.9. MS (EI): Found m/z = 562.19 $[M]^+$ for $C_{32}H_{22}N_2O_8$ (calcd. 562.14). Elemental analysis: Found C, 68.27; H, 3.99; N, 4.95; Calcd. C, 68.32; H, 3.94; N, 4.98 for $C_{32}H_{22}N_2O_8$.

## 3.2. Emergence and Autoregulation in Dynamic Molecular Assemblies

Autoregulation is the process by which a system actuates and modulates its responses automatically for an external stimulus.[48-51] Such mechanisms are extremely critical for the smooth functioning of almost all biochemical processes. On the other hand, emergence is the process by which complex systems and patterns arise out of multitude of relatively simple interactions.[52,53] These emergent behaviors/properties are often unpredictable, unprecedented and represent the advanced stages of the system's evolution.[54,55] Even the origin and evolution of life from inanimate matter is a resultant of emergence.[56,57] Besides, it's literal meaning 'to arise', in general terms emergence is defined as 'the whole being greater than the sum of its parts'. Although, the unusual characteristic features of superconductors, topological insulators *etc*., are all attributed to emergence, they are no such reports in abiotic molecular assemblies, to the best of our knowledge.[58-61] Intriguingly, given the context of evolution of life, it is imperative that such systems are developed and/or studied both for our fundamental understanding and *de novo* designs of synthetic biological systems. In this regard, we present the experimental evidences of emergent and autoregulatory behavior in an abiotic molecular assembly.

In order to realize an emergent behavior, firstly it is necessary to envision a delicate interplay of multiple interactions. In general, as more and more complex sets of interactions involve, the complexity of the system also increases.[62,63] On the other hand, it need not be true for a complex multitude of interactions to result in novel properties, as the system could either implode or succumb due to relatively weaker effects in a complex environment. Thus, finding an optimal balance of such interactions is one of the most

daunting tasks to embark on. In our earlier work, we had proposed that bioinspired design strategies could in principle be the best way to efficiently engineer the molecular assemblies and could also provide better opportunities to understand our natural world.[31,42,64-67] Our design strategy primarily involves amino acids due to their extraordinary molecular recognition, stereoselectivity and sequence-specific self-assembling properties. Moreover, the rigorous natural selection of several billion years has effectively tailored the chemical functionalities of aminoacids, so as to inculcate multiple interactions like hydrogen bonding, hydrophilic interactions, hydrophobic interactions, and aromatic interactions amongst others. Most importantly, all the functionalities are designed to interact rather synergistically by means of their compact size and positions. Thus, we believe that by derivatizing amino acids with abiotic functional molecules, a wide variety of functional systems are possible with unique properties and applications.[64]

Herein we have thoughtfully employed NDI and pyrene as the functional molecules due to their molecular structural symmetry ($D_{2h}$) and complementary π-character.[66] NDI is π-acidic with an estimated quadrupole moment (*Q*zz) of +18.6 B (Buckinghams) and pyrene is π-basic with a *Q*zz of -13.8 B.[68] Interestingly, theoretical calculations carried out in our earlier work, have showed that the interaction energies for π-π stacking of NDI-NDI, pyrene-pyrene and NDI-pyrene are -27.17, -16.45 and -23.35 kcal $mol^{-1}$ respectively, and by appropriate molecular designs the self-sorting or alternating stack could be realized.[66] In a separate study, we have also shown that the kinetically controlled self-assemblies could be achieved via designer molecules under suitable conditions.[31] Inspired by these earlier successes, we have designed a much more

complicated system of amino acid interlinked triads, comprising NDI and pyrene. The designed molecular systems include six triads of pyrene-NDI-pyrene consisting of alanine, phenylalanine and isoleucine as the interlinking amino acids, so as to modulate their assemblies via different stereochemical information. **LL**, **DD**, **LD** and **RAC** are alanine appended triads, whereas **C1** and **C2** are phenylalanine and isoleucine derivatives respectively. **LL**, **DD** and **LD** represent the stereochemistry of the alanine linker, while the **RAC** molecule was synthesized from a racemic mixture of alanine precursor. **C1** and **C2** serve as controls for the study to emphasize the importance of the molecular design.

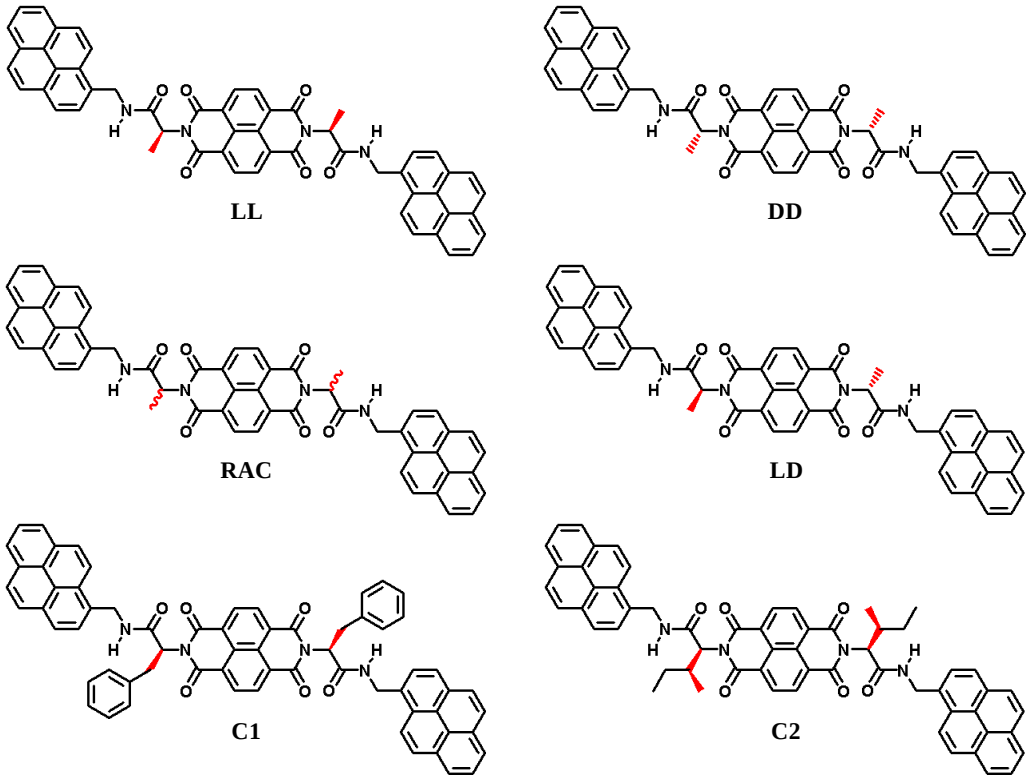


### 3.2.1. Dynamic helical assembly

UV–vis absorption spectra of **LL** in *N*-methyl-2-pyrrolidone (NMP) exhibited absorption bands in the region of 270-400 nm due to characteristic π-π* transitions of pyrene and

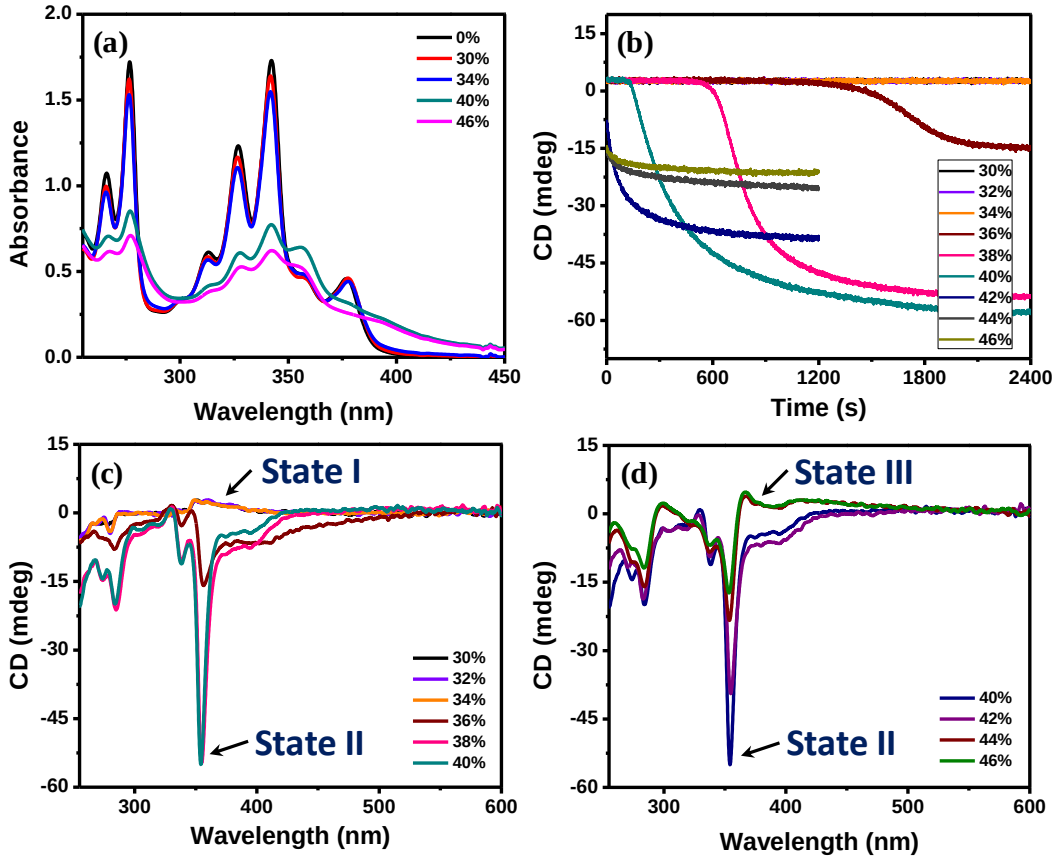


**Figure 11**. (a) Absorption spectra of 200 µM solution of **LL** in (0 to 46%) aqueous NMP. (b) Time-dependent CD spectra of 200 µM solution of **LL** in (0 to 46%) aqueous NMP monitored at 350 nm. (c) and (d) The CD spectra of 200 µM solution of **LL** showing the transitions from ***State I*** to ***State II*** and from ***State II*** to ***State III*** respectively. The values represent the various percentages of water in aqueous NMP. For (a), (c) and (d) the spectrum was recorded either on reaching saturation of CD amplitude or after 40 min.

NDI (Figure 11a). With successive increase of water content in the 200 µM NMP solution of **LL**, a decrease in absorption intensity as well as broadening of the bands was observed due to π-π stacking of **LL** under the enhanced hydrophobic forces of water. Further CD studies rendered remarkable insights into the nature of their assembly. The triad **LL** showed time-dependent dynamic self-assembly behavior in aqueous NMP, once the onset of aggregation was induced by hydrophobic forces (Figure 11b). The CD signals arising due to excitonic coupling of transition dipole moments of NDI and pyrene

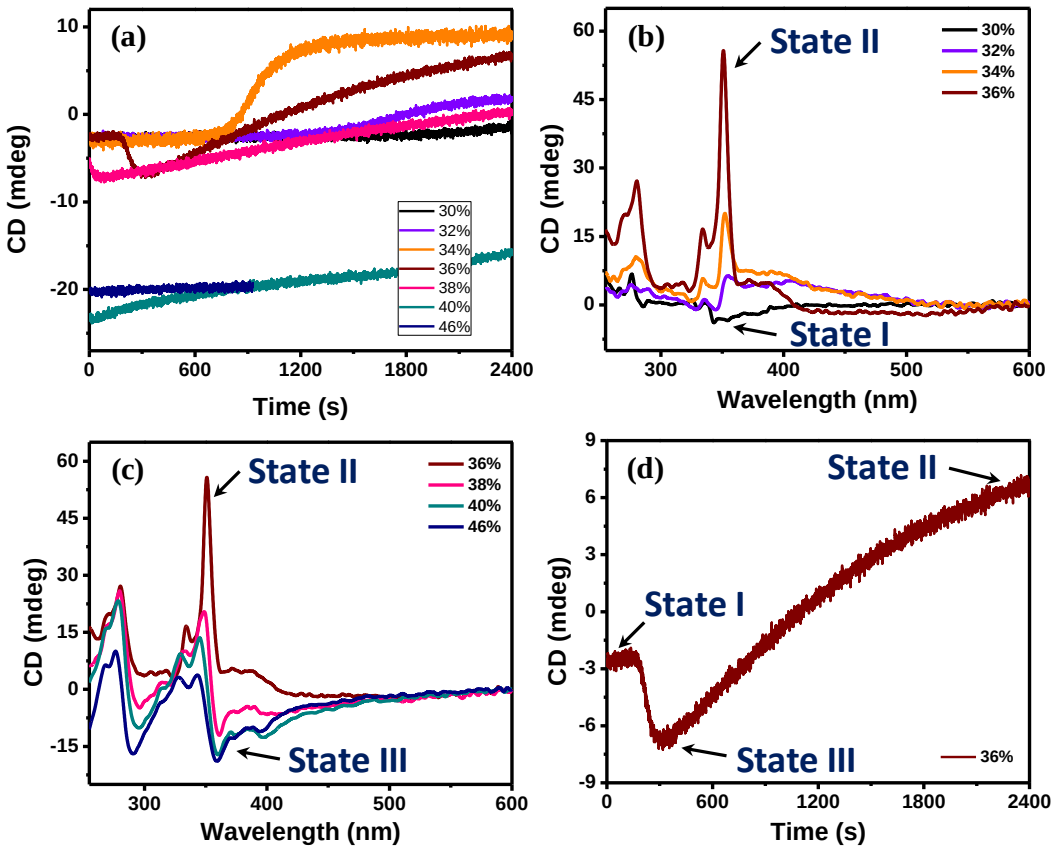


**Figure 12**. (a) Time-dependent CD spectra of 200 µM solution of **DD** in (0 to 46%) aqueous NMP monitored at 360 nm. (b) and (c) The CD spectra of 200 µM solution of **DD** showing the transitions from ***State I*** to ***State II*** and from ***State II*** to ***State III*** respectively. The spectrum was recorded either on reaching saturation of CD amplitude or after 40 min. (d) Time-dependent CD spectra of 200 µM solution of **DD** showing the transitions to various aggregation states. The values represent the various percentages of water in aqueous NMP.

were found to have distinct spectral features as a function of solvent composition. Notably, three main aggregation states could be described namely ***State I***, ***State II*** and ***State III*** (Figure 11c,d). Up to 34% of aqueous content in NMP, **LL** retains ***State I***. With successive increase of water content transition of ***State I*** to ***State II*** (40% aqueous NMP) and in turn to ***State III*** (46% aqueous NMP) was observed. On the other hand, **DD** enantiomer exhibited similar characteristics as that of **LL** with some slight interesting variations (Figure 12a). Herein, the transition from ***State I*** to ***State II*** occurs from 30%

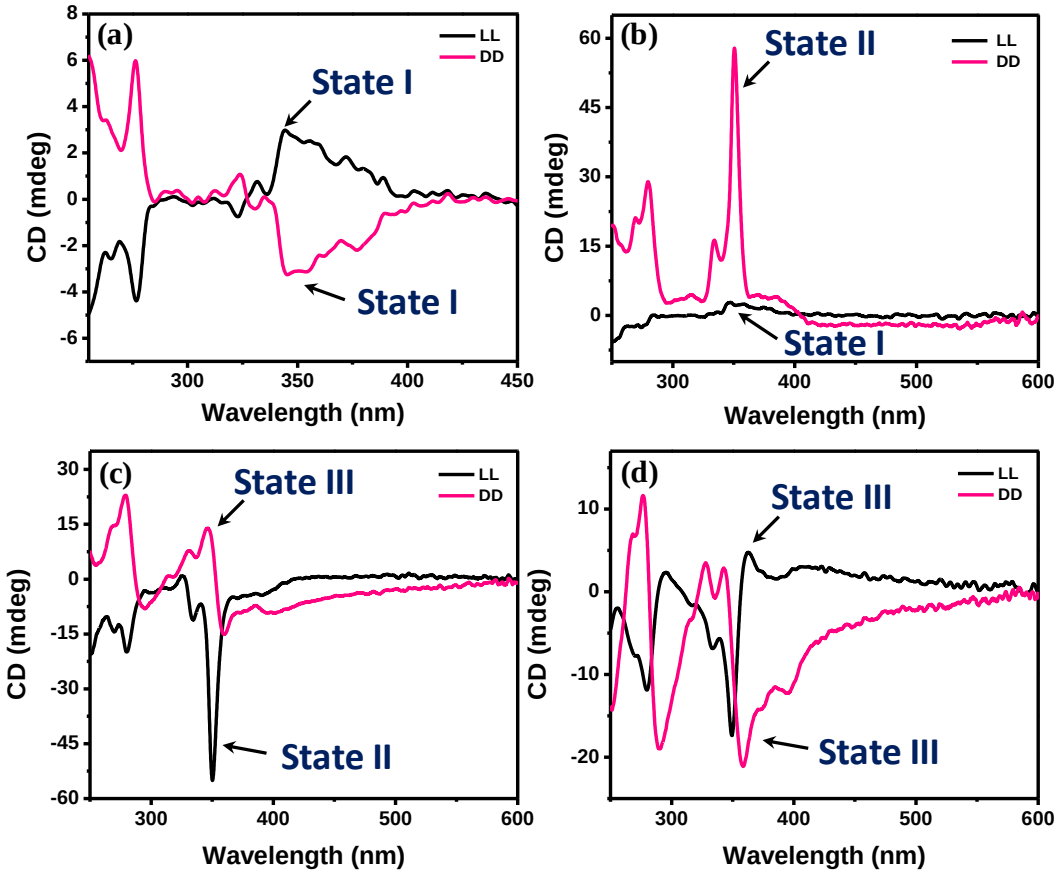


**Figure 13**. (a), (b), (c) and (d) The CD spectra of 200 µM solution of **LL** and **DD** in ***Sol30*** (30% aqueous NMP), ***Sol36*** (36% aqueous NMP), ***Sol40*** (40% aqueous NMP) and ***Sol46*** (46% aqueous NMP) respectively.

aqueous content of NMP itself, instead of 34% as seen in case of **LL** (Figure 12b). The transition from ***State I*** to ***State II*** completes in ~ 36% of aqueous NMP and above which a transition occurs to ***State III*** (Figure 12c). Intriguingly, we have observed an unprecedented sequential transition involving all three distinct aggregation states of **DD** in 36% aqueous NMP (Figure 12d). Such aggregation pathway complexities involving transitions from ***State I*** to ***State III*** and in turn to ***State II*** occurring over several minutes time scale is indeed one of the most striking aspects of this molecular system.

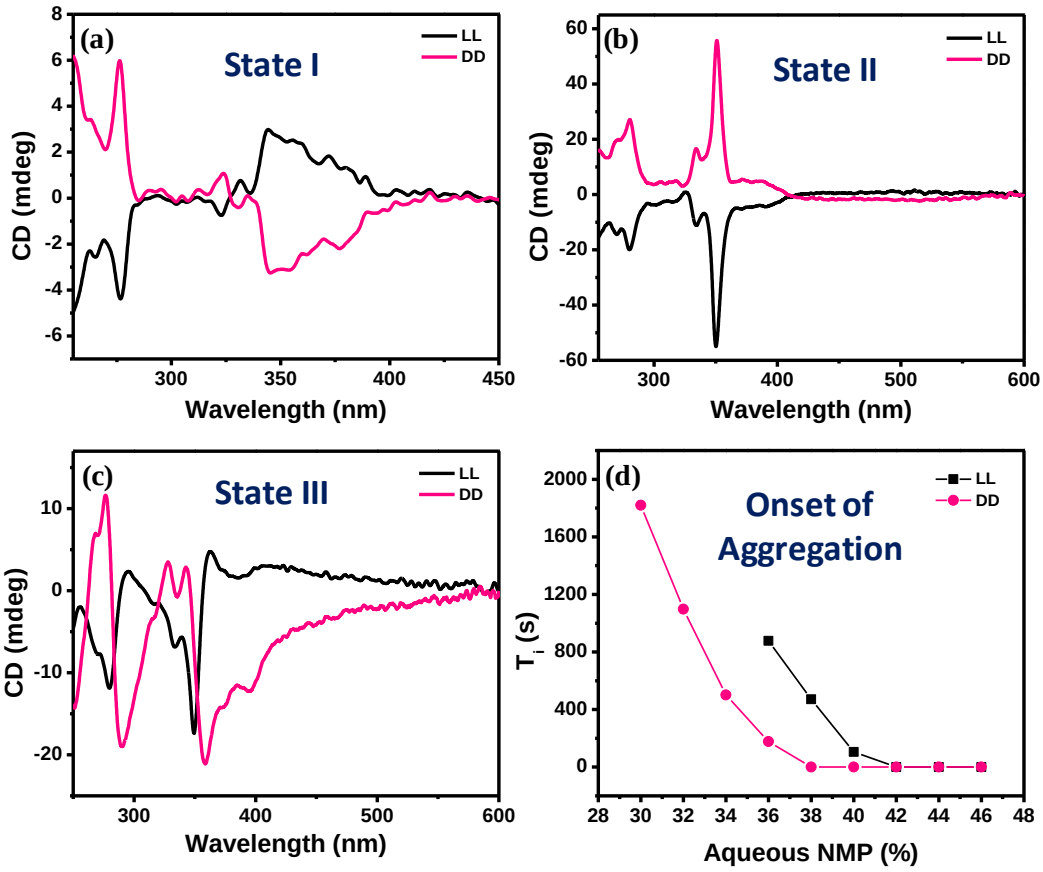


**Figure 14**. (a), (b) and (c) The CD spectra of 200 µM solution of **LL** and **DD** exhibiting ***State I***, ***State II*** and ***State III*** respectively. (d) The plot of onset of aggregation of **LL** and **DD** as a function of solvent composition. $T_i$ is the time at which the aggregation initiates.

The above described molecular self-assembly behavior indicates four important solvent compositions namely 30%, 36%, 40% and 46% of aqueous NMP (denoted as ***Sol30***, ***Sol36***, ***Sol40*** and ***Sol46*** respectively), wherein which different combinations of **LL** and **DD** aggregation states exist. In ***Sol30*** (Figure 13a), both **LL** and **DD** exist in ***State I***, while in ***Sol36*** (Figure 13b); **LL** retains ***State I***, whereas **DD** attains ***State II***. In ***Sol40*** (Figure 13c), **LL** possesses ***State II*** and **DD** reaches ***State III***. However in ***Sol46*** (Figure 13d), both **LL** and **DD** show the existence of ***State III***. In Figure 14a, 14b and 14c, we show the three different states of **LL** and **DD** namely ***State I***, ***State II*** and ***State***

***III*** respectively. Further in Figure 14d, we have shown a plot of solvent composition against the time at which aggregation initiates (represented as $T_i$), to provide a better perspective of the relative differences in the onset of aggregation of **LL** and **DD**. On the other hand, as expected **RAC**, the triad synthesized from racemic triad did not show any CD signals, suggesting the absence of any enantiomeric excess to induce biased helical assembly (Figure 15a). In addition, **LD** also did not show any CD signals in NMP due to opposing biasing effect of the L and D isomers (Figure 15b). However, under enhanced hydrophobic forces even **LD** shows bisignated CD signals due to probable chiral symmetry breaking.[69]

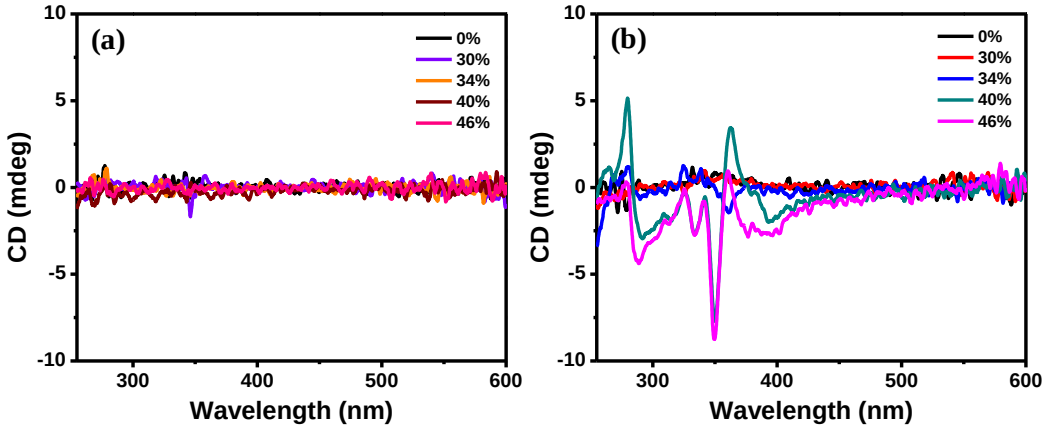


**Figure 15**. (a) and (b) The CD spectra of 200 µM solution of **RAC** and **LD** in aqueous NMP respectively. The values represent the various percentages of water in aqueous NMP.

### 3.2.2. Majority-rule experiment

We envisioned that it would be interesting to subject **LL** and **DD** enantiomers for a majority-rule experiment, as they exist in similar as well as dissimilar aggregation states in different solvent compositions. In a majority-rule experiment, when two enantiomers

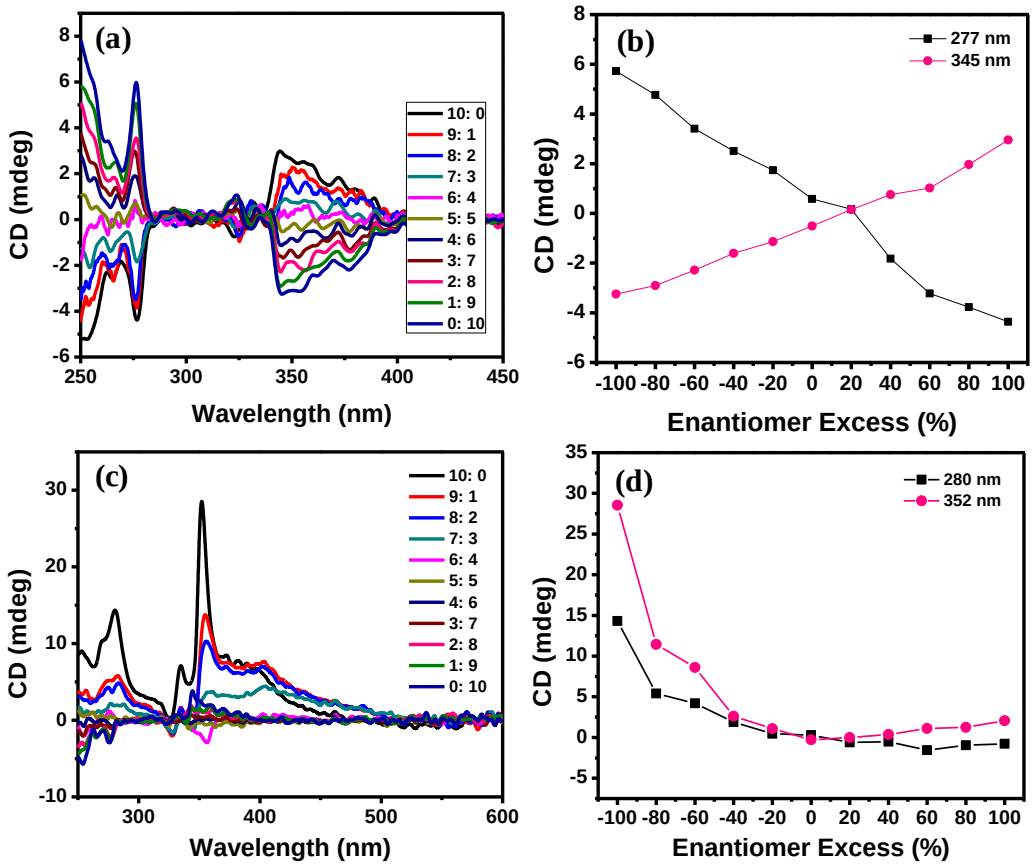


**Figure 16**. (a) and (c) The CD spectra of 200 µM solutions of **LL** and **DD** mixed under a majority-rule experiment in ***Sol30*** (30% aqueous NMP) and ***Sol36*** (36% aqueous NMP), respectively. The spectra were recorded after 40 min. The values represent the various stoichiometric ratios of **LL** and **DD**. (b) and (d) Plot of CD amplitude monitored at specific wavelengths for various enantiomeric excesses corresponding to (a) and (c), respectively.

of different stoichiometric ratios are mixed in a single column, infidelitic behavior could be observed giving rise to CD signal amplification. In ***Sol30***, both **LL** and **DD** are in ***State I***, and the majority-rule experiment did not show any appreciable CD signal amplification (Figure 16a). The plot of CD intensity against the enantiomeric excess shows a linear relation, which is an indication of fidelitic behavior of **LL** and **DD** (Figure 16b).[43] Further similar CD characteristics were observed in ***Sol36*** as well with minimal

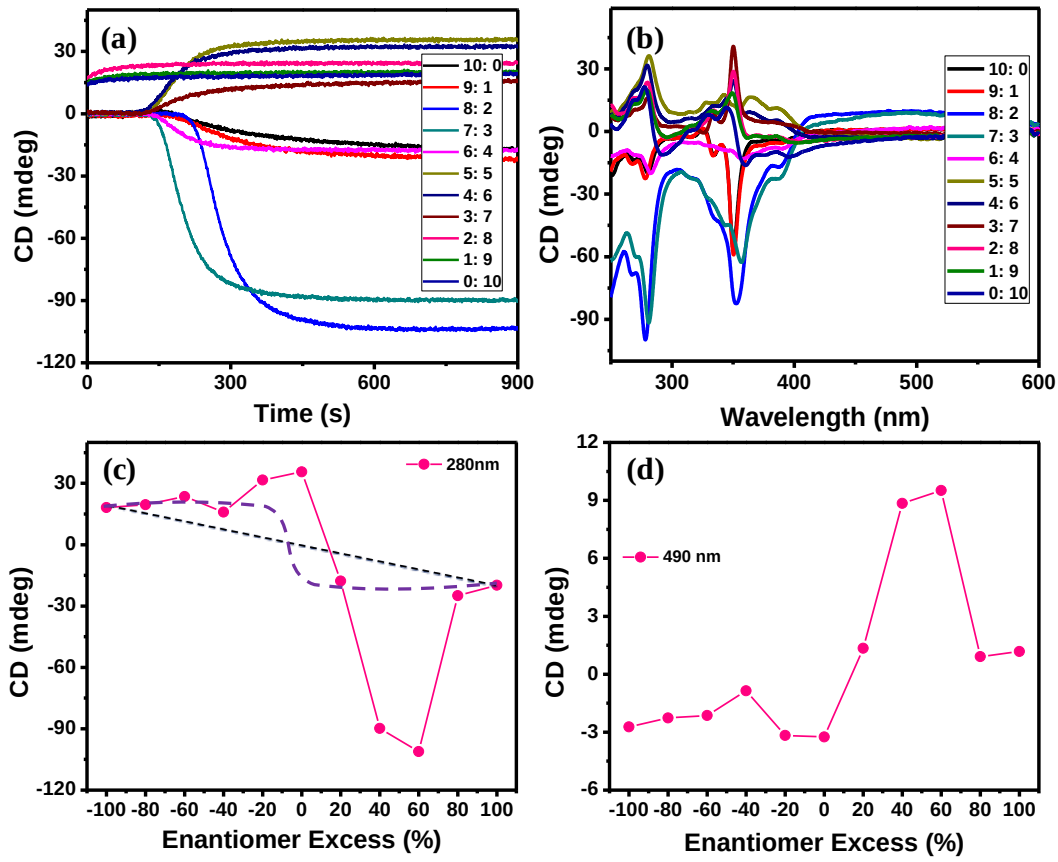


**Figure 17**. (a) Time-dependent CD spectra of 200 µM solutions of **LL** and **DD** mixed under a majority-rule experiment in ***Sol40*** (40% aqueous NMP). (b) The corresponding CD spectra of (a) recorded either on saturation or after 40 min. The values represent the various stoichiometric ratios of **LL** and **DD**. (c) and (d) Plot of CD amplitude monitored at specific wavelengths for various enantiomeric excesses corresponding to (b). The black and purple dashed lines represent the two extreme cases of typical non-fidelitic and fidelitic behavior under majority-rule condition, respectively.

signal amplification (Figure 16c,d). However, in ***Sol40*** an unprecedented dynamic assembly behavior under the majority-rule condition was observed. Herein as well, the mixture of **LL** and **DD** showed time-dependent dynamic assembly behavior (Figure 17a). The CD studies revealed rather unusual spectral features for the mixture of **LL** and **DD** in various stoichiometric ratios (Figure 17b). In order to get greater insights into the spectral data, the intensity of CD signal at 277 nm was plotted against the enantiomeric excess

and the data points were clearly non-linear (Figure 17c). Typically for a fidelitic assembly behavior of enantiomers, a linear plot would result (as shown in Figure 16b), and is represented with a black dashed line as a reference in Figure 17c. If there were to be CD signal amplification due to majority-rule then, even the best possible data would have data points along the purple dashed line shown in Figure 17c.[43] Such non-linear plot arises due to mixed stacking of minor and major enantiomers in a single column, giving rise to strong and weak CD signals at low and high enantiomeric excess values, respectively. Besides experimental observation in molecular and macromolecular systems, theoretical validation of such non-linearity has also been reported in the literature.[70] Surprisingly, our data points are way beyond the conventional non-linearity and moreover, the nature of the resulting spectra is also quite distinct from others. We have attributed this novel characteristic behavior observed in the dynamic molecular self-assembly to emergence, for the reasons discussed *vide infra*.

It is important to note that the CD amplitude (*A*) depends upon several factors namely square of extinction coefficient (ε) of chromophore, inverse square of inter-chromophore distance (R) and the angle between the transition dipole moments of the chromophores (maximum at ~$70^{o}$).[71] Ideally, for a given molecule under specific solvent composition, *A* should be constant as ε, R and the twist angles are essentially same. Additionally, in case of molecules having non-identical chromophores, meaning two different chromophores such as NDI and pyrene, there could be a possibility of hetero-chromophore excitonic coupling due to their high ε and close proximity in terms of spatial positions as well as their absorption maxima.[71] Even in the latter scenario, if such hetero-chromophore coupling were to occur then, it should have been present for all the

enantiomeric excesses employed in the majority-rule. Unexpectedly, anomalous spectral features were obtained at several stoichiometric ratios and which is what is termed as emergence. In order to account for this anomalous behavior, several speculations could be made such as the dynamicity and/or the hetero-chromophore excitonic coupling and/or the presence of two distinct aggregation states of **LL** (***State II***) and **DD** (***State III***). Interestingly, a careful inspection revealed that the plot of CD intensity at 480 nm for various enantiomeric excesses (Figure 17d) was found to be complementary to that at 277 nm (Figure 17c). This new band in the range of 400 - 600 nm could be attributed to the well-known charge transfer complexation of NDI and pyrene and in turn was thought to play the crucial role in our system for the resulting emergence. Similarly, various stoichiometric ratios of **LL** and **DD** in ***Sol46*** exhibit distinct CD signals (Figure 18a). Here as well, the plot of CD intensity against the enantiomeric excesses showed the non-linearity beyond the conventional type (Figure 18b). This suggests that different

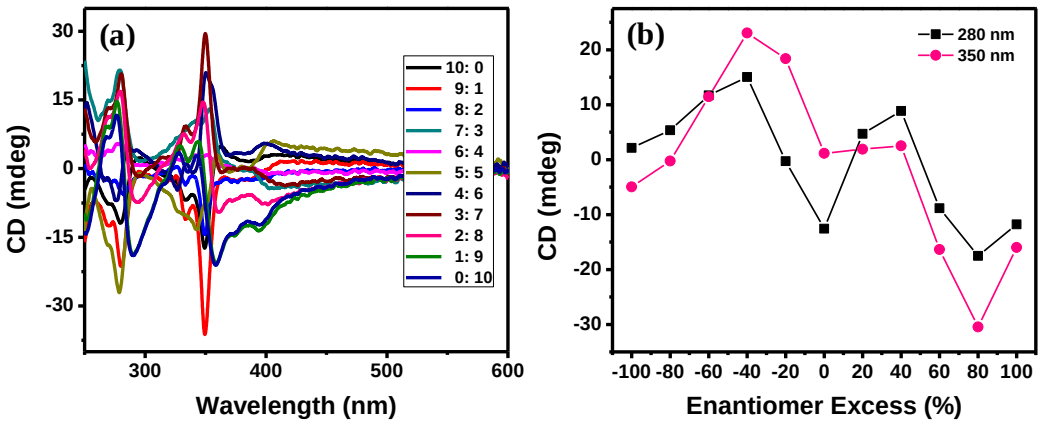


**Figure 18**. (a) The CD spectra of 200 µM solutions of **LL** and **DD** mixed under a majority-rule experiment in ***Sol46*** (46% aqueous NMP). The spectrum was recorded as soon as prepared. The values represent the various stoichiometric ratios of **LL** and **DD**. (b) Plot of CD amplitude monitored at specific wavelengths for various enantiomeric excesses corresponding to (a).

aggregation states of **LL** and **DD** are not necessary to achieve the non-linearity of non-conventional type, as both **LL** and **DD** exist in ***State III*** for ***Sol46*.**

### 3.2.3. Seeding experiment

Next we subjected our triads for seeding experiment, wherein which seeds (biased helical aggregates) of enantiomers like **LL** and **DD** were added with **RAC** and **LD** with an anticipation of probable stereoselective amplification behavior. Firstly, for a fixed

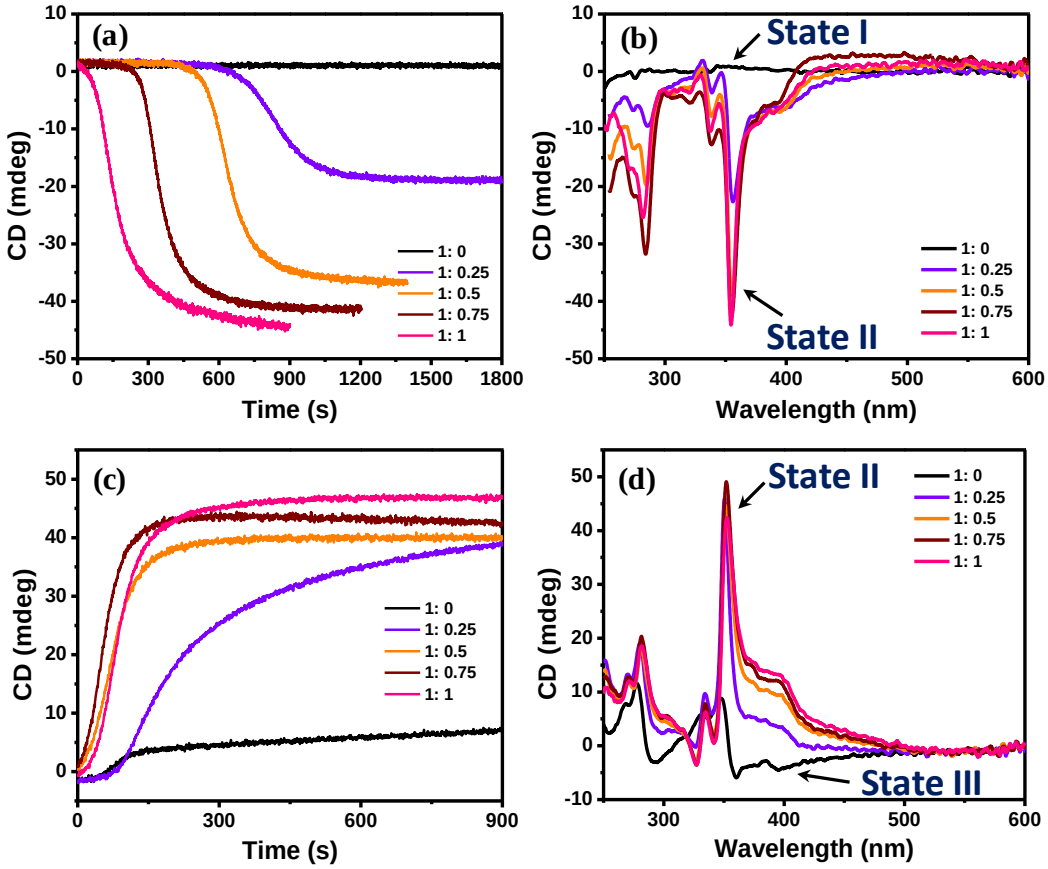


**Figure 19**. (a) and (c) Time-dependent CD spectra of 200 µM solutions of **LL** and **DD** upon mixing with **RAC** under a seeding experiment in ***Sol40*** (40% aqueous NMP). (b) and (d) The corresponding CD spectra of (a) and (c) respectively recorded either on saturation or after 40 min. The values represent the various stoichiometric ratios of **LL**/**DD** and **RAC**.

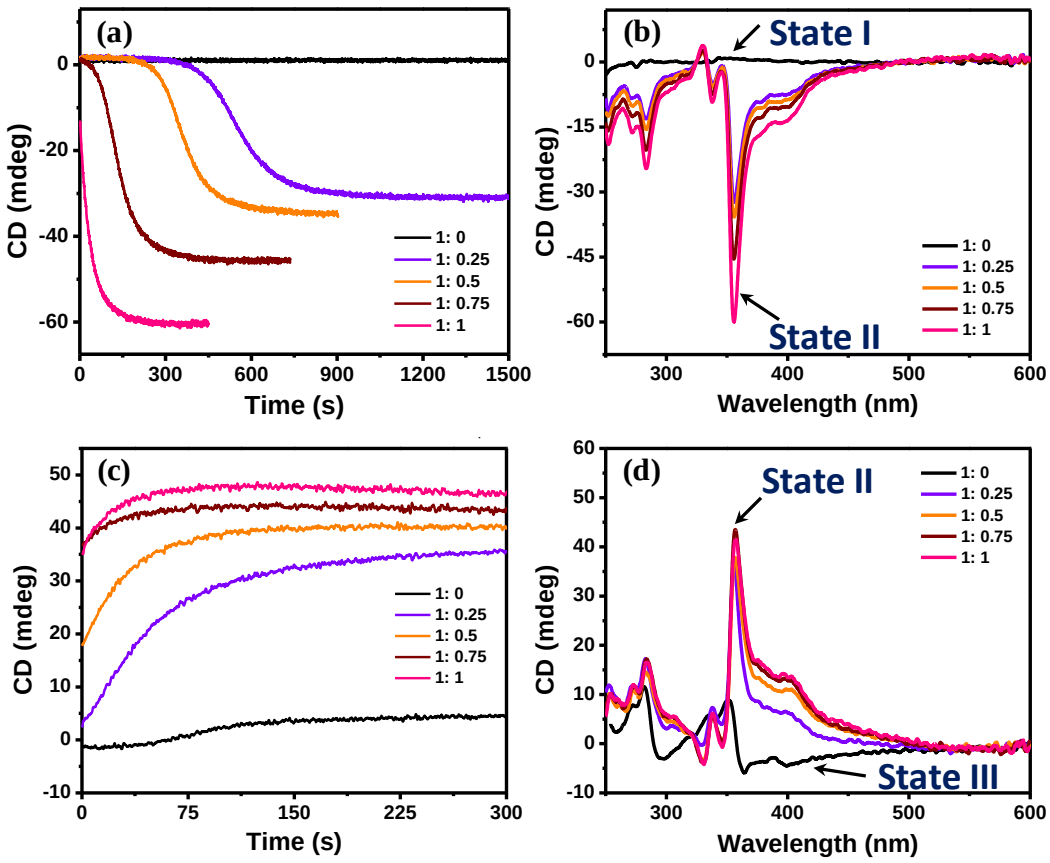


**Figure 20**. (a) and (c) Time-dependent CD spectra of 200 µM solutions of **LL** and **DD** upon mixing with **LD** under a seeding experiment in ***Sol40*** (40% aqueous NMP). (b) and (d) The corresponding CD spectra of (a) and (c) respectively recorded either on saturation or after 40 min. The values represent the various stoichiometric ratios of **LL**/**DD** and **LD**.

amount of **LL** in ***Sol40***, the addition of various stoichiometric ratios of **RAC** showed dynamic helical assembly behavior (Figure 19a). The CD study showed the transition from ***State I*** to ***State II*** upon addition of **RAC** to **LL** (Figure 19b). Similar behavior was observed for the seeding experiment done with **DD** and **RAC** in ***Sol40*** (Figure 19c,d). Interestingly, in the latter case a transition from ***State III*** to ***State II*** was observed upon addition of **RAC** to **DD**. Further, we were curious to know the fate of the resulting aggregates if a heterochiral **LD** could be employed instead of **RAC**, in the seeding experiment. Evidently, here as well dynamic assembly behavior and the characteristic

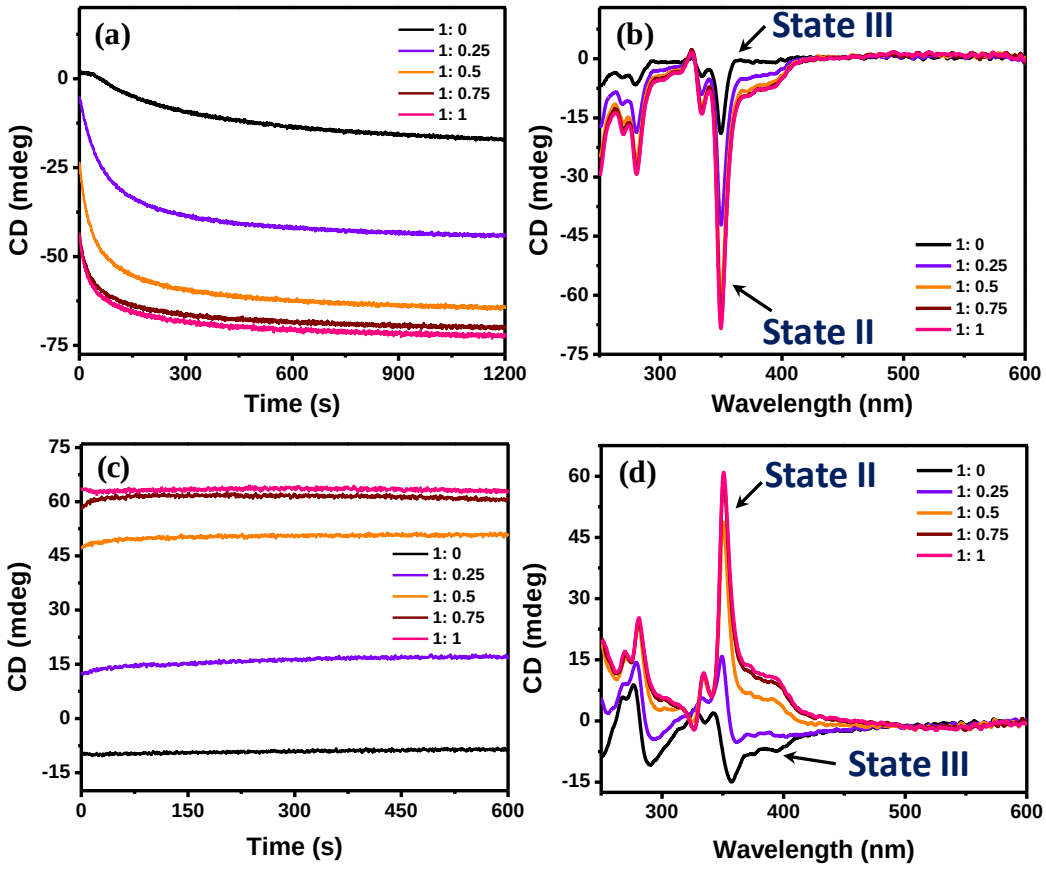


**Figure 21**. (a) and (c) Time-dependent CD spectra of 200 µM solutions of **LL** and **DD** upon mixing with **RAC** under a seeding experiment in ***Sol46*** (46% aqueous NMP). (b) and (d) The corresponding CD spectra of (a) and (c) respectively recorded either on saturation or after 40 min. The values represent the various stoichiometric ratios of **LL**/**DD** and **RAC**.

transition from ***State I*** to ***State II*** in case of **LL**, while a transition from ***State III*** to ***State II*** for **DD** was observed (Figure 20a-d). In order to probe the effect of solvent composition if any on the transition of aggregation states in seeding experiment, we performed additional studies in ***Sol46*** as well. Intriguingly, successive addition of **RAC** to **LL** or **DD** in ***Sol46***, revealed the dynamic nature by facilitating the transition from ***State III*** to ***State II*** (Figure 21a-d). From the above experiments, it is evident that irrespective of solvent compositions (***Sol40***/***Sol46***) and the stereochemistry (**RAC**/**LD**) of the added moieties a transition from either ***State I*** or ***State III*** to ***State II*** was obtained.

This characteristic property of our molecular system to mitigate the formation of ***State II*** from various constraints is in line with the autoregulatory behavior.

### 3.2.4. Concentration and temperature-dependent CD studies

In order to explain these complicated behaviors of our molecules, few additional studies were undertaken and some of the preliminary studies are provided here, while a detailed account would be available in due course of time. Concentration dependent studies

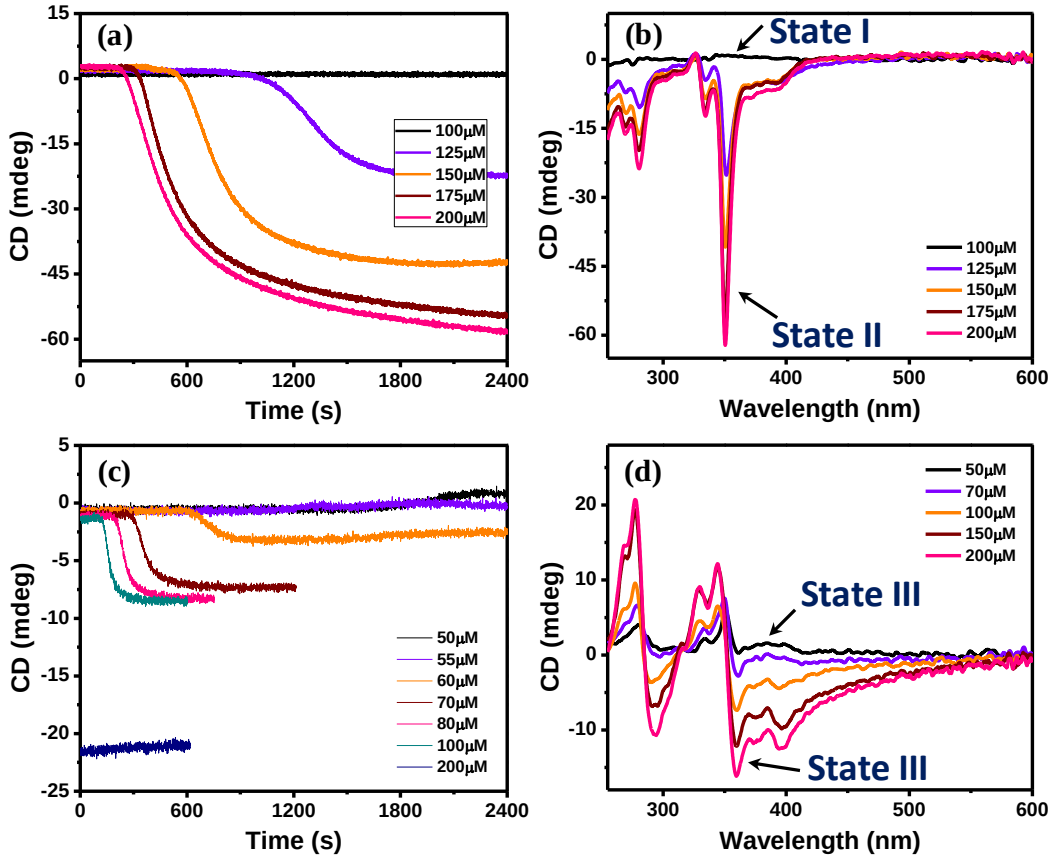


**Figure 22**. (a) and (c) Time-dependent CD spectra of **LL** and **DD** for various concentrations in ***Sol40*** (40% aqueous NMP). (b) and (d) The corresponding CD spectra of (a) and (c) respectively recorded either on saturation or after 40 min. The values represent the various concentrations of **LL** /**DD**.

revealed that with increasing concentration of **LL** from 100 µM to 200 µM, transition from ***State I*** to ***State II*** could be achieved in ***Sol40*** (Figure 22a,b). The same could thus be attributed for the transition of ***State I*** to ***State II*** observed in case of **LL** during seeding experiment with **RAC**/**LD** in ***Sol40*** (Figure 19b,20b). On the other hand, **DD** showed the existence of ***State III*** from 50 µM to 200 µM concentrations in ***Sol40*** (Figure 22c,d). As a result of which, the transition from ***State III*** to ***State II*** for the seeding experiment of **DD** with **RAC**/**LD** in ***Sol40*** could not be accounted (Figure 19d,20d). The probable reasons for such behavior were made possible by temperature dependent CD studies. The gist of the latter study is that all the three aggregation states of **LL** and **DD** namely ***State I***, ***State II*** and ***State III*** are kinetically controlled aggregates. ***State I*** is a kinetically trapped state, as the aggregates do not melt even at 90 $^{o}$C, while ***State II*** and ***State III*** exhibit chiral denaturation behavior similar to that observed in the previous sub-chapter (Figure 5b).[31,43] As the transition occurs from ***State III*** to ***State II*** during seeding experiments as well as in the time dependent aggregation of **DD** in ***Sol36***, we have termed ***State III*** and ***State II*** as kinetically controlled aggregate and pseudo-thermodynamically controlled aggregate, respectively. In addition, **C1** and **C2** do not show any anomalous behavior mainly due to their bulky side chains, which could effectively hinder the interactions amongst NDI and pyrene functionalities.

### 3.2.5. Conclusions

In conclusion, a bioinspired design strategy was employed to develop abiotic functional molecular systems with novel properties. With the aid of thoughtfully designed molecular

triads, the most complicated molecular self-assembly was successfully illustrated. By facilitating suitable conditions, dynamic molecular assemblies were developed and the relative differences in the aggregation tendencies of two enantiomers were exploited to obtain the unprecedented emergent behavior for the first time in molecular systems. Further, an autoregulatory behavior leading to formation of a particular aggregate from different aggregate states as well as precursors was observed. Such design approaches and the resulting unusual properties could be instrumental in shedding interesting insights in to the biochemical processes and its exploits thereafter for various technological implications are envisioned.

### 3.2.6. Experimental section

#### *3.2.6.1. Materials and methods*

*Materials*: 1,4,5,8-Naphthalenetetracarboxylic acid dianhydride, 1-pyrenemethylamine hydrochloride and *N*,*N*-diisopropylethylamine were obtained from Sigma-Aldrich, 1-hydroxybenzotriazole, L-alanine, D-alanine, Rac-alanine, L-phenylalanine and L-isoleucine from Spectrochem Pvt. Ltd. (Mumbai, India). All other reagents and solvents were of reagent grade and used without further purification.

*NMR Spectroscopy, Mass Spectrometry (MS), and Elemental Analysis*: $^{1}$H and $^{13}$C NMR spectra were recorded on a Bruker AV-400 spectrometer with chemical shifts reported as ppm (in DMSO-$d_6$ with tetramethylsilane as internal standard). Mass spectra were obtained from Shimadzu 2020 LC-MS. Elemental analysis was carried out on ThermoScientific FLASH 2000 Organic Element Analyzer.

*Absorption Spectroscopy*: UV–vis spectra were recorded on a Perkin Elmer Model Lambda 900 spectrophotometer. 200 μM solutions of the samples were analyzed in quartz cuvette of 1 mm path length.

*Circular Dichroism (CD)*: CD measurements were carried out on a Jasco J-815 spectropolarimeter under nitrogen atmosphere. Solutions of the samples of appropriate concentrations were analyzed in quartz cuvette of 1 mm path length. For time-dependent studies, water was added to the solution of the compound in NMP (so as to obtain a required concentration and solvent composition) and was mixed manually. The entire process of addition of water, mixing and placing the cuvette in the sample holder of the instrument typically lasts for about 60 sec. All the measurements were done at 25 $^{o}$C unless otherwise mentioned.

### *3.2.6.2. Synthesis of LL*

*Synthesis of L-alanine appended NDI (L-Ala-NDI-L-Ala)*: 1,4,5,8-naphthalenetetracarboxylic acid dianhydride (100 mg, 0.37 mmol) and L-alanine (66.46

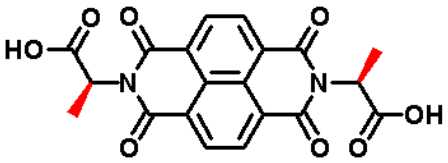


mg, 0.74 mmol) were taken in 20 mL of *N*,*N*-dimethylformamide and the mixture was sonicated for 5 min. The resulting suspension was heated to reflux for 13 h at 110 $^{o}$C and then solvent was concentrated to 5 mL under reduced pressure. The residue was purified by precipitation and washed in diethyl ether to afford yellow solid in quantitative yield.

Compound L-Ala-NDI-L-Ala (100 mg, 0.24 mmol), 1-ethyl-3-(3-dimethylaminopropyl)carbodiimide (102.8 mg, 0.54 mmol), hydroxybenzotriazole (72.96 mg, 0.54 mmol) were dissolved in *N*,*N*-dimethylformamide (10 mL) and stirred in ice bath for about 15 min under inert atmosphere.

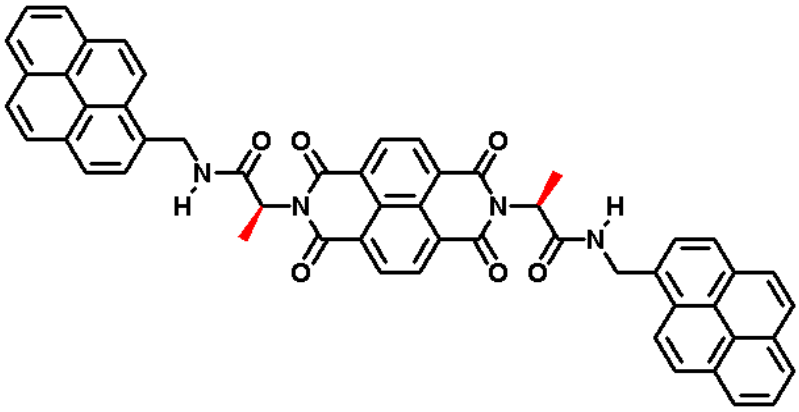

1-Pyrenemethylamine hydrochloride (131 mg, 0.5 mmol) and diisopropylethyl amine (0.3 mL) were added to the reaction mixture. The resulting solution was stirred at room temperature for 24 h and the red colored precipitate was filtered and washed with excess methanol to afford the red solid, **LL** in 63% yield. $^{1}$H NMR (400 MHz, DMSO-$d_6$, $\delta$ in ppm): 8.63(m, 6H), 8.12(m, 18H), 5.59(q, 2H), 4.99(t, 4H), 1.63(d, 6H). $^{13}$C NMR (100 MHz. DMSO-$d_6$, $\delta$ in ppm): 168.9, 162.4, 132.6, 130.7, 130.2, 129.9, 127.9, 127.4, 127.3, 126.9, 126.6, 126.5, 126.2, 125.1, 125.1, 124.5, 123.8, 123.8, 123.1, 49.9, 41.0, 14.3. MS (EI): m/z = 836.31 $[M]^+$ for $C_{54}H_{36}N_4O_6$ (calc. 836.26). Elemental analysis: Found: C, 77.47; H, 4.40; N, 6.62; Calcd: C, 77.50; H, 4.34; N, 6.69 for $C_{54}H_{36}N_4O_6$.

### *3.2.6.3. Synthesis of DD*

*Synthesis of D-alanine appended NDI (D-Ala-NDI-D-Ala)*: 1,4,5,8-naphthalenetetracarboxylic acid dianhydride (100 mg, 0.37 mmol) and D-alanine (66.46 mg, 0.74 mmol) were taken in 20 mL of *N*,*N*-dimethylformamide and the mixture was

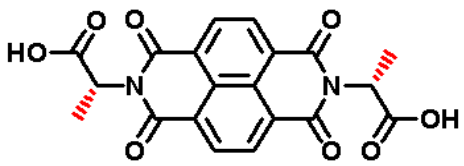

sonicated for 5 min. The resulting suspension was heated to reflux for 13 h at 110 $^{o}$C and then solvent was concentrated to 5 mL under reduced pressure. The residue was purified by precipitation and washed in diethyl ether to afford yellow solid in quantitative yield.

Compound D-Ala-NDI-D-Ala (100 mg, 0.24 mmol), 1-ethyl-3-(3-dimethylaminopropyl)carbodiimide (102.8 mg, 0.54 mmol), hydroxybenzotriazole (72.96

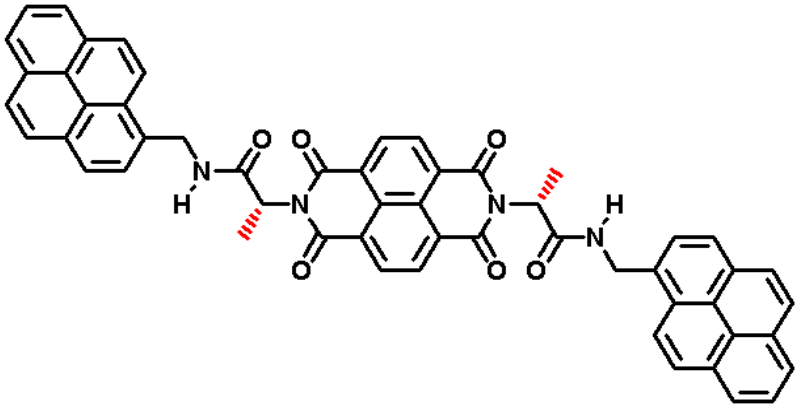

mg, 0.54 mmol) were dissolved in *N*,*N*-dimethylformamide (10 mL) and stirred in ice bath for about 15 min under inert atmosphere. 1-Pyrenemethylamine hydrochloride (131 mg, 0.5 mmol) and diisopropylethyl amine (0.3 mL) were added to the reaction mixture. The resulting solution was stirred at room temperature for 24 h and the red colored precipitate was filtered and washed with excess methanol to afford the red solid, **DD** in 64% yield. $^{1}$H NMR (400 MHz, DMSO-$d_6$, $\delta$ in ppm): 8.62(m, 6H), 8.10(m, 18H), 5.60(q, 2H), 4.98(t, 4H), 1.64(d, 6H). $^{13}$C NMR (100 MHz. DMSO-$d_6$, $\delta$ in ppm): 168.9, 162.5, 132.6, 130.7, 130.2, 129.9, 128., 127.4, 127.3, 126.9, 126.6, 126.5, 126.2, 126.1, 125.1, 125.1, 124.5, 123.9, 123.8, 123.1, 49.9, 41.0, 14.4. MS (EI): m/z = 836.37 $[M]^{+}$ for $C_{54}H_{36}N_4O_6$ (calc. 836.26). Elemental analysis: Found: C, 77.49; H, 4.39; N, 6.65; Calcd: C, 77.50; H, 4.34; N, 6.69 for $C_{54}H_{36}N_4O_6$.

### *3.2.6.4. Synthesis of RAC*

*Synthesis of Rac-alanine appended NDI (Rac-Ala-NDI-Rac-Ala)*: 1,4,5,8-naphthalenetetracarboxylic acid dianhydride (100 mg, 0.37 mmol) and Racemic mixture

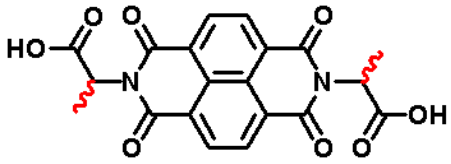

of alanine (66.46 mg, 0.74 mmol) were taken in 20 mL of *N*,*N*-dimethylformamide and the mixture was sonicated for 5 min. The resulting suspension was heated to reflux for 13 h at 110 $^{o}$C and then solvent was concentrated to 5 mL under reduced pressure. The residue was purified by precipitation and washed in diethyl ether to afford yellow solid in quantitative yield.

Compound Rac-Ala-NDI-Rac-Ala (100 mg, 0.24 mmol), 1-ethyl-3-(3-dimethylaminopropyl)carbodiimide (102.8 mg, 0.54 mmol), hydroxybenzotriazole (72.96

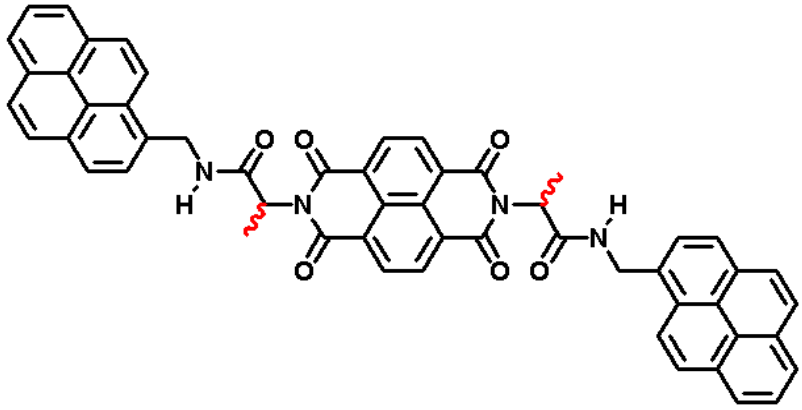

mg, 0.54 mmol) were dissolved in *N*,*N*-dimethylformamide (10 mL) and stirred in ice bath for about 15 min under inert atmosphere. 1-Pyrenemethylamine hydrochloride (131 mg, 0.5 mmol) and diisopropylethyl amine (0.3 mL) were added to the reaction mixture. The resulting solution was stirred at room temperature for 24 h and the red colored precipitate was filtered and washed with excess methanol to afford the red solid, **RAC** in 63% yield. $^{1}$H NMR (400 MHz, DMSO-$d_6$, $\delta$ in ppm): 8.61(m, 6H), 8.08(m, 18H), 5.57(q, 2H), 4.96(t, 4H), 1.62(d, 6H). MS (EI): m/z =

836.35 $[M]^+$ for $C_{54}H_{36}N_4O_6$ (calc. 836.26). Elemental analysis: Found: C, 77.46; H, 4.37; N, 6.65; Calcd: C, 77.50; H, 4.34; N, 6.69 for $C_{54}H_{36}N_4O_6$.

### *3.2.6.5. Synthesis of LD*

*Coupling of Boc-L-alanine with pyrenemethylamine (Py-L-Ala-Boc)*: To a 5 mL DMF solution of Boc-protected L-alanine (353 mg, 1.86 mmol) HOBT (1-

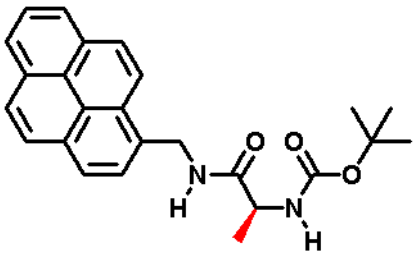

hydroxybenzotriazole; 277 mg, 2.05 mmol), HBTU (O-benzotriazole-*N*,*N*,*N*',*N*'-tetramethyl-uronium-hexafluoro phosphate; 778 mg, 2.05 mmol), and DIPEA (*N*,*N*-diisopropylethylamine; 716 µl, 4.10 mmol) were added and maintained in an inert atmosphere. The reaction contents were stirred for 30 min. To this 1-pyrenemethylamine hydrochloride (500 mg, 1.86 mmol) was added and the contents were stirred for 48 h. The reaction mixture was concentrated under vacuo. The crude product was purified by column chromatography. Yield 58 %. $^1$H NMR (400 MHz, $CDCl_3$, $\delta$ in ppm): 8.12 (m, 9H), 6.53 (b, 1H), 5.16 (b, 2H), 4.94 (b, 1H), 4.18 (b, 1H), 1.40 (d, 3H), 1.30 (s, 9H). $^{13}$C NMR (100 MHz. $CDCl_3$, $\delta$ in ppm): 172.2, 131.2, 130.9, 130.8, 129.0, 128.2, 127.5, 127.3, 126.9, 126.1, 125.4, 125.3, 125.0, 124.8, 124.7, 122.7, 41.9, 28.1.

*Synthesis of Py-L-Ala-NDI-D-Ala*: Firstly, to a solution of Py-L-Ala-Boc (400 mg) in dichloromethane maintained at 0 $^o$C, TFA (trifluoroacetic acid; 3 ml) and TIPS (triisopropylsilane; 50 µl) were added and the contents were stirred at room temperature for 2 h. The solvent was removed under reduced pressure. The resulting solid (Boc-

deprotected Py-L-Ala) was washed with toluene, chloroform and methanol and dried under vacuo. After which, 1,4,5,8-naphthalenetetracarboxylic acid dianhydride (193 mg, 0.72 mmol), Boc-deprotected Py-L-Ala (300 mg, 0.72 mmol) and D-alanine (66.46 mg, 0.74 mmol) were taken in 20 mL of *N*,*N*-dimethylformamide and the mixture was sonicated for 5 min. The resulting suspension was heated to reflux for 13 h at 110 $^{o}$C and then solvent was concentrated to 5 mL under reduced pressure. The residue was precipitated, washed with diethyl ether and then purified by column chromatography to obtain Py-L-Ala-NDI-D-Ala in quantitative yield. $^{1}$H NMR (400 MHz, DMSO-$d_6$, $\delta$ in ppm): 8.66(m, 5H), 8.11(m, 9H), 5.62(q, 1H), 5.33(b, 1H), 5.00(b, 2H), 1.66(d, 3H), 1.57(d, 3H).

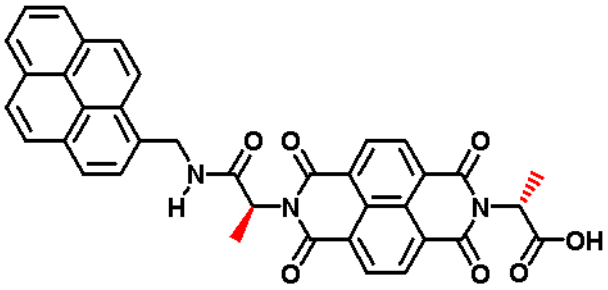

Compound Py-L-Ala-NDI-D-Ala (140 mg, 0.22 mmol), 1-ethyl-3-(3-dimethylaminopropyl)carbodiimide (52 mg, 0.26 mmol), hydroxybenzotriazole (36 mg, 0.26 mmol) were dissolved in *N*,*N*-dimethylformamide (10 mL) and stirred in ice bath for about 15 min under inert atmosphere. 1-Pyrenemethylamine hydrochloride (60 mg, 0.22 mmol) and diisopropylethyl amine (0.1 mL) were added to the reaction mixture. The resulting solution was stirred at room

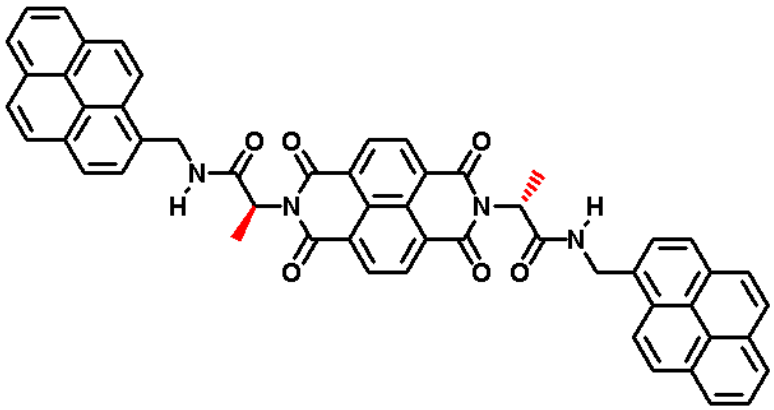

temperature for 24 h and the red colored precipitate was filtered and washed with excess methanol to afford the red solid, **LD** in 63% yield. $^1$H NMR (400 MHz, DMSO-$d_6$, $\delta$ in ppm): 8.63(m, 6H), 8.11(m, 18H), 5.60(q, 2H), 5.00(t, 4H), 1.63(d, 6H). MS (EI): m/z = 836.39 $[M]^+$ for $C_{54}H_{36}N_4O_6$ (calc. 836.26). Elemental analysis: Found: C, 77.46; H, 4.38; N, 6.63; Calcd: C, 77.50; H, 4.34; N, 6.69 for $C_{54}H_{36}N_4O_6$.

### *3.2.6.6. Synthesis of C1*

*Synthesis of L-phenylalanine appended NDI (L-Phe-NDI-L-Phe)*: 1,4,5,8-naphthalenetetracarboxylic acid dianhydride (100 mg, 0.37 mmol) and L-phenylalanine

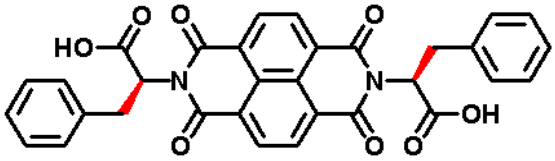


(124 mg, 0.74 mmol) were taken in 20 mL of *N*,*N*-dimethylformamide and the mixture was sonicated for 5 min. The resulting suspension was heated to reflux for 16 h at 110 $^o$C and then solvent was concentrated to 5 mL under reduced pressure. The residue was purified by precipitation and washed in diethyl ether to afford brown solid in quantitative yield.

Compound L-Phe-NDI-L-Phe (70 mg, 0.12 mmol), 1-ethyl-3-(3-dimethylaminopropyl)carbodiimide (52.52 mg, 0.27 mmol), hydroxybenzotriazole (37 mg, 0.27 mmol) were dissolved in *N*,*N*-dimethylformamide (10 mL) and stirred in ice bath for about 15 min under inert atmosphere. 1-Pyrenemethylamine hydrochloride (67 mg, 0.24 mmol) and diisopropylethyl amine (0.5 mL) were added to the reaction mixture. The resulting solution was stirred at room temperature for 24 h and the red colored precipitate was filtered and washed with excess methanol to afford the red solid, **C1** in

52% yield. $^{1}$H NMR (400 MHz, DMSO-$d_6$, $\delta$ in ppm): 8.72(t, 2H), 8.53(s, 4H), 8.13(m, 18H), 6.96(m, 10H), 5.86(q, 2H), 5.02(m, 4H), 3.73(dd, 2H), 3.38(dd, 2H). $^{13}$C NMR (100 MHz. DMSO-$d_6$, $\delta$ in ppm): 168.1, 162.4, 138.0, 132.5, 130.7, 130.4, 130.2, 130.0, 128.9, 128.0, 127.9, 127.4, 127.3, 126.9, 126.2, 125.8, 125.2, 125.1, 124.5, 123.9, 123.8, 123.1, 55.4, 40.9, 33.8. MS (EI): m/z = 988.48 $[M]^+$ for $C_{66}H_{44}N_4O_6$ (calc. 988.32). Elemental analysis: Found: C, 80.21; H, 4.54; N, 5.61; Calcd: C, 80.15; H, 4.48; N, 5.66 for $C_{66}H_{44}N_4O_6$.

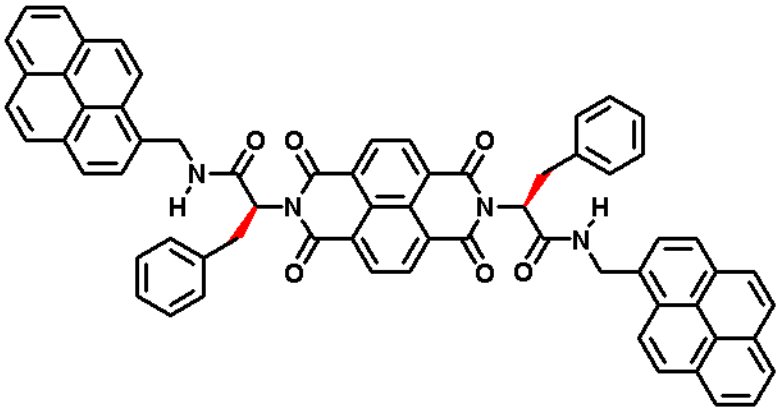

### *3.2.6.7. Synthesis of C2*

*Synthesis of L-isoleucine appended NDI (L-Ile-NDI-L-Ile)*: 1,4,5,8-naphthalenetetracarboxylic acid dianhydride (100 mg, 0.37 mmol) and L-isoleucine (98 mg, 0.74 mmol) were taken in 20 mL of *N*,*N*-dimethyl formamide and the mixture was sonicated for 5 min. The resulting suspension was heated to reflux for 24 h at 110 $^{o}$C and then solvent was concentrated to 5 mL under reduced pressure. The residue was purified by precipitation and washed in diethyl ether to afford brown solid in quantitative yield.

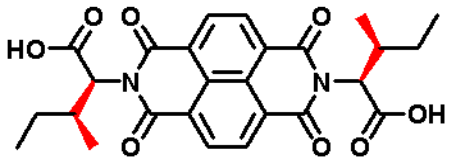

Compound L-Ile-NDI-L-Ile (400 mg, 0.81 mmol), 1-ethyl-3-(3-dimethylaminopropyl)carbodiimide (342 mg, 1.78 mmol), hydroxybenzotriazole (241 mg, 1.781 mmol) were dissolved in *N*,*N*-dimethylformamide (15 mL) and stirred in ice bath for about 15 min. under inert atmosphere.

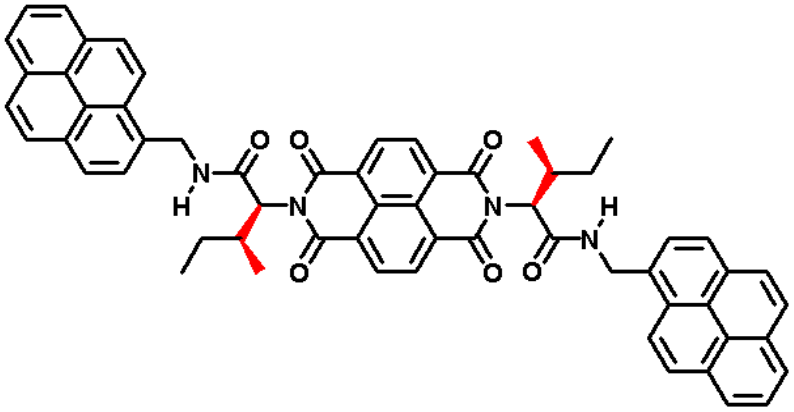

1-Pyrenemethylamine hydrochloride (437 mg, 1.61 mmol) and diisopropylethyl amine (0.5 mL) were added to the reaction mixture. The resulting solution was stirred at room temperature for 24 h and the red colored precipitate was filtered and washed with excess methanol to afford the red solid, **C2** in 55% yield. $^{1}$H NMR(400 MHz, DMSO-$d_6$, $\delta$ in ppm): 8.62(m, 6H), 8.13(m, 18H), 5.18(d, 2H), 4.96(m, 4H), 2.60(m, 2H), 1.19(m, 8H), 0.85(m, 2H), 0.73(t, 6H). $^{13}$C NMR(100 MHz. DMSO-$d_6$, $\delta$ in ppm): 168.0, 162.7, 132.6, 130.7, 130.7, 130.2, 129.9, 128.0, 127.3, 126.8, 126.6, 126.2, 126.1, 125.1, 125.0, 124.4, 123.8, 123.8, 123.1, 58.6, 40.9, 32.7, 24.5, 18.6, 11.1. MS (EI): m/z = 920.45 $[M]^+$ for $C_{60}H_{48}N_4O_6$ (calc. 920.35). Elemental analysis: Found: C, 78.31; H, 5.34; N, 6.11; Calcd: C, 78.24; H, 5.25; N, 6.08 for $C_{60}H_{48}N_4O_6$.

### 3.2.7. Appendix

- $^{1}H$ and $^{13}C$ NMR of **1**
- $^{1}H$ and $^{13}C$ NMR of **2**
- $^{1}H$ and $^{13}C$ NMR of **3**
- $^{1}H$ and $^{13}C$ NMR of **LL**
- $^{1}H$ and $^{13}C$ NMR of **DD**
- $^{1}H$ and NMR of **RAC**
- $^{1}H$ and NMR of **LD**
- $^{1}H$ and $^{13}C$ NMR of **C1**
- $^{1}H$ and $^{13}C$ NMR of **C2**

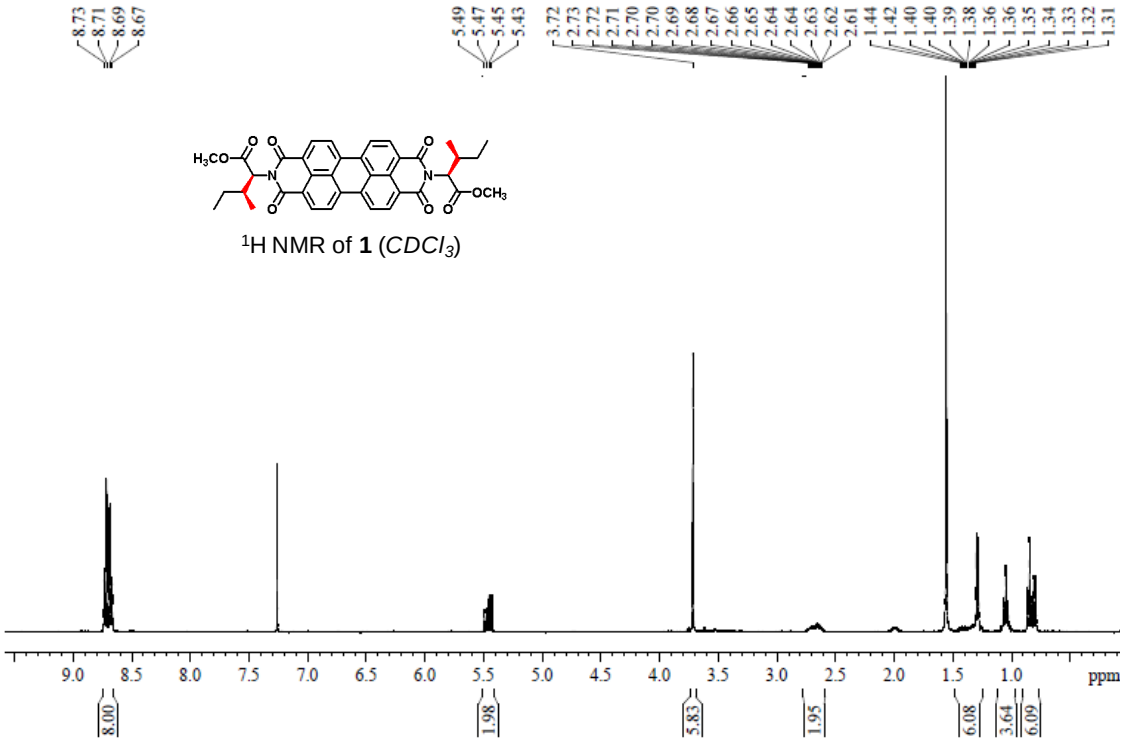


$^{1}$H NMR of **1** ($CDCl_3$)

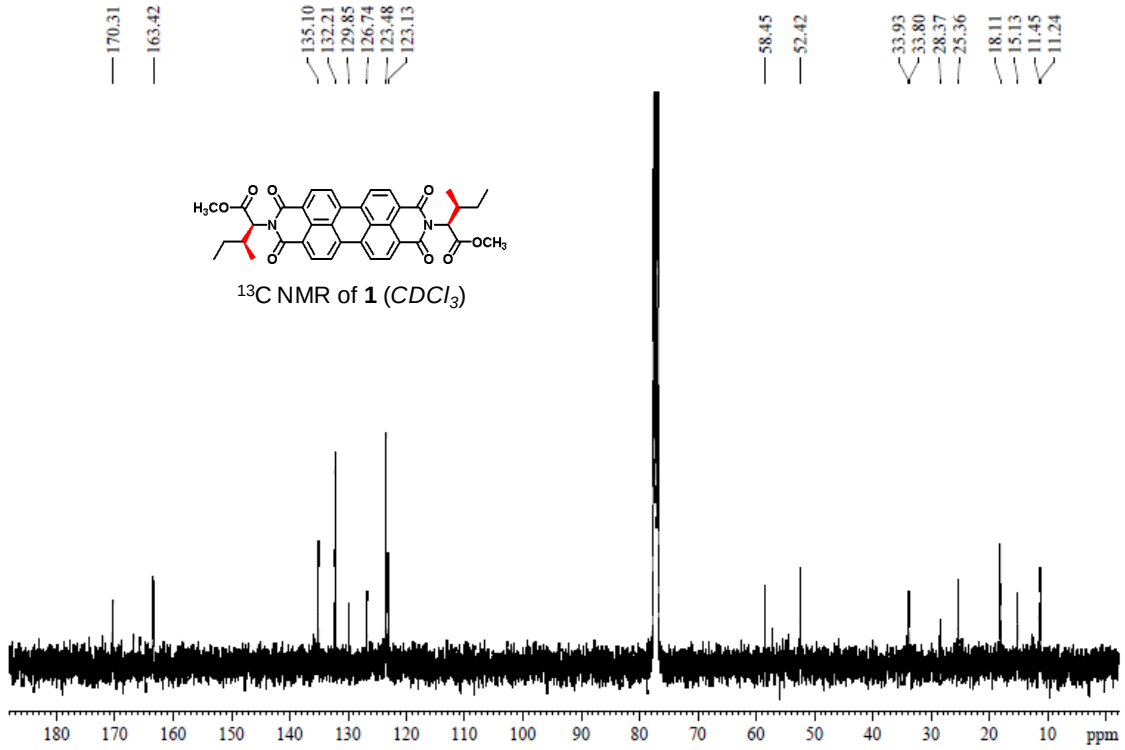


$^{13}$C NMR of **1** ($CDCl_3$)

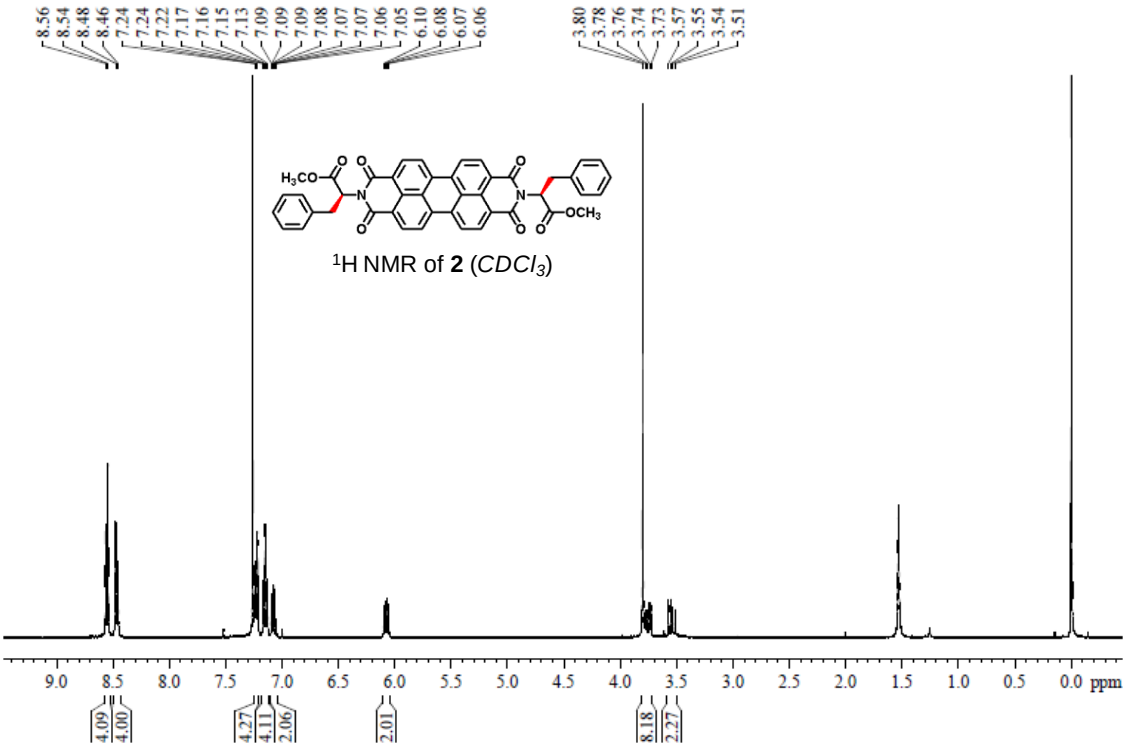


$^{1}$H NMR of **2** (*CDCl$_3$*)

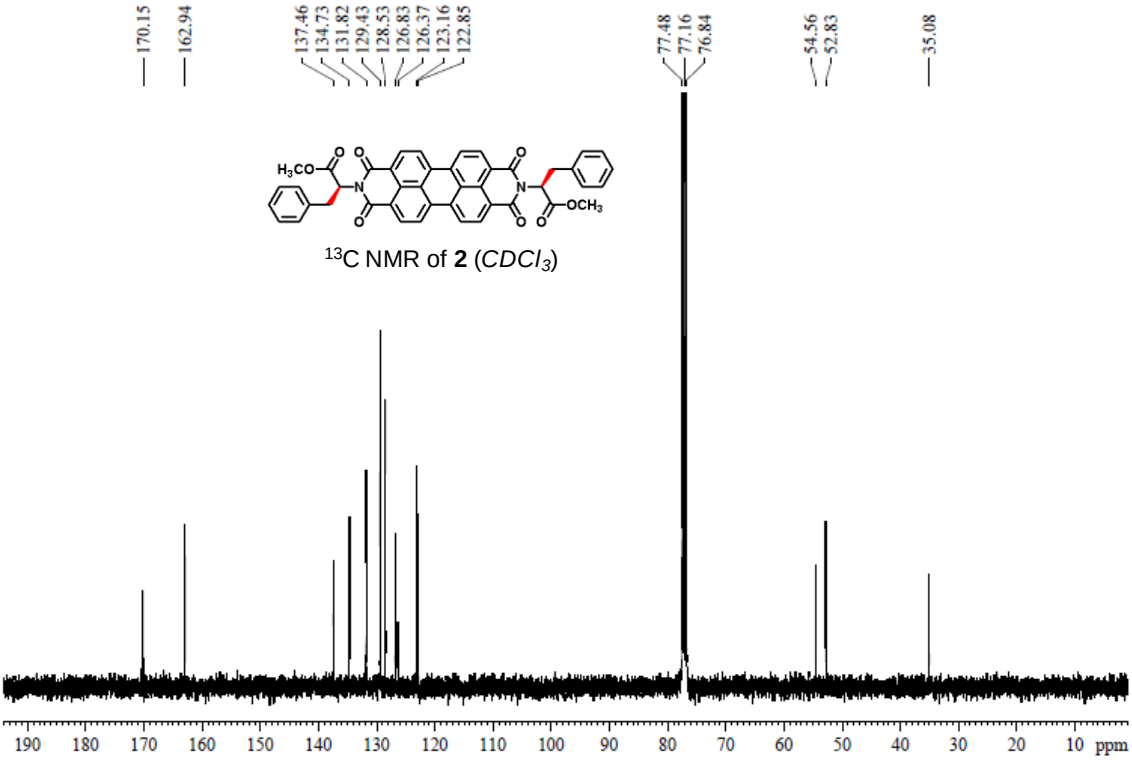


$^{13}$C NMR of **2** (*CDCl$_3$*)

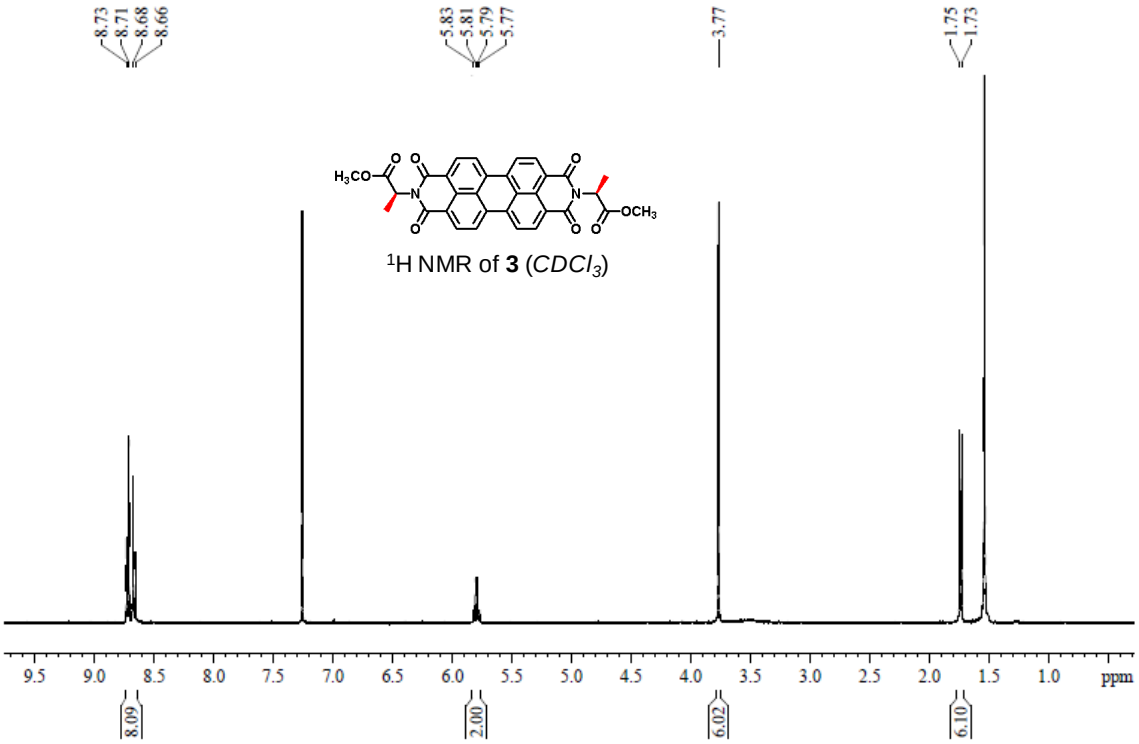


$^{1}$H NMR of **3** ($CDCl_3$)

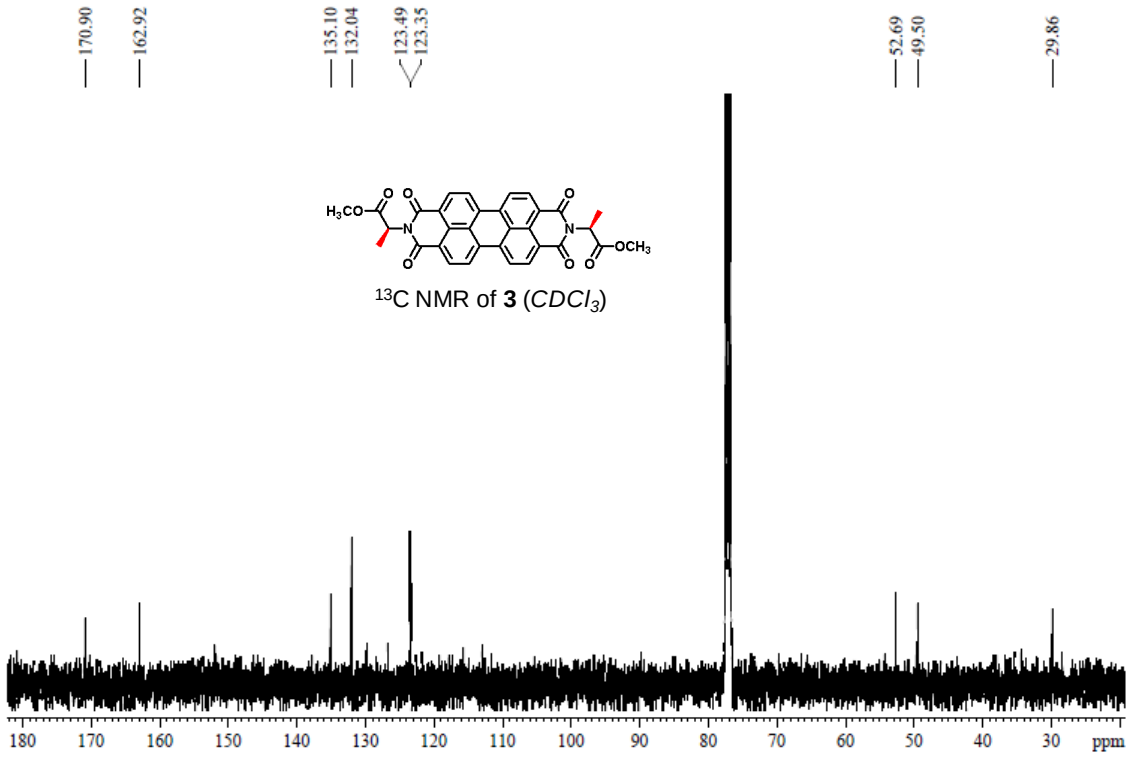


$^{13}$C NMR of **3** ($CDCl_3$)

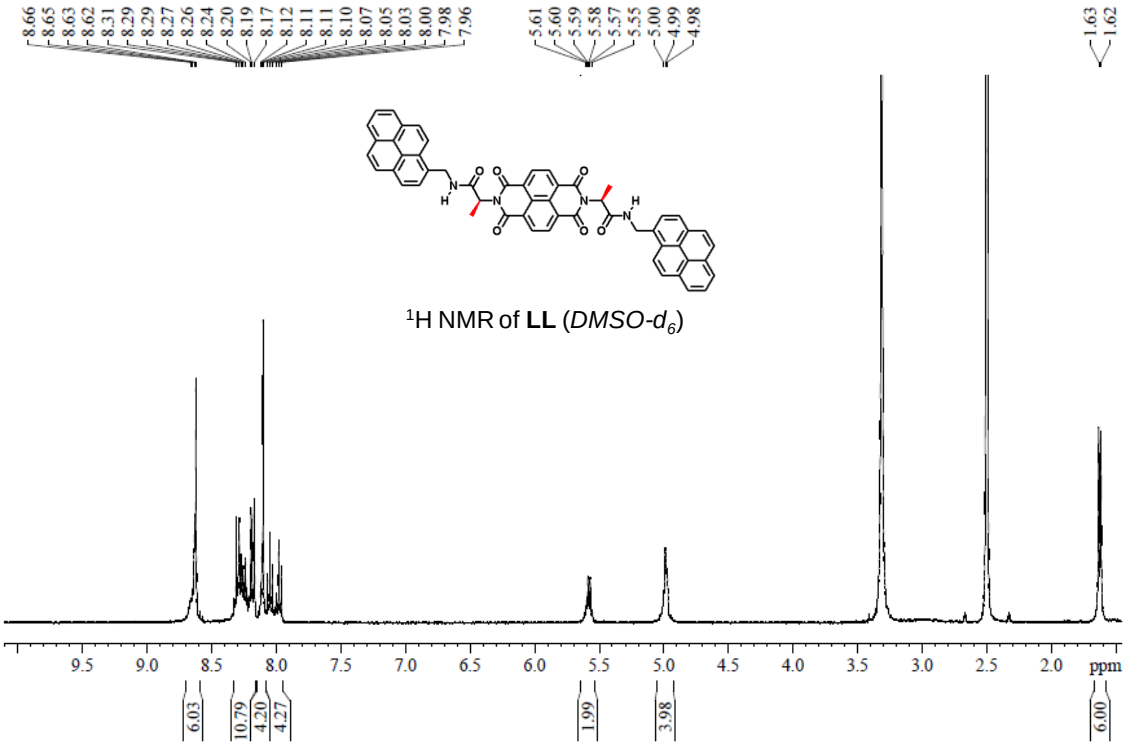


$^{1}$H NMR of **LL** (*DMSO-$d_6$*)

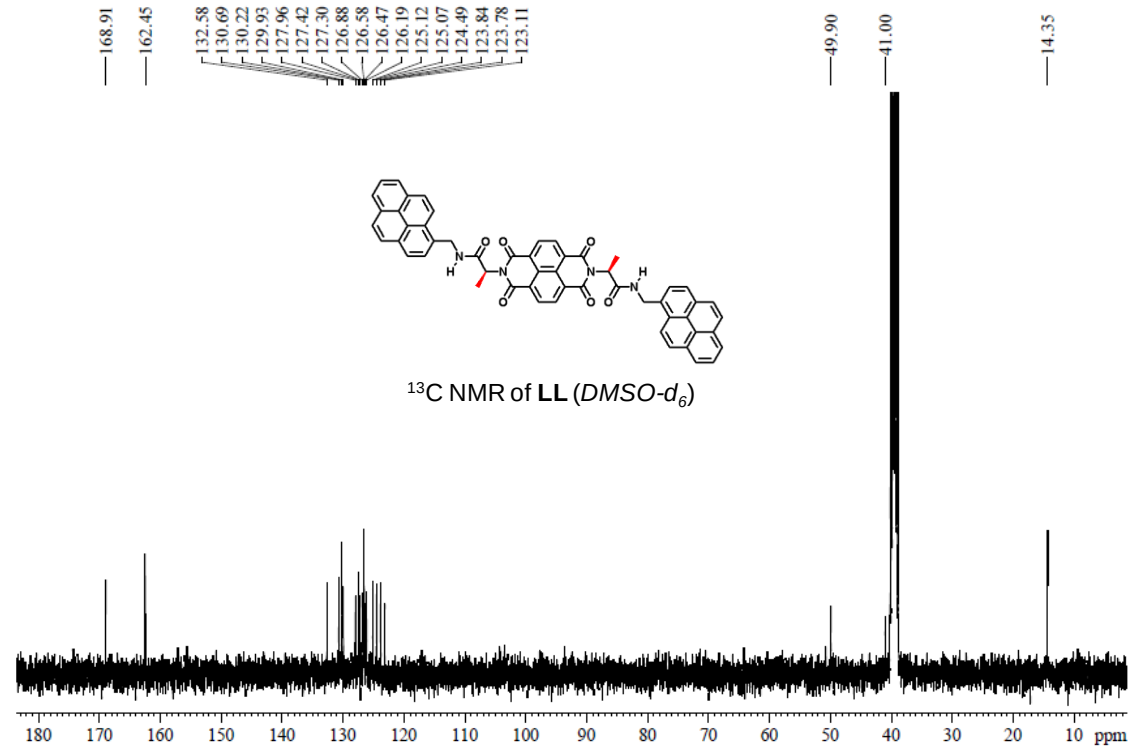


$^{13}$C NMR of **LL** (*DMSO-$d_6$*)

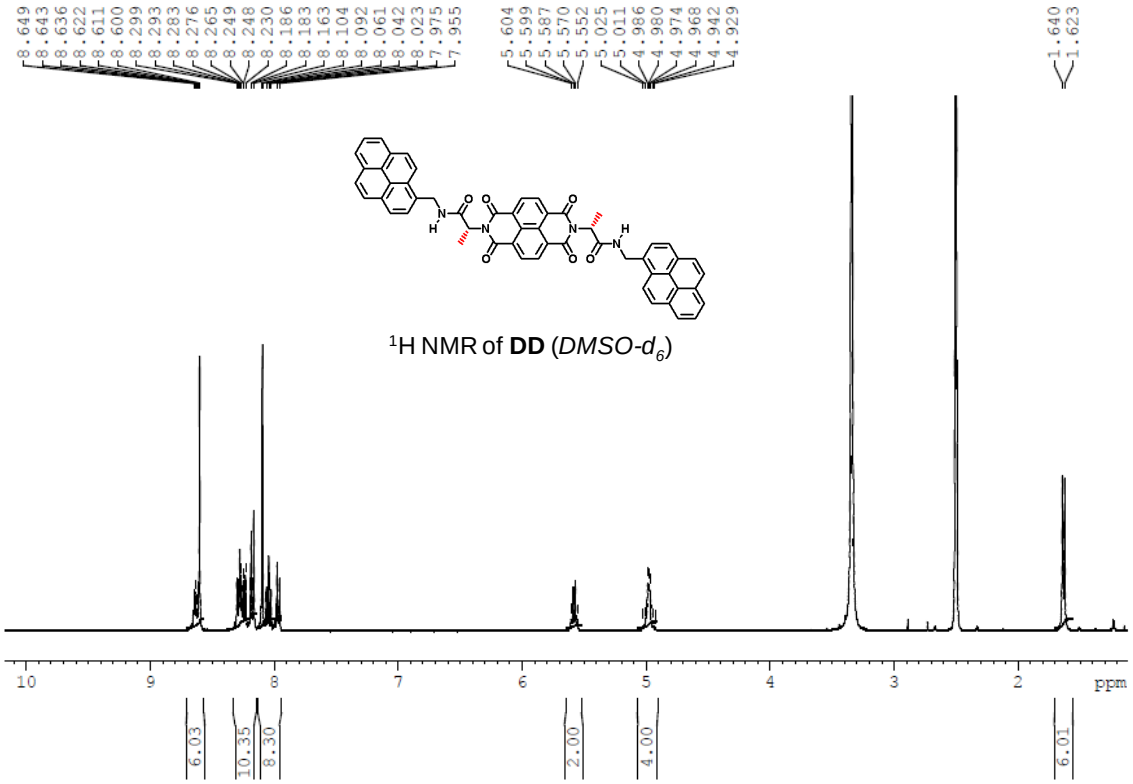


$^{1}$H NMR of **DD** (*DMSO-$d_6$*)

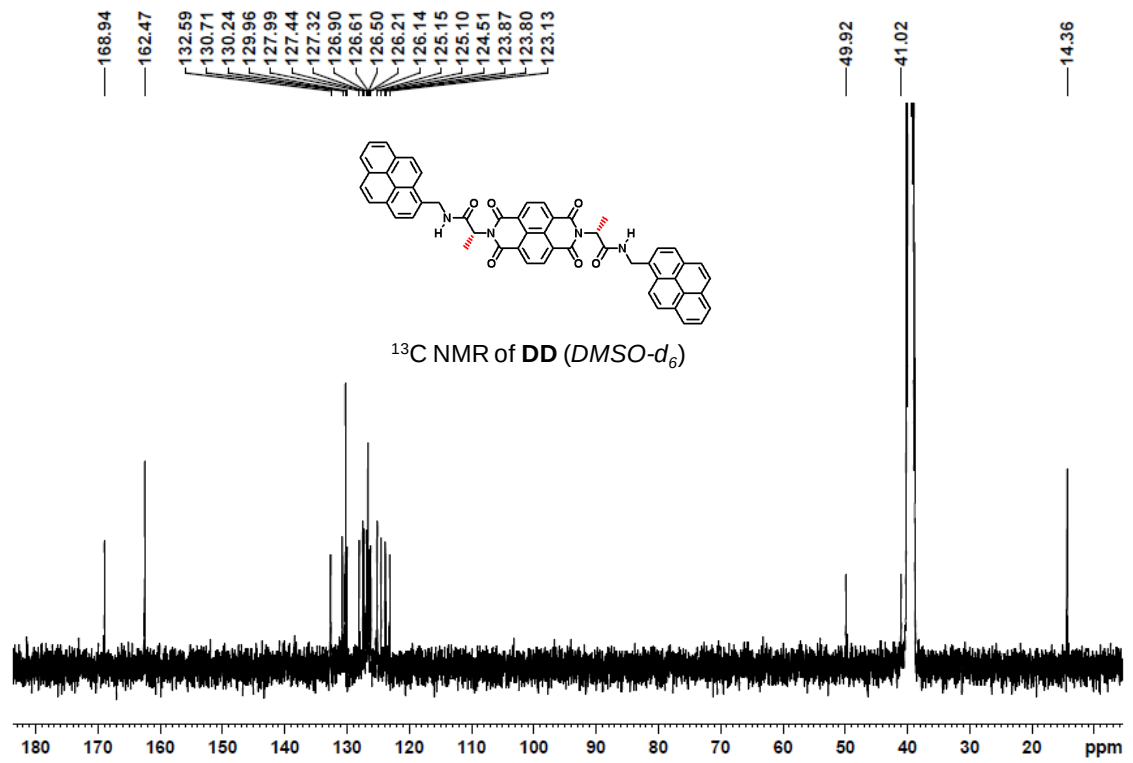


$^{13}$C NMR of **DD** (*DMSO-$d_6$*)

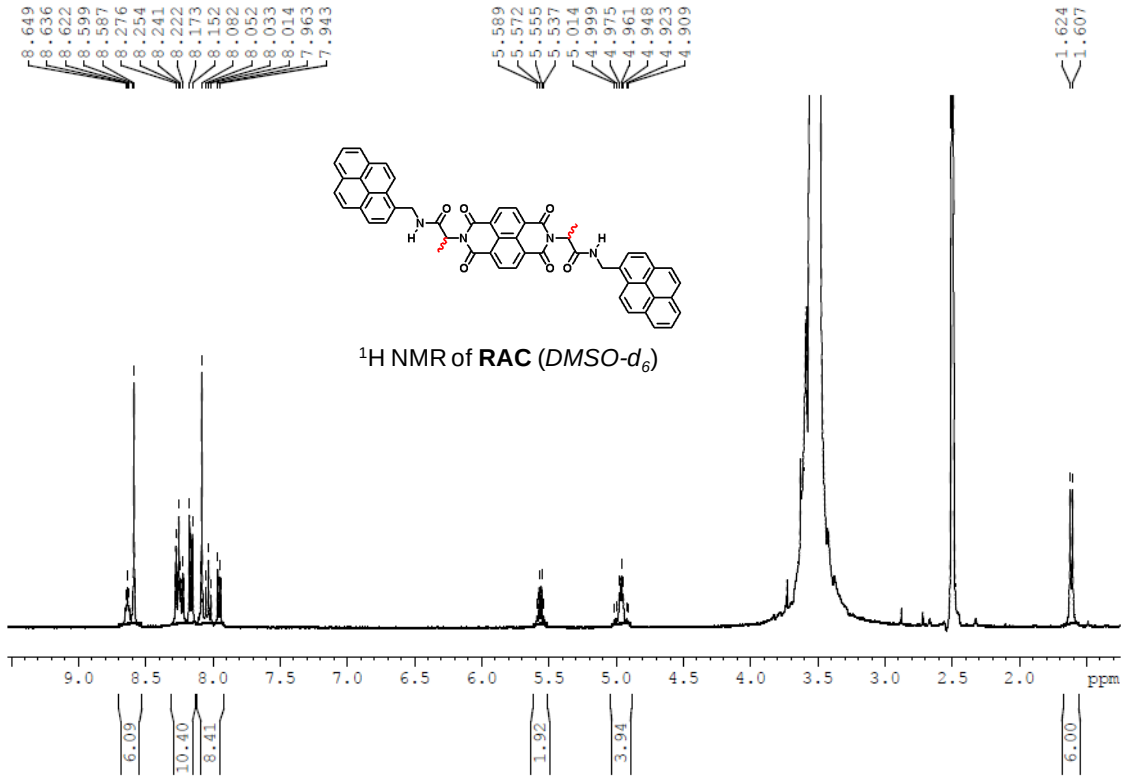


$^1$H NMR of **RAC** (*DMSO-$d_6$*)

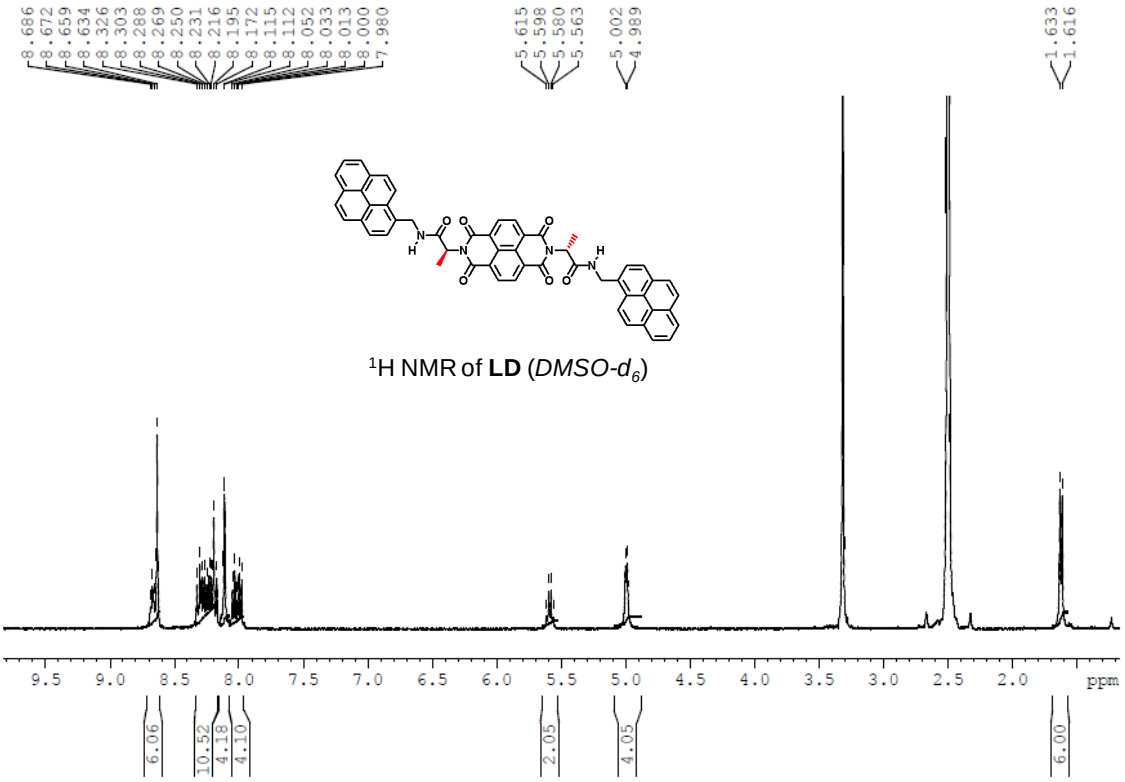


$^1$H NMR of **LD** (*DMSO-$d_6$*)

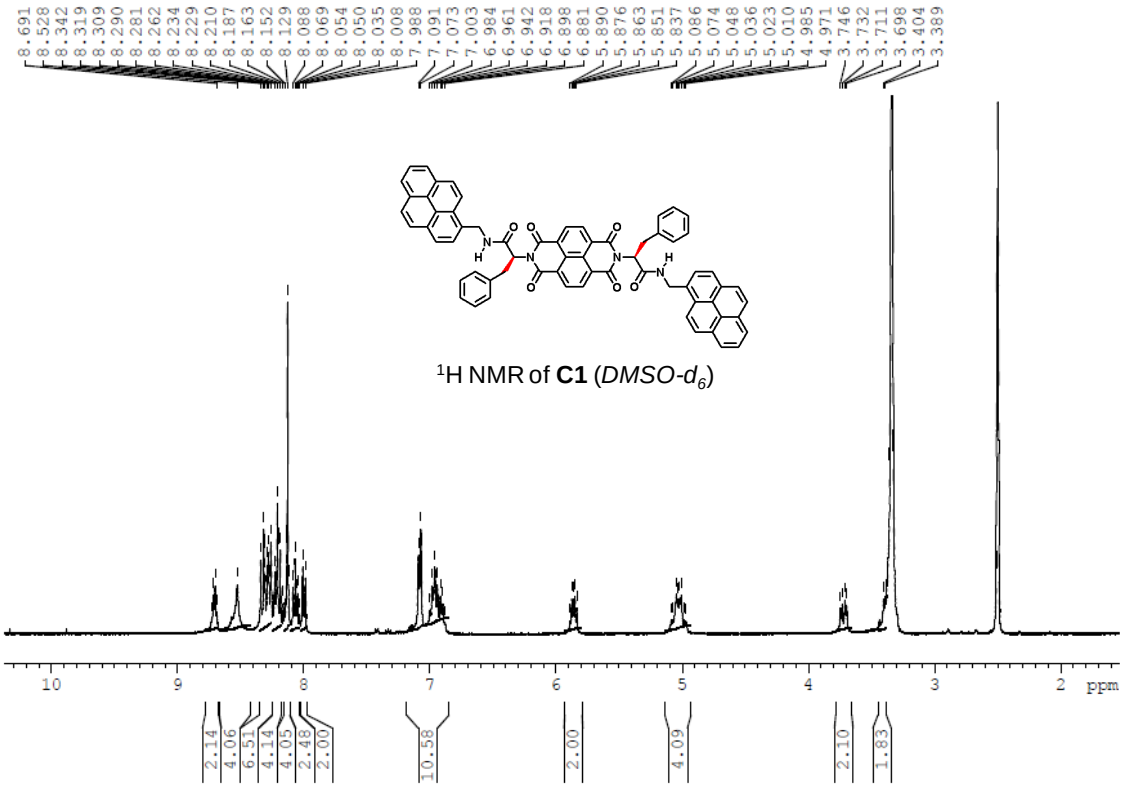


$^{1}$H NMR of **C1** (*DMSO-$d_6$*)

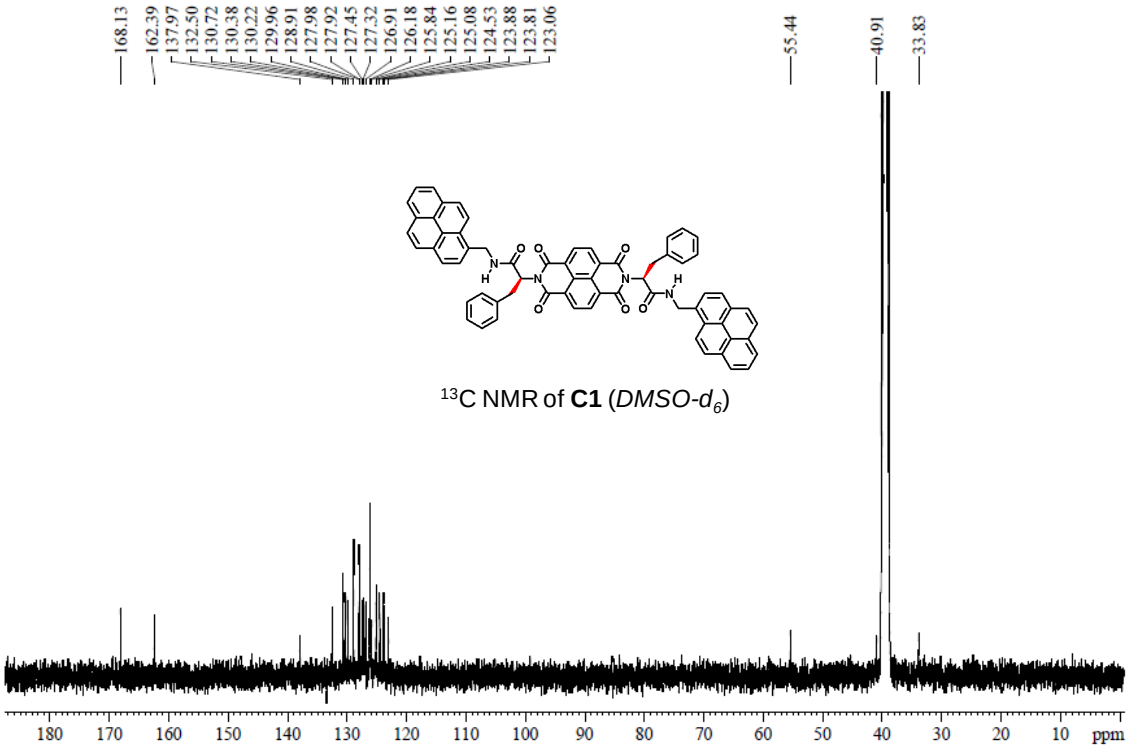


$^{13}$C NMR of **C1** (*DMSO-$d_6$*)

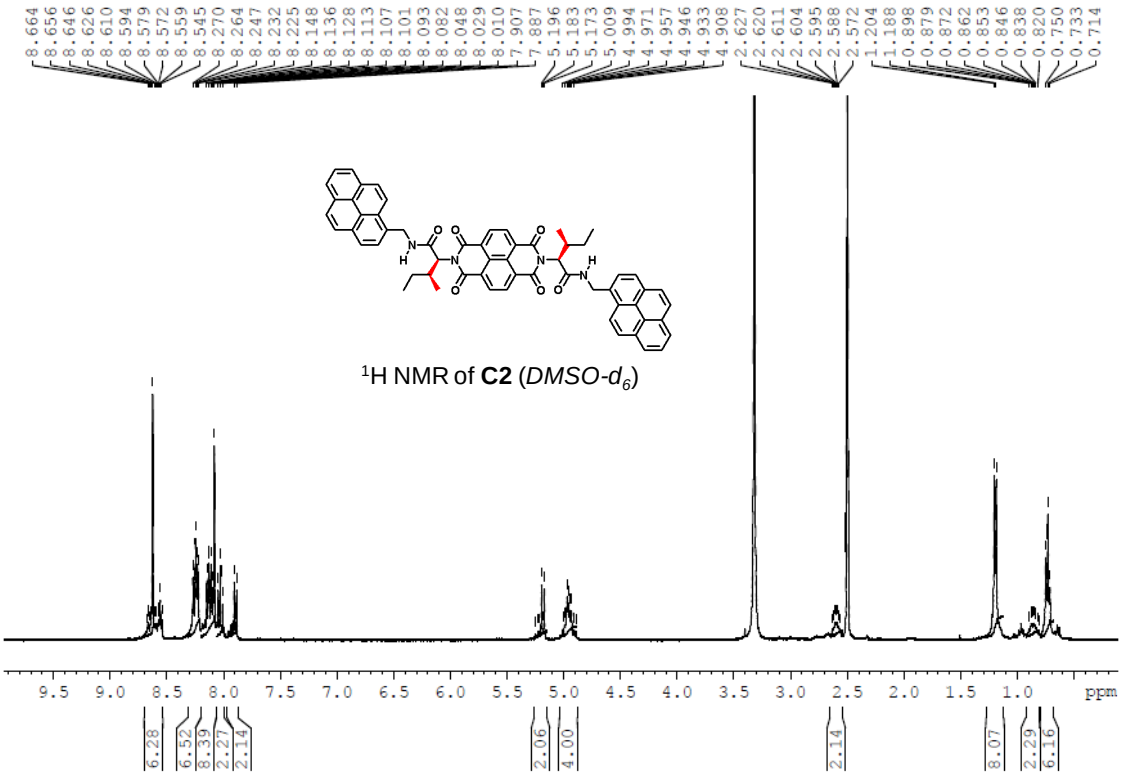

$^{1}$H NMR of **C2** (*DMSO-$d_6$*)

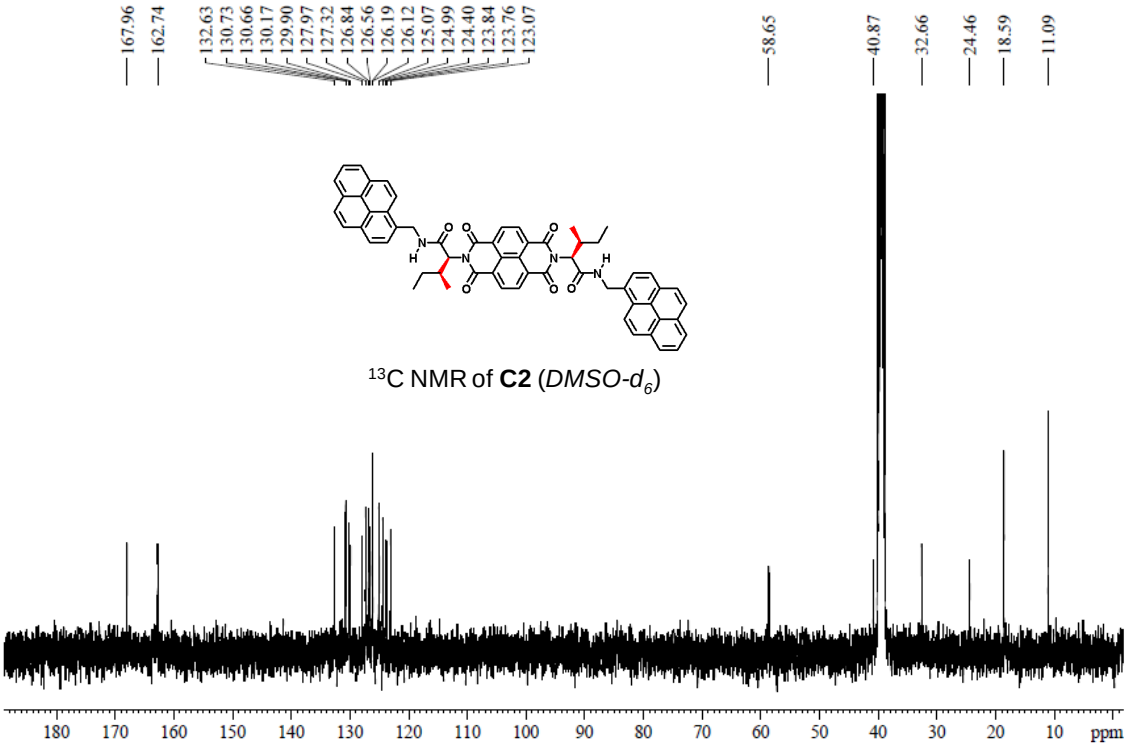

$^{13}$C NMR of **C2** (*DMSO-$d_6$*)

### 3.2.8. References

1. Corbett, P. T.; Leclaire, J.; Vial, L.; West, K. R.; Wietor, J.-L.; Sanders, J. K.; Otto, S., Dynamic combinatorial chemistry. *Chem. Rev.* **2006,** *106*, 3652-3711.

2. Lehn, J.-M., Toward complex matter: Supramolecular chemistry and self-organization. *Proc. Natl. Acad. Sci. U.S.A.* **2002,** *99*, 4763-4768.

3. Cousins, G. R.; Poulsen, S.-A.; Sanders, J. K., Molecular evolution: dynamic combinatorial libraries, autocatalytic networks and the quest for molecular function. *Curr. Opin. Chem. Biol.* **2000,** *4*, 270-279.

4. Kuhn, H., Is the transition from chemistry to biology a mystery. *J. Syst. Chem.* **2010,** *1*, 3.

5. Ludlow, R. F.; Otto, S., Systems chemistry. *Chem. Soc. Rev.* **2008,** *37*, 101-108.

6. von Kiedrowski, G., Chemistry: a way to the roots of biology. *Chem. Bio. Chem.* **2001,** *2*, 597-598.

7. Ball, P., Life's lessons in design. *Nature* **2001,** *409*, 413-416.

8. Lehn, J.-M., Toward self-organization and complex matter. *Science* **2002,** *295*, 2400-2403.

9. Ball, P., Natural strategies for the molecular engineer. *Nanotechnology* **2002,** *13*, R15.

10. Kurihara, K.; Tamura, M.; Shohda, K.-i.; Toyota, T.; Suzuki, K.; Sugawara, T., Self-reproduction of supramolecular giant vesicles combined with the amplification of encapsulated DNA. *Nat. Chem.* **2011,** *3*, 775-781.

11. Murphy, W. L.; Mooney, D. J., Molecular-scale biomimicry. *Nat. Biotechnol.* **2002,** *20*, 30-31.

12. Bowden, N. B.; Weck, M.; Choi, I. S.; Whitesides, G. M., Molecule-mimetic chemistry and mesoscale self-assembly. *Acc. Chem. Res.* **2001,** *34*, 231-238.

13. Zhang, S., Emerging biological materials through molecular self-assembly. *Biotechnol. Adv.* **2002,** *20*, 321-339.

14. Gust, D.; Moore, T. A.; Moore, A. L., Mimicking Photosynthetic Solar Energy Transduction. *Acc. Chem. Res.* **2000,** *34*, 40-48.

15. Czyzewski, A. M.; Barron, A. E., Protein and peptide biomimicry: Gold-mining inspiration from Nature's ingenuity. *AIChE J.* **2008,** *54*, 2-8.

16. Tu, R. S.; Tirrell, M., Bottom-up design of biomimetic assemblies. *Adv. Drug Delivery Rev.* **2004,** *56*, 1537-1563.

17. Reinhoudt, D.; Crego-Calama, M., Synthesis beyond the molecule. *Science* **2002,** *295*, 2403-2407.

18. Corbett, P. T.; Sanders, J. K.; Otto, S., Systems chemistry: pattern formation in random dynamic combinatorial libraries. *Angew. Chem. Int. Ed.* **2007,** *46*, 8858-8861.

19. Otto, S.; Furlan, R. L.; Sanders, J. K., Dynamic combinatorial chemistry. *Drug Discov. Today* **2002,** *7*, 117-125.

20. Mann, S., The Origins of Life: Old Problems, New Chemistries. *Angew. Chem. Int. Ed.* **2013,** *52*, 155-162.

21. Joyce, G. F., RNA evolution and the origins of life. *Nature* **1989,** *338*, 217-224.

22. Lewandowski, B.; De Bo, G.; Ward, J. W.; Papmeyer, M.; Kuschel, S.; Aldegunde, M. J.; Gramlich, P. M.; Heckmann, D.; Goldup, S. M.; D'Souza, D. M., Sequence-specific peptide synthesis by an artificial small-molecule machine. *Science* **2013,** *339*, 189-193.

23. Bertran-Vicente, J.; Hackenberger, C. P., A Supramolecular Peptide Synthesizer. *Angew. Chem. Int. Ed*. **2013**, *52*, 6140-6142.

24. Kouwer, P. H.; Koepf, M.; Le Sage, V. A.; Jaspers, M.; van Buul, A. M.; Eksteen-Akeroyd, Z. H.; Woltinge, T.; Schwartz, E.; Kitto, H. J.; Hoogenboom, R., Responsive biomimetic networks from polyisocyanopeptide hydrogels. *Nature* **2013,** *493*, 651-655.

25. Huebsch, N.; Mooney, D. J., Inspiration and application in the evolution of biomaterials. *Nature* **2009,** *462*, 426-432.

26. Kindermann, M.; Stahl, I.; Reimold, M.; Pankau, W. M.; von Kiedrowski, G., Systems chemistry: kinetic and computational analysis of a nearly exponential organic replicator. *Angew. Chem. Int. Ed.* **2005,** *44*, 6750-6755.

27. Harold, F. M., Molecules into cells: specifying spatial architecture. *Microbiol. Mol. Biol. Rev.* **2005,** *69*, 544-564.

28. Ramanathan, S.; Broach, J., Do cells think? *Cell. Mol. Life Sci.* **2007,** *64*, 1801-1804.

29. Pinheiro, V. B.; Taylor, A. I.; Cozens, C.; Abramov, M.; Renders, M.; Zhang, S.; Chaput, J. C.; Wengel, J.; Peak-Chew, S.-Y.; McLaughlin, S. H., Synthetic genetic polymers capable of heredity and evolution. *Science* **2012,** *336*, 341-344.

30. Bensaude-Vincent, B.; Arribart, H.; Bouligand, Y.; Sanchez, C., Chemists and the school of nature. *New J. Chem.* **2002,** *26*, 1-5.

31. Avinash, M.; Govindaraju, T., Extremely Slow Dynamics of an Abiotic Helical Assembly: Unusual Relevance to the Secondary Structure of Proteins. *J. Phys. Chem. Lett.* **2013,** *4*, 583-588.

32. Korevaar, P. A.; George, S. J.; Markvoort, A. J.; Smulders, M. M. J.; Hilbers, P. A. J.; Schenning, A. P. H. J.; De Greef, T. F. A.; Meijer, E. W., Pathway complexity in supramolecular polymerization. *Nature* **2012,** *481*, 492-496.

33. Tidhar, Y.; Weissman, H.; Wolf, S. G.; Gulino, A.; Rybtchinski, B., Pathway-Dependent Self-Assembly of Perylene Diimide/Peptide Conjugates in Aqueous Medium. *Chem. Eur. J.* **2011,** *17*, 6068-6075.

34. Radford, S. E., Protein folding: progress made and promises ahead. *Trends Biochem. Sci.* **2000,** *25*, 611-618.

35. Dobson, C. M., Protein folding and misfolding. *Nature* **2003,** *426*, 884-890.

36. Haran, G., How, when and why proteins collapse: the relation to folding. *Curr. Opin. Struct. Biol.* **2012,** *22*, 14-20.

37. Smith, B. A.; Hecht, M. H., Novel proteins: from fold to function. *Curr. Opin. Chem. Biol.* **2011,** *15*, 421-426.

38. Anfinsen, C. B., Principles that Govern the Folding of Protein Chains. *Science* **1973,** *181*, 223-230.

39. Sosnick, T. R.; Barrick, D., The folding of single domain proteins-have we reached a consensus? *Curr. Opin. Struct. Biol.* **2011,** *21*, 12-24.

40. Bowman, G. R.; Voelz, V. A.; Pande, V. S., Taming the complexity of protein folding. *Curr. Opin. Struct. Biol.* **2011,** *21*, 4-11.

41. Dobson, C. M., Experimental investigation of protein folding and misfolding. *Methods* **2004,** *34*, 4-14.

42. Avinash, M. B.; Govindaraju, T., Engineering Molecular Organization of Naphthalenediimides: Large Nanosheets with Metallic Conductivity and Attoliter Containers. *Adv. Funct. Mater.* **2011,** *21*, 3875-3882.

43. De Greef, T. F. A.; Smulders, M. M. J.; Wolffs, M.; Schenning, A. P. H. J.; Sijbesma, R. P.; Meijer, E. W., Supramolecular Polymerization. *Chem. Rev.* **2009,** *109*, 5687-5754.

44. Ponnuswamy, N.; Pantoş, G. D.; Smulders, M. M. J.; Sanders, J. K. M., Thermodynamics of Supramolecular Naphthalenediimide Nanotube Formation: The Influence of Solvents, Side Chains, and Guest Templates. *J. Am. Chem. Soc.* **2011,** *134*, 566-573.

45. Smulders, M. M. J.; Nieuwenhuizen, M. M. L.; de Greef, T. F. A.; van der Schoot, P.; Schenning, A. P. H. J.; Meijer, E. W., How to Distinguish Isodesmic from Cooperative Supramolecular Polymerisation. *Chem. Eur. J.* **2010,** *16*, 362-367.

46. Würthner, F.; Thalacker, C.; Diele, S.; Tschierske, C., Fluorescent J-type Aggregates and Thermotropic Columnar Mesophases of Perylene Bisimide Dyes. *Chem. Eur. J.* **2001,** *7*, 2245-2253.

47. Huang, C.; Barlow, S.; Marder, S. R., Perylene-3,4,9,10-tetracarboxylic Acid Diimides: Synthesis, Physical Properties, and Use in Organic Electronics. *J. Org. Chem.* **2011,** *76*, 2386-2407.

48. Restituito, S.; Khatri, L.; Ninan, I.; Mathews, P. M.; Liu, X.; Weinberg, R. J.; Ziff, E. B., Synaptic autoregulation by metalloproteases and γ-secretase. *J. Neurosci.* **2011,** *31*, 12083-12093.

49. Rodríguez-Llansola, F.; Meijer, E., Supramolecular Autoregulation. *J. Am. Chem. Soc.* **2013,** *135*, 6549-6553.

50. Hudmon, A.; Schulman, H., Neuronal CA2+/calmodulin-dependent protein kinase II: the role of structure and autoregulation in cellular function. *Annu. Rev. Biochem.* **2002,** *71*, 473-510.

51. Hordijk, W.; Steel, M., Autocatalytic sets extended: Dynamics, inhibition, and a generalization. *J. Sys. Chem.* **2012,** *3*, 1-12.

52. Voytek, S. B.; Joyce, G. F., Emergence of a fast-reacting ribozyme that is capable of undergoing continuous evolution. *Proc. Natl. Acad. Sci. USA* **2007,** *104*, 15288-15293.

53. Filisetti, A.; Graudenzi, A.; Serra, R.; Villani, M.; De Lucrezia, D.; Füchslin, R. M.; Kauffman, S. A.; Packard, N.; Poli, I., A stochastic model of the emergence of autocatalytic cycles. *J. Sys. Chem.* **2011,** *2*, 1-10.

54. Saggiomo, V.; Hristova, Y. R.; Ludlow, R. F.; Otto, S., Systems chemistry: using thermodynamically controlled networks to assess molecular similarity. *J. Sys. Chem.* **2013,** *4*, 1-6.

55. Campbell, V. E.; De Hatten, X.; Delsuc, N.; Kauffmann, B.; Huc, I.; Nitschke, J. R., Cascading transformations within a dynamic self-assembled system. *Nat. Chem.* **2010,** *2*, 684-687.

56. Pross, A., Toward a general theory of evolution: extending Darwinian theory to inanimate matter. *J. Sys. Chem.* **2011,** *2*, 1-14.

57. Pross, A., On the emergence of biological complexity: life as a kinetic state of matter. *Origins Life Evol. B.* **2005,** *35*, 151-166.

58. Bahramy, M.; Yang, B.-J.; Arita, R.; Nagaosa, N., Emergence of non-centrosymmetric topological insulating phase in BiTeI under pressure. *Nat. Commun.* **2012,** *3*, 679.

59. Yamakage, A.; Tanaka, Y.; Nagaosa, N., Evolution of Edge States and Critical Phenomena in the Rashba Superconductor with Magnetization. *Phys. Rev. Lett.* **2012,** *108*, 087003.

60. Hwang, H.; Iwasa, Y.; Kawasaki, M.; Keimer, B.; Nagaosa, N.; Tokura, Y., Emergent phenomena at oxide interfaces. *Nat. Mater.* **2012,** *11*, 103-113.

61. Nagaosa, N.; Tokura, Y., Emergent electromagnetism in solids. *Phys. Scr.* **2012,** *2012*, 014020.

62. Ghosh, S.; Mukhopadhyay, P.; Isaacs, L., Deconvolution of a multi-component interaction network using systems chemistry. *J. Sys. Chem.* **2010,** *1*, 6.

63. Sarma, R. J.; Nitschke, J. R., Self-Assembly in Systems of Subcomponents: Simple Rules, Subtle Consequences. *Angew. Chem. Int. Ed.* **2008,** *47*, 377-380.

64. Avinash, M. B.; Govindaraju, T., Amino Acid Derivatized Arylenediimides: A Versatile Modular Approach for Functional Molecular Materials. *Adv. Mater.* **2012,** *24*, 3905-3922.

65. Avinash, M.; Govindaraju, T., A bio-inspired design strategy: Organization of tryptophan-appended naphthalenediimide into well-defined architectures induced by molecular interactions. *Nanoscale* **2011,** *3*, 2536-2543.

66. Avinash, M. B.; Samanta, P. K.; Sandeepa, K. V.; Pati, S. K.; Govindaraju, T., Molecular Architectonics of Stereochemically Constrained π-Complementary Functional Modules. *Eur. J. Org. Chem.* **2013,** *2013*, 5838-5847.

67. Pandeeswar, M.; Avinash, M.; Govindaraju, T., Chiral Transcription and Retentive Helical Memory: Probing Peptide Auxiliaries Appended with Naphthalenediimides for Their One-Dimensional Molecular Organization. *Chem. Eur. J.* **2012,** *18*, 4818-4822.

68. Sakai, N.; Mareda, J.; Vauthey, E.; Matile, S., Core-substituted naphthalenediimides. *Chem. Commun.* **2010,** *46*, 4225-4237.

69. Palmans, A. R.; Meijer, E. e. W., Amplification of chirality in dynamic supramolecular aggregates. *Angew. Chem. Int. Ed.* **2007,** *46*, 8948-8968.

70. Markvoort, A. J.; Ten Eikelder, H. M.; Hilbers, P. A.; de Greef, T. F.; Meijer, E., Theoretical models of nonlinear effects in two-component cooperative supramolecular copolymerizations. *Nat. Commun.* **2011,** *2*, 509.

71. Berova, N.; Nakanishi, K.; Woody, R. W., *Circular dichroism: principles and applications*. Wiley-VCH New York: 2000; Vol. 912.

# CHAPTER 4 MOLECULAR MATERIALS

Programmed molecular assemblies with molecular-level precision have always intrigued mankind in the quest to master the art of molecular engineering. The controlled self-assembly of small molecules into well-defined, ordered nano- and microstructures is of current interest for potential applications in photavoltaics,[1] photonic crystals,[2] tissue engineering,[3] single-cell analysis,[4] microreactors,[5] superhydrophobic coatings[6] and many others. This bottom-up molecular assembly approach has been elegantly utilized by nature to form a variety of functional materials.[7,8] However, it is only now that chemists have begun to understand the underlying supramolecular design principles[9-12] in an ongoing effort to construct ordered two-dimensional (2D) or three-dimensional (3D) patterns and arrays, which could ultimately lead to complex architectures and functions.

In this regard, we demonstrate examples based on bioinspired design strategies for developing functional molecular materials. This chapter is categorized into three sub-chapters pertaining to self-cleanability inspired by lotus leaf, extraordinary stiffness inspired by spider silk and high charge transport achieved in the bulk state by our bioinspired modular approach. In these sub-chapters, we provide detailed descriptions of the working principles of the natural systems along with their potential applications and the molecular design strategies employed by us to mimic them. Such efforts are believed to empower our molecular engineering skills for not just developing the molecular materials but also to infuse additional functionalities by a simple and efficient process of self-assembly. We strongly believe that with increasing constraints on energy, health and environment, the demand for efficient processes and materials would inevitably increase in due course of time.

## 4.1. Self-Cleaning Functional Molecular Materials

Self-cleaning is the remarkable property of a surface, by which it can clean itself without any human intervention.[13,14] This unusual property draws its inspiration from the lotus effect exhibited by lotus leaves.[15] Although lotus plants grow in muddy ponds, its leaves are always clean, which is due to a surface property known as superhydrophobicity.[16] The surface of lotus leaves comprises of micron sized bud-like structures known as papillae followed by a coating of nanometer-sized wax crystalloids (Figure 1). This combination of hierarchical surface roughness and low-surface energy coating results in superhydrophobicity, often ascribed to a water contact angle greater than 150$^{o}$.

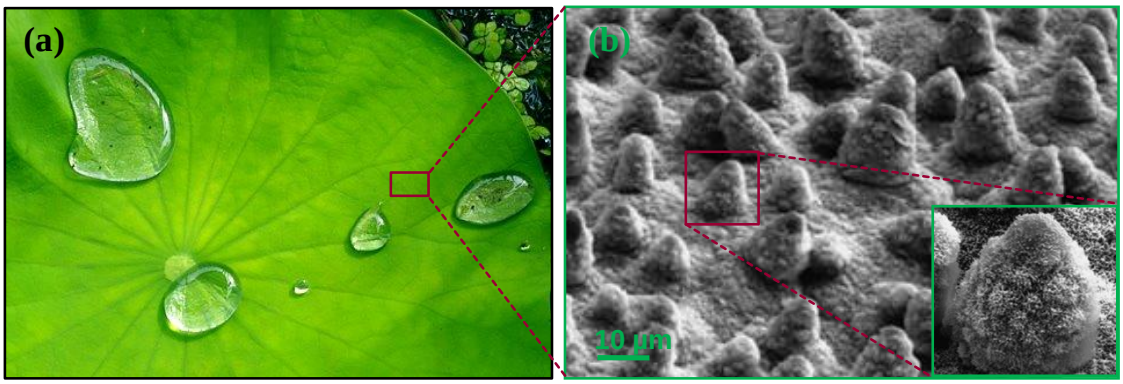


**Figure 1**. (a) Photograph of a self-cleanable lotus leaf along with the water droplets. (b) SEM image of the lotus leaf and the inset show papillae and wax crystalloids. Adapted with permission of RSC from reference 17.

Contact angle is the angle between the tangent and the surface at the point of contact of water droplet with the surface (Figure 2). For any non-superhydrophobic surface, the water droplets just glide down the inclined surface under the influence of gravity (Figure 2). During which the dust particles if any, would only be displaced along

the path of water droplets but cannot be removed completely. On the other hand, for a superhydrophobic surface the very high surface tension of water enforces it to attain spherical shape and also the dust particles experience greater affinity for the water droplet than to the surface (Figure 2). As a result of which, when the water droplet rolls down on such an inclined surface, the dust gets removed completely and which is what is termed as self-cleaning. For better performances as a self-cleaning surface, the contact angle hysteresis ($\Delta\theta$) and the slide/tilt angle ($\alpha$) has to be as low as possible, typically less than $10^{o}$ (Figure 2). $\alpha$ is the minimum angle to which the surface has to be inclined, so as to facilitate the rolling of water droplets under the action of gravity. $\Delta\theta$ is the difference between the advancing and receding contact angles.

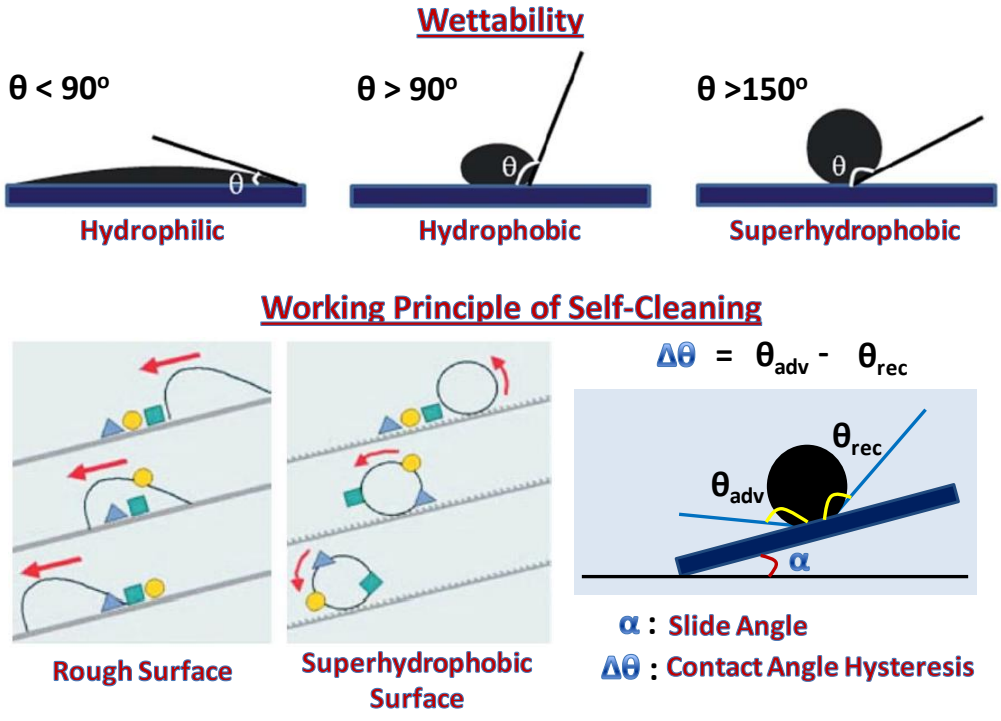


**Figure 2**. Schematic representation of contact angles for hydrophilic, hydrophobic and superhydrophobic surfaces, and the working principle of self-cleaning. Adapted with permission of RSC from reference 18 and Springer Science and Business Media from reference 19.

In recent years, superhydrophobic surfaces in particular have come into focus, partly by the motivation to mimic nature and owing to their promising applications.[20-24] Over the years, a variety of chemical and physical methods for the fabrication of rough surfaces with subsequent low-surface-energy coatings have been explored by lithography,[25] sublimation,[26] plasma techniques,[27] self-assembled monolayers (SAM),[28,29] and electrochemical methods[30,31]. Furthermore, the so called breath-figure technique (BFT)[32] has also been explored owing to its simple solution processability, robustness, and the excellent tunability of size over three orders of magnitude (nm to mm). When a solution is drop-cast on a surface under humid air, the evaporation of the volatile solvent facilitates condensation of water droplets on the cold surface. This evaporative cooling and subsequent solidification of the solute under favorable conditions produces highly ordered arrays of well-defined cavities with diameters of 50 nm to 20 μm, called breath-figure arrays. However, the use of BFT has been limited to date to certain classes of macromolecules, such as star polymers,[33] cross-linked star polymers,[34] hyper-branched polymers,[35] conjugated polymers,[36] and dendronized polymers,[37] with an exception of only a few organogelators.[38-40] It has been argued that viscous polymer solutions with additional polar functionalities are required in BFT to form a stable interface with the water droplet. In contrast, small molecules either crystallize or unspecifically aggregate and thus lack the ability to stabilize water rafts.[41-43]

We serendipitously discovered that a NDI-based molecule **1** that forms highly-ordered self-assembled breath-figure arrays from dichloromethane solvent.[44] Depending on the concentration of **1**, the surface roughness of the self-assembled materials changes and thus the surface wettability for water can be varied from a contact angle of $60^{o}$ to

135°. Furthermore, upon sputtering a thin layer of gold onto these microarrays, we could ultimately successfully mimic the self-cleaning properties of the lotus leaf (contact angle of 156° and tilt angle of 3°). Furthermore, fluorescent dyes, such as perylenediimide, rhodamine B, and coumarines, can be incorporated within the self-assembled microarrays of **1**, giving rise to highly fluorescent hydrophobic materials.

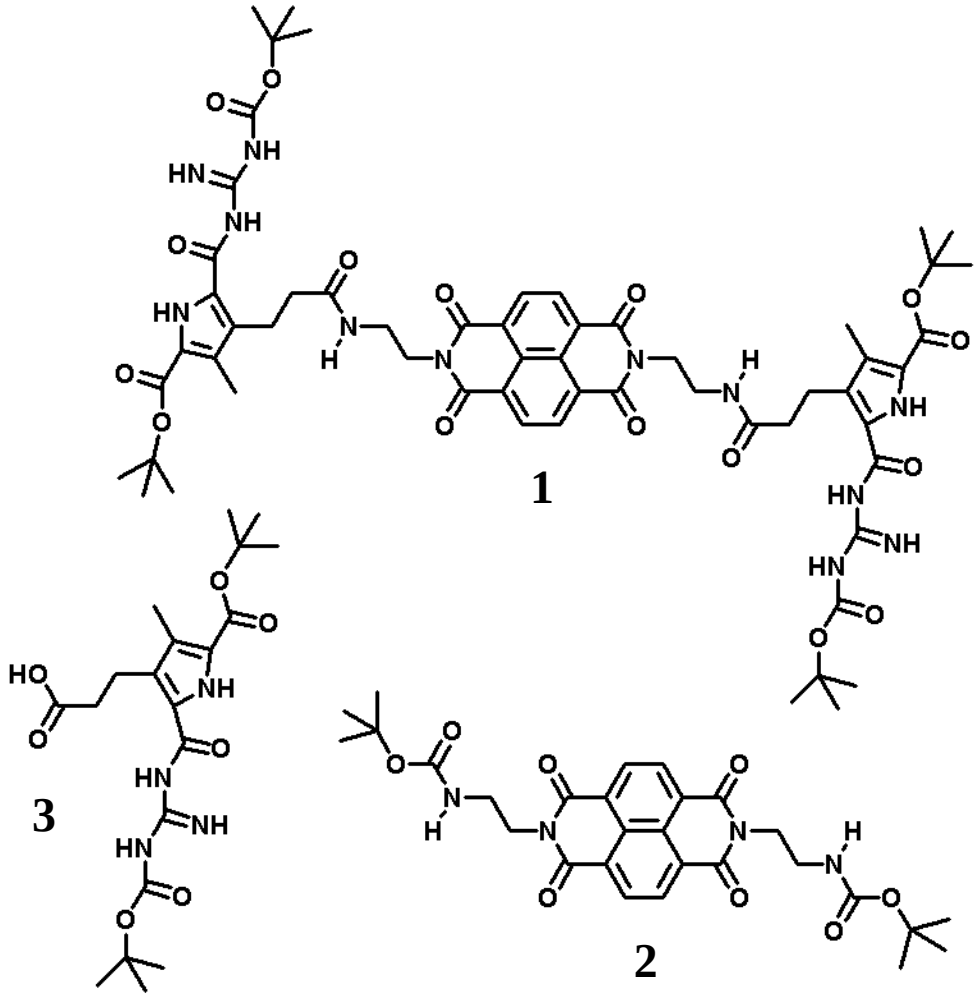


### 4.1.1. Effect of solvent

The presence of both polar and non-polar functional groups in **1** ensures solubility in various organic solvents of different polarity index and should also allow for self-

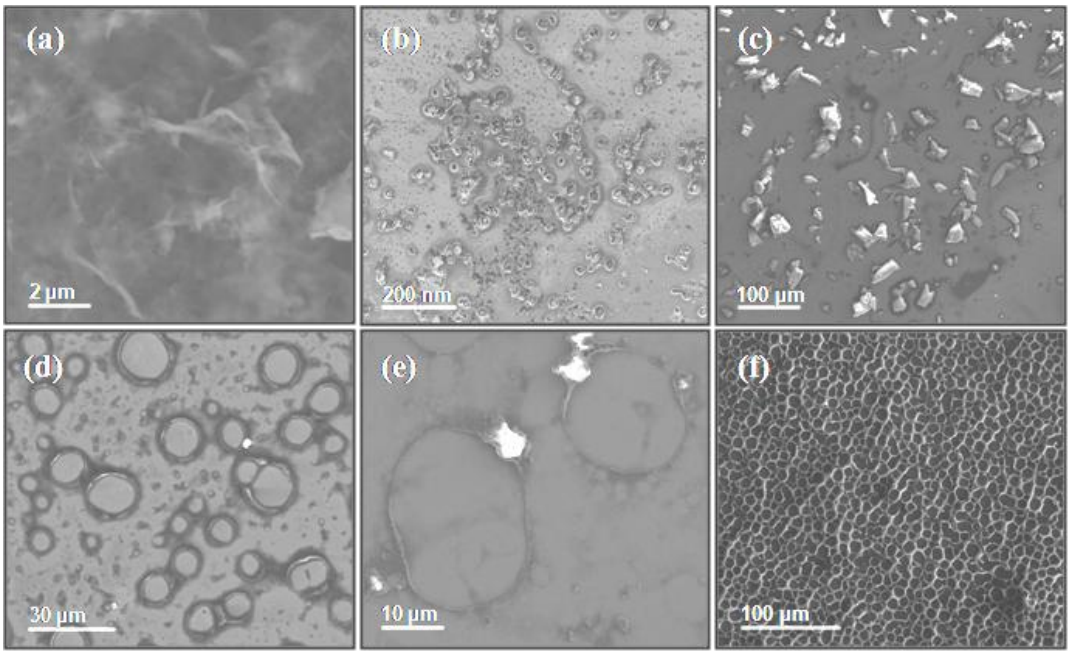


**Figure 3**. FESEM micrographs of **1** drop-casted from (a) 1 mM acetonitrile solution, (b) 1 mM tetrahydrofuran solution, (c) 1 mM dimethylsulfoxide solution, (d) 1 mM chloroform solution, (e) 1 mM carbontetrachloride solution and (f) 1 mM dichloromethane solution.

assembly. Indeed, **1** formed self-assembled structures of different morphologies from various organic solvents, as observed with field-emission scanning electron microscopy (FESEM) after drop-casting solutions of **1** onto silicon (111) substrates; particulate as well as film like morphologies are obtained from acetonitrile, random nanometer- and micrometer-sized particulate-like aggregates from tetrahydrofuran and dimethylsulfoxide, and discrete microwells from chloroform and carbon tetrachloride solutions (Figure 3a-e). To our surprise, from another chlorinated solvent, dichloromethane, **1** self-assembled into honeycomb-like microarrays (Figure 3f). Obviously, chlorinated solvents had a peculiar impact on the formation of microwells or microarrays. Previously we had encountered a similar situation wherein chlorinated co-solvents were found to be crucial in the formation of attoliter containers of NDIs.[45] In this earlier work, we had shown with

the help of single-crystal X-ray data that chlorinated solvents interact with the carbonyl functionalities of NDI by means of halogen bonding interactions. Therefore, it is reasonable to assume that similar halogen bonding interactions occur with **1**, which might explain why **1** forms microwells and microarrays exclusively from chlorinated solvents.

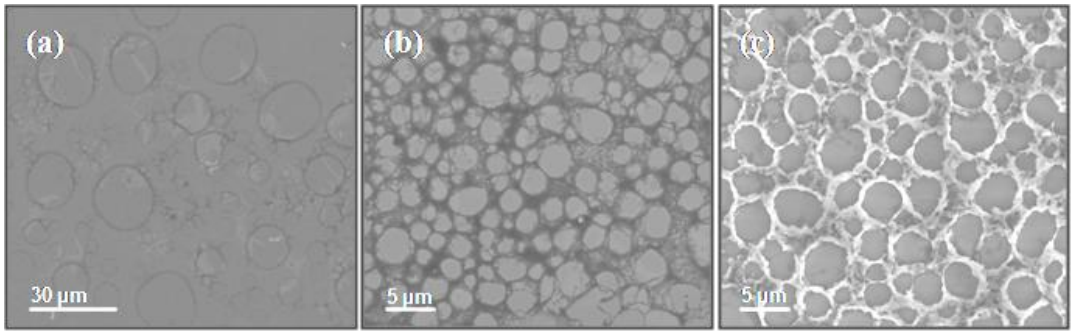


**Figure 4**. FESEM micrographs of **1** drop-casted from (a) 1 µM dichloromethane solution, (b) 10 µM dichloromethane solution and (c) 100 µM dichloromethane solution.

### 4.1.2. Effect of concentration

The exact morphology of the self-assembled structures depends on the concentration of **1** (Figure 4). A 1 µM dichloromethane solution of **1** resulted only in discrete faint microwell-like features amongst groups of smaller microwells (Figure 4a). With a 10-fold increase in concentration (10 µM), a microarray-like morphology formed from entangled nanobelts was observed (Figure 4b). Increasing the concentration further to 100 µM led to a microarray with an internal diameter of less than 5 µm (Figure 4c). Thus, as the concentration of **1** increases (see Figure 3f for 1 mM solution), the microarray structuring also increases with a gradual enhancement in the topographical thickness. An optical profiler was utilized to obtain a 3D image of the microarrays obtained from a 1 mM solution (Figure 5). The section analysis revealed microarrays with an internal diameter of 10-25 µm with a topographical thickness of 10-15 µm.

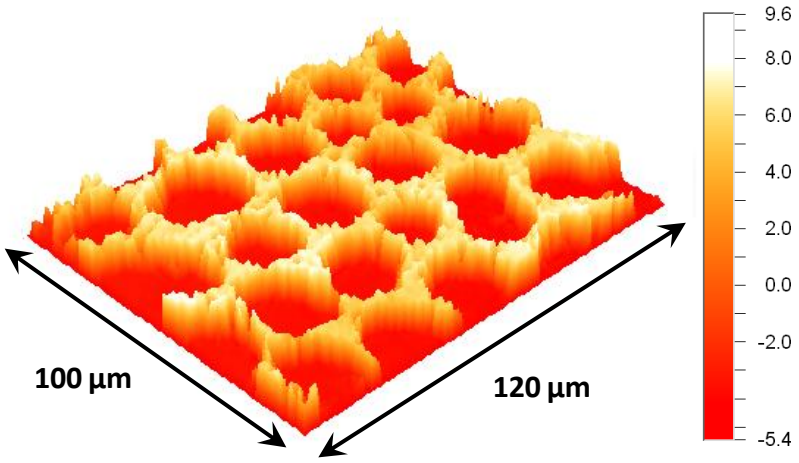


**Figure 5**. An optical profiler 3D image depicting the dimensions of honeycomb-like microarrays obtained from 1 mM dichloromethane solution of **1**.

### 4.1.3. Effect of substrate

To study the effect of the surface on morphogenesis, we also employed mica and glass as other substrates. On mica, microarrays were formed as well with an internal diameter ranging from 15 to 35 µm (Figure 6a,b). Furthermore, within these large microwells, smaller discrete microwells were observed that are most likely due to smaller breath figures. On the contrary, a glass surface produced significantly smaller microwells of only 1 to 6 µm internal diameter, with the rest of the surface being covered with a network of belt like aggregates (Figure 6c,d).

### 4.1.4. The mechanism

A literature survey suggested a probable role of BFT for the formation of such honeycomb-like microarrays, even though breath-figure arrays to date were mainly

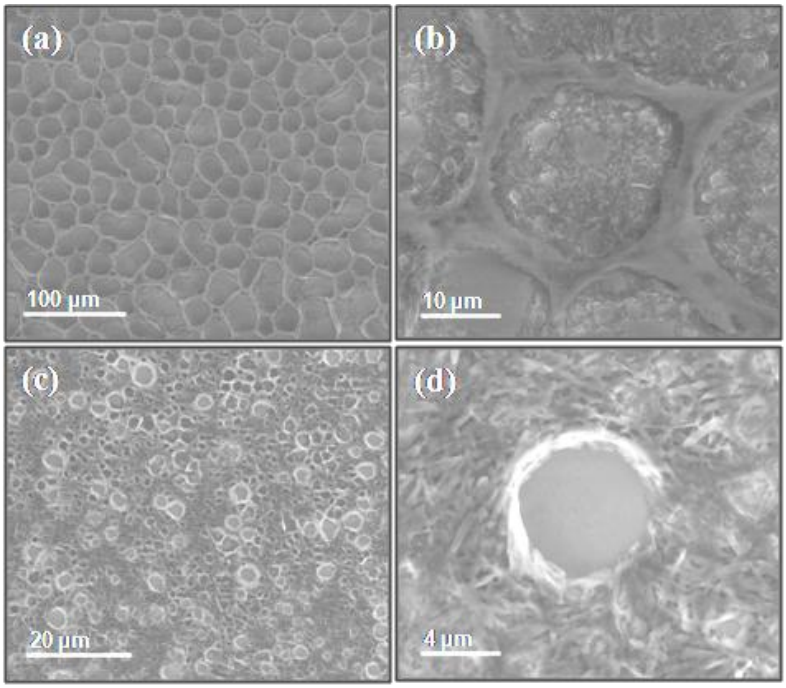


**Figure 6**. FESEM micrographs of 1 mM dichloromethane solution of **1** drop-casted on (a) and (b) freshly cleaved mica, (c) and (d) glass, as substrates.

observed for polymers but not small low-molecular-weight compounds such as **1**. Nevertheless, to test the hypothesis whether BFT might be important for structure formation in our case, we studied the self-assembly of **1** in atmospheres with different relative humidity (RH). When a 1 mM dichloromethane solution of **1** was drop-casted on a silicon substrate in an inert atmosphere with about 0% RH, only random aggregates without any indication for the formation of microarrays were observed (Figure 7a). This strongly indicated the importance of humidity as required in BFT. To study the effect of RH on microarray formation quantitatively, a set up was developed to maintain and control the humidity during the self-assembly process. Dichloromethane solutions of **1** were drop-casted under five different RH values of 35%, 50%, 65%, 80%, and 95%. At 35% RH, the wells of the microarrays had dimensions in the range of 40 to 100 µm

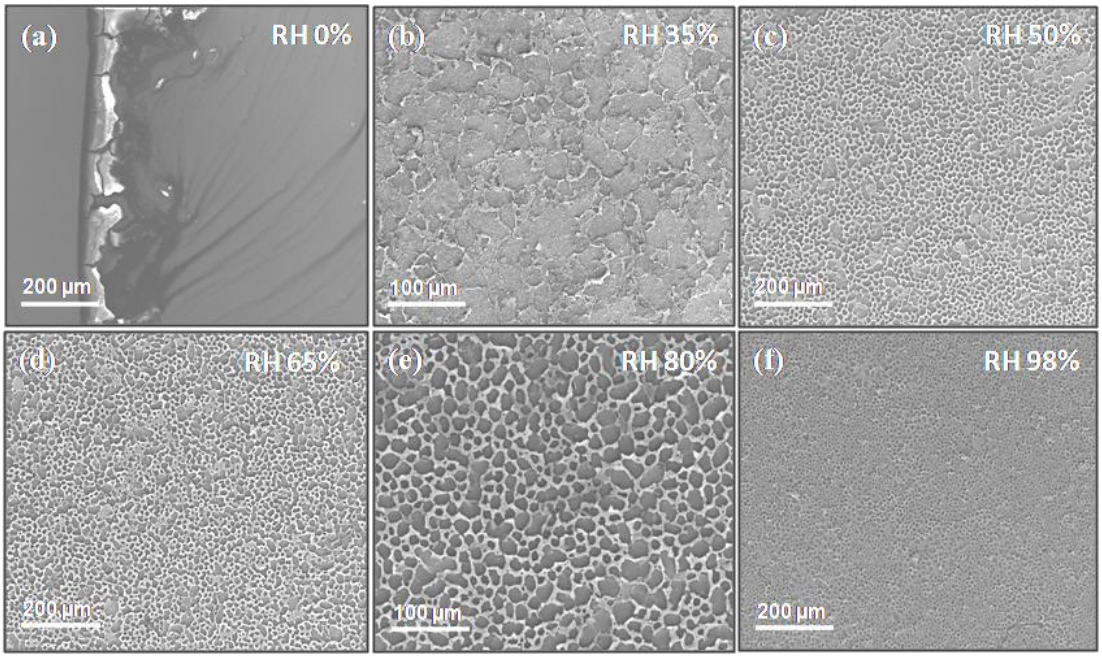


**Figure 7**. FESEM micrographs obtained from dichloromethane solution of **1** drop casted on Si (111) surface at different relative humidity (RH). The inset in (a) to (f) corresponds to respective relative humidity (in %).

(Figure 7b). However, the microwells were of uneven topographical thickness and most often the wells were fused with their neighbors. With increasing RH, significantly better structured microarrays were observed (Figure 7c-f). Moreover, the internal diameter of the microwells decreased with increasing RH. To further elucidate the mechanism of microarray formation, dynamic light-scattering (DLS) measurements were performed. In a 1 mM dichloromethane solution of **1** self-assembled aggregates having a hydrodynamic diameter of about 220 nm were observed (Figure 8a). Upon increasing the concentration to 5 mM, even large aggregates of about 784 nm sizes among the smaller aggregates of about 161 nm were observed (Figure 8b). Thus, **1** self-assembles into supramolecular polymeric aggregates in dichloromethane, which is most likely due to the strong hydrogen bonding of the *N*-*t*Boc(tert-butoxycarbonyl)-protected guanidinocarbonyl

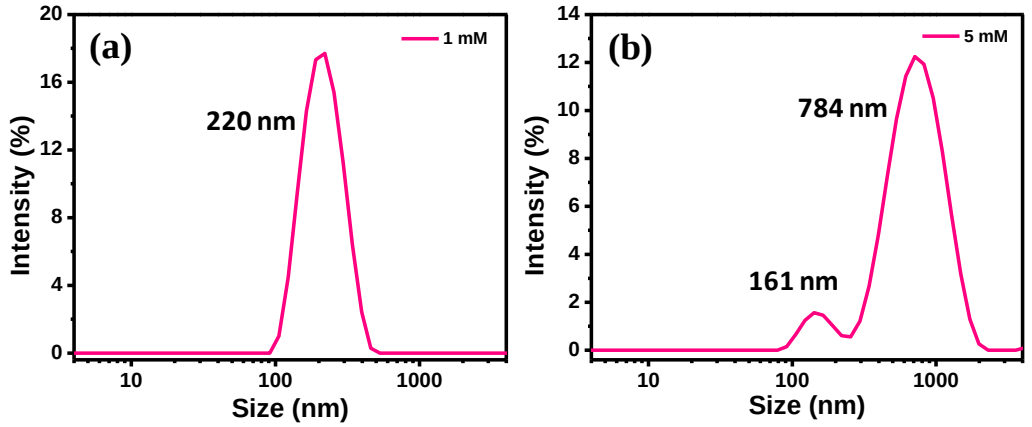


**Figure 8**. Dynamic light scattering (DLS) spectra of **1** obtained from (a) 1 mM and (b) 5 mM dichloromethane solution respectively.

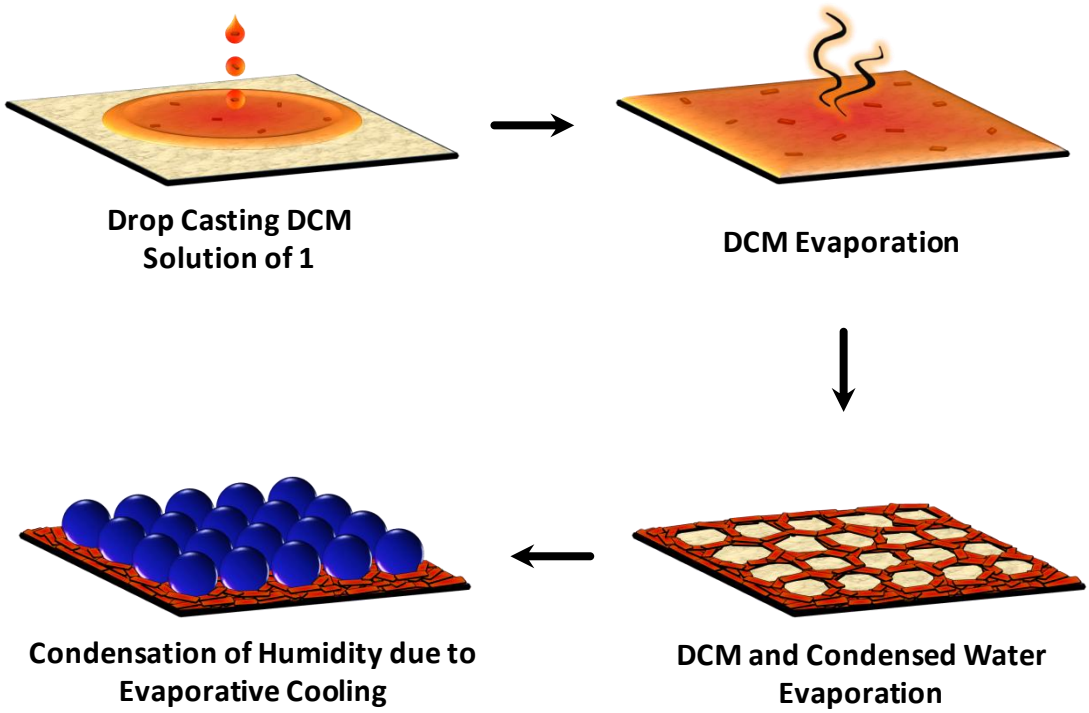


**Figure 9**. The formation of honeycomb-like microarrays from self-assembled structures of **1** by means of breath-figure technique (BFT). Not to scale.

pyrrole (GCP) groups in this solvent. Furthermore, in more concentrated solutions the size of the aggregates increases significantly, which is probably due to the weaker π-π interactions of the NDI core. These findings now allow presenting a plausible mechanism

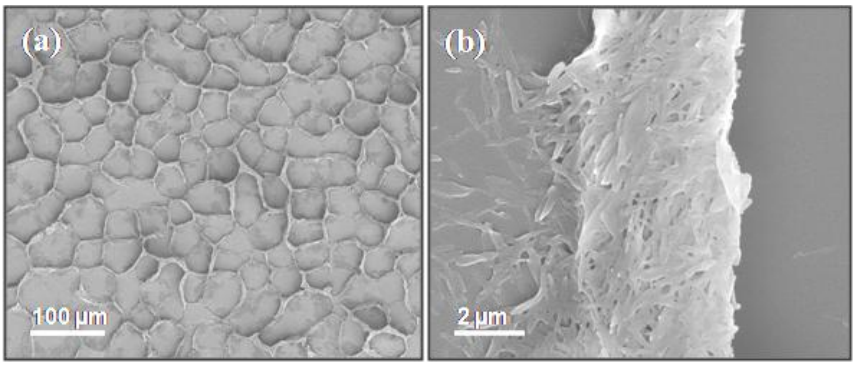


**Figure 10**. (a) and (b) FESEM micrographs of gold coated surface (1 mM dichloromethane solution of **1**). The microarray side wall comprising a pile of nanobelts is shown in (b).

for structure formation (Figure 9). Thus, when a dichloromethane solution of **1** is drop-cast on a substrate, the evaporative cooling owing to the evaporation of the volatile solvent dichloromethane causes a decrease in the surface temperature, which induces condensation of water vapors present in humid air. However, the condensed water droplets on the surface are stabilized and protected from coalescing by interaction with the self-assembled aggregates of **1** already present in solution (Figure 10). Upon further evaporation of dichloromethane, the hexagonally packed array of water rafts then induces the formation of self-assembled honeycomb-like microarrays of **1**. As the microscopy image of the walls of the microarrays shows, the original aggregates in solution most likely consist of nanobelt-like structures. A representation of this breath-figure mechanism is shown in Figure 9. The presence of the different polar and aromatic functionalities in **1** is believed to synergistically stabilize both the self-assembled structures of **1** and the water droplets at their interface. The rigidity of the nanobelt-like aggregates of **1** then facilitates a hexagonal assembly around the water droplets, which is then responsible for the formation of distorted hexagonal cavities in the BFT microarrays. Furthermore, the breath-figure arrays produced from chlorinated solvents most likely

involve halogen bonding. For such halogen bonding, carbonyl functionalities in **1** seem to play a crucial role.[32,45] Also the fact that dichloromethane is immiscible in water is important for BFT.

### 4.1.5. Developing the self-cleanable molecular material

The enhanced surface roughness properties associated with nano- and microstructured surfaces is utilized by nature to control water wettability in different systems, such as lotus leaves, desert beetles, mosquito eyes, and water striders. As with increasing concentration of **1**, the topographical thickness and thus the surface roughness of the self-assembled microarrays increases, the wettability of the surfaces should decrease, accordingly turning the material into a hydrophobic coating. Indeed, the contact angle of a 4 µL water droplet increases gradually from $60^{o}$ for the surface obtained from a 1 µM solution of **1** to $134^{o}$ for a 1 mM solution (Figure 11). Thus, simply by varying the concentration of **1**, the surface wettability of the same material could be tuned from hydrophilic to strongly hydrophobic owing to concentration-dependent changes in the morphology and thus the roughness of the surface (Figure 4a-c and 3f). To increase the

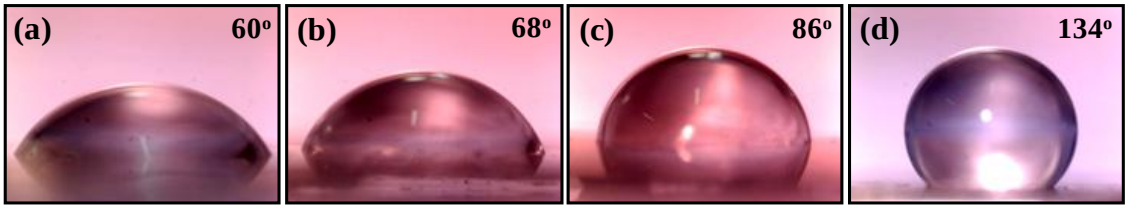


**Figure 11**. Optical images of the contact angle exhibited by a 4 µL water droplet on a microarray surface of **1** produced from (a) 1 µM dichloromethane solution, (b) 10 µM dichloromethane solution, (c) 100 µM dichloromethane solution and (d) 1 mM dichloromethane solution

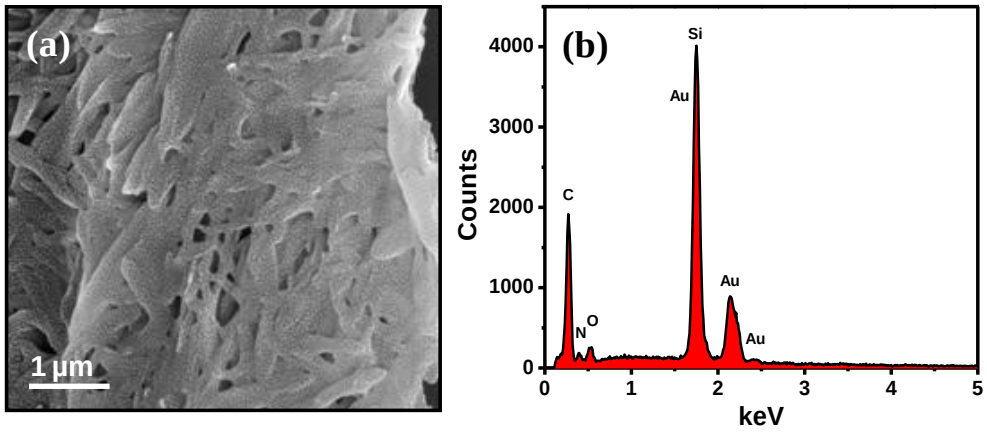


**Figure 12**. (a) FESEM micrograph of gold coated surface obtained from 1 mM dichloromethane solution of **1**. (b) The energy dispersive X-ray analysis (EDAX) spectra show the presence of gold.

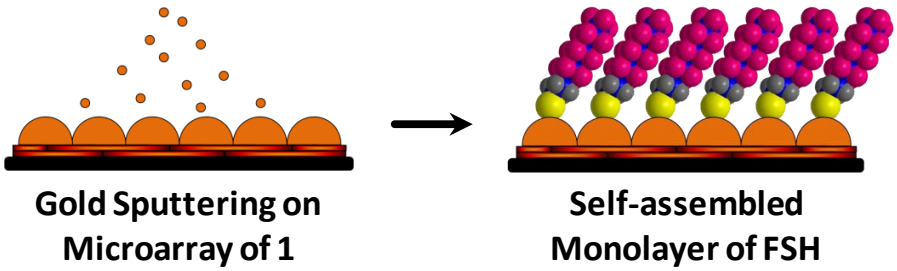


**Figure 13**. Gold sputtering and subsequent functionalization with self-assembled monolayer of FSH on BFT microarray of **1**.

hydrophobicity even further, a low-surface-energy coating of the microarray was produced by sputtering gold onto the surface. The sputtered gold was about 100 nm thick with circa 100 nm sized particulates (Figure 12). The nanostructured gold coating not only serves as a stable inert coating on the self-assembled microarray surface but also allows for further chemical modifications of the microarrays using self-assembled monolayers of thiols (SAMs; Figure 13).[46] These can be simply obtained by immersing the gold covered surface in 5 mM ethanol solution of different thiols for a duration of 24 h (Figure 14a,b).[47,48]

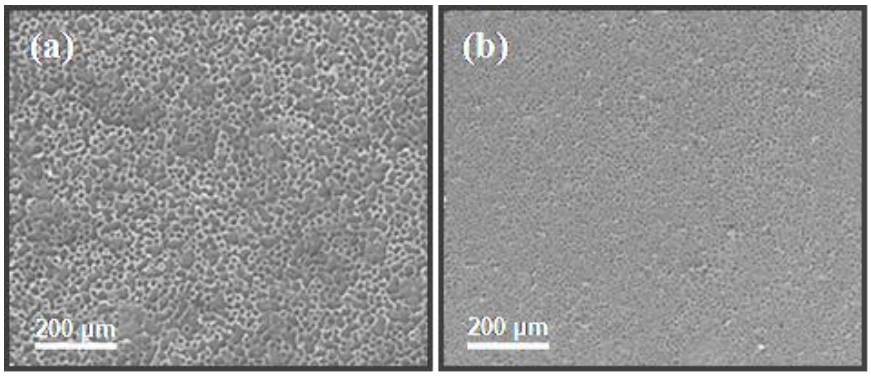


**Figure 14**. FESEM micrographs of honeycomb-like microarrays produced at relative humidity of (a) 65% and (b) 95%, which are then coated with gold by sputtering, followed by a self-assembled monolayer of FSH.

We have used three different thiols in our experiments, namely 11-mercaptoundecanoic acid (MSH), 1*H*, 1*H*, 2*H*, 2*H*-perfluorodecanethiol (FSH), and 1-dodecanethiol (DSH) to provide SAMs with different chemical functionalities (MSH: negatively charged, FSH: fluorinated, DSH: nonpolar), which affect the surface wettability differently. The gold coating on the surface of the microarray obtained from a 1 mM dichloromethane solution of **1** exhibits a contact angle of 125$^{o}$ (Figure 15a), which is similar to the non-covered surface (134$^{o}$). The MSH coating gave a decreased contact angle of 105$^{o}$ owing to the presence of the terminal polar COOH groups (Figure 15b). In contrast, the nonpolar DSH coating resulted in a superhydrophobic surface with an increased contact angle of 150$^{o}$ (Figure 15c). The fluorinated FSH coating pushed the contact angle of the superhydrophobic surface even further to 156$^{o}$ (Figure 15d). Artificial superhydrophobic surfaces are often not self-cleaning surfaces even though they have a large contact angle, because they suffer from a high tilt angle and high contact angle hysteresis. In contrast, the FSH coating on the microarray of **1** exhibit a tilt angle of only 3$^{o}$ and a very low contact angle hysteresis of only 1$^{o}$ (Figure 15e).

Accordingly, black carbon dust placed on the surface could be self-cleaned by water without any trace of remaining carbon dust or water stains (Figure 15f–h).

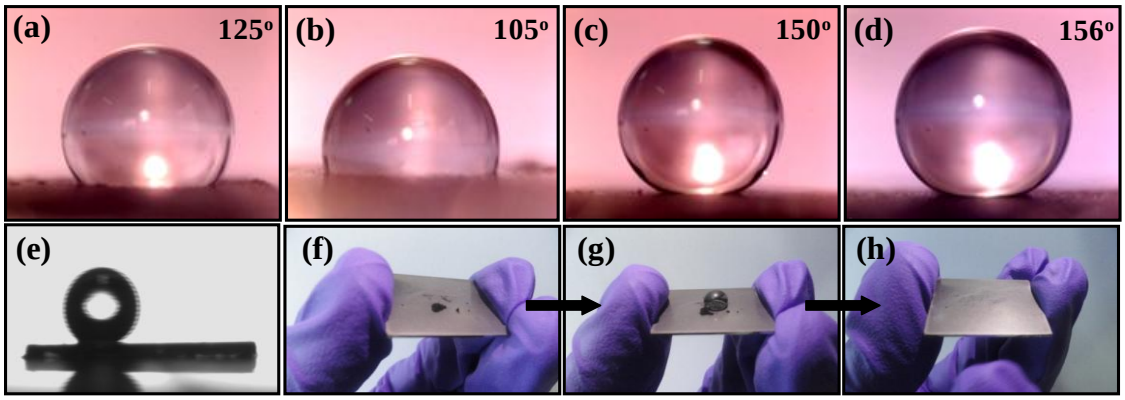


**Figure 15**. Optical images showing the contact angle exhibited by a 4 µL water droplet on a microarray surface produced from: (a) 1 mM dichloromethane solution followed by gold coating; (b) 1 mM dichloromethane solution followed by gold coating and a SAM of 11-mercaptoundecanoic acid; (c) 1 mM dichloromethane solution followed by gold coating and a SAM of 1-dodecanethiol; (d) 1 mM dichloromethane solution followed by gold coating and a SAM of 1H,1H,2H,2H-perfluorodecanethiol. The values in (a) to (d) are the corresponding contact angles. (e) Optical image showing the rolling of a water droplet for a tilt angle of 3°. (f), (g), and (h) Images of a gold sputtered honeycomb-like microarray surface coated with 1H,1H,2H,2H-perfluorodecanethiol showing self-cleanability.

Furthermore, to provide this material with additional interesting optical properties, we incorporated fluorescent dyes into the hierarchical molecular self-assemblies of **1** (Figure 16a,b). Such dyes should be soluble in dichloromethane so that they can be mixed with **1** in specific proportions and still allow the formation of breath-figure arrays. As the self-assembled structure of **1** is partly based on π-π interactions, aromatic dyes seemed most attractive. As a first illustration, we thus incorporated rhodamine B (rhoB; 100 µM) in a dichloromethane solution of **1** (1 mM), which on drop-casting resulted again in a honeycomb-like microarray (Figure 16c). The presence of the rhoB dye did not interfere with structure formation but made the microarrays highly

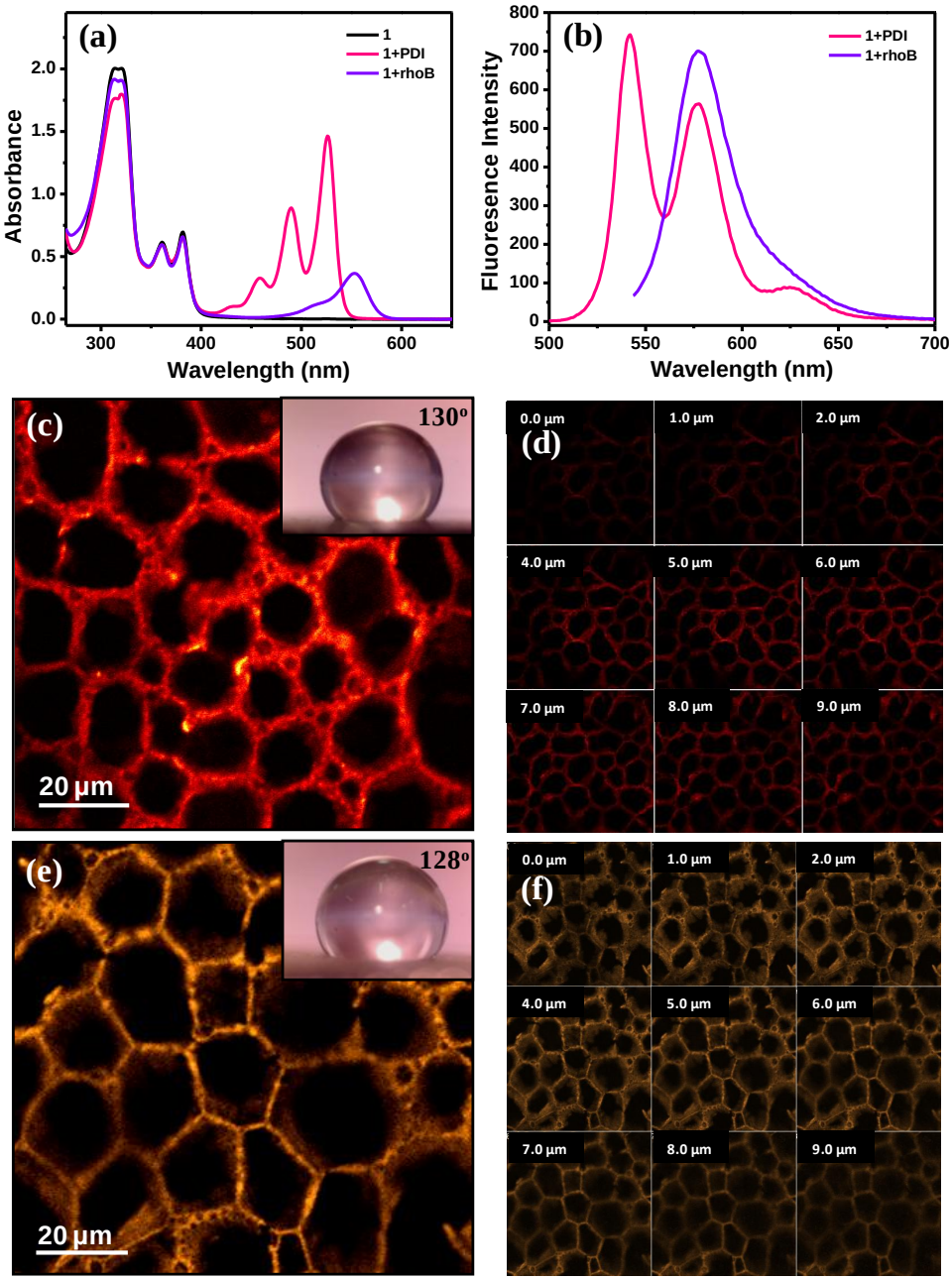


**Figure 16**. (a) Absorption and (b) fluorescence spectra of dichloromethane solutions of **1**, rhodamine B incorporated **1** (**1**+rhoB) and isoleucinemethylester appended perylenediimide incorporated **1** (**1**+PDI). Confocal micrographs obtained from a mixture containing 10:1 ratio (1 mM: 100 µM) of (c) **1**+rhoB and (e) **1**+PDI in dichloromethane. (d) and (f) Fluorescent confocal micrographs with a cross sectional analysis at different topographical heights of (c) and (e) respectively. The insets in (c) and (e) are the corresponding contact angles for a 4 µL water droplet.

fluorescent. A cross-sectional analysis of the microarray at different topographical heights using fluorescent confocal microscopy confirmed a homogeneous distribution of the dye throughout the microarray (Figure 16d). Therefore, the dye is not only present on the surface but an integral part of the self-assembled structure itself. The same finding was obtained with an isoleucine methyl ester appended PDI dye. The yellowish orange fluorescence of the PDI again appeared only along the walls of the microarray (Figure 16e,f). The contact angle for the microarrays with the incorporated rhoB and PDI were $130^{o}$ (inset, Figure 16c) and $128^{o}$ (inset, Figure 16e), respectively. These angles are more or less the same as of the non-functionalized microarrays ($134^{o}$; Figure 11d), confirming again that the dyes did not alter the self-assembly of **1** significantly. Furthermore, a blue fluorescent 7-amino-4-trifluoromethyl coumarin and a green fluorescent coumarin dye could also be incorporated into the microarrays similar to rhoB and the PDI. Unfortunately, fluorescent confocal micrographs for these coumarin dyes (absorption in the UV region) were hampered by reflections caused by the silicon substrate preventing a more detailed analysis of the distribution of the dyes within the microarrays.

### 4.1.6. Conclusions

In conclusion, the unexpected spontaneous hierarchical molecular assembly of a small low-molecular-weight NDI derivative **1** into microarrays was achieved by a simple solution-processing technique (breath-figure technique). These arrays could be employed to fabricate self-cleaning surfaces with very low slide angle ($3^{o}$) and contact angle hysteresis ($1^{o}$). This finding is rather surprising as it was commonly believed that BFT

cannot be used effectively for small non-polymeric molecules. The molecular design could influence the formation of honeycomb-like microarrays and thereby provide better insights for future endeavors. However, it is known that in case of polymers, the internal diameter of the microarray formed using BFT increases linearly with increasing RH.[15] In contrast to these polymers, our results on **1** show that the microwell size actually decreases with increasing RH. Nevertheless, our work demonstrates that advanced functional molecular materials can be obtained, even from small molecules based on a simple and easy-to-use solution process. Furthermore, the resulting microstructures are very robust and can be easily functionalized by simply adding additional molecules into the solution as demonstrated by the incorporation of different dyes into the arrays. Using this approach and the three primary colors red, green, and blue, white-light-emitting as well as other rainbow-colored hydrophobic decorative molecular materials, and in addition potential applications in electronics and miniaturized biochemical assays are envisioned.

## 4.1.7. Experimental section

### *4.1.7.1. Materials and methods*

1,4,5,8-naphthalenetetracarboxylic dianhydride, 1*H*,1*H*,2*H*,2*H*-perfluorodecanethiol, 11-mercaptoundecanoic acid, *N*,*N*-diisopropylethylamine and rhodamine B were obtained Sigma-Aldrich, 1-dodecanethiol from Alfa-Aesar, O-benzotriazole-*N*,*N*,*N*',*N*'-tetramethyl-uronium-hexafluoro phosphate from Chem-Impex International (IL, USA), 1-hydroxybenzotriazole, triisopropylsilane and di-tert-butyldicarbonate from

Spectrochem Pvt. Ltd. (Mumbai, India) and ethylenediamine from SD Fine-Chem Limited (Mumbai, India). All other reagents and solvents were of reagent grade and used without further purification.

*NMR Spectroscopy, Mass Spectrometry (MS), and Elemental Analysis*: $^{1}H$ and $^{13}C$ NMR were recorded on a Bruker AV-400 spectrometer with chemical shifts reported as ppm (in $CDCl_3$ with tetramethylsilane as internal standard). Mass spectra were obtained from Shimadzu 2020 LC-MS. Elemental analysis was carried out on ThermoScientific FLASH 2000 Organic Element Analyzer.

*Absorption Spectroscopy*: UV–vis spectra were recorded on a Perkin Elmer Model Lambda 900 spectrophotometer. Dichloromethane solutions of the samples were analyzed in quartz cuvette of 1 mm path length.

*Fluorescence Spectroscopy*: Fluorescence spectra were recorded on a Perkin Elmer Model LS 55 spectrophotometer. Dichloromethane solutions of the samples were analyzed in a quartz cuvette of 1 mm path length with an excitation at 490 nm for perylenediimide and 535 nm for rhodamine B.

*Infrared (IR) Spectroscopy*: IR spectra were recorded on a Bruker IFS 66/V spectrometer on a sodium chloride crystal. The solution of **1** was drop-casted and was allowed to dry naturally on the sodium chloride crystal.

*Fluorescence Confocal Microscopy*: Fluorescence confocal microscopy images were obtained from LSM 510 META-Carl Zeiss. Excitation wavelengths of 543 nm and 490 nm were used to excite the rhodamine B and isoleucine methylester appended perylenediimide respectively. A two-photon laser was employed to excite the blue

fluorescent 7-amino,4-trifluoromethylcoumarin and green fluorescent coumarin dyes. The LSM image examiner was utilized for processing the images.

*Field Emission Scanning Electron Microscopy*: FESEM images were acquired with a FEI Nova nanoSEM-600 equipped with a field-emission gun operating at 15 kV. Energy dispersive spectroscopy (EDS) analysis was performed with an EDAX genesis instrument attached to the SEM column. The sample was prepared by drop-casting either onto a Si (111) or freshly cleaved mica or glass substrate.

*Optical Profiler*: Height profiles of the microarrays were acquired with a Wyko NT9100 Optical Profiler (Veeco, USA) in Vertical Scanning Interferometry (VSI) mode.

*Gold Sputtering*: Gold was sputtered with a Polaron SC502 Sputter Coater (FISONS Instruments) in argon atmosphere. Sputtering for 1 min could render a thickness of ~100 nm of gold.

*Relative humidity*: The weather at Bangalore, India could furnish a relative humidity from 30-75% for our experiments. Moreover, an artificial set up comprising a 12 $m^3$ closed room furnished with cold or hot water sprinkler and an outlet door was utilized for producing and maintaining the relative humidity in the range of 35-95%. A dedicated humidity meter, testo 410-2 (Germany) with an accuracy of ±2.5 % RH was employed in our experiments.

*Contact angle*: Contact angles were measured mostly using an indigenous set up coupled with a Logitech camera for capturing the images. Contact angles were also measured using dedicated contact angle analyzer, OCA30 from Data Physics instrument (GmbH, Germany). 4 µL of the sessile water droplets were employed for measuring the static contact angles. A minimum of ten measurements were made for each surface.

*Preparation of microarrays*: Drop casting a dichloromethane solution of **1** (e.g. 1 mM) on a Si (111) substrate results in honeycomb-like microarrays within 5-10 min by breath figure technique.

*Preparation of SAM*: The Si (111) substrate containing the gold sputtered microarray was completely immersed in 5 mM ethanol solutions of 11-mercaptoundecanoic acid or 1*H*, 1*H*, 2*H*, 2*H*-perfluorodecanethiol or 1-dodecanethiol for duration of 24 h.

*Dynamic Light Scattering (DLS)*: The hydrodynamic diameter measurements were carried out using Zetasizer Nano ZS (Malvern Instruments) by employing 1/5 mM DCM solutions of **1** at 20$^{o}$C.

### *4.1.7.2. Synthesis of* 2

*Mono tBoc protection of ethylenediamine*: To a solution of ethylenediamine (3.06 mL, 45.8 mmol) in chloroform (300 mL), di-tert-butyldicarbonate (1 g, 4.58 mmol) in

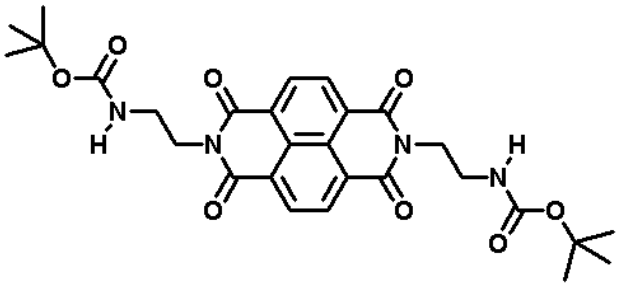

chloroform (250 mL) was added drop-wise using pressure equalizer under vigorous stirring at 0 °C. The reaction was monitored by using TLC (thin layer chromatography). After completion of the reaction, the reaction mixture was filtered and concentrated under vacuo. The compound was extracted to organic layer and the unreacted ethylenediamine lies in water layer. Organic layer was dried over anhydrous sodium sulfate and concentrated under vacuo. The obtained product was used for further reaction without any additional purification.

The above mono *t*Boc protected ethylenediamine (238.7 mg, 1.49 mmol) was added to 1,4,5,8-naphthalenetetracarboxylicdianhydride (200 mg, 0.74 mmol) in 15 ml of dry DMF (*N*,*N*-dimethylformamide). The contents were stirred for 15 h at 75 $^{o}$C. The crude product was extracted to organic (chloroform) layer and concentrated under vacuo. The crude product was further purified by column chromatography (1 % methanol in chloroform). Yield 80%. $^{1}$H NMR (400 MHz, $CDCl_3$): δ 8.76 (s, 4H), 4.85 (s, 2H), 4.38 (t, 2H), 3.56 (q, 2H), 1.22 (s, 18H); $^{13}$C NMR (100 MHz, $CDCl_3$): δ 163.2, 131.0, 126.7, 126.6, 79.3, 40.7, 39.2, 28.1; MS (EI): m/z = 552.22 $[M]^+$ for $C_{28}H_{32}N_4O_8$ (calc. 552.57).

### *4.1.7.3: Synthesis of* **3**

Compound **3** was obtained following the previous report.[49]

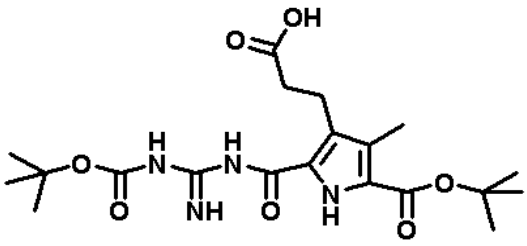


### *4.1.7.4. Synthesis of* **1**

*tBoc deprotection of 2*: To a solution of **2** (100 mg) in dichloromethane maintained at 0 $^{o}$C, TFA (trifluoroacetic acid; 3 ml) and TIPS (triisopropylsilane; 50 µL) were added and the contents were stirred at room temperature for 1 h. The solvent was removed under reduced pressure. The resulting brownish yellow solid was washed with toluene, chloroform and methanol and dried under vacuo.

To a 5 ml DMF solution of **3** (80 mg, 0.18 mmol) HOBT (1-hydroxybenzotriazole; 27.2 mg, 0.2 mmol), HBTU (O-benzotriazole-*N*,*N*,*N*',*N*'-tetramethyl-uronium-hexafluoro phosphate; 76.12 mg, 0.2 mmol), and DIPEA (N,N-diisopropylethylamine; 80 µl, 0.45 mmol) were added, maintained in an inert atmosphere. The reaction contents were stirred for 30 min. To this *t*Boc deprotected **2**

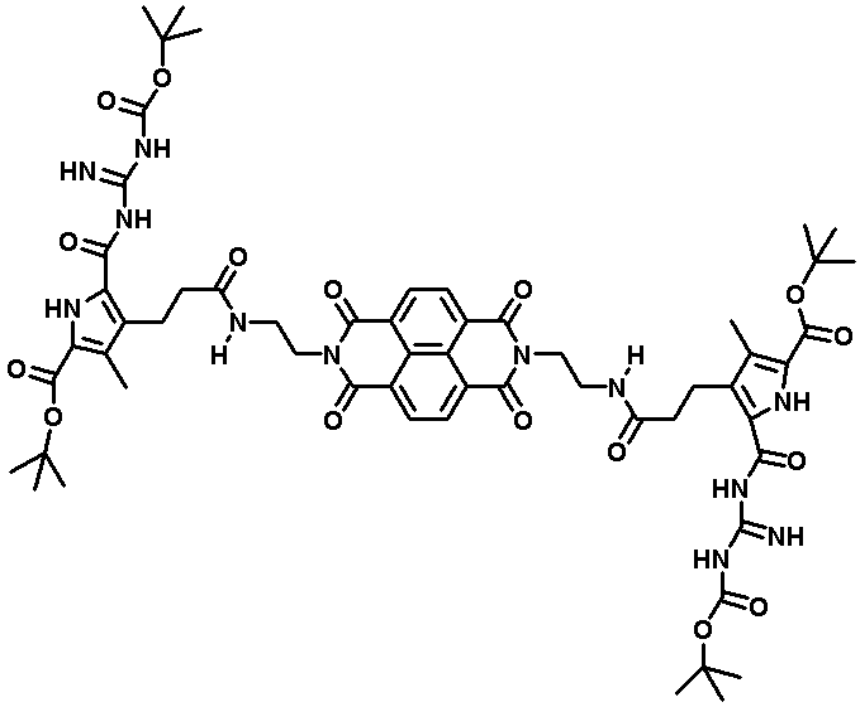

(32.17 mg, 0.09 mmol) was added and the contents were stirred for 48 h. The reaction mixture was concentrated under vacuo. The crude product (**1**) was purified by column chromatography (1% methanol in chloroform). Yield 58 %. $^{1}$H NMR (400 MHz, $CDCl_3$): δ 9.91 (b, 1H), 9.54 (b, 1H), 8.95 (b, 4H), 8.58 (s, 4H), 8.38 (b, 2H), 7.77 (b, 2H), 4.39 (t, 4H), 3.66 (q, 4H), 2.98 (t, 4H), 2.45 (t, 4H), 2.14 (s, 6H), 1.58 (s, 18H), 1.57 (s, 18H); $^{13}$C NMR (100 MHz, $CDCl_3$): δ 174.1, 171.8, 163.4, 160.8, 158.6, 153.5, 130.9, 128.2, 128.1, 127.0, 126.4, 122.1, 83.6, 81.5, 40.3, 38.1, 37.0, 28.6, 28.2; MS (EI): m/z = 1193.519 $[M]^+$ for $C_{58}H_{72}N_{12}O_{16}$ (calc. 1193.26); Elemental analysis: Calcd. for $C_{58}H_{72}N_{12}O_{16}$: C, 58.38; H, 6.08; N, 14.09. Found: C, 58.35; H, 6.12; N, 14.12.

## 4.2. A Bioinspired Reductionistic Modular Approach for Stiffest Organic Materials

The inspiration to this work is drawn from the strongest and stiffest known protein material *viz.* spider silk (Figure 17a).[50] An orb-weaving spider produces three main types of silks namely the catching spiral, webframe and dragline silk (Figure 17b).[51] Dragline silk is the toughest material and it is five times stronger by weight than steel. Dragline silk possesses a toughness of 160 MJ $m^{-3}$, stiffness of 10 GPa, strength of 1.1 GPa and a hysteresis of 65%.[52] This unusual combination of toughness and strength of spider silk has been one of the hallmarks of Nature's superior engineering skills. They find numerous applications as biological implants, sutures, drug-delivery systems, bullet-proof vests and light weight automotives amongst others.[52] In order to cater such

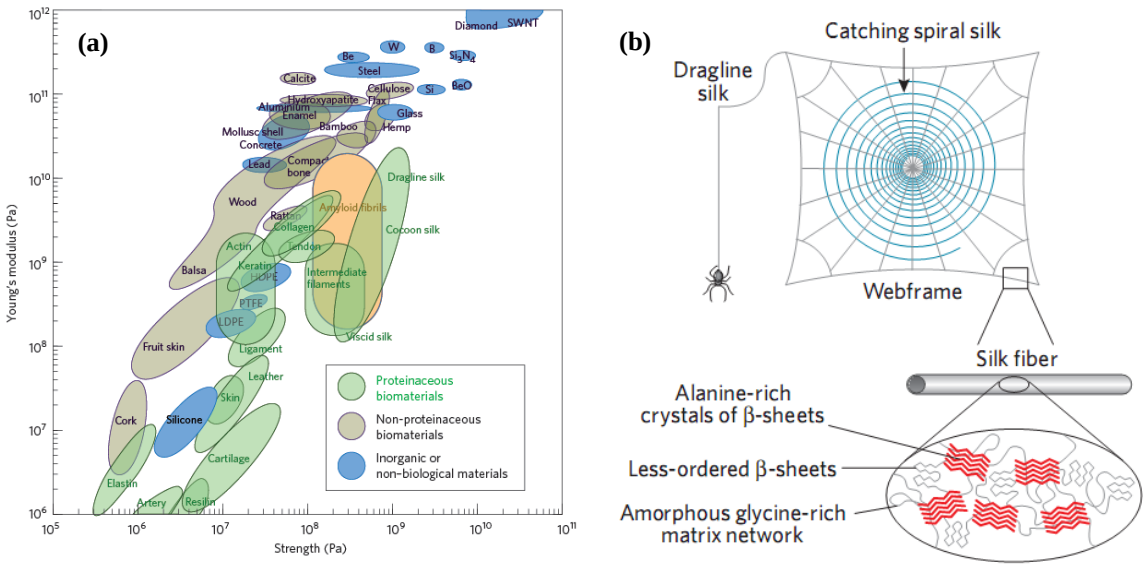


**Figure 17**. (a) Plot of Young's modulus *vs.* strength of various biological and non-biological materials. (b) Schematic of the orb web of a spider and the ordering of silk proteins within the fiber. (a) and (b) Reproduced with permission of NPG from references 50 and 51 respectively.

commercial prospects, large scale production becomes inevitable. However, the domesticated production of spider silk is difficult due to their cannibalic nature and also for the more complex and smaller quantities of silk mixtures generated in orb webs. On the other hand, production approaches by genetic engineering, abiotic synthesis as well as from synthetic molecules are all marred with inferior mechanical properties, besides issues relating to scalability and cost effectiveness.[53-63] Therefore, there is an inherent need for alternative and novel approaches to develop new materials with spider silk-like mechanical properties.

Typically spider silks are made up of proteins with >3000 amino acids contributing to very high molecular weights of about 200-350 kDa.[52] Spider silk proteins consists of unique amino acid sequences, which are primarily rich in glycine and alanine residues, giving rise to crystalline β-sheets in conjunction with less-ordered and amorphous domains.[51] The crystalline and amorphous domains of silk impart rigidity and extensibility, respectively. The extraordinary strength of spider silk is thus an outcome of ingeniously engineered hydrogen bonding. Theoretical predictions also estimate the Young's modulus of about 10 GPa for hydrogen bonding, which are effectively achieved in spider silks.[50] Moreover, it has been proposed that additional non-covalent interactions can further enhance the mechanical properties by synergic effect.[50] Therefore, essentially the research problem at hand boils down to engineering the hydrogen bonded molecular assemblies to emulate the mechanical properties of silk.

### 4.2.1. Design strategy

We envisioned that CDPs, which are the simplest forms of peptides could be instrumental in extracting hydrogen bonding to obtain favorable mechanical properties.[64-69] Depending on the nature of the side chains, the CDPs could in principle be tailored into hydrogen bonded 1D molecular chains and 2D molecular layers (Figure 18). In an effort to extract optimum hydrogen bonding interactions, CDPs of alanine (**CDP-Ala**) was employed, whereas CDPs of phenylalanine (**CDP-Phe**) and that of an unnatural amino acid phenylglycine (**CDP-Phg**) were thought to render additional aromatic interactions, preferably by a synergic effect for better mechanical properties. Notably, our CDPs have

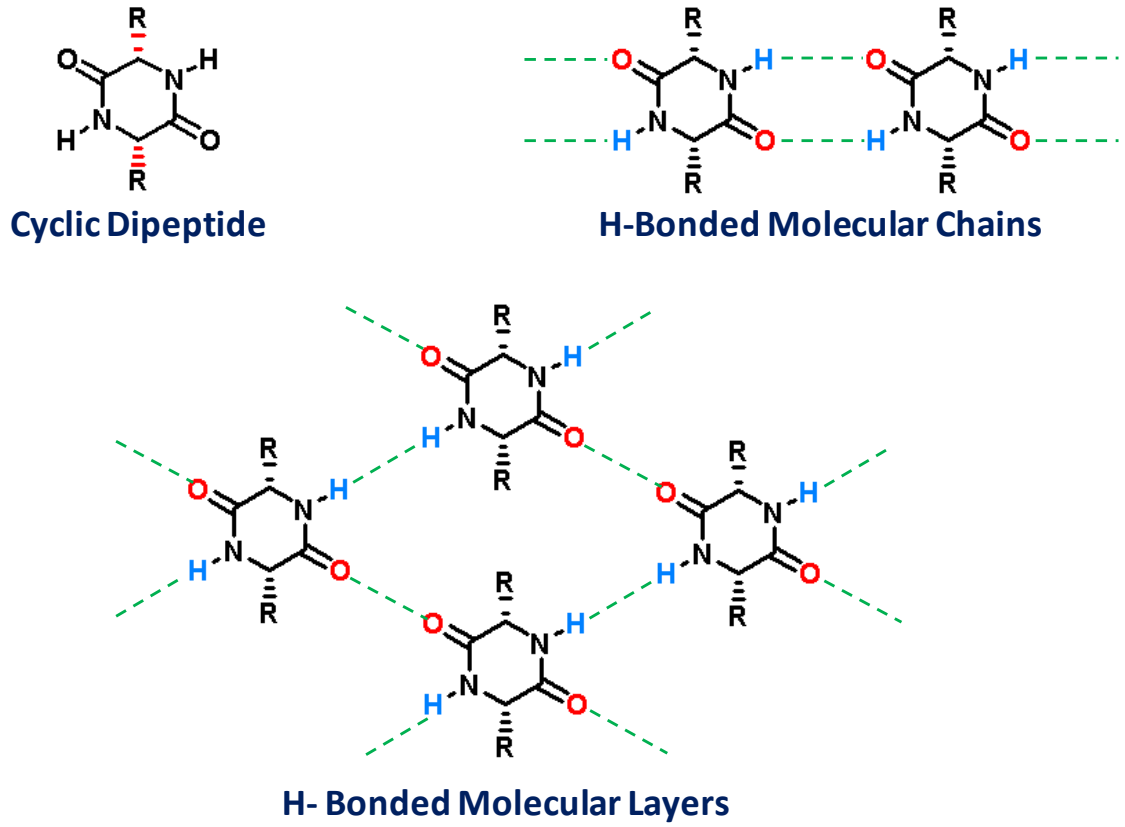


**Figure 18**. Schematic representation of ordering of cyclic dipeptides into hydrogen bonded 1D molecular chains and 2D molecular layers.

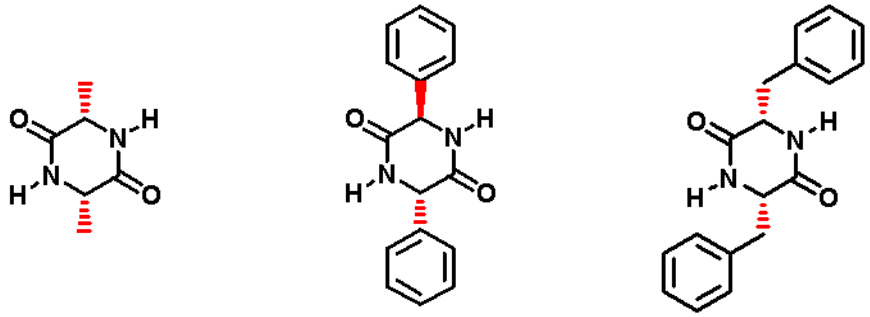

CDP-Ala CDP-Phg CDP-Phe

nearly three orders of magnitude smaller molecular weights (0.15-0.3 kDa) compared to that of spider silks. In addition, the following salient features are thought to provide greater advantages;

- ✓ Rigid structural motifs
- ✓ Self-complementary motifs
- ✓ Biocompatibility
- ✓ Solution processability
- ✓ Ease of synthesis
- ✓ Large scale production

### 4.2.2. Molecular self-assembly

**CDP-Ala** formed 2D sheets in a non-polar solvent like chloroform (Figure 19a). These sheets possess widths of 1-3 µm, lengths of 5-20 µm and thickness of 100-500 nm. Interestingly, even when the methyl groups of **CDP-Ala** are replaced with phenyl groups (as in **CDP-Phg**) also facilitates the formation of 2D sheets of several microns (Figure 19b).[64] On the other hand, **CDP-Phe** formed micron-sized rods with diameters of few

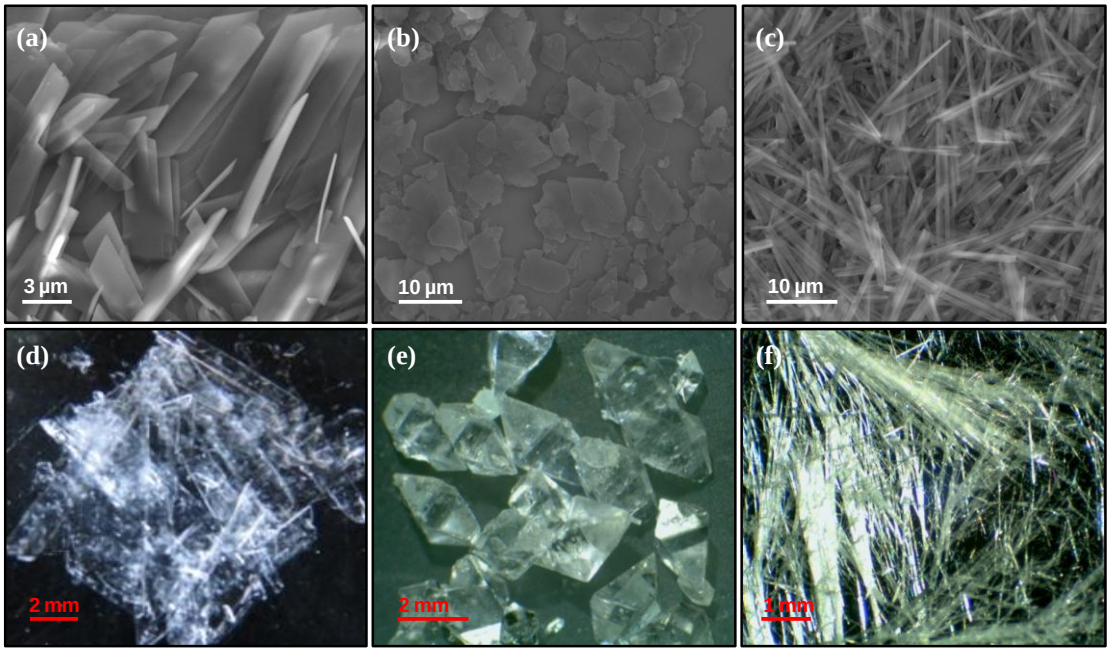


**Figure 19**. FESEM micrograph of (a) **CDP-Ala**, (b) **CDP-Phg** and (c) **CDP-Phe** obtained from chloroform solution. Optical micrographs of (d) **CDP-Ala**, (e) **CDP-Phg** and (f) **CDP-Phe** obtained from 50/50 (v/v) methanol/dichloromethane solution.

hundred nanometers (Figure 19c).[65] In order to have bigger self-assembled structures beyond micrometer dimensions, all three CDPs *viz*. **CDP-Ala**, **CDP-Phe** and **CDP-Phg** were subjected to assembly in 50/50 (v/v) dichloromethane/methanol solvent system. Here as well, **CDP-Ala** formed sheets but were of macroscopic in nature (Figure 19d). These transparent sheets were of 0.5 to 3 mm width and 0.1 to 1 cm length. **CDP-Phg** formed glittering rhombohedral structures of few millimeter dimensions, while **CDP-Phe** formed fibers of over 0.5 cm lengths (Figure 19e,f).

### 4.2.3. X-ray diffraction studies

The rhombohedral self-assembled structure of **CDP-Phg** obtained from 50/50 (v/v) methanol/dichloromethane was found to be single-crystalline in nature and hence was

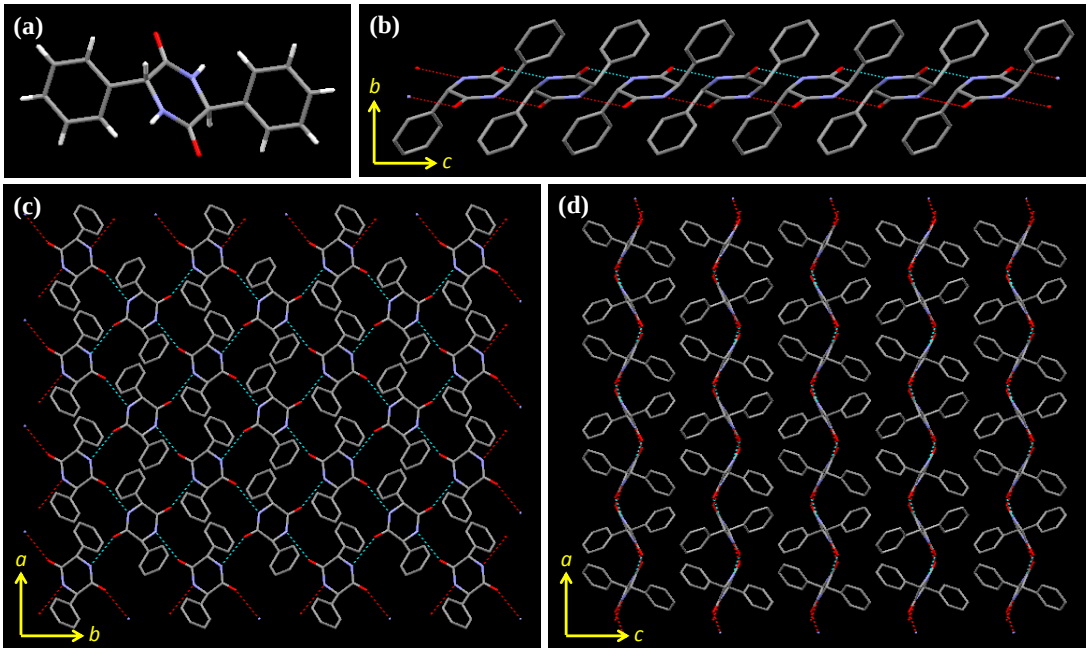


**Figure 20**. (a) Molecular model of **CDP-Phg**. Molecular interactions induced ordering of **CDP-Phg** along the crystallographic (b) *bc* plane, (c) *ab* plane and (d) *ac* plane.

subjected to single-crystal X-ray diffraction studies to understand their molecular interactions. **CDP-Phg** was found to crystallize in orthorhombic *P*bca space group and the phenyl rings are orthogonally placed on either sides of the diketopiperazine ring (Figure 20a,b). As each **CDP-Phg** consists of two sets of N-H (donor) and C=O (acceptor) functionalities, they facilitate self-complementary intermolecular hydrogen bonding interactions. All in all, each **CDP-Phg** unit forms hydrogen bonding with four different **CDP-Phg** neighbors, resulting in corrugated molecular layers spanning across the crystallographic *ab* plane (Figure 20c). Notably, a bond distance of 2.093 Å was found for all these four hydrogen bonds indicating their strong interactions (dotted line; Figure 20c). Further, these corrugated molecular layers stack on top of each other along the crystallographic *c* direction to form the 3D rhombohedral single crystals (Figure 20d).

Later, the self-assembled macroscopic structures of **CDP-Ala** and **CDP-Phe** were subjected to PXRD studies. The macroscopic sheets of **CDP-Ala** exhibited highly crystalline ordering with diffraction intensity counts of over $8*10^5$ (Figure 21a). The lower angle peak ($2\theta = 11.52^o$) corresponding to a *d*-spacing of 7.67 Å could be ascribed to the intermolecular distances of **CDP-Ala**. Further the higher angle peaks with *d*-spacing of 3.84 Å, 2.56 Å and 1.92 Å indicate lamellar-type ordering of **CDP-Ala** motifs in the macroscopic sheets. On the other hand, the **CDP-Phe** fibers were relatively less crystalline and the *d*-spacing of 12.24 Å could be attributed to the molecular length of **CDP-Phe** (Figure 21b). The *d*-spacing values 2-3 Å and ~4 Å could be assigned to probable hydrogen bonding and aromatic interactions respectively.

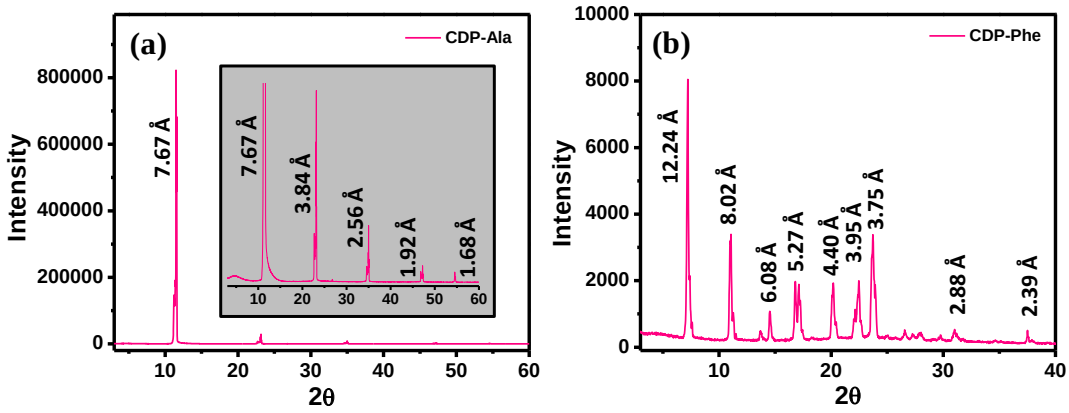


**Figure 21**. X-ray diffraction profile of (a) **CDP-Ala** sheets and (b) **CDP-Phe** fibers obtained from 50/50 (v/v) methanol/dichloromethane solution.

### 4.2.4. Nanoindentation studies

Nanoindentation is an effective technique employed to determine the mechanical properties of a material.[70,71] In a typical experiment, a hard tip of known mechanical properties is pressed into the test sample. During the course of this indentation, a record

of applied load, penetration depth, area of the indent and other parameters can be determined to obtain a plot known as load-displacement curve. These curves can be further utilized to extract various mechanical properties like Young's modulus, hardness and stiffness. Young's modulus is a measure of the stiffness of the material and is defined as the ratio of stress to strain for which Hooke's law holds good. Hardness represents the resistance of a material to various types of permanent shape variation, when subjected to an external force. Stiffness is defined as the resistance exerted by a material to deformation.

Nanoindentation studies performed on the macroscopic fibers of **CDP-Phe** revealed that they have Young's modulus, hardness and stiffness values of 0.32 GPa, 0.04 GPa and 375 $Nm^{-1}$, respectively (Table 1, Figure 22a). On the other hand, **CDP-Ala** showed remarkable optimization in the mechanical properties by nearly an order of magnitude (Figure 22b). A Young's modulus of 7.12 GPa, hardness of 0.64 GPa and a stiffness of 3216 $Nm^{-1}$ was obtained for **CDP-Ala** sheets. The rhombohedral crystals of **CDP-Phg** showed further improvements as can be noted by their Young's modulus of 10.86 GPa, hardness of 1.17 GPa and stiffness of 7989 $Nm^{-1}$ (Figure 22c). The Young's modulus of 0.32 GPa, 7.12 GPa and 10.86 GPa of our CDPs are comparable to that of different varieties of spider silk (0.1-10 GPa). The extraordinary stiffness values of 3216 $Nm^{-1}$ and 7989 $Nm^{-1}$ of our **CDP-Ala** and **CDP-Phg** respectively makes them the stiffest known organic materials. The immediate best stiffness value known to the best of our knowledge is 885 $Nm^{-1}$.[72] Thus, by effectively exploiting hydrogen bonding interactions alone Young's modulus of 7.12 GPa and a stiffness of 3216 $Nm^{-1}$ was achieved by our modular **CDP-Ala** motifs. The relatively low values obtained for **CDP-Phe** can be

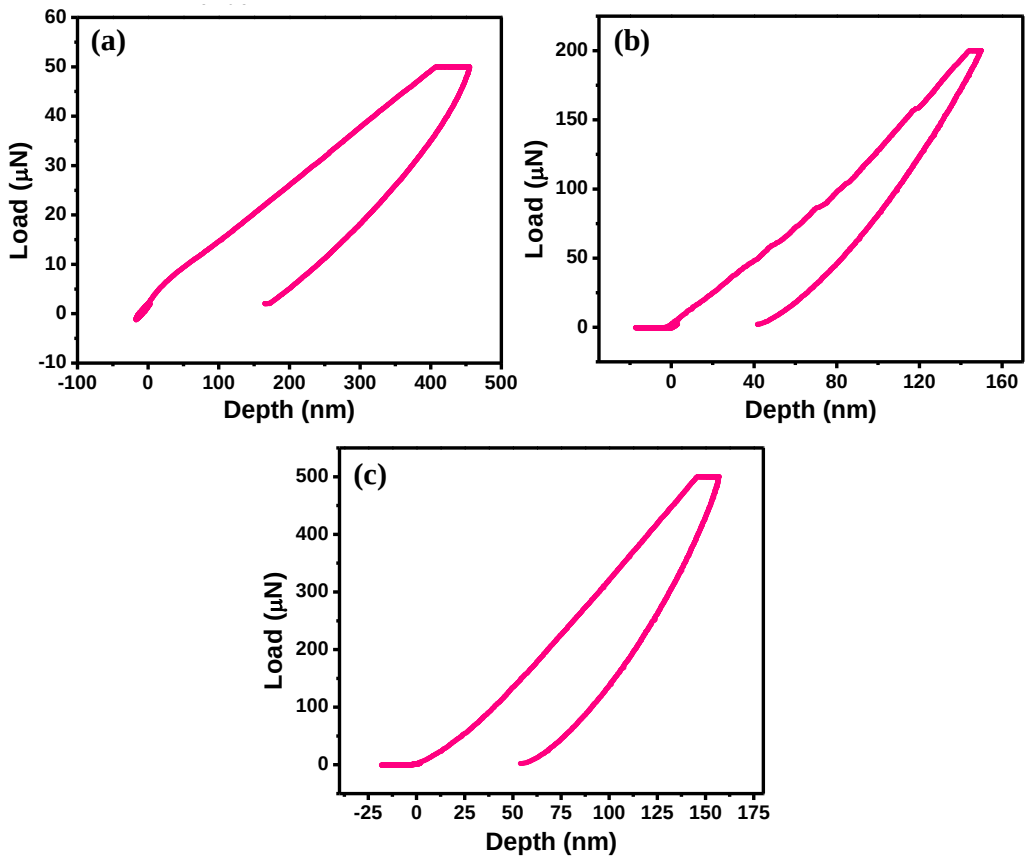


**Figure 22**. Load-displacement curves of (a) **CDP-Phe** fibers, (b) **CDP-Ala** sheets and (c) **CDP-Phg** rhombohedral crystals obtained from 50/50 (v/v) methanol/dichloromethane solution.

attributed to their reduced crystallinity (Figure 21b) and the nature of hydrogen bonding interactions. As evident from the crystal structure, **CDP-Phg** forms hydrogen-bonded 2D molecular layers whereas the **CDP-Phe** fibers are known to form 1D molecular chains with a weaker van der Waals interactions between the adjacent chains.[65,66] The best mechanical properties obtained for **CDP-Phg** can be attributed to the synergic contributions of aromatic interactions alongside 2D hydrogen bonding interactions. Additional efforts are under way in order to determine the effect of stereochemical information of CDPs in modulating the non-covalent interactions.

**Table 1**. Mechanical properties of cyclic dipeptides (CDPs).

| Molecule | Young's Modulus, *E* [GPa] | Hardness, *H* [GPa] | Stiffness, *S* [$Nm^{-1}$] |
|---|---|---|---|
| CDP-Phe | 0.32 | 0.04 | 375 |
| CDP-Ala | 7.12 | 0.64 | 3216 |
| CDP-Phg | 10.86 | 1.17 | 7989 |

### 4.2.5. Conclusions

In conclusion, a bioinspired design strategy was undertaken to emulate the mechanical properties of spider silk. By employing a simple rigid motif like CDP, we were successful in achieving mechanical properties spanning nearly two orders of magnitude. Specifically, Young's modulus (10.86 GPa) of our **CDP-Phg** was as high as the best values reported for dragline silk (10 GPa). As of now, with values of 3216 $Nm^{-1}$ and 7989 $Nm^{-1}$, **CDP-Ala** and **CDP-Phg** are the stiffest known organic materials. Although, our designer CDPs were not intended to bestow toughness, we strongly believe that it can also be achieved by appropriate modular strategies. Nevertheless, with the availability of different macroscopic self-assembled structures as well as the mechanical properties, we foresee a wide variety of potential applications in both biological and non-biological systems.

## 4.2.6. Experimental section

### *4.2.6.1. Materials and methods*

All the solvents and reagents were obtained from Sigma-Aldrich and used as received unless otherwise mentioned.

*NMR Spectroscopy, Mass Spectrometry (MS), and Elemental Analysis*: $^{1}H$ and $^{13}C$ NMR were recorded on a Bruker AV-400 spectrometer with chemical shifts reported as ppm (in $CDCl_3$ with tetramethylsilane as internal standard). Mass spectra were obtained from Shimadzu 2020 LC-MS. Elemental analysis was carried out on ThermoScientific FLASH 2000 Organic Element Analyzer.

*Field Emission Scanning Electron Microscopy*: FESEM images were acquired with a FEI Nova nanoSEM-600 equipped with a field-emission gun operating at 15 kV. The sample was prepared by drop-casting onto a Si (111) substrate.

*Nanoindentation*: Nanoindentation studies were performed by utilizing a nanoindenter (Triboindenter of Hysitron, Minneapolis, USA) with an in-situ imaging capability.

*Powder X-ray diffraction (PXRD):* PXRD patterns were recorded with a Rigaku-99 (Miniflex) diffractometer using Cu Kα radiation (λ = 1.5406 Å). The self-assembled structures of CDPs were drop-casted on a glass slide.

### *4.2.6.2. Synthesis of CDP-Ala*

9-Fluorenylmethoxycarbonyl protected L-alanine (Fmoc-Ala-OH) and L-alanine methylester (H-Ala-OMe) were prepared by using standard protection protocols. Fmoc-

Ala-OH (2 g, 5.16 mmol) dissolved in dichloromethane was added with H-Ala-OMe

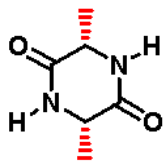

(1.23 g, 5.67 mmol), 1-ethyl-3-(3-dimethylaminopropyl)carbodiimide (EDC.HCl, 1.19 g, 6.19 mmol) and 1-hydroxybenzotriazole (HOBt, 1.2 g, 6.19 mmol). The solution was maintained at ice cold temperature. Diisopropylethylamine (DIPEA, 2.14 g, 16.51 mmol) was added and the reaction mixture was stirred at ice temperature for 1 h and then at room temperature for 5 h. The reaction progress was monitored by thin layer chromatography (TLC). Reaction mixture was evaporated to dryness and extracted from dichloromethane, washed with water, dried over anhydrous sodium sulfate. The solvent was evaporated to obtain Fmoc-Ala-Ala-OMe in quantitative yield. The dipeptide Fmoc-Ala-Ala-OMe (1 g, 1.82 moles) when subjected to Fmoc-deprotection in 15% piperidine/dichloromethane, the deprotected dipeptide undergo cyclization to give **CDP-Ala**, which was filtered, washed with dichloromethane, methanol and the white solid material was dried to obtain **CDP-Ala**. $^{1}$H NMR ($CDCl_3$-$CF_3COOH$, 400 MHz, δ) 8.29 (s, 2H), 4.26 (q, 2H), 1.60 (d, 6H); $^{13}$C NMR ($CDCl_3$-$CF_3COOH$, 100 MHz, δ) 171.6, 50.9, 19.7; MS (EI): $m/z$ = 142.15 $[M]^+$ for $C_6H_{10}N_2O_2$ (calc. 142.15); Elemental analysis: Calcd. for $C_6H_{10}N_2O_2$: C, 50.69; H, 7.09; N, 19.71. Found: C, 50.65; H, 7.14; N, 19.69.

### *4.2.6.3. Synthesis of CDP-Phg*

9-Fluorenylmethoxycarbonyl protected L-phenylglycine (Fmoc-Phg-OH) and D-phenylglycine methylester (H-Phg-OMe) were prepared by using standard protection protocols. Fmoc-Phg-OH (2 g, 5.16 mmol) dissolved in dichloromethane was added with

H-Phg-OMe (1.23 g, 5.67 mmol), 1-ethyl-3-(3-dimethylaminopropyl)carbodiimide

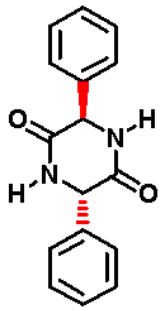

(EDC.HCl, 1.19 g, 6.19 mmol) and 1-hydroxybenzotriazole (HOBt, 1.2 g, 6.19 mmol). The solution was maintained at ice cold temperature. Diisopropylethylamine (DIPEA, 2.14 g, 16.51 mmol) was added and the reaction mixture was stirred at ice temperature for 1 h and then at room temperature for 5 h. The reaction progress was monitored by thin layer chromatography (TLC). Reaction mixture was evaporated to dryness and extracted from dichloromethane, washed with water, dried over anhydrous sodium sulfate. The solvent was evaporated to obtain Fmoc-Phg-Phg-OMe in quantitative yield. The dipeptide Fmoc-Phg-Phg-OMe (1 g, 1.82 moles) when subjected to Fmoc-deprotection in 15% piperidine/dichloromethane, the deprotected dipeptide undergo cyclization to give **CDP-Phg**. The cyclic dipeptide spontaneously self-assembled to form 2D sheets, which was filtered, washed with dichloromethane, methanol and the white solid material was dried to obtain **CDP-Phg**. $^{1}$H NMR ($CDCl_3$-$CF_3COOH$, 400 MHz, δ) 8.31 (s, 2H), 7.39 (m, 10H), 5.40 (s, 2H); $^{13}$C NMR ($CDCl_3$-$CF_3COOH$, 100 MHz, δ) 169.9, 134.1, 130.3, 129.8, 127.3, 59.4; MS (EI): *m/z* = 266.31 $[M]^+$ for $C_{16}H_{14}N_2O_2$ (calc. 266.29); Elemental analysis: Calcd. for $C_{16}H_{14}N_2O_2$: C, 72.16; H, 5.30; N, 10.52. Found: C, 72.11; H, 5.34; N, 10.55.

### *4.2.6.5. Synthesis of CDP-Phe*

9-Fluorenylmethoxycarbonyl protected L-phenylalanine (Fmoc-Phe-OH) and L-phenylalanine methylester (H-Phe-OMe) were prepared by using standard protection

protocols. Fmoc-Phe-OH (2.0 g, 5.16 mmol) dissolved in dichloromethane was added

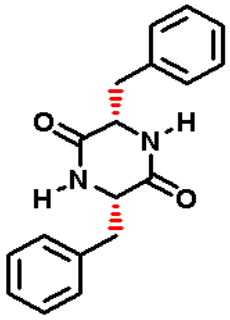

with H-Phe-OMe (1.23 g, 5.67 mmol), 1-ethyl-3-(3-dimethylaminopropyl)carbodiimide (EDC.HCl, 1.19 g, 6.19 mmol) and 1-hydroxybenzotriazole (HOBt, 1.2 g, 6.19). The solution was cooled to ice-cold temperature. Diisopropylethylamine (DIPEA, 2.14 g, 16.51mmol) was added and the reaction mixture was stirred on ice for 1 h and then at room temperature for 5 h. The reaction progress was monitored by thin layer chromatography. The reaction mixture was evaporated to dryness and extracted from dichloromethane, washed with water and dried over anhydrous sodium sulphate. The solvent was evaporated to obtain Fmoc-Phe-Phe-OMe in quantitative yield. Further, Fmoc-Phe-Phe-OMe (1.0 g, 1.82mol) was subjected to Fmoc-deprotection in 10% piperidine/dichloromethane for 2 h. The reaction mixture was evaporated to dryness and the residue was re-dissolved into dichloromethane. The **CDP-Phe** spontaneously forms insoluble fibres. The suspension was filtered, washed with dichloromethane and methanol, and dried to obtain **CDP-Phe**. $^{1}$H NMR ($CDCl_3$-$CF_3COOH$, 400 MHz, δ) 7.83 (s, 2H), 7.30 (m, 6H), 7.04 (m, 4H), 4.29 (t, 2H), 2.97 (dd, 2H), 2.19 (dd, 2H); $^{13}$C NMR ($CDCl_3$-$CF_3COOH$, 100 MHz, δ) 170.2, 133.7, 130.0, 129.6, 128.6, 56.5, 39.9; MS (EI): *m*/*z* = 294.42 $[M]^+$ for $C_{18}H_{18}N_2O_2$ (calc. 294.34); Elemental analysis: Calcd. for $C_{18}H_{18}N_2O_2$: C, 73.45; H, 6.16; N, 9.52. Found: C, 73.49; H, 6.21; N, 9.55.

## 4.3. Designer Auxiliaries to Engineer the Molecular Assembly and Bulk Charge Transport of Naphthalenediimides

In this sub-chapter we have extended our bioinspired design strategy to tailor the assembly of NDIs and in turn find structure-property correlations with their electronic properties. As emphasized earlier in Section 1.9, NDIs are among the most promising organic n-type semiconductors and the necessity to improve the performance of n-type semiconductors analogous to p-type counterparts has been one of the driving forces for active research in this field.[73-77] With such an objective in mind, we had demonstrated in Chapter 2 that the functionalization of amino acid derivatives with NDI is a versatile strategy to engineer their assemblies.[78] Specifically, we had shown that **L-NDI** self-assembles into 2D sheets. In addition, these sheets were found to exhibit remarkable conductivity of 1.6 $Scm^{-1}$, which is unusually high for a non doped semiconductor like NDI.[79] This value obtained from C-AFM studies motivated us for its further exploration towards charge transport properties. Besides **L-NDI**, four additional NDI derivatives were employed in this study in an effort to correlate molecular structure, assembly and charge transport properties. **NDI-PhgOMe**, **NDI-TyrOMe**, **NDI-TrpOMe** and **NDI-IleOMe** are the additional NDI derivatives functionalized with phenylglycine, tyrosine,

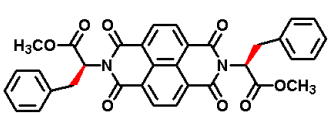


L-NDI

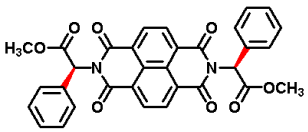


NDI-PhgOMe

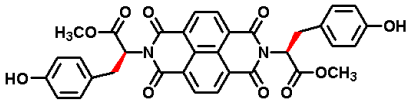


NDI-TyrOMe

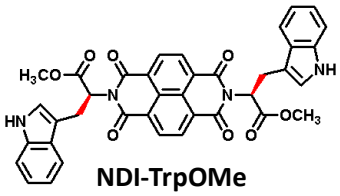


NDI-TrpOMe

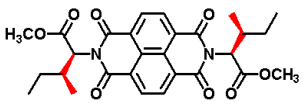


NDI-IleOMe

tryptophan and isoleucine methylesters respectively.

### 4.3.1. Photophysical studies

As the self-assembled sheets of **L-NDI** were obtained from acetonitrile-water solvent system (Section 2.2.1.2), the other NDI derivatives were also subjected to photophysical studies in the same solvent system in order to enforce identical solvophobic effect. A 100 µM solution of **NDI-PhgOMe** in acetonitrile showed the characteristic absorption spectra in the range of 200 - 400 nm corresponding to the π-π* transitions of NDI and phenyl

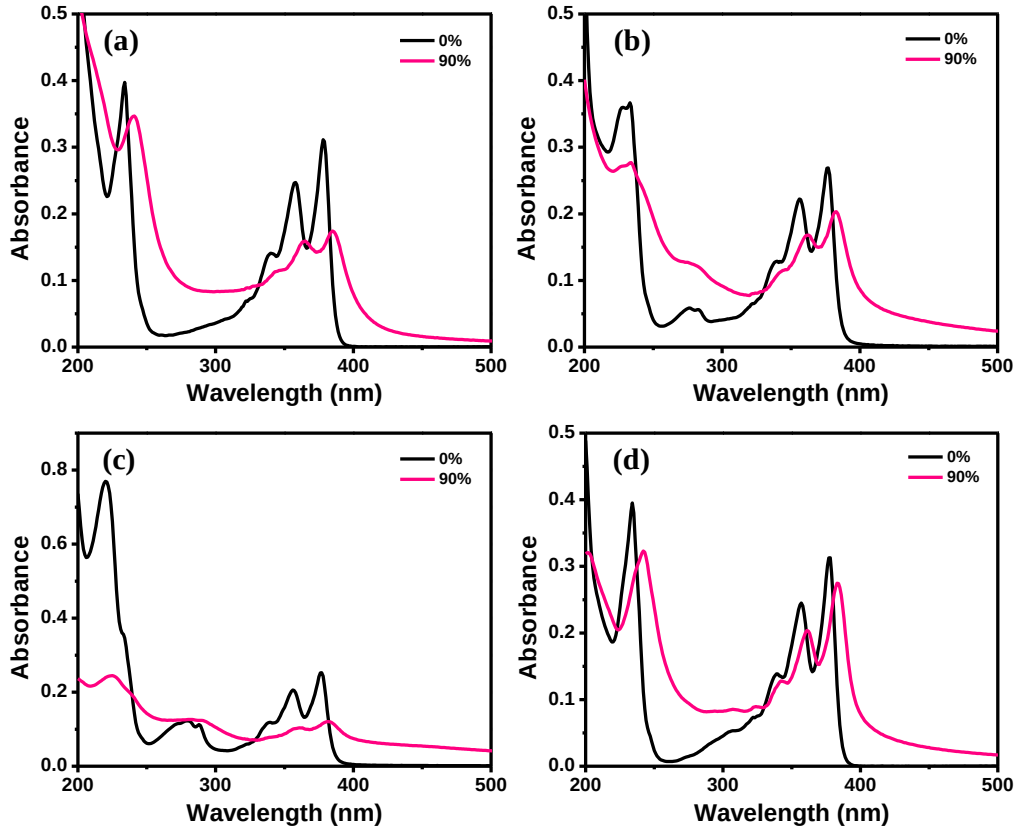


**Figure 23**. Absorption spectra of 100 µM solutions of (a) **NDI-PhgOMe**, (b) **NDI-TyrOMe**, (c) **NDI-TrpOMe** and (d) **NDI-IleOMe** in aqueous acetonitrile. The values represent the various percentages of water in acetonitrile.

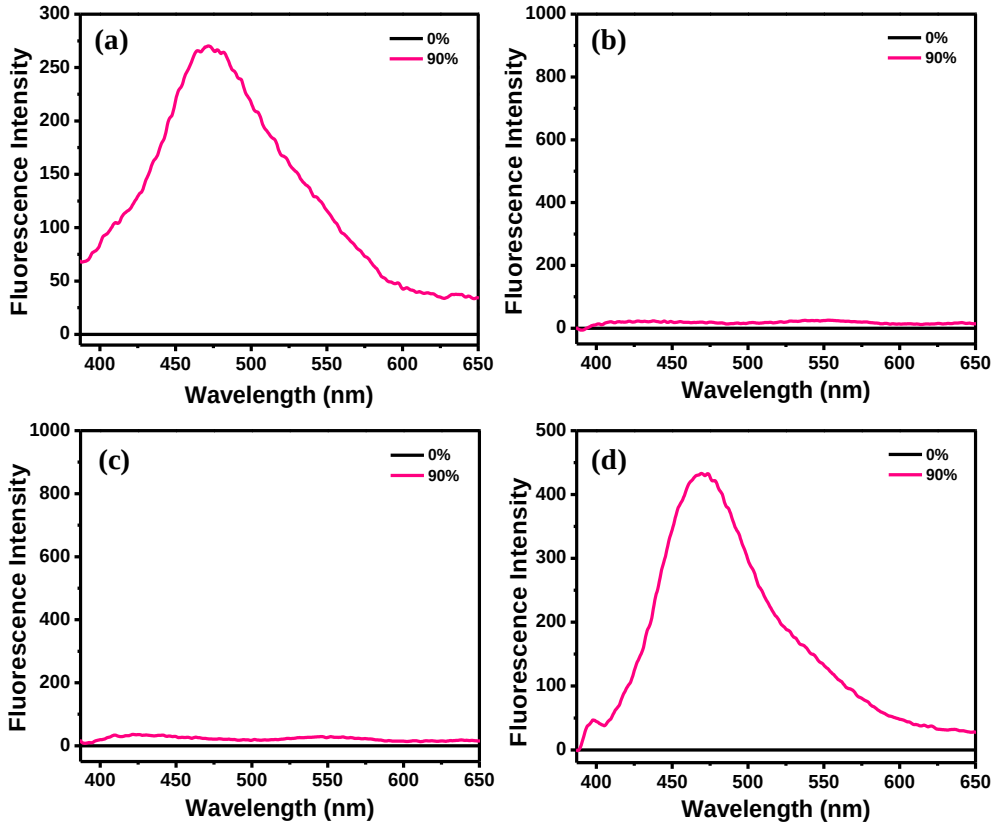


**Figure 24**. Fluorescence spectra of 100 µM solutions of (a) **NDI-PhgOMe**, (b) **NDI-TyrOMe**, (c) **NDI-TrpOMe** and (d) **NDI-IleOMe** in aqueous acetonitrile. The values represent the various percentages of water in acetonitrile.

functionalities (Figure 23a). Further, a bathochromic shift of 7 nm for the 378 nm band was observed in 90% aqueous acetonitrile. Similarly, bathochromic shifts of 6 nm, 5 nm and 6 nm was obtained for **NDI-TyrOMe**, **NDI-TrpOMe** and **NDI-IleOMe** respectively for 90% aqueous acetonitrile (Figure 23b-d). These absorption characteristics suggest J-type stacking of NDI chromophores under enhanced hydrophobic forces. In addition, all the four NDI derivatives *viz.* **NDI-PhgOMe**, **NDI-TyrOMe**, **NDI-TrpOMe** and **NDI-IleOMe** did not show any fluorescence in acetonitrile, similar to that of **L-NDI** (Figure 24a-d). Moreover, only **NDI-PhgOMe** and **NDI-IleOMe** showed excimer-like emission ($\lambda_{max}$ = 470 nm) in 90% aqueous acetonitile, whereas **NDI-TyrOMe** and **NDI-TrpOMe**

were non-fluorescent. This suggests that the non-polar functionalities like phenyl groups as in **L-NDI** and **NDI-PhgOMe** as well as the butyl groups of **NDI-IleOMe** favor excimer-like emission. The presence of polar functionalities like hydroxyl of **NDI-TyrOMe** and indole (N-containing heterocycle) of **NDI-TrpOMe** are believed to render additional dipole-dipole interactions with solvent water molecules and thereby prohibits excimer-like emission.

### 4.3.2. Morphological studies

As discussed in Section 2.2.1.2, **L-NDI** forms 2D sheets in 90% aqueous acetonitrile due to hydrophobic force induced assembly (Figure 25a). Typically, these free-floating aggregates are formed in an hour and would precipitate out within a day's time, when the solution is subjected for external constraints like manual mixing or sonication. In the absence of these external constraints, the assembly occurs slowly with the process extending to a week's time. The latter gives rise to larger aggregates of **L-NDI** having lateral dimensions of up to 200 μm (Figure 25b). As the phenyl functionalities of **NDI-PhgOMe** provide additional aromatic interactions orthogonally, they also facilitate 2D organization (Figure 25c). However, these 2D sheets were of 1-5 μm lateral dimensions with the topographical thickness of 100-500 nm. **NDI-TyrOMe** also formed 2D micron-sized flakes, which are further interconnected to form flower-like extended architectures (Figure 25d). These extended organizations could be ascribed to hydroxyl group induced additional dipole-dipole interactions. Although, these dipole-dipole interactions are possible in case of **NDI-TrpOMe**, the relatively larger indole group is thought to favor

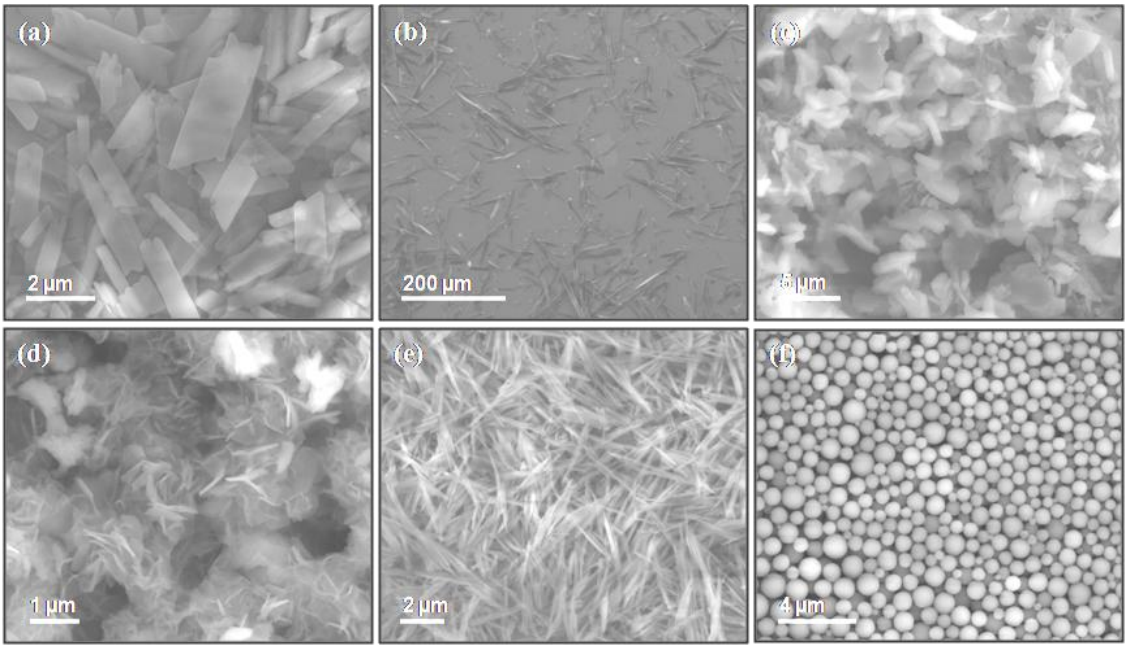


**Figure 25**. FESEM micrograph of (a,b) **L-NDI**, (c) **NDI-PhgOMe**, (d) **NDI-TyrOMe**, (e) **NDI-TrpOMe** and (f) **NDI-IleOMe** obtained from 90% aqueous acetonitrile. For (a) the aggregates were formed at a faster rate, while slow for that of (b).

1D organization (Figure 25e). It has to be noted that **NDI-Trp** (which lacks the methyl group) forms random particles and hence protection of carboxylic group with methyl moiety is also essential for **NDI-TrpOMe** to form 1D fiber. The absence of any aromatic functionalities and the presence of a relatively bulky butyl group in **NDI-IleOMe** could be hypothesized to result in 0D spheres of 0.2 – 2 µm diameter (Figure 25f).

### 4.3.3. X-ray diffraction studies

Later the NDI derivatives in their aggregated states were subjected to X-ray diffraction studies to get greater insights about the nature of molecular assembly. The slow rate of assembly of **L-NDI** engenders high crystalline ordering as can be inferred from their

intense diffraction peaks (Figure 26a). Although, the faster assembly process of **L-NDI** reduced the diffraction peak intensities, their organization is essentially into the same tetragonal crystal system as obtained by indexing in DICVOL program (Figure 26b). Interestingly, the 2D sheets of **NDI-PhgOMe** show reasonable crystallinity, whereas the 2D flower-like architectures of **NDI-TyrOMe** exhibit poor crystallinity (Figure 26c,d). On the other hand, 1D fibers of **NDI-TrpOMe** and 0D spheres of **NDI-IleOMe** reveal appreciable crystalline ordering (Figure 26e,f).

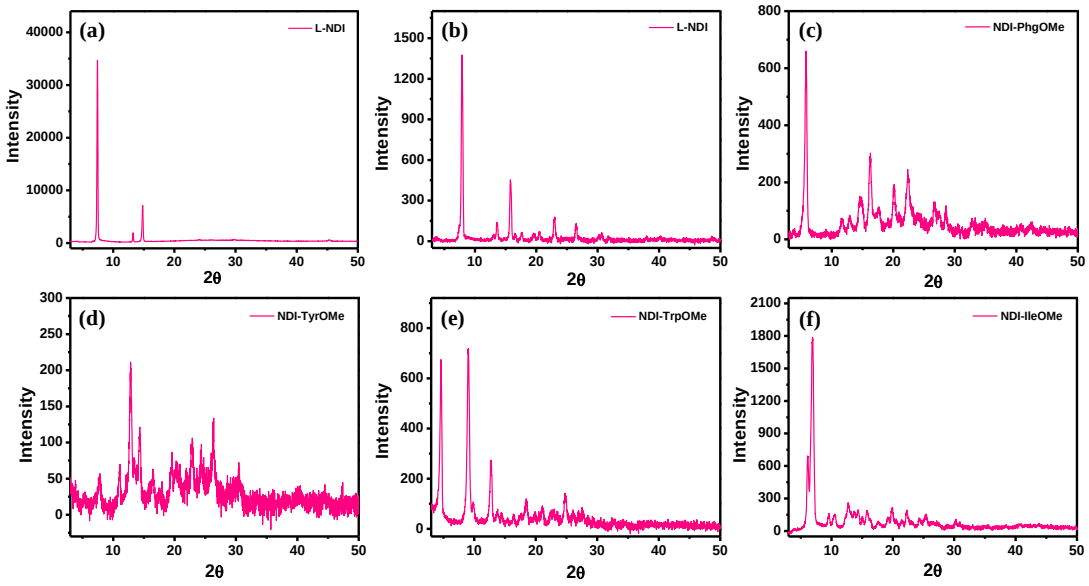


**Figure 26**. X-ray diffraction profiles of (a,b) **L-NDI**, (c) **NDI-PhgOMe**, (d) **NDI-TyrOMe**, (e) **NDI-TrpOMe** and (f) **NDI-IleOMe** obtained from 90% aqueous acetonitrile. For (a) the aggregates were formed at a slower rate, while fast for that of (b).

### 4.3.4. Cyclic voltammetry studies

Initial characterization to estimate the LUMO level of NDI was studied through cyclic voltammetry (CV). NDI was reduced at 0.36 V *vs*. Ag/AgCl in acetonitrile (Figure 27a). From this we estimated the LUMO level to be at -4.16 eV, which is consistent with the

literature reports.[80,81] However, under the same conditions the reduction peak was shifted to 0.25 V when the molecule was dissolved in DMF (Figure 27b). The probable reason could be due to lowering of the LUMO level upon π-π stacking.[82,83] This lowering of the LUMO level reduces the metal-semiconductor barrier thus facilitating ease of injection of charge carriers.

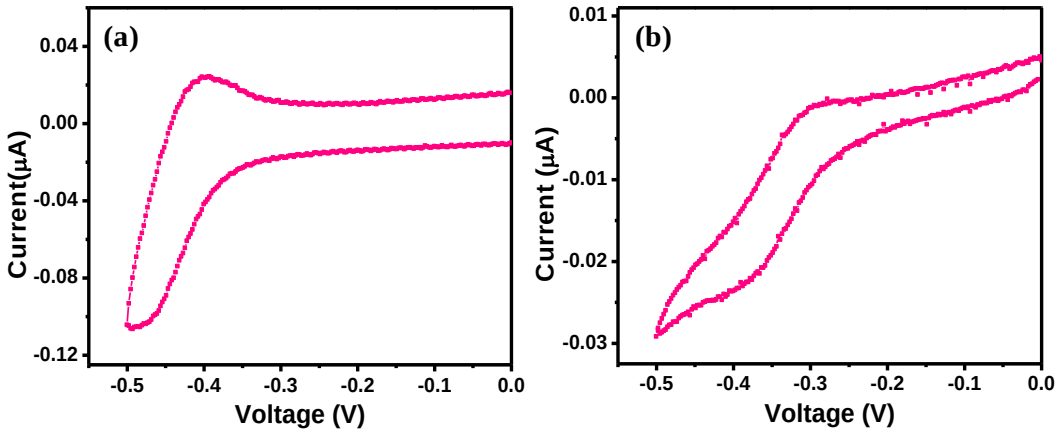


**Figure 27**. Cyclic voltammograms of 0.1 mM **L-NDI** in (a) acetonitrile and (b) *N*,*N*-dimethylformamide solution.

### 4.3.5. Bulk charge transport studies

Steady state space charge limited current (SCLC) measurements were employed to measure the electron mobilities of the NDI derivatives. The advantage of this method over conventional methods such as time of flight is that materials with low charge density can be probed.[84,85] The device structure used in this technique is shown in Figure 28, where the semiconductor is sandwiched between two injecting metal electrodes ITO and Aluminium. The electrodes are selected in such a way so as to reduce the injection barrier between the LUMO level of the semiconductor and the work function of the metal. The results from SCLC measurements for all the five NDI derivatives are shown in Figure 29.

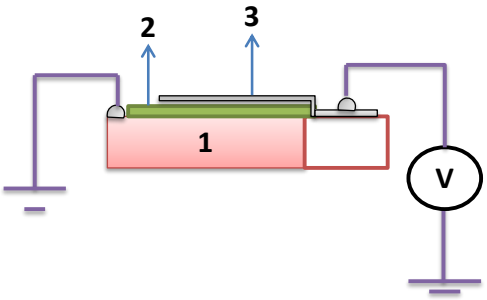


1. **Etched ITO coated glass**
2. **Semiconductor (5-10 micron)**
3. **Aluminum top electrode (100-200 nm)**

**Figure 28**. Schematic representation of the device structure employed for SCLC measurements

In all the cases, the I-V curves show a linear dependence of current with respect to voltage (I α V) up to a certain voltage and a trap-free SCLC regime thereafter, which can be fitted for I α $V^2$. Mobility (μ) in the trap free limit is calculated using the Mott- Gurney relation

$$J = \frac{9}{8}\mu\epsilon\epsilon_0\frac{V^2}{d^3}$$

where ε is the relative permittivity of the semiconductor (taken to be 3 for organic molecules) and $\varepsilon_0$ is the permittivity of vacuum. *d* is the thickness of the semiconductor film and *J* is the current density for an area *A* of the semiconductor.

**L-NDI** gives the highest mobility of 1 $cm^2$/V.s for a bulk sample of 2D sheets formed by a slower assembly process (Figure 29a). On the other hand, the 2D sheets of **L-NDI** formed under a faster rate renders mobilities of $9.1*10^{-3}$ $cm^2$/V.s (Figure 29b). Similarly, the bulk sample of **NDI-TrpOMe** fibers also exhibits mobilities of $3.2*10^{-3}$ $cm^2$/V.s (Figure 29c), whereas **NDI-PhgOMe**, **NDI-IleOMe** and **NDI-TyrOMe** showed very low mobilities of $4.7*10^{-5}$ $cm^2$/V.s (Figure 29d), $4.5*10^{-6}$ $cm^2$/V.s (Figure 29e) and $9*10^{-8}$ $cm^2$/V.s (Figure 29f), respectively. **L-NDI** also exhibits a pronounced temperature

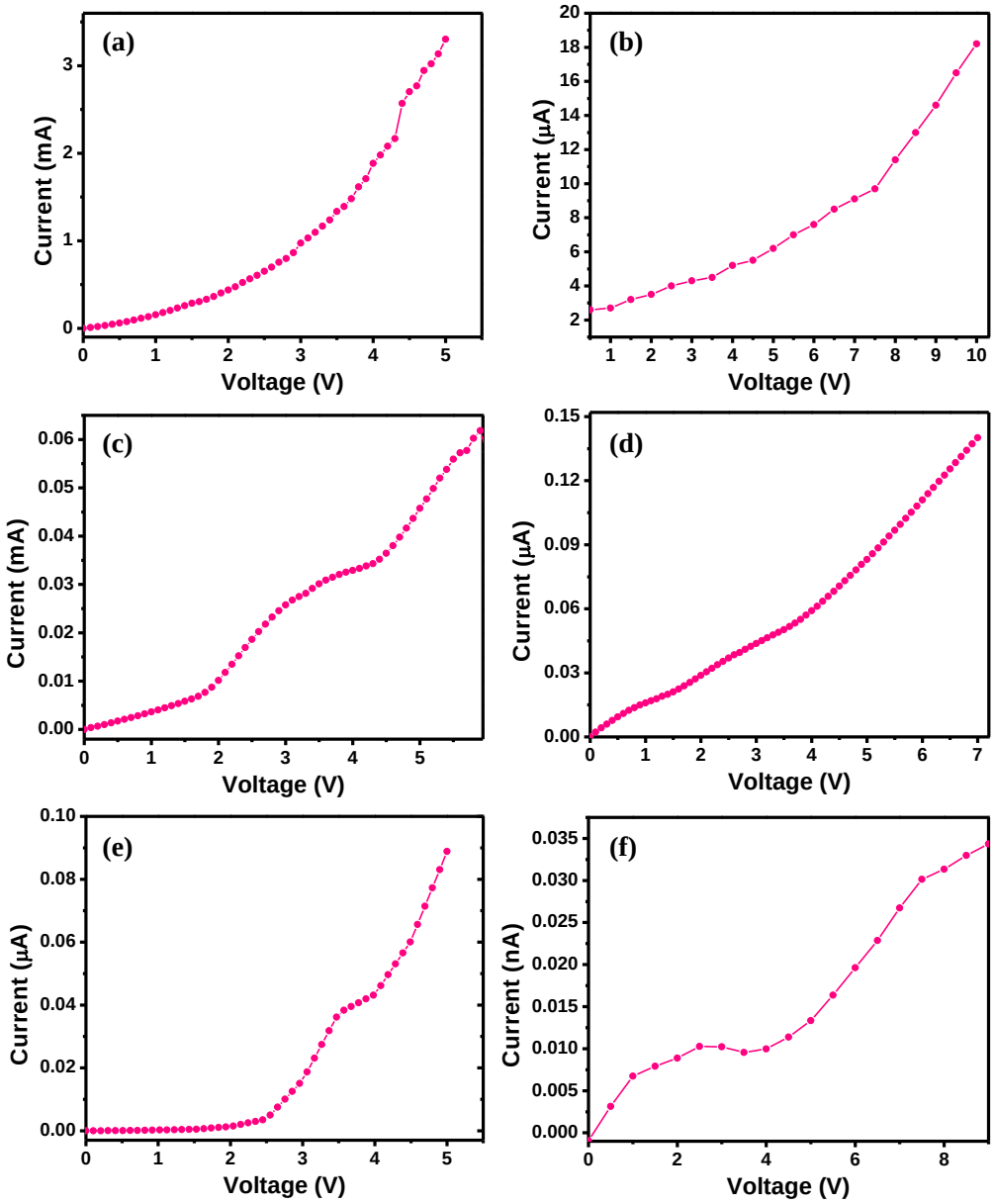


**Figure 29**. I-V plots of (a,b) **L-NDI**, (c) **NDI-TrpOMe**, (d) **NDI-PhgOMe**, (e) **NDI-IleOMe** and (f) **NDI-TyrOMe** obtained from 90% aqueous acetonitrile. For (a) the aggregates were formed at a slower rate, while fast for that of (b).

dependence which is typical to the class of disordered organic semiconductors.[76,86,87] In Figure 30 we show the temperature dependent I-V characteristics of **L-NDI** for the temperature range of 120 K to 300 K. This reveals a hopping like behavior of charge

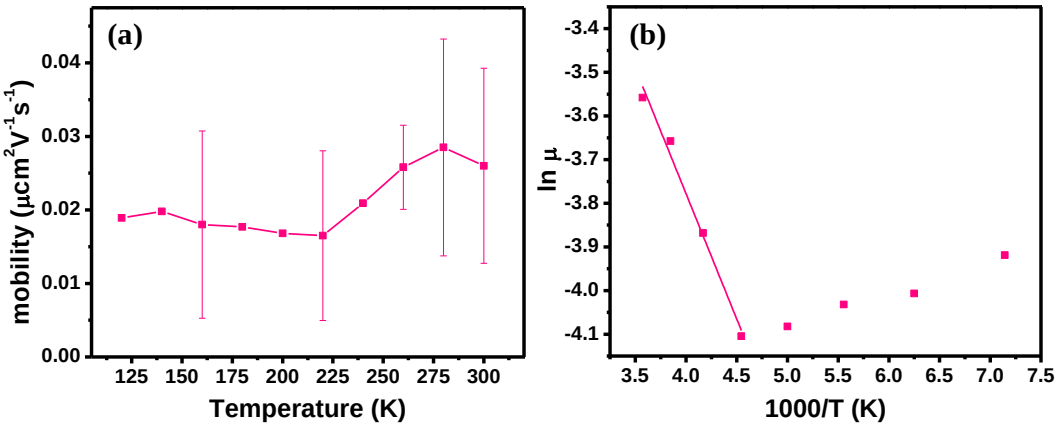


**Figure 30**. (a) and (b) Plots of mobility of **L-NDI** as a function of temperature.

carriers in the high temperature regime, which can be explained by the activation model by Arrhenius.[85] However it deviates from Arrhenius behavior below 220K. The activation energy ($E_a$) of hopping can be obtained from the equation

$$\mu(T) = \mu_0 e^{\frac{-E_a}{KT}}$$

which gives a value of 50 meV. Such a small value of activation energy and deviation from thermal activation behavior suggests that the transport becomes band-like at lower temperatures.[85] However, since trapping effects are not considered in this study, the behavior of transport below 220 K cannot be predicted with certainty from our experiments.

### 4.3.6. Discussion and conclusions

Although, better mobilities are expected for a 2D sheet-like semiconductor layer sandwiched between two injecting electrodes, the obtained distinctly different mobilities

of **L-NDI**, **NDI-PhgOMe** and **NDI-TyrOMe** could be ascribed to following reasons, i) the π-π stacking of chromophores is not perpendicular with respect to the two electrodes, ii) the extent of crystalline ordering in a single self-assembled structure and iii) limited by the orientations of these self-assembled structures (termed as orientational disorder) for charge transport in a bulk sample. Although, we do not have precise evidences about the direction of π-π stacking, it appears to us that the extremely low mobilities of **NDI-TyrOMe** could be attributed to low-crystalline ordering (Figure 26d) and the orientation disorder (Figure 25d), which in turn affects the net direction of π-π stacking. In case of **L-NDI**, a difference of nearly two orders of magnitude can be directly correlated with the crystalline ordering as seen in X-ray diffraction studies (Figure 26a,b) and the inter-sheet limited charge transport changes arising due to their aggregates sizes (Figure 25a,b). Similarly, the latter reasons as well as the orientational disorder may limit the mobilities of **NDI-PhgOMe** to the order of $10^{-5}$.

Interestingly, in case of **NDI-TrpOMe** the π-π stacking is most likely to be along the longer axis of the fibers and hence the mobilities of the order of $10^{-3}$ can be accounted by orientational disorder (Figure 25e) and crystallinity (Figure 26e). On the other hand, the **NDI-IleOMe** motifs has to be oriented in all possible directions to form the spherical structures, as a result orientational disorder lies within the single self-assembled structure itself. In addition, the mobilities would be limited by the charge transport across the spheres in a bulk sample.

Thus, with the aid of available results, we have shown that a small modification in the structure of the molecule can bring about significant variations to their organization, crystallinity and in turn to their electronic properties. As SCLC studies are a collective

phenomenon arising from measurements done on the bulk of the material, a direct correlation with their single self-assembled structure and/or molecular structure is not appropriate. Therefore, additional experiments are underway for a much detailed account of structural-property correlations. Such studies if successful could be beneficial in designing high performance electronic devices.

### 4.3.7. Experimental section

#### *4.3.7.1. Materials and methods*

All the solvents and reagents were obtained from Sigma-Aldrich and used as received unless otherwise mentioned.

*NMR Spectroscopy, Mass Spectrometry (MS), and Elemental Analysis*: $^{1}H$ and $^{13}C$ NMR were recorded on a Bruker AV-400 spectrometer with chemical shifts reported as ppm (in $CDCl_3$ with tetramethylsilane as internal standard). Mass spectra were obtained from Shimadzu 2020 LC-MS. Elemental analysis was carried out on ThermoScientific FLASH 2000 Organic Element Analyzer.

*Absorption Spectroscopy*: UV–vis spectra were recorded on a Perkin Elmer Model Lambda 900 spectrophotometer. A 100 μM solution of the sample was analyzed in quartz cuvette of 1 mm path length.

*Fluorescence Spectroscopy*: Fluorescence spectra were recorded on a Perkin Elmer Model LS 55 spectrophotometer. A 100 μM solution of the sample were analyzed in a quartz cuvette of 1 mm path length with an excitation at 375 nm.

*Field Emission Scanning Electron Microscopy*: FESEM images were acquired with a FEI Nova nanoSEM-600 equipped with a field-emission gun operating at 15 kV. The sample was prepared by drop-casting onto a Si (111) substrate.

*Powder X-ray diffraction (PXRD):* PXRD patterns were recorded with a Rigaku-99 (Miniflex) diffractometer using Cu Kα radiation (λ = 1.5406 Å). The free-floating self-assembled structures of NDI derivatives were drop-casted on a glass slide. The diffraction peaks were indexed with the DICVOL program.

*Cyclic Voltammetry:* Cyclic Voltammetry was performed using Metrohm's Autolab PGSTAT101 with Ag/AgCl reference electrode, Platinum wire as counter electrode and Platinum disc as working electrode. 10 mL of 0.1 M solution of tetra-n-butylammonium hexafluorophosphate($TBAPF_6$) was used as the electrolyte in anhydrous acetonitrile/*N*,*N*-dimethylformamide(DMF) and 0.1 mM of **L-NDI** dissolved in acetonitrile/DMF was added to the above prepared solution. Ultra pure nitrogen was used to purge the sealed cell containing the solution and electrodes ten minutes before the experiment and a blanket of nitrogen was maintained throughout the experiment. The I-V curve was recorded at a scan rate of 0.5 V/s.

*Device fabrication*: ITO coated glass substrates were cleaned by ultra-sonication in soap solution followed by sonication in acetone and isopropyl alcohol. This was followed by standard RCA treatment; substrates in a mixture of ammonium hydroxide ($NH_4OH$), hydrogen peroxide ($H_2O_2$) and water (1:1:4 by volume) were heated at 80 $^oC$ for 15 min. The semiconductor was drop-casted on the cleaned ITO coated glass from 90% aqueous acetonitrile solution and left to dry overnight under ambient conditions. The resulting film thickness ranges from 1-10 μm. Aluminum top electrode which determines the

device area was then evaporated by physical vapor deposition ($10^{-6}$ mbar vacuum and 100 nm thick) to complete the sandwich structure. All measurements were carried out in inert atmosphere using a standard Keithley 4200 semi-conductor parameter analyzer. Temperature dependent measurements were done using a liquid helium based cryostat from Cryogenic Technologies Ltd.

#### *4.3.7.2. Synthesis of L-NDI*

Refer section 2.2.4.2

#### *4.3.7.3. Synthesis of NDI-TrpOMe*

Refer section 2.1.8.3

#### *4.3.7.4. Synthesis of NDI-PhgOMe*

*Synthesis of L-phenylglycine methylester hydrochloride*: Anhydrous methanol (50 mL)

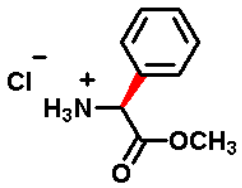


was placed into a 100 mL two-necked round-bottom flask, fitted with a reflux condenser and an additional dropping funnel, and cooled to ice temperature (0 $^{o}$C). Acetyl chloride (3 mL) was added drop-wise through the dropping funnel. After 15 min, L-phenylglycine (3 g, 18.16 mmol) was added, and the reaction mixture was refluxed overnight at 70 $^{o}$C. The reaction

mixture was dried in vacuo to obtain L-phenylglycine methylester hydrochloride in quantitative yield and used for further reaction without purification.

1,4,5,8-naphthalenetetracarboxylic dianhydride (200 mg, 0.74 mmol) and L-phenylglycine methylester hydrochloride (322 mg 1.49 mmol) were suspended in DMF

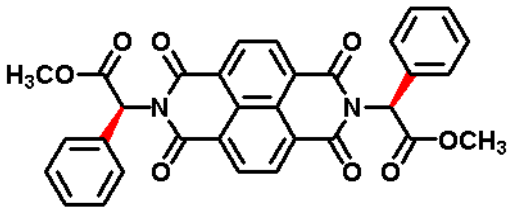


(20 mL) in a 100 mL round-bottom flask. To this suspension, triethylamine (0.6 mL) was added under inert atmosphere. The reaction mixture was refluxed at 75 $^{o}$C for 24 h. The solvent was evaporated in vacuo, and the residue was purified by column chromatography (1% methanol in chloroform). Yield 70%. $^{1}$H NMR (400 MHz, $CDCl_3$, δ): 8.77 (s, 4H), 7.69 (m, 4H), 7.34 (m, 6H), 6.84 (s, 2H), 3.82 (s, 6H); $^{13}$C NMR (100 MHz, $CDCl_3$, δ): 168.4, 162.2, 134.3, 131.5, 130.5, 128.7, 128.4, 126.8, 126.6, 57.1, 52.9; MS (EI): $m/z$ = 562.16 $[M]^+$ for $C_{34}H_{26}N_2O_8$ (calc. 562.14); Elemental analysis: Calcd. for $C_{32}H_{22}N_2O_8$: C, 68.32; H, 3.94; N, 4.98. Found: C, 68.29; H, 3.98; N, 4.95.

### *4.3.7.5. Synthesis of NDI-TyrOMe*

*Synthesis of L-tyrosine methylester hydrochloride*: Anhydrous methanol (50 mL) was

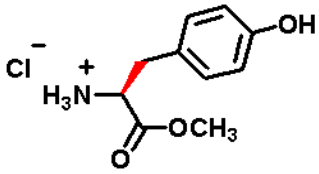


placed into a 100 mL two-necked round-bottom flask, fitted with a reflux condenser and an additional dropping funnel, and cooled to ice temperature (0 $^{o}$C). Acetyl chloride (3 mL) was added drop-wise through the dropping funnel. After 15 min, L-tyrosine (3 g, 18.16 mmol) was added, and the reaction mixture was refluxed overnight at 70 $^{o}$C. The reaction

mixture was dried in vacuo to obtain L-tyrosine methyl ester hydrochloride in quantitative yield and used for further reaction without purification.

1,4,5,8-naphthalenetetracarboxylic dianhydride (200 mg, 0.74 mmol) and L-tyrosine methyl ester hydrochloride (322 mg 1.49 mmol) were suspended in DMF (20 mL) in a 100 mL round-bottom flask. To this suspension, triethylamine (0.6 mL) was added under inert atmosphere. The reaction mixture was refluxed at 75 $^{o}$C for 24 h. The solvent was evaporated in vacuo, and the residue was purified by column chromatography (1% methanol in chloroform). Yield 68%. $^{1}$H NMR (400 MHz, $CDCl_3$, δ): 9.09 (s, 2H), 8.65 (s, 4H), 6.95 (d, 4H), 6.49 (d, 4H), 5.90 (q, 2H), 3.65 (s, 6H), 3.50 (dd, 2H, $J$ = 8Hz, 4Hz), 3.22 (dd, 2H, $J$ = 8 Hz, 4 Hz); $^{13}$C NMR (100 MHz, $CDCl_3$, δ) 169.4, 161.9, 155.74, 131.4, 130.0, 127.2, 126.1, 125.6, 115.0, 54.6, 52.4, 33.2; MS (EI): $m/z$ = 622.27 $[M]^+$ for $C_{34}H_{26}N_2O_{10}$ (calc. 622.16); Elemental analysis: Calcd. for $C_{34}H_{26}N_2O_{10}$: C, 65.59; H, 4.21; N, 4.50. Found: C, 65.57; H, 4.25; N, 4.53.

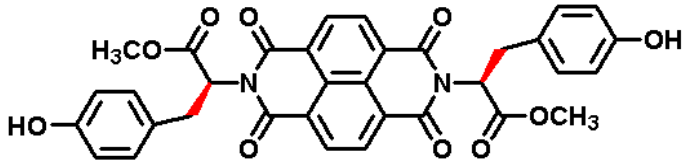


### *4.3.7.6. Synthesis of NDI-IleOMe*

*Synthesis of L-isoleucine methyl ester hydrochloride*: Anhydrous methanol (50 mL) was placed into a 100 mL two-necked round-bottom flask, fitted with a reflux condenser and an additional dropping funnel, and cooled to ice temperature (0 $^{o}$C). Acetyl chloride (3 mL) was added drop-wise through the dropping funnel. After 15 min, L-isoleucine (3 g, 18.16 mmol) was

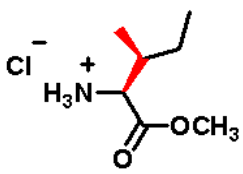

added, and the reaction mixture was refluxed overnight at 70 °C. The reaction mixture was dried in vacuo to obtain L-isoleucine methyl ester hydrochloride in quantitative yield and used for further reaction without purification.

1,4,5,8-naphthalenetetracarboxylic dianhydride (200 mg, 0.74 mmol) and L-isoleucine methyl ester hydrochloride (322 mg 1.49 mmol) were suspended in DMF (20 mL) in a 100 mL round-bottom flask. To this suspension, triethylamine (0.6 mL) was added under inert atmosphere. The reaction mixture was refluxed at 75 °C for 24 h. The solvent was evaporated in vacuo, and the residue was purified by column chromatography (1% methanol in chloroform). Yield 78%. $^{1}$H NMR (400 MHz, $CDCl_3$, δ): 8.79 (s, 4H), 5.42 (d, 2H), 3.69 (s, 6H), 2.63 (m, 2H), 1.30 (m, 8H), 1.03 (m, 2H), 0.84 (m, 6H); $^{13}$C NMR (100 MHz, $CDCl_3$, δ) 169.9, 162.8, 131.7, 127.2, 126.6, 58.7, 52.5, 33.7, 25.4, 18.1, 11.1; MS (EI): $m/z$ = 522.16 $[M]^+$ for $C_{28}H_{30}N_2O_8$ (calc. 522.20); Elemental analysis: Calcd. for $C_{28}H_{30}N_2O_8$: C, 64.36; H, 5.79; N, 5.36. Found: C, 64.30; H, 5.84; N, 5.39.

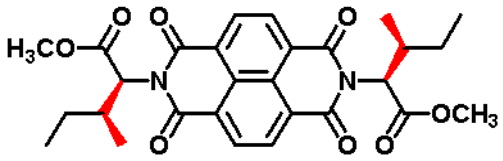

### 4.3.8. Appendix

- $^{1}H$ and $^{13}C$ NMR of **1**
- $^{1}H$ and $^{13}C$ NMR of **CDP-Ala**
- $^{1}H$ and $^{13}C$ NMR of **CDP-Phg**
- $^{1}H$ and $^{13}C$ NMR of **CDP-Phe**
- $^{1}H$ and $^{13}C$ NMR of **NDI-PhgOMe**
- $^{1}H$ and $^{13}C$ NMR of **NDI-TyrOMe**
- $^{1}H$ and $^{13}C$ NMR of **NDI-IleOMe**

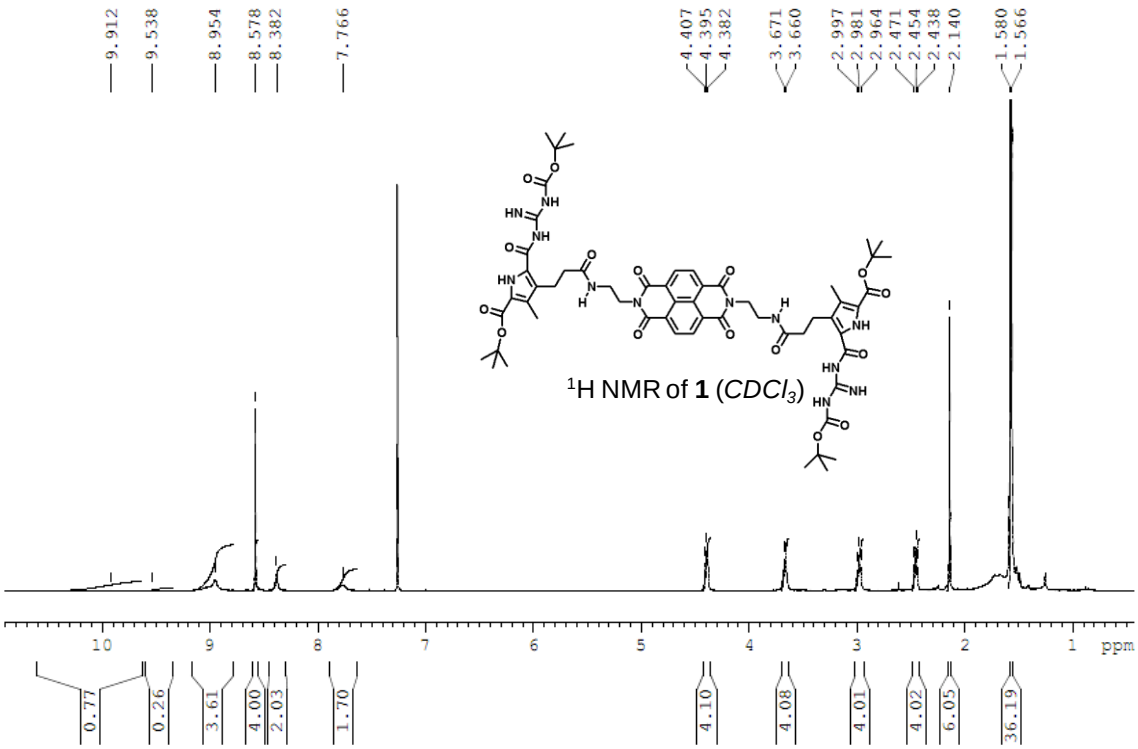


$^{1}$H NMR of **1** ($CDCl_3$)

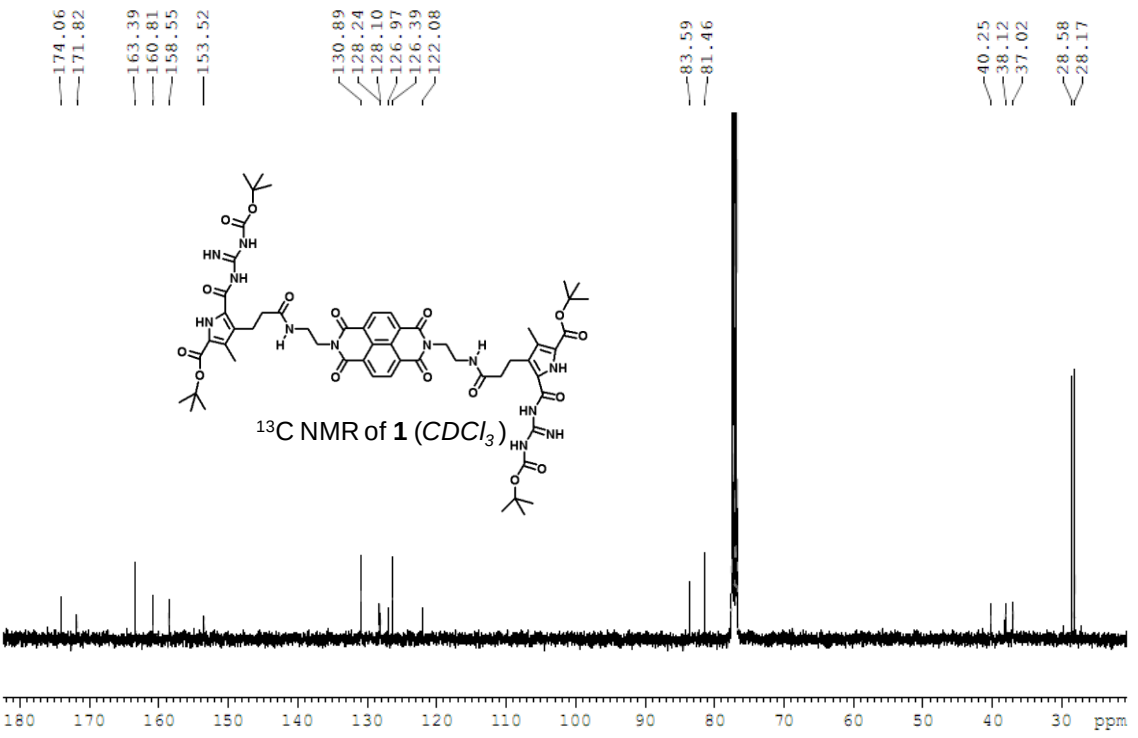


$^{13}$C NMR of **1** ($CDCl_3$)

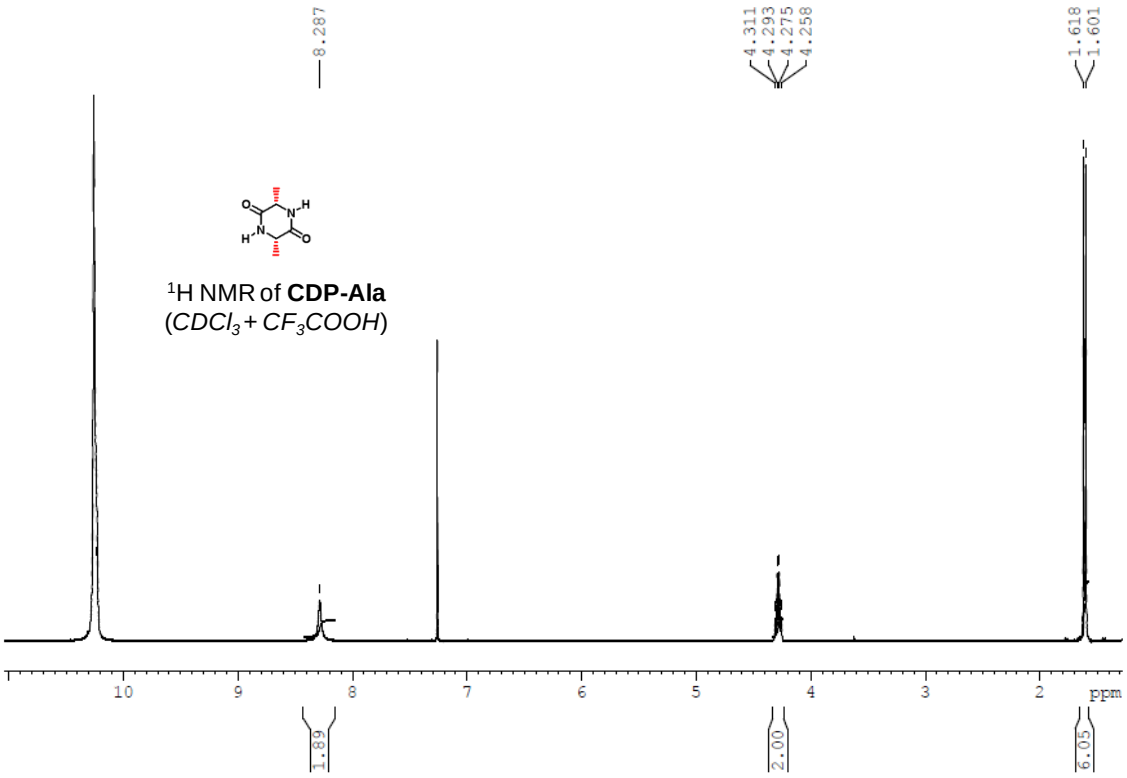


$^{1}$H NMR of **CDP-Ala**
(*$CDCl_3$ + $CF_3COOH$*)

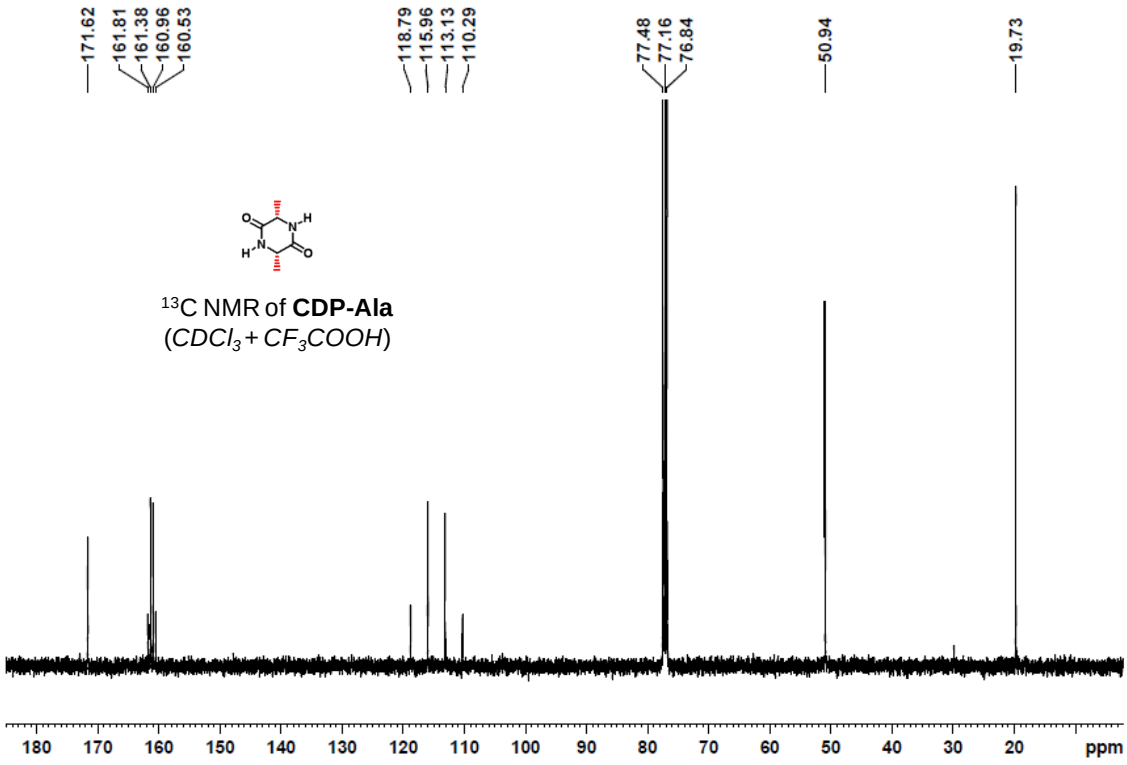


$^{13}$C NMR of **CDP-Ala**
(*$CDCl_3$ + $CF_3COOH$*)

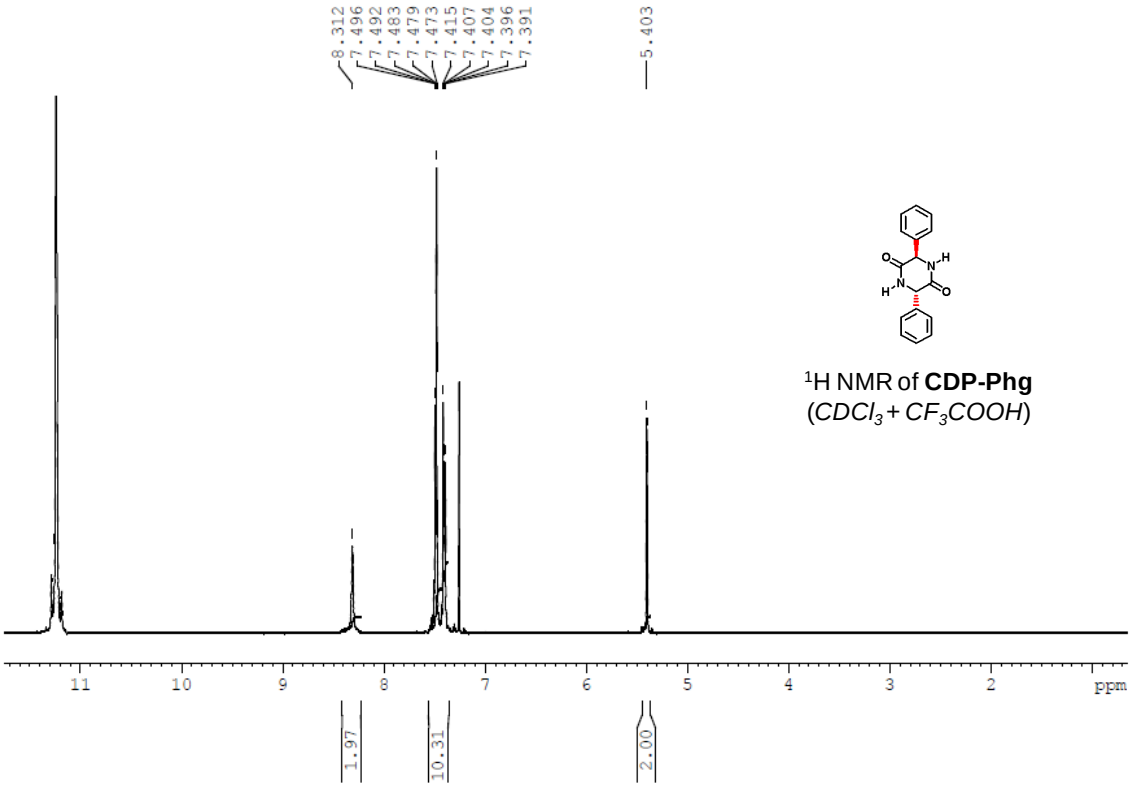


$^{1}$H NMR of **CDP-Phg**
(*$CDCl_3$ + $CF_3COOH$*)

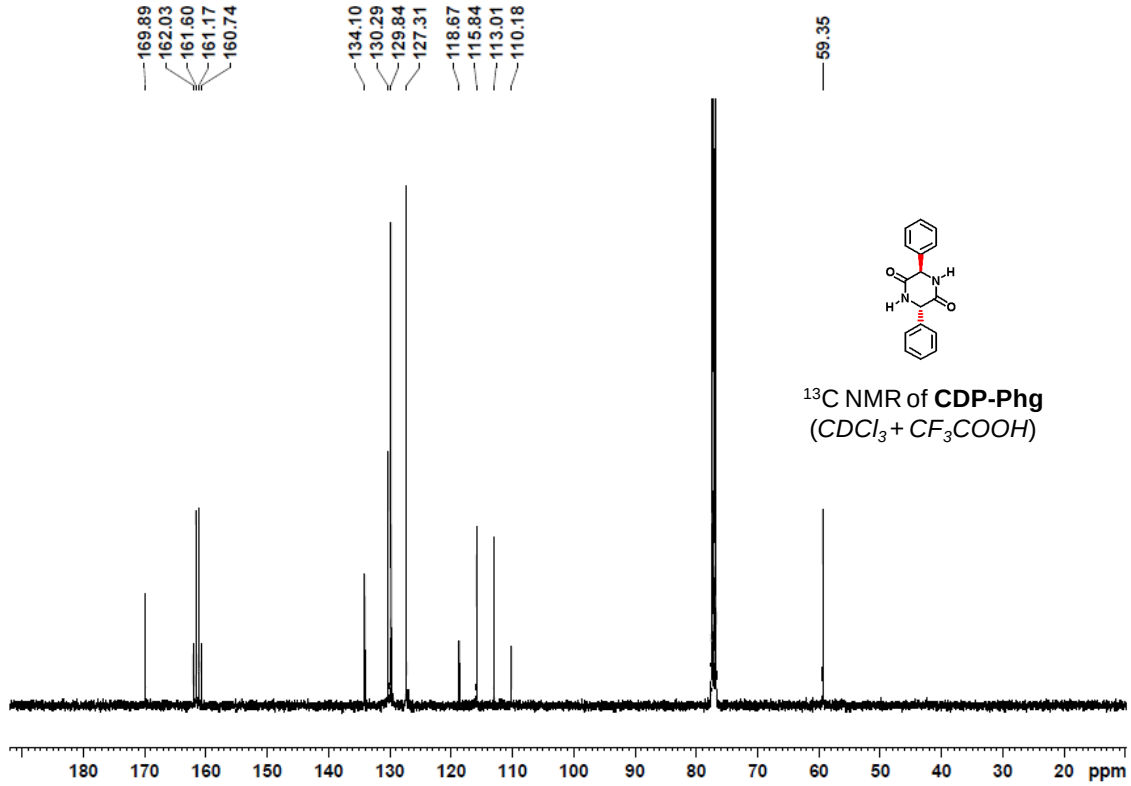


$^{13}$C NMR of **CDP-Phg**
(*$CDCl_3$ + $CF_3COOH$*)

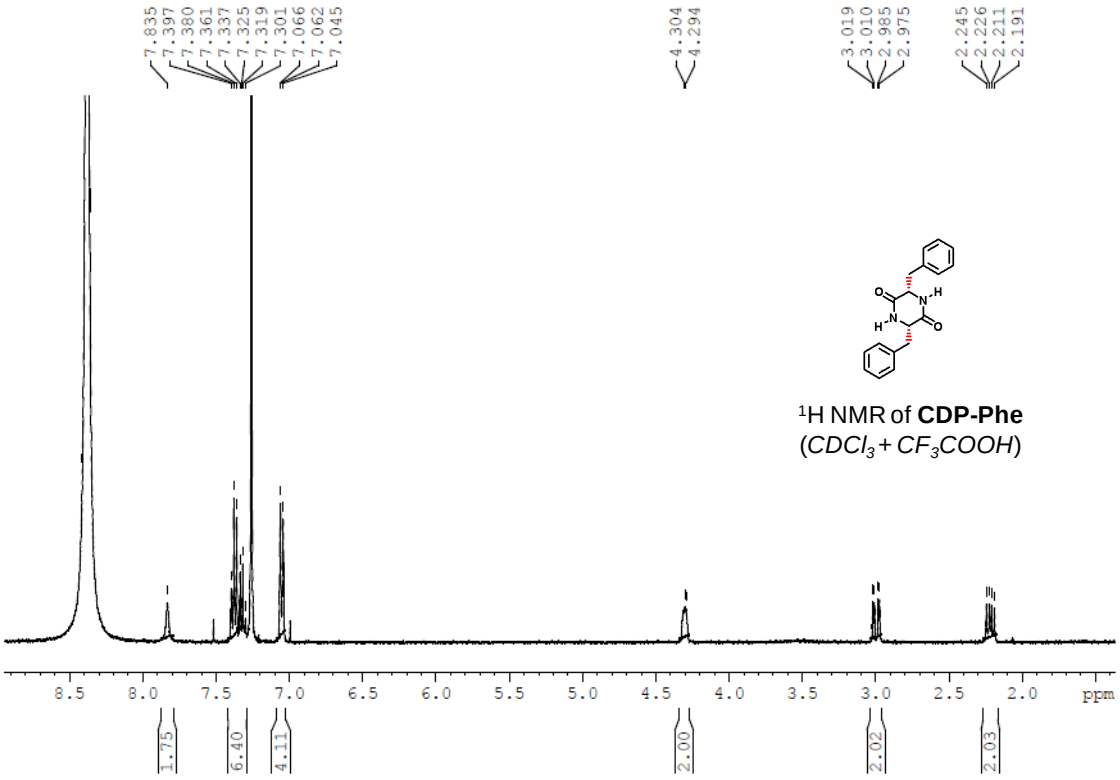


$^{1}$H NMR of **CDP-Phe**
($CDCl_3 + CF_3COOH$)

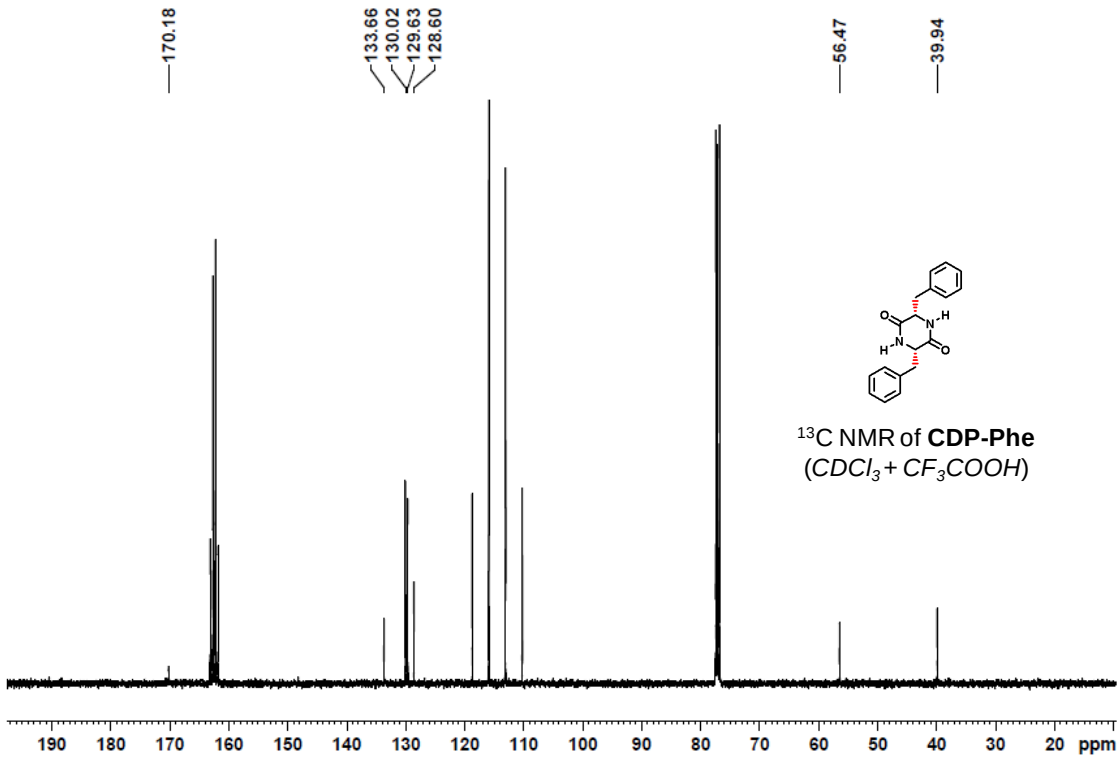


$^{13}$C NMR of **CDP-Phe**
($CDCl_3 + CF_3COOH$)

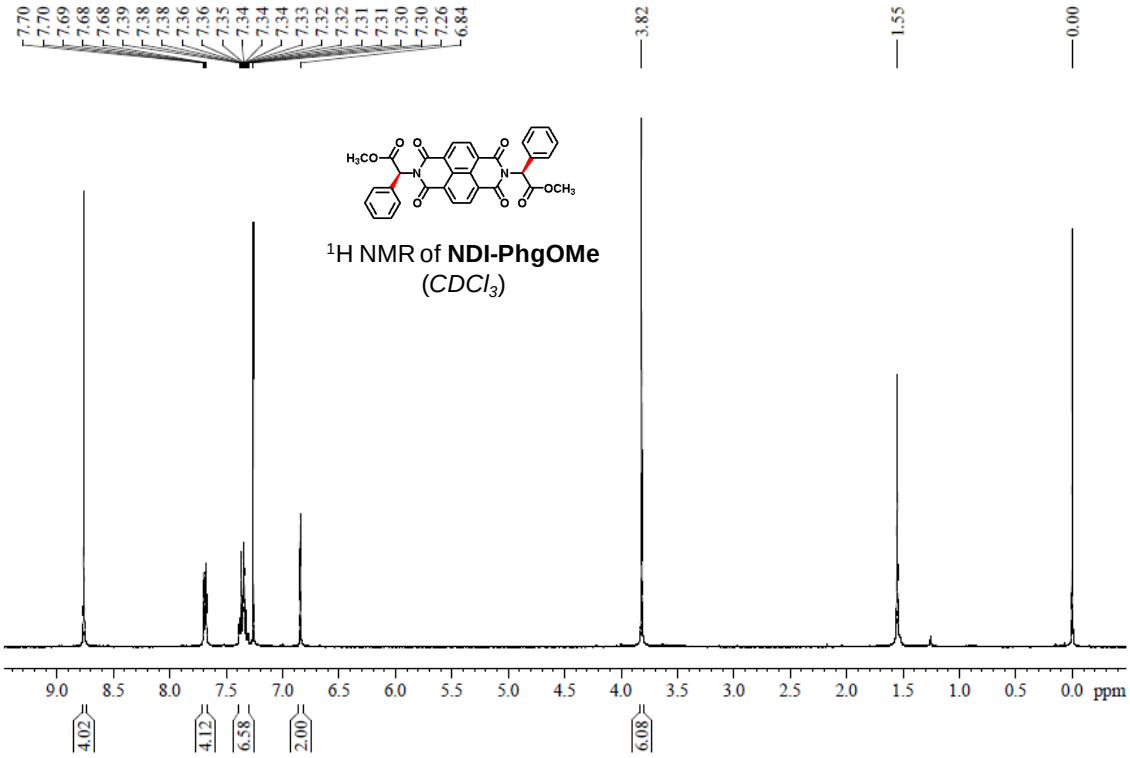


$^{1}$H NMR of **NDI-PhgOMe** ($CDCl_3$)

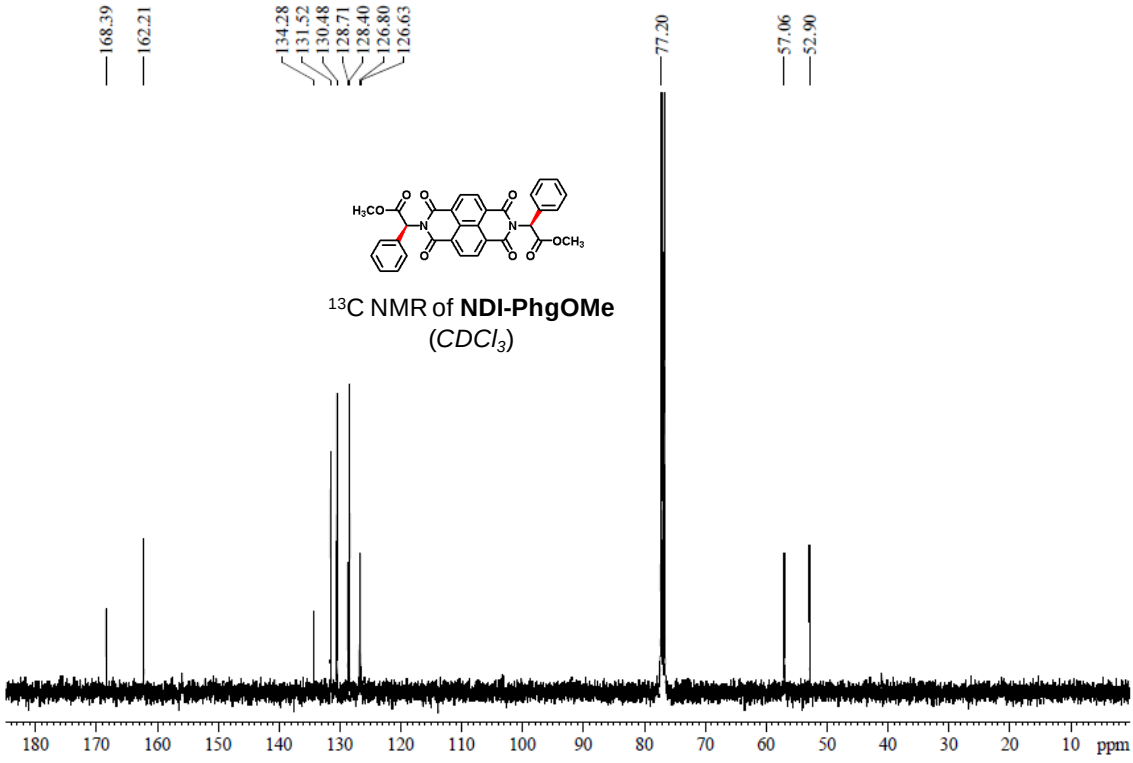


$^{13}$C NMR of **NDI-PhgOMe** ($CDCl_3$)

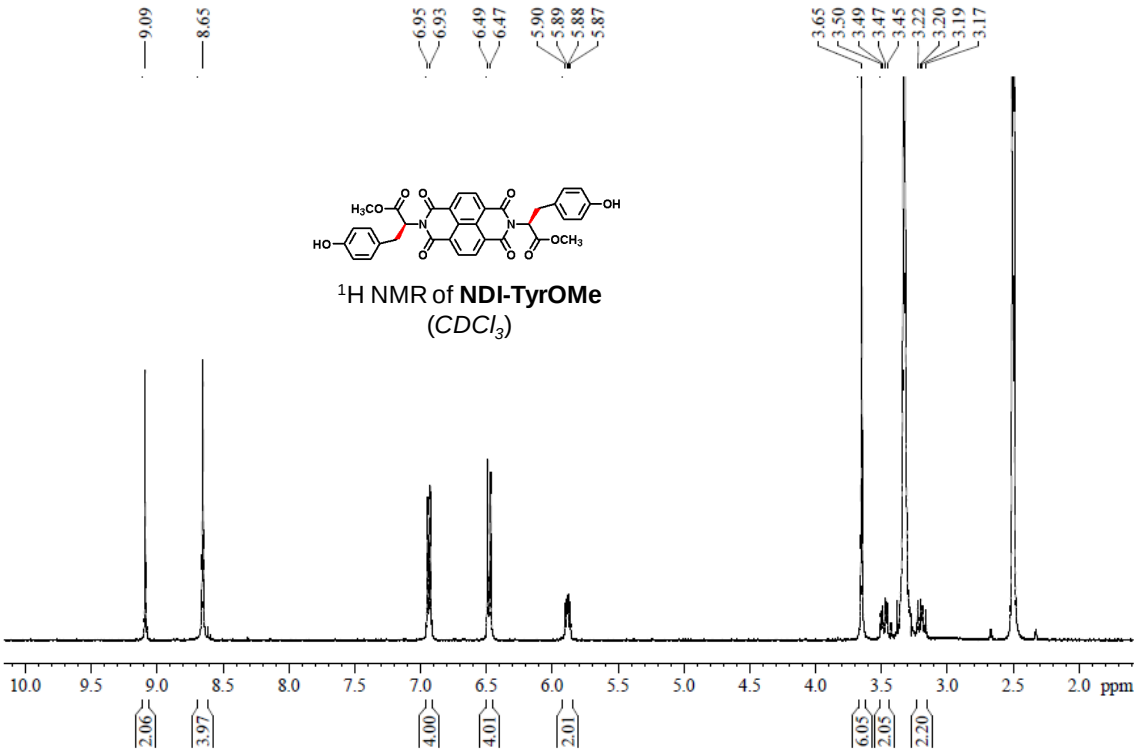


$^{1}$H NMR of **NDI-TyrOMe** ($CDCl_3$)

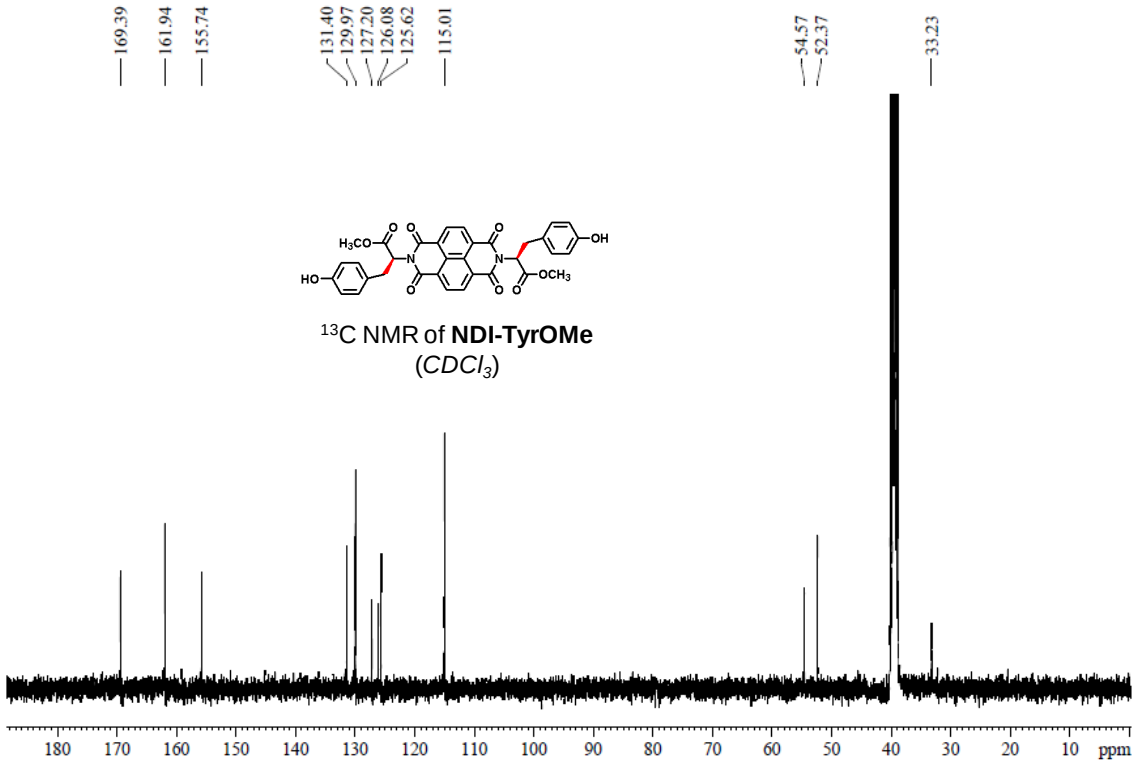


$^{13}$C NMR of **NDI-TyrOMe** ($CDCl_3$)

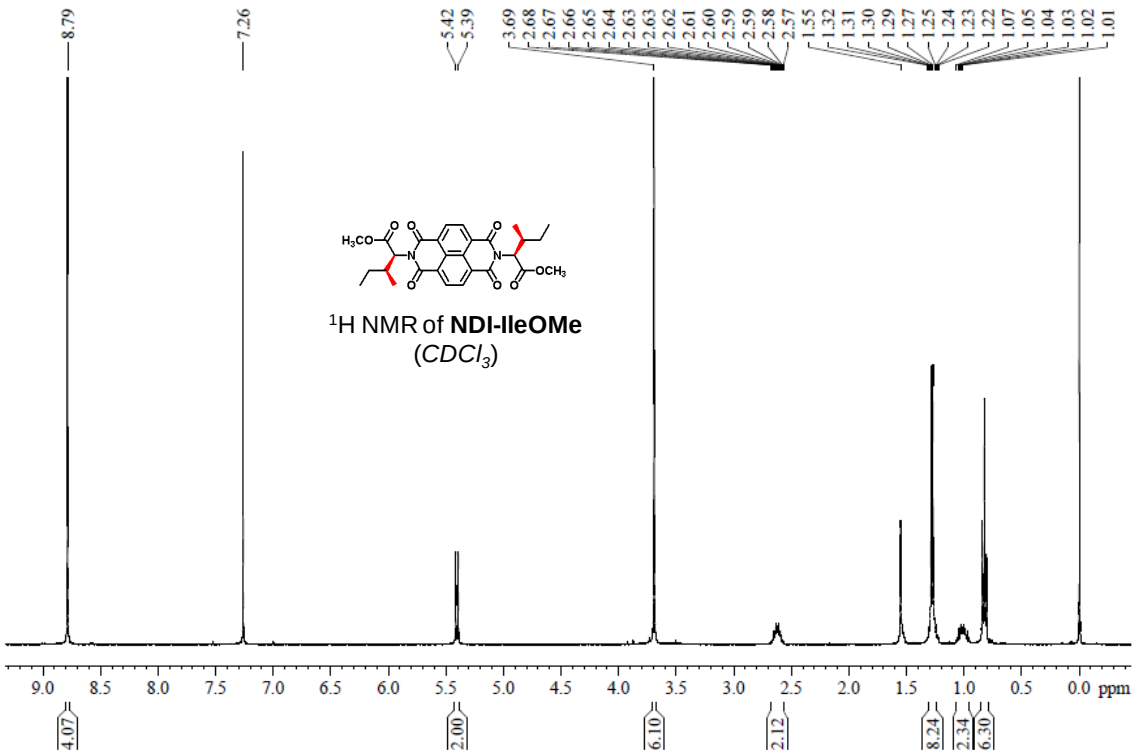


$^{1}$H NMR of **NDI-IleOMe** ($CDCl_3$)

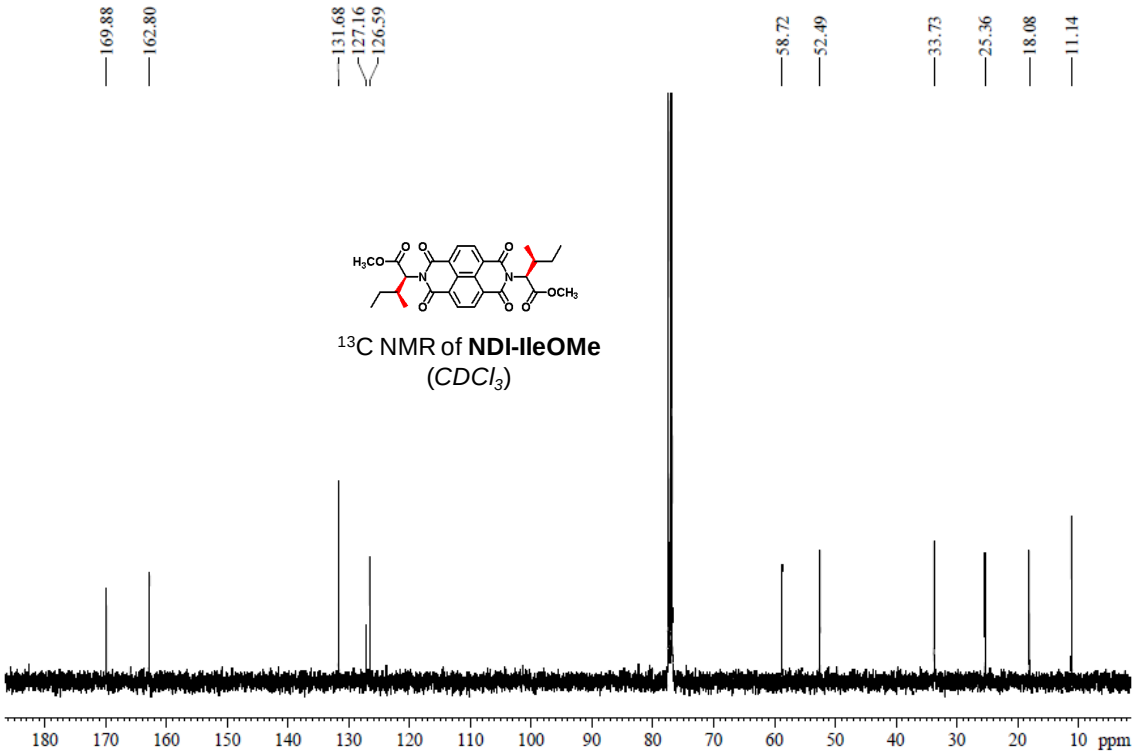


$^{13}$C NMR of **NDI-IleOMe** ($CDCl_3$)

### 4.3.9. References

1. Kwak, E. S.; Lee, W.; Park, N.-G.; Kim, J.; Lee, H., Compact Inverse-Opal Electrode Using Non-Aggregated TiO2 Nanoparticles for Dye-Sensitized Solar Cells. *Adv. Funct. Mater.* **2009,** *19*, 1093-1099.

2. Kubo, S.; Gu, Z.-Z.; Takahashi, K.; Fujishima, A.; Segawa, H.; Sato, O., Tunable Photonic Band Gap Crystals Based on a Liquid Crystal-Infiltrated Inverse Opal Structure. *J. Am. Chem. Soc.* **2004,** *126*, 8314-8319.

3. Shastri, V. P.; Martin, I.; Langer, R., Macroporous polymer foams by hydrocarbon templating. *Proc. Natl. Acad. Sci.* **2000,** *97*, 1970-1975.

4. Walling, M. A.; Shepard, J. R. E., Cellular heterogeneity and live cell arrays. *Chem. Soc. Rev.* **2011,** *40*, 4049-4076.

5. Haswell, S. J.; Skelton, V., Chemical and biochemical microreactors. *TrAC Trends Anal. Chem.* **2000,** *19*, 389-395.

6. Zhang, X.; Shi, F.; Niu, J.; Jiang, Y.; Wang, Z., Superhydrophobic surfaces: from structural control to functional application. *J. Mater. Chem.* **2008,** *18*, 621-633.

7. Sanchez, C.; Arribart, H.; Giraud Guille, M. M., Biomimetism and bioinspiration as tools for the design of innovative materials and systems. *Nat. Mater.* **2005,** *4*, 277-288.

8. Xia, F.; Jiang, L., Bio-Inspired, Smart, Multiscale Interfacial Materials. *Adv. Mater.* **2008,** *20*, 2842-2858.

9. Aida, T.; Meijer, E. W.; Stupp, S. I., Functional Supramolecular Polymers. *Science* **2012,** *335*, 813-817.

10. Shao, H.; Seifert, J.; Romano, N. C.; Gao, M.; Helmus, J. J.; Jaroniec, C. P.; Modarelli, D. A.; Parquette, J. R., Amphiphilic Self-Assembly of an n-Type Nanotube. *Angew. Chem. Int. Ed.* **2010,** *49*, 7688-7691.

11. Sakai, N.; Bhosale, R.; Emery, D.; Mareda, J.; Matile, S., Supramolecular n/p-Heterojunction Photosystems with Antiparallel Redox Gradients in Electron- and Hole-Transporting Pathways. *J. Am. Chem. Soc.* **2010,** *132*, 6923-6925.

12. Yagai, S.; Seki, T.; Karatsu, T.; Kitamura, A.; Würthner, F., Transformation from H- to J-Aggregated Perylene Bisimide Dyes by Complexation with Cyanurates. *Angew. Chem. Int. Ed.* **2008,** *47*, 3367-3371.

13. Blossey, R., Self-cleaning surfaces—virtual realities. *Nat. Mater.* **2003,** *2*, 301-306.

14. Liu, K.; Yao, X.; Jiang, L., Recent developments in bio-inspired special wettability. *Chem. Soc. Rev.* **2010,** *39*, 3240-3255.

15. Nishimoto, S.; Bhushan, B., Bioinspired self-cleaning surfaces with superhydrophobicity, superoleophobicity, and superhydrophilicity. *RSC Advances* **2013,** *3*, 671-690.

16. Liu, K.; Jiang, L., Bio-inspired self-cleaning surfaces. *Annu. Rev. Mater. Res.* **2012,** *42*, 231-263.

17. Koch, K.; Bhushan, B.; Jung, Y. C.; Barthlott, W., Fabrication of artificial Lotus leaves and significance of hierarchical structure for superhydrophobicity and low adhesion. *Soft Matter* **2009,** *5*, 1386-1393.

18. Li, X.-M.; Reinhoudt, D.; Crego-Calama, M., What do we need for a superhydrophobic surface? A review on the recent progress in the preparation of superhydrophobic surfaces. *Chem. Soc. Rev.* **2007,** *36*, 1350-1368.

19. Barthlott, W.; Neinhuis, C., Purity of the sacred lotus, or escape from contamination in biological surfaces. *Planta* **1997,** *202*, 1-8.

20. Ueda, E.; Levkin, P. A., Emerging Applications of Superhydrophilic-Superhydrophobic Micropatterns. *Adv. Mater.* **2013**, *25*, 1234-1247.

21. Verho, T.; Bower, C.; Andrew, P.; Franssila, S.; Ikkala, O.; Ras, R. H., Mechanically durable superhydrophobic surfaces. *Adv. Mater.* **2011,** *23*, 673-678.

22. Xia, D.; Johnson, L. M.; López, G. P., Anisotropic Wetting Surfaces with One-Dimesional and Directional Structures: Fabrication Approaches, Wetting Properties and Potential Applications. *Adv. Mater.* **2012,** *24*, 1287-1302.

23. Banerjee, I.; Pangule, R. C.; Kane, R. S., Antifouling coatings: recent developments in the design of surfaces that prevent fouling by proteins, bacteria, and marine organisms. *Adv. Mater.* **2011,** *23*, 690-718.

24. Yao, X.; Song, Y.; Jiang, L., Applications of Bio-Inspired Special Wettable Surfaces. *Adv. Mater.* **2011,** *23*, 719-734.

25. Öner, D.; McCarthy, T. J., Ultrahydrophobic Surfaces. Effects of Topography Length Scales on Wettability. *Langmuir* **2000,** *16*, 7777-7782.

26. Nakajima, A.; Fujishima, A.; Hashimoto, K.; Watanabe, T., Preparation of Transparent Superhydrophobic Boehmite and Silica Films by Sublimation of Aluminum Acetylacetonate. *Adv. Mater.* **1999,** *11*, 1365-1368.

27. Coulson, S. R.; Woodward, I. S.; Badyal, J. P. S.; Brewer, S. A.; Willis, C., Ultralow Surface Energy Plasma Polymer Films. *Chem. Mater.* **2000,** *12*, 2031-2038.

28. Jiang, Y.; Wan, P.; Smet, M.; Wang, Z.; Zhang, X., Self-Assembled Monolayers of a Malachite Green Derivative: Surfaces with pH- and UV-Responsive Wetting Properties. *Adv. Mater.* **2008,** *20*, 1972-1977.

29. Love, J. C.; Gates, B. D.; Wolfe, D. B.; Paul, K. E.; Whitesides, G. M., Fabrication and Wetting Properties of Metallic Half-Shells with Submicron Diameters. *Nano Lett.* **2002,** *2*, 891-894.

30. Darmanin, T.; de Givenchy, E. T.; Amigoni, S.; Guittard, F., Superhydrophobic Surfaces by Electrochemical Processes. *Adv. Mater.* **2013**, *25*, 1378-1394.

31. Zhang, X.; Shi, F.; Yu, X.; Liu, H.; Fu, Y.; Wang, Z.; Jiang, L.; Li, X., Polyelectrolyte Multilayer as Matrix for Electrochemical Deposition of Gold Clusters: Toward Super-Hydrophobic Surface. *J. Am. Chem. Soc.* **2004,** *126*, 3064-3065.

32. Bunz, U. H. F., Breath Figures as a Dynamic Templating Method for Polymers and Nanomaterials. *Adv. Mater.* **2006,** *18*, 973-989.

33. Lord, H. T.; Quinn, J. F.; Angus, S. D.; Whittaker, M. R.; Stenzel, M. H.; Davis, T. P., Microgel stars viaReversible Addition Fragmentation Chain Transfer (RAFT) polymerisation - a facile route to macroporous membranes, honeycomb patterned thin films and inverse opal substrates. *J. Mater. Chem.* **2003,** *13*, 2819-2824.

34. Connal, L. A.; Vestberg, R.; Gurr, P. A.; Hawker, C. J.; Qiao, G. G., Patterning on Nonplanar Substrates: Flexible Honeycomb Films from a Range of Self-assembling Star Copolymers. *Langmuir* **2007,** *24*, 556-562.

35. Liu, C.; Gao, C.; Yan, D., Honeycomb-Patterned Photoluminescent Films Fabricated by Self-Assembly of Hyperbranched Polymers. *Angew. Chem. Int. Ed.* **2007,** *46*, 4128-4131.

36. Erdogan, B.; Song, L.; Wilson, J. N.; Park, J. O.; Srinivasarao, M.; Bunz, U. H. F., Permanent Bubble Arrays from a Cross-Linked Poly(para-phenyleneethynylene): Picoliter Holes without Microfabrication. *J. Am. Chem. Soc.* **2004,** *126*, 3678-3679.

37. Cheng, C. X.; Tian, Y.; Shi, Y. Q.; Tang, R. P.; Xi, F., Porous Polymer Films and Honeycomb Structures Based on Amphiphilic Dendronized Block Copolymers. *Langmuir* **2005,** *21*, 6576-6581.

38. Kim, J. H.; Seo, M.; Kim, S. Y., Lithographically Patterned Breath Figure of Photoresponsive Small Molecules: Dual-Patterned Honeycomb Lines from a Combination of Bottom-Up and Top-Down Lithography. *Adv. Mater.* **2009,** *21*, 4130-4133.

39. Babu, S. S.; Mahesh, S.; Kartha, K. K.; Ajayaghosh, A., Solvent-Directed Self-Assembly of π Gelators to Hierarchical Macroporous Structures and Aligned Fiber Bundles. *Chem. Asian J.* **2009,** *4*, 824-829.

40. Yu, Y.; Ma, Y., Breath figure fabrication of honeycomb films with small molecules through hydrogen bond mediated self-assembly. *Soft Matter* **2011,** *7*, 884-886.

41. Du, M.; Zhu, P.; Yan, X.; Su, Y.; Song, W.; Li, J., Honeycomb Self-Assembled Peptide Scaffolds by the Breath Figure Method. *Chem. Eur. J.* **2011,** *17*, 4238-4245.

42. Gao, Y.-F.; Huang, Y.-J.; Xu, S.-Y.; Ouyang, W.-J.; Jiang, Y.-B., Ordered Honeycomb Microporous Films from Self-Assembly of Alkylated Guanosine Derivatives. *Langmuir* **2011,** *27*, 2958-2964.

43. Chen, J.; Yan, X.; Zhao, Q.; Li, L.; Huang, F., Adjustable supramolecular polymer microstructures fabricated by the breath figure method. *Polym. Chem.* **2012,** *3*, 458-462.

44. Avinash, M. B.; Verheggen, E.; Schmuck, C.; Govindaraju, T., Self-Cleaning Functional Molecular Materials. *Angew. Chem. Int. Ed.* **2012,** *51*, 10324-10328.

45. Avinash, M. B.; Govindaraju, T., Engineering Molecular Organization of Naphthalenediimides: Large Nanosheets with Metallic Conductivity and Attoliter Containers. *Adv. Funct. Mater.* **2011,** *21*, 3875-3882.

46. Vericat, C.; Vela, M. E.; Benitez, G.; Carro, P.; Salvarezza, R. C., Self-assembled monolayers of thiols and dithiols on gold: new challenges for a well-known system. *Chem. Soc. Rev.* **2010,** *39*, 1805-1834.

47. Love, J. C.; Estroff, L. A.; Kriebel, J. K.; Nuzzo, R. G.; Whitesides, G. M., Self-Assembled Monolayers of Thiolates on Metals as a Form of Nanotechnology. *Chem. Rev.* **2005,** *105*, 1103-1170.

48. Govindaraju, T.; Bertics, P. J.; Raines, R. T.; Abbott, N. L., Using Measurements of Anchoring Energies of Liquid Crystals on Surfaces To Quantify Proteins Captured by Immobilized Ligands. *J. Am. Chem. Soc.* **2007,** *129*, 11223-11231.

49. Gröger, G.; Meyer-Zaika, W.; Böttcher, C.; Gröhn, F.; Ruthard, C.; Schmuck, C., Switchable supramolecular polymers from the self-assembly of a small monomer with two orthogonal binding interactions. *J. Am. Chem. Soc.* **2011,** *133*, 8961-8971.

50. Knowles, T. P.; Buehler, M. J., Nanomechanics of functional and pathological amyloid materials. *Nat. Nanotechnol.* **2011,** *6*, 469-479.

51. Linke, W. A., Biomaterials: Spider strength and stretchability. *Nat. Chem. Biol.* **2010,** *6*, 702-703.

52. Omenetto, F. G.; Kaplan, D. L., New opportunities for an ancient material. *Science* **2010,** *329*, 528-531.

53. Xia, X.-X.; Qian, Z.-G.; Ki, C. S.; Park, Y. H.; Kaplan, D. L.; Lee, S. Y., Native-sized recombinant spider silk protein produced in metabolically engineered Escherichia coli results in a strong fiber. *Proc. Natl. Acad. Sci.USA* **2010,** *107*, 14059-14063.

54. Chung, H.; Kim, T. Y.; Lee, S. Y., Recent advances in production of recombinant spider silk proteins. *Curr. Opin. Biotechnol.* **2012,** *23*, 957-964.

55. An, B.; Hinman, M. B.; Holland, G. P.; Yarger, J. L.; Lewis, R. V., Inducing β-sheets formation in synthetic spider silk fibers by aqueous post-spin stretching. *Biomacromolecules* **2011,** *12*, 2375-2381.

56. Xia, X.-X.; Xu, Q.; Hu, X.; Qin, G.; Kaplan, D. L., Tunable self-assembly of genetically engineered silk–elastin-like protein polymers. *Biomacromolecules* **2011,** *12*, 3844-3850.

57. Wendt, H.; Hillmer, A.; Reimers, K.; Kuhbier, J. W.; Schäfer-Nolte, F.; Allmeling, C.; Kasper, C.; Vogt, P. M., Artificial skin–culturing of different skin cell lines for generating an artificial skin substitute on cross-weaved spider silk fibres. *PLoS One* **2011,** *6*, e21833.

58. Humenik, M.; Smith, A. M.; Scheibel, T., Recombinant Spider Silks—Biopolymers with Potential for Future Applications. *Polymers* **2011,** *3*, 640-661.

59. Vollrath, F.; Knight, D. P., Liquid crystalline spinning of spider silk. *Nature* **2001,** *410*, 541-548.

60. Scheller, J.; Gührs, K.-H.; Grosse, F.; Conrad, U., Production of spider silk proteins in tobacco and potato. *Nat. Biotechnol.* **2001,** *19*, 573-577.

61. Hagn, F.; Eisoldt, L.; Hardy, J. G.; Vendrely, C.; Coles, M.; Scheibel, T.; Kessler, H., A conserved spider silk domain acts as a molecular switch that controls fibre assembly. *Nature* **2010,** *465*, 239-242.

62. Fahnestock, S.; Irwin, S., Synthetic spider dragline silk proteins and their production in Escherichia coli. *Appl. Microbiol. Biotechnol.* **1997,** *47*, 23-32.

63. Lazaris, A.; Arcidiacono, S.; Huang, Y.; Zhou, J.-F.; Duguay, F.; Chretien, N.; Welsh, E. A.; Soares, J. W.; Karatzas, C. N., Spider silk fibers spun from soluble recombinant silk produced in mammalian cells. *Science* **2002,** *295*, 472-476.

64. Govindaraju, T.; Pandeeswar, M.; Jayaramulu, K.; Jaipuria, G.; Atreya, H. S., Spontaneous self-assembly of designed cyclic dipeptide (Phg-Phg) into two-dimensional nano-and mesosheets. *Supramol. Chem.* **2011,** *23*, 487-492.

65. Govindaraju, T., Spontaneous self-assembly of aromatic cyclic dipeptide into fibre bundles with high thermal stability and propensity for gelation. *Supramol. Chem.* **2011,** *23*, 759-767.

66. Joshi, K. B.; Verma, S., Participation of aromatic side chains in diketopiperazine ensembles. *Tetrahedron Lett.* **2008,** *49*, 4231-4234.

67. Palacin, S.; Chin, D. N.; Simanek, E. E.; MacDonald, J. C.; Whitesides, G. M.; McBride, M. T.; Palmore, G. T. R., Hydrogen-Bonded Tapes Based on Symmetrically Substituted

Diketopiperazines: A Robust Structural Motif for the Engineering of Molecular Solids. *J. Am. Chem. Soc.* **1997,** *119*, 11807-11816.

68. Ghosh, S.; Reches, M.; Gazit, E.; Verma, S., Bioinspired Design of Nanocages by Self-Assembling Triskelion Peptide Elements. *Angew. Chem. Int. Ed.* **2007,** *46*, 2002-2004.

69. Gdaniec, M.; Liberek, B., Structure of cyclo(-l-phenylalanyl-l-phenylalanyl-). *Acta Crystallographica Section C* **1986,** *42* (10), 1343-1345.

70. Varughese, S.; Kiran, M.; Ramamurty, U.; Desiraju, G. R., Nanoindentation in Crystal Engineering: Quantifying Mechanical Properties of Molecular Crystals. *Angew. Chem. Int. Ed.* **2013**, *52*, 2701-2712.

71. Mishra, M. K.; Varughese, S.; Ramamurty, U.; Desiraju, G. R., Odd–Even Effect in the Elastic Modulii of α, ω-Alkanedicarboxylic Acids. *J. Am. Chem. Soc.* **2013**, *135*, 8121-8124.

72. Adler-Abramovich, L.; Kol, N.; Yanai, I.; Barlam, D.; Shneck, R. Z.; Gazit, E.; Rousso, I., Self-Assembled Organic Nanostructures with Metallic-Like Stiffness. *Angew. Chem. Int. Ed.* **2010,** *49*, 9939-9942.

73. Katz, H. E.; Lovinger, A. J.; Johnson, J.; Kloc, C.; Siegrist, T.; Li, W.; Lin, Y. Y.; Dodabalapur, A., A soluble and air-stable organic semiconductor with high electron mobility. *Nature* **2000,** *404*, 478-481.

74. Zaumseil, J.; Sirringhaus, H., Electron and Ambipolar Transport in Organic Field-Effect Transistors. *Chem. Rev.* **2007,** *107*, 1296-1323.

75. Bhosale, S. V.; Jani, C. H.; Langford, S. J., Chemistry of naphthalene diimides. *Chem. Soc. Rev.* **2008,** *37*, 331-342.

76. Zhan, X.; Facchetti, A.; Barlow, S.; Marks, T. J.; Ratner, M. A.; Wasielewski, M. R.; Marder, S. R., Rylene and Related Diimides for Organic Electronics. *Adv. Mater.* **2011,** *23*, 268-284.

77. Naraso; Nishida, J.-i.; Kumaki, D.; Tokito, S.; Yamashita, Y., High Performance n- and p-Type Field-Effect Transistors Based on Tetrathiafulvalene Derivatives. *J. Am. Chem. Soc.* **2006,** *128*, 9598-9599.

78. Avinash, M. B.; Govindaraju, T., Amino Acid Derivatized Arylenediimides: A Versatile Modular Approach for Functional Molecular Materials. *Adv. Mater.* **2012,** *24*, 3905-3922.

79. Prasanthkumar, S.; Gopal, A.; Ajayaghosh, A., Self-Assembly of Thienylenevinylene Molecular Wires to Semiconducting Gels with Doped Metallic Conductivity. *J. Am. Chem. Soc.* **2010,** *132*, 13206-13207.

80. Jones, B. A.; Facchetti, A.; Wasielewski, M. R.; Marks, T. J., Tuning Orbital Energetics in Arylene Diimide Semiconductors. Materials Design for Ambient Stability of n-Type Charge Transport. *J. Am. Chem. Soc.* **2007,** *129*, 15259-15278.

81. Usta, H.; Facchetti, A.; Marks, T. J., n-Channel Semiconductor Materials Design for Organic Complementary Circuits. *Acc. Chem. Res.* **2011,** *44*, 501-510.

82. Chikamatsu, M.; Mikami, T.; Chisaka, J.; Yoshida, Y.; Azumi, R.; Yase, K.; Shimizu, A.; Kubo, T.; Morita, Y.; Nakasuji, K., Ambipolar organic field-effect transistors based on a low band gap semiconductor with balanced hole and electron mobilities. *Appl. Phys. Lett.* **2007,** *91*, 043506.

83. Xiao, K.; Liu, Y.; Qi, T.; Zhang, W.; Wang, F.; Gao, J.; Qiu, W.; Ma, Y.; Cui, G.; Chen, S.; Zhan, X.; Yu, G.; Qin, J.; Hu, W.; Zhu, D., A Highly π-Stacked Organic Semiconductor for Field-Effect Transistors Based on Linearly Condensed Pentathienoacene. *J. Am. Chem. Soc.* **2005,** *127*, 13281-13286.

84. Steyrleuthner, R.; Schubert, M.; Jaiser, F.; Blakesley, J. C.; Chen, Z.; Facchetti, A.; Neher, D., Bulk Electron Transport and Charge Injection in a High Mobility n-Type Semiconducting Polymer. *Adv. Mater.* **2010,** *22*, 2799-2803.

85. Coropceanu, V.; Cornil, J.; da Silva Filho, D. A.; Olivier, Y.; Silbey, R.; Brédas, J.-L., Charge transport in organic semiconductors. *Chem. Rev.* **2007,** *107*, 926-952.

86. Brütting, W.; Berleb, S.; Mückl, A. G., Space-charge limited conduction with a field and temperature dependent mobility in Alq light-emitting devices. *Synth. Met.* **2001,** *122*, 99-104.

87. Zheng, Y.; Wee, A. T. S.; Troadec, C.; Chandrasekhar, N., Temperature-dependent transition from injection-limited to space-charge-limited current in metal-organic diodes. *Appl. Phys. Lett.* **2009,** *95*, 143303.

# List of Publications

## *For PhD Thesis - Published*

- **M. B. Avinash** and T. Govindaraju, *A Bio-Inspired Design Strategy: Organization of Tryptophan-Appended Naphthalenediimide into Well-Defined Architectures Induced by Molecular Interactions*, ***Nanoscale***, **2011**, *3*, 2536-2543. (Cover Page)

- **M. B. Avinash** and T. Govindaraju, *Engineering Molecular Organization of Naphthalenediimides: Large Nanosheets with Metallic Conductivity and Attoliter Containers*, ***Adv. Funct. Mater.***, **2011**, *21*, 3875-3882. (Back Cover Page)

- **M. B. Avinash**, Elisabeth Verheggen, Carsten Schmuck and T. Govindaraju, *Self-Cleaning Functional Molecular Materials*, ***Angew. Chem. Int. Ed.***, **2012**, *51*, 10324-10328. (**Chosen as a "Hot Paper" by the Editors for its importance in a rapidly evolving field of high current interest**)

  Highlighted in "***ChemistryViews***" and "Sciencia"

- **M. B. Avinash** and T. Govindaraju, *Amino Acid Derivatized Arylenediimides: A Versatile Modular Approach for Functional Molecular Materials*, ***Adv. Mater.***, **2012**, *24*, 3905-3922. (A Review)

- T. Govindaraju and **M. B. Avinash**, *Two-Dimensional Nanoarchitectonics: Organic and Hybrid Materials*, ***Nanoscale***, **2012**, *4*, 6102-6117. (A Review; Cover Page)

- **M. B. Avinash** and T. Govindaraju, *Extremely Slow Dynamics of an Abiotic Helical Assembly: Unusual Relevance to the Secondary Structure of Proteins*, ***J. Phys. Chem. Lett.***, **2013**, *4*, 583-588.

- **M. B. Avinash**, Pralok K. Samanta, K. V. Sandeepa, Swapan K. Pati, and T. Govindaraju, *Molecular Architectonics of Stereochemically Constrained π-Complementary Functional Modules*, ***Eur. J. Org. Chem.***, **2013**, 5838-5847.

- **M. B. Avinash**, K. V. Sandeepa and T. Govindaraju, *Molecular Assembly of Amino Acid Interlinked, Topologically Symmetric, π–Complementary Donor–Acceptor–Donor Triads*, ***Beilstein J. Org. Chem.***, **2013**, 9, 1565-1571.

## *For PhD Thesis & Miscellaneous - Under Submission/Preparation*

- **M. B. Avinash**, K. V. Sandeepa and T. Govindaraju, *Evidence for Emergence in a Dynamic Molecular Assembly* (manuscript under submission).

- **M. B. Avinash**, Devraj Raut, U. Ramamurty and T. Govindaraju, *A Bioinspired Reductionistic Modular Approach for Stiffest Organic Materials* (manuscript under submission).

- **M. B. Avinash**, Swati, K. S. Narayan and T. Govindaraju, *Designer Auxiliaries to Engineer the Molecular Assembly and Bulk Charge Transport of Naphthalenediimides* (manuscript under preparation).

- **M. B. Avinash** and T. Govindaraju, *Emerging Engineering Strategies for Advanced Functional Self-Cleaning Materials* (manuscript under submission).

- **M. B. Avinash** and T. Govindaraju, *Molecular Architectonics for Advanced Functional Materials* (manuscript under submission).

- **M. B. Avinash**, Pralok K. Samanta, K. V. Sandeepa, Swapan K. Pati, and T. Govindaraju, *Self-Replicating Dynamic Molecular Assembly* (manuscript under preparation).

- **M. B. Avinash**, K. V. Sandeepa and T. Govindaraju, *Anti-Retentive Helical Memory: A Novel Insight into Chiral Selection during Molecular Assembly* (manuscript under preparation).

## ***Miscellaneous - Published***

- **M. B. Avinash**, K. S. Subrahmanyam, Y. Sundarayya and T. Govindaraju, *Covalent Modification and Exfoliation of Graphene Oxide Using Ferrocene*, ***Nanoscale***, **2010**, *2*, 1762-1766. (Most Accessed Article)

  Selected for *Physics Nobel 2010 Web Collection: Graphene*

- M. Pandeeswar, **M. B. Avinash**, and T. Govindaraju, *Chiral Transcription and Retentive Helical Memory: Probing Peptide Auxiliaries Appended with Naphthalenediimides for Their One-Dimensional Molecular Organization*, ***Chem. Eur. J.***, **2012**, 18, 4818- 4822. (Inside Cover Page)

- A. Thirumurugan, **M. B. Avinash** and C. N. R. Rao, *1, 2-, 1, 3 - and 1, 4-Cyclohexanedicarboxylates of Cd and Mn with Chain and Layered Structures*, ***Dalton Trans.***, **2006**, 221-228.

- Nagarjun Narayanaswamy, **M. B. Avinash** and T. Govindaraju, *Exploring Hydrogen Bonding and Weak Aromatic Interactions Induced Assembly of Adenine and Thymine Functionalised Naphthalenediimides*, ***New J. Chem.***, **2013**, 37, 1302-1306. (Most Accessed Article)

- Yosuke Hisamatsu, Supratim Banerjee, **M. B. Avinash**, T. Govindaraju, and Carsten Schmuck, *A Supramolecular Gel from a Quadruple Zwitterion that Responds to both Acid and Base*, ***Angew. Chem. Int. Ed.***, **2013**, *52*, 12550-12554. (**Chosen as a "Hot Paper" by the Editors**)

## **Patents**

- T. Govindaraju, **M. B. Avinash**, M. Pandeeswar, *Self-Assembly of Naphthalenediimide Derivatives and Process thereof*, WO Patent 2012098439, 2012.

## Miscellaneous Highlights of PhD Work

✓ **Best Poster Award** at "In-house Symposium-2009", Jawaharlal Nehru Centre for Advanced Scientific Research (JNCASR), Bangalore, India.

✓ **Best Poster Award** at "Chemistry of Functional Materials-2011", organized by Indian Institute of Technology-Bombay (IITB) and International Centre for Material Science (ICMS).

✓ Selected for Oral Presentation and was awarded **Best Speaker** at "Winter School on Frontiers in Material Science-2012", organized by University of Cambridge and ICMS at Bangalore, India.

✓ Appreciated with **Gandhian Young Technological Innovation Award** (GYTI-2013) under SRISTI Technological Edge/Strategic Innovation Category at Indian Institute of Management-Ahmedabad (IIMA).

✓ Our Artworks were featured on the **Journal Cover Pages** of *Nanoscale* and *Advanced Functional Materials*.

## Brief Curriculum Vitae

**M. B. Avinash** obtained his Integrated M.Sc. (Hons.) in Applied Chemistry from Kuvempu University, Karnataka, India in 2008. He was selected for the Project Oriented Chemical Education (POCE, 2004-2006) and Summer Research Fellowship (SRF, 2007) programs of Jawaharlal Nehru Centre for Advanced Scientific Research (JNCASR). He received Prof. C. N. R. Rao Foundation Gold Medal and Jayamma & Mudegoudra Veerabhadrappa Gold Medal for having secured the First Rank and being the topper of the Master's degree. After his post graduation, he worked as a Research and Development personnel of Defence Research and Development Organization (DRDO) project at JNCASR. He was presented with Gandhian Young Technological Innovation Award (Appreciation GYTI-2013) under SRISTI Technological Edge/ Strategic Innovation Category at Indian Institute of Management-Ahmedabad. He has worked for his PhD at JNCASR under the supervision of Dr. T. Govindaraju. His research interests include bio-inspired design strategies to engineer molecular assemblies for structure-function correlations, *de novo* properties and advanced functional molecular materials.